TNFα-activated fibroblasts support tumor progression in Luminal A breast cancer

Zhivka Ivanova Hristova

Oral examination: 01.09.2022

TNFα-activated fibroblasts support tumor progression in Luminal A breast cancer

Referees: Apl. Prof. Dr. Stefan Wiemann

Apl. Prof. Dr. Viktor Umansky

Inaugural dissertation

for

obtaining the doctoral degree

of the

Combined Faculty of Mathematics, Engineering and Natural Sciences

of the

Ruprecht - Karls - University

Heidelberg

Presented by

M.Sc. Zhivka Ivanova Hristova

born in: Svilengrad, Bulgaria

Oral examination: 01.09.2022

Declaration of authorship

I hereby declare that the work presented in my dissertation was carried out between August 2018 and June 2022 under the supervision of Prof. Dr. Stefan Wiemann in the group of Molecular Genome Analysis at the German Cancer Research Center (DKFZ, Heidelberg, Germany).

If not stated differently and referenced within the text, the experiments included in my dissertation have been designed and performed by me. The data presented is original, has been gathered by me and has not yet been presented as a part of a university examination. Any data from other sources has been cited accordingly. All main sources have been referenced appropriately. I, as the author, hereby declare no potential conflict of interest.

Heidelberg, _____

Zhivka Ivanova Hristova

Table of contents

List of Figures

List of Tables

Acknowledgements

I would like to thank my supervisors Prof. Dr. Stefan Wiemann and Dr. Cindy Körner for their guidance the last almost four years. In that respect, I would also like to express my gratitude to the members of my TAC, Prof. Dr. Viktor Umansky and Prof. Dr. Adit Ben-Baruch, for the advice and critical review of my work. I believe under your guidance I have become an even better scientist. I would also like to thank Prof. Dr. Tobias Dick and Prof. Dr. Dr. Georg Stoecklin for agreeing to serve on my thesis defense committee.

Four years is a long time and yet as if it was yesterday, when I joined the Division of Molecular Genome Analysis. In fact, it was February 2017 when I started as an intern in the lab. So, in the past more than five years, I had the pleasure to meet many wonderful people. First, I would like to thank our wonderful technicians, Heike, Angelika, Sara, Corinna, Daniela H., and Sabine for all the guidance with technical issues, willingness to help and even serve as a crying shoulder at times. I would also like to thank Daniela F. for all the help with orders, HR, etc. throughout the years, and for the little sweet presents that miraculously appeared on everyone's desk almost every Christmas. Working with you all has been a pleasure!

Next, I would like to express my gratitude to Dr. Mireia Berdiel-Acer for introducing me to the world of CAFs during my Master studies. I guess I became so captivated with them that I decided to make them my babies for several years. Thank you, Mireia, for the support and for making me a part of the CAF story.

Special gratitude goes as well to all the other CAF/TME ladies that have been on this journey with me at some point or another- Nese, Ana, Christina, Ani, Alessandra, Sophia, and Manio. It was a pleasure learning together more about the CAF world. This journey would not have been the same without you. It is always nice to have a travel-buddy or two to share the research experience with. For that I thank you.

This thesis would not have been possible without the wonderful support of the DKFZ core facilities. Special thanks go to Dr. Rainer Will, Katja and Birgit for all the help with the generation of the various cell lines I used during my Master and PhD studies. Without you, I would literally not have had cells to work with. Thank you, Rainer, for always answering all my questions, for all the drawings you did for me to explain important concepts and for all the guidance.

I would also like to thank the mass spectrometry and sequencing facilities for their excellent services. Special thanks go to Martin Schneider from the mass spec facility for the help with the mass spec data analysis. Without his help, my work would have been incomplete. I would also like to thank Dr. Bernd Heßling and Dr. Dominic Helm for the advice on how to set up my mass spec experiments and how to interpret the data, respectively.

I would like to also thank Dr. Simone Borgoni, Lukas Beumers and Nooraldeen Tarade for their assistance with the RPPA, and Dr. Birgitta Michels and Dr. Efstathios-Iason Vlachavas for their help with the analysis of the RNA-seq data. Your help has been invaluable and is truly appreciated.

Five years at the same division is a long time, so it will take me pages to mention everyone I have had the pleasure to meet here and all the ways they have contributed to my growth, personal and as a scientist. Honorable mention goes to the Girls office, Xiaoya and Janine for all the laughter, tears, food, and anything in between. You have been my rock to lean on and shoulder to cry on. Thank you for being there for me for literally anything – from a failed experiment to a broken heart. Thank you for fixing my soul, whenever I needed it. Thank you for being my friends.

Janina, Sophia, Manio and Dennis, thank you as well for being there for me. It was fun having you around and hope to be able to stay in touch in the future. My little vampires (always staying in the dark), the office is just not the same without you. Thank you, Lab girls + Dennis, for all the birthday surprises, sunset watching through the office window, tea/wine breaks and burger dinners. Dennis, thank you for the puzzle times. Your moral support, ladies, and a gentleman, during the final stages of my PhD was truly a life-saver. I hope to be able to repay you all one day.

My dearest friend, Raisa, in an ever-changing world, thank you for being a constant in my life. When I am scared, you give me strength. When I feel alone, you are there for me. When I think that I cannot do it, you remind me that I can. Just thinking about all the little and big ways you have been there for me, makes me emotional. I know that I can always rely on you for anything, and I hope you know I would do the same for you too. Thank you, Raisa, Ilma and Ihsan, for being my home away from home. For all the Christmases spent together, for all the support and for making life easier even at its hardest moments. We have survived the troubles of academic (Master and PhD) life together, been there for each other during family medical emergencies, even a pandemic and a war did not break our bond. I hope we have this forever, regardless of where life takes us next. I hope we always have each other's back.

Last, I would like to thank my family and especially my mom and dad for all the support, for being there for me, for encouraging me to never stop pursuing my dreams. I know I am not the perfect daughter, but I hope to be able to make you proud. Even if we are an ocean apart, I know I can always rely on you to put me back together, whenever I feel like I am falling apart. For all the packages with goodies from home, long video calls and words of encouragement, I will never be able to repay you. Thank you for loving me in my least lovable moments. Thank you for teaching me by example how to live an honest life. You taught me that integrity always comes first, and that is a lesson I will pass one day to my own children.

To my niece and nephews, I love you to the moon and back and then to the moon again. Although you drive me nuts sometimes, I still love you and always will. Sorry I have been working so much. I will try to do better in the future. I have missed so many of your milestones, but hopefully that will change for the better soon. Thank you for your patience with me and for continuing to ask me when I will be coming home to see you. I miss you too. But you know those fancy toys you ask me for will not pay for themselves, so Aunty has to work sometimes.

At the very last but not least, thank you, Grandpa! You are the reason I do what I do. Say hi to the angels from me, please. Miss you and love you!

SUMMARY

Breast carcinoma is the leading cause of cancer-related death in women worldwide. The most common breast cancer subtype is Luminal A. Most patients with this subtype initially respond well to standard endocrine therapies. However, many of them develop metastasis years later. It is well-known that the tumor microenvironment (TME) plays an important role in supporting tumor progression. A major component of the TME are the cancer-associated fibroblasts (CAFs), which have been reported to have multiple tumor-promoting functions. The exact mechanisms though are still under investigation, and no successful anti-CAF therapies have been discovered yet.

In my PhD studies, presented in this thesis, I investigated the role of CAFs in Luminal A breast cancer progression. To this end, I utilized CAFs isolated from Luminal A patient biopsies, as well as the classical *in vitro* models of Luminal A breast cancer – the MCF7 and T47D cell lines. In the TME, CAFs are exposed to many factors that activate them and drive them into a tumor-promoting phenotype. Previously, it has been shown that the combination of TNFα and TGFβ1 was sufficient to confer CAF-like properties on CAF precursor cells. Therefore, to mimic CAF activation in *vitro,* I stimulated the CAFs with these two cytokines. To study how the cytokine-activated CAFs could support breast cancer progression, the effect of CAF-conditioned medium (CM) on migration, autophagy and recovery post chemotherapy was examined in MCF7 and T47D cells. The goal was to identify novel CAF-secreted factors and/or signaling pathways that they activate in the breast cancer cells to support Luminal A relapse. To this aim, via mass spectrometry analysis, I studied the effect of the stimulation on the CAF secretome and full proteome. In addition, utilizing RNA sequencing, I investigated the effect of the cytokine-activated CAF CM on the MCF7 cells, and compared it to the effect of the CM from unstimulated CAFs. Finally, I compared the results from both analyses to better understand the complex crosstalk between CAFs and Luminal A breast cancer cells and how it could contribute to Luminal A breast cancer progression.

First, I demonstrated that the stimulation with TNFα was sufficient to induce the CAFs to secrete factors with pro-migratory effect on the Luminal A cells. Second, I was able to identify upregulation of STAT/IFNβ1 signaling in the CAFs in response to the TNFα stimulation. In addition, the CAFs were able to relay the STAT signaling to the breast cancer cells via secretion of IFNβ1. Third, I identified STAT2 to work in a STAT1-independent manner as the transcription factor necessary for the TNFα-stimulated induction of the ISG (interferon-stimulated gene) signature in the CAFs. Although I could not show a clear connection between the CAF interferon signaling and the breast cancer migratory phenotype, the stimulation with TNFα appeared to potentially impede with the CAFs ability to support Luminal A recovery post chemotherapy. Thus, TNFα seemed to play a double role in the complex CAF-Luminal A crosstalk. While TNFα-stimulated CAFs secreted factors, which increased Luminal A breast cancer migration, some of these factors and/or even TNFα itself seemed to prevent the recovery of the tumor cells after

chemotherapy. Further investigation of the complex CAF-Lum A crosstalk and the role of TNFα in it is necessary. Meanwhile the role of TNFα as a double-edge sword in the TME-cancer crosstalk is something to consider when deciding on the next best therapeutic option for treatment of refractory Luminal A breast cancer.

ZUSAMMENFASSUNG

Brustkrebs stellt weltweit die häufigste Ursache für krebsbedingte Tode unter Frauen dar. Der am häufigsten festgestellte Subtyp von Brustkrebs ist Luminal A. Die meisten Patientinnen mit diesem Subtyp profitieren zunächst von der gängigen endokrinen Therapie. Allerdings entwickeln viele der Patientinnen Jahre später Metastasen. Es ist bekannt, dass die Tumor-Mikroumgebung (TME) eine wichtige Rolle in der Tumorprogression spielt. Einen Hauptbestandteil der TME bilden die Krebs-assoziierten Fibroblasten (CAFs), welchen vielseitige tumorfördernde Funktionen zugeschrieben werden. Die genauen Mechanismen hierfür werden allerdings noch untersucht, und es wurden bislang keine erfolgreichen anti-CAF Therapien entwickelt.

In meiner Doktorarbeit habe ich die Rolle von CAFs in der Progression von Brustkrebs des Luminal A Subtyps untersucht. Hierfür habe ich nebem den klassischen *in vitro* Modellen für Luminal A Brustkrebs – den Zellinien MCF7 und T47D – CAFs verwendet, die aus Biopsien von Luminal A Tumoren gewonnen worden sind. In der TME sind die CAFs einer Vielzahl an Faktoren ausgesetzt, die die CAFs aktivieren und damit in einen tumorförderlichen Phänotyp überführen können. Es wurde zuvor gezeigt, dass eine Kombinationsbehandlung mit TNFα und TGFβ1 ausreichend war, um in CAF-Vorläuferzellen einen CAF-ähnlichen Phänotyp zu induzieren. Aus diesem Grund habe ich CAFs mit diesen beiden Zytokinen stimuliert, um die Aktivierung der CAFs *in vitro* nachzustellen. Um zu untersuchen, wie die aktivierten CAFs die Progression von Brustkrebs beeinflussen können, wurden die Auswirkungen von CAF-konditioniertem Medium auf Migration, Autophagie und die Erholung nach einer Chemotherapiebehandlung in MCF7 und T47D Zellen untersucht. Dabei war es das Ziel, neue Faktoren zu identifizieren, die von den CAFs ausgeschüttet werden und die Signalwege zu untersuchen, die durch diese Faktoren in den Brustkrebszellen aktiviert werden und potentiell zu erneutem Tumorwachstum in Luminal A Patientinnen führen können. Hierfür habe ich mittels Massenspektrometrie den Effekt der Stimulation auf das CAF Sekretom und das CAF Proteom untersucht. Zusätzlich habe ich mittels RNA Sequenzierung den Effekt der durch Zytokine aktivierten CAFs auf das Transkriptom von MCF7 Zellen im Vergleich zu unstimulierten CAFs quantifiziert. Zuletzt habe ich die Ergebnisse beider Analysen vergleichen, um das komplexe Zusammenspiel zwischen CAFs und den Luminal A Brustkrebszellen und dessen Beitrag zur Progression der Krankheit besser zu verstehen.

Zuerst habe ich gezeigt, dass die Stimulation mit TNFα ausreichend war, um die CAFs zur Ausschüttung von Faktoren mit migrationsförderlicher Wirkung auf die Luminal A Zellen anzuregen. Zweitens war ich in der Lage, die Aktivierung des STAT/IFNβ1 Signalwegs in den CAFs als Reaktion auf die Stimulation mit TNFα zu identifizieren. Zudem waren die CAFs in der Lage, durch Sekretion von IFNβ1 den STAT Signalweg auch in den Brustkrebszellen zu induzieren. Des Weiteren konnte ich zeigen, dass STAT2 die durch TNFα induzierte Expression der interferon-stimulierten Gensignatur in den CAFs unabhängig von STAT1 vermittelte. Obwohl ich keine klare Verbindung zwischen der Aktivierung des Interferon-Signalwegs in den CAFs und dem migratorischen Phänotyp in den Brustkrebszellen aufzeigen konnte, schien die Stimulation mit TNFα die Fähigkeit der

CAFs zu beeinträchtigen, die Erholung von Luminal A Brustkrebszellen nach einer Chemotherapiebehandlung voranzutreiben. TNFα scheint also eine duale Rolle im komplexen Zusammenspiel zwischen CAFs und Brustkrebszellen zu spielen.

Während TNFα-stimulierte CAFs Faktoren ausschütteten, welche die Migration von Luminal A Brustkrebszellen verstärkten, schienen einige dieser Faktoren und/oder TNFα selbst der Erholung der Tumorzellen nach einer Chemotherapiebehandlung entgegenzuwirken. Weitere Untersuchungen sind notwendig, um das komplexe Zusammenspiel zwischen CAFs und Luminal A Brustkrebszellen sowie speziell die Rolle von TNFα zu verstehen. Dabei sollte die Rolle von TNFα als zweischneidiges Schwert bei der Entscheidung über Behandlungsmöglichkeiten für refraktären Luminal A Brustkrebs berücksichtigt werden.

1. INTRODUCTION

1.1. Breast Cancer. Subtypes and Standard Therapies

Breast carcinoma is the leading cause of cancer-related mortality in women. According to the Global Cancer Statistics (Globocan), in 2020, one in six female cancer deaths was due to breast cancer, which then claimed 685 000 lives. The same year, worldwide, an estimated 2.3 million women were diagnosed with breast cancer. Thus, with 11.7% of all new cancer cases recorded in 2020, female breast cancer, surpassing lung cancer, has become the most commonly diagnosed malignancy (Sung *et al*., 2021).

Breast cancer is a highly-heterogeneous disease with several molecular subtypes. Determining the subtype at diagnosis is important because it can guide towards targeted treatment and spare chemotherapy, with its severe side effects, for patients who will not benefit from it. The classification is based primarily on the level of expression of 1) three cell signaling receptors, namely, ER (estrogen receptor), PR (progesterone receptor) and HER2 (human epidermal growth factor receptor 2); 2) proliferation markers, such as Ki-67; and 3) basal markers. Although the number of subtypes varies according to the different studies, there are three major ones, which are used the most at the clinics: Triple Negative Breast Cancer (TNBC), HER2-enriched, and Luminal. The Luminal subtype is further divided into at least two subgroups, Luminal A and B (Dai *et al*., 2015, Johnson *et al*., 2021). The main characteristics of these breast cancer subtypes are summarized in Figure 1.

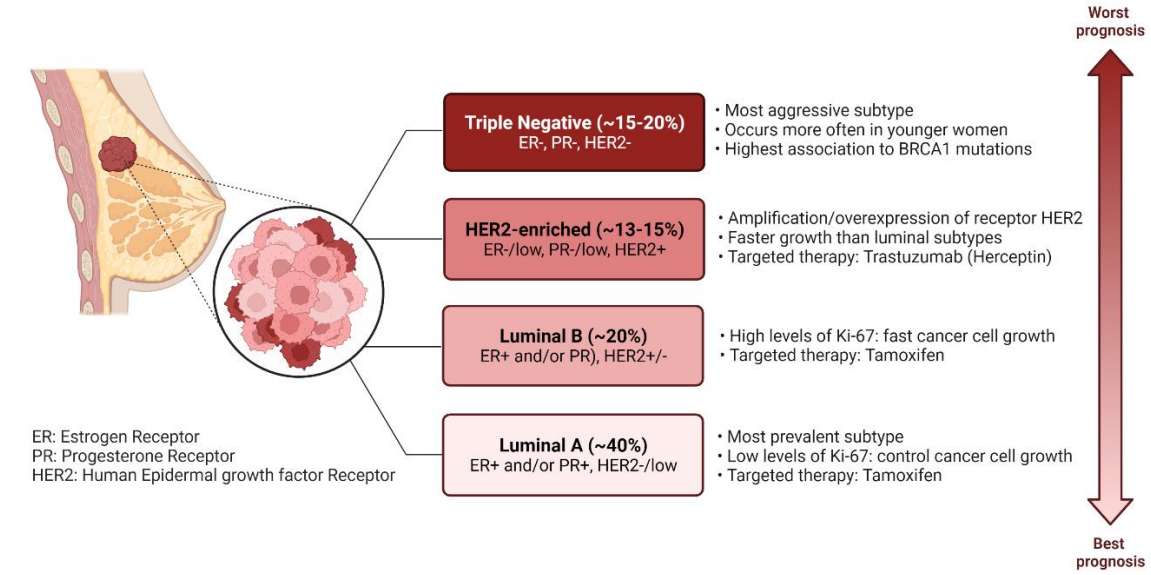

Figure 1. Intrinsic molecular breast cancer subtypes. Although according to the different classifications, there are several breast cancer subtypes, only four are used in the clinic on a regular basis: Triple Negative Breast Cancer (TNBC), HER2-enriched, Luminal A and B. TNBC is considered to have the worst prognosis, and Luminal A – the best prognosis. Luminal A is also the most commonly diagnosed breast cancer subtype. Adapted from "Intrinsic and Molecular Subtypes of Breast Cancer", by BioRender.com (2022). Retrieved from https://app.biorender.com/biorender-templates.

Triple negative breast cancer (TNBC) gets its name from the fact that it does not express ER, PR and HER2 receptors. The majority of TNBC tumors are basal-like, meaning that their expression profile resembles that of breast basal epithelial cells – they express laminin, keratins 5/6 and 17 and integrin β4 (Perou *et al*., 2000). This subtype is very heterogeneous and can itself be divided into at least four subgroups- two basal-like BL1 and BL2, mesenchymal (M) and luminal androgen receptor (LAR) subtypes (Lehmann *et al*., 2016). Because, unlike the other breast cancer subtypes, TNBC lacks expression of drug-targetable receptors, the main treatment for this disease is chemotherapy. Although some TNBC patients respond very well to the chemotherapy, this subtype is considered to have the worst prognosis (Hennigs *et al*., 2016; van Maaren *et al*., 2019).

HER2-enriched breast tumors are hormonal receptor low or negative. As the name suggests, they overexpress the *HER2* oncogene, which codes for the receptor tyrosine kinase HER2. The *HER2* gene, also known as *ERRB2*, is amplified in 13-15% of breast cancers (Harbeck *et al*., 2019). HER2 is an orphan receptor, meaning that it has no known ligands. It belongs to the HER family of four type I transmembrane growth factor receptors, which includes, in addition to HER2, also HER1, HER3 and HER4. HER2 forms heterodimers with the other members of the HER family, when the latter are bound by their respective ligands. The dimerization elicits a series of downstream phosphorylation events, such as activation of the PI3K/Akt and MAPK/ERK pathways. This ultimately results in induction of cell responses, e.g., survival, growth, proliferation, and migration. Hyperactive HER signaling leads to tumorigenesis (Yarden and Sliwkowski, 2001; Moasser *et al*., 2007; Yarden and Pines, 2012). The HER2-enriched subtype may harbor *TP53* mutations, which in the context of breast cancer are associated with increased mortality (Silwal-Pandit *et al*., 2014). HER2-targeted therapy, e.g., the anti-HER2 monoclonal antibodies trastuzumab (also known as Herceptin) and pertuzumab, is the treatment of choice for HER2-enriched breast cancers (Brandão *et al*., 2018).

The luminal subtypes are named after the breast luminal epithelial cells with which they share similarities in gene expression profiles (Perou *et al*., 2000). They are characterized by expression of the hormone receptors ER and/or PR, as well as ER-associated genes. Epithelial in nature, the luminal subtypes express also cytokeratins 8/18 (Perou *et al*., 2000). Based on the expression of the proliferation marker Ki-67, there are two luminal subtypes, A and B with low (<14%) and high (≥14%) Ki-67 index, respectively (Cheang *et al*., 2009; Johnson *et al*., 2021). Some Luminal B cancers are also HER2+.

Luminal A is the most common breast cancer subtype accounting for about 40% of all breast tumors (Johnson *et al*., 2021). It has also the most favorable prognosis among all breast cancer types (Hennigs *et al*., 2016; Gao and Swain, 2018; van Maaren *et al*., 2019). Endocrine therapy which targets the estrogen receptor signaling, e.g., tamoxifen (for premenopausal patients) and fulvestrant (approved for postmenopausal patients), or targets the estrogen production, i.e.,

aromatase inhibitors, is the standard of care for Luminal A and B breast cancers. Luminal A patients are recommended to take endocrine therapy for at least 5 years after surgery. Some patients though develop resistance to endocrine therapy and eventually must undergo alternative treatments, such as CDK4/6 inhibitors and chemotherapy, (Harbeck *et al*., 2019).

Chemotherapy is also recommended for early-stage luminal HER2-negative patients with high risk of relapse (>10% in 10 years) as well as last resort for patients with luminal-like (ER+ and/or PR+ and HER2-) advanced breast cancer. The standard chemotherapy for such patients is an anthracycline, such as epirubicin, and a taxane, such as paclitaxel, given sequentially (Harbeck *et al*., 2019). Anthracyclines are DNA intercalating agents causing DNA breaks and adducts which inhibit DNA and RNA synthesis. Anthracyclines also generate reactive oxygen species (ROS), which lead to further DNA damage (Coukell and Faulds., 1997; Schick *et al*., 2021). Taxanes bind to beta-tubulin, thus stabilizing the microtubules and preventing their assembly into a mitotic spindle. As a result, taxanes cause a G2/M arrest and inhibit the cell cycle (Horwitz 1994; Schick *et al*., 2021). Both classes of chemotherapy ultimately lead to apoptosis of highly-proliferative cells, such as the tumor cells.

1.2 The Concept of Tumor Microenvironment

Although Luminal A carcinomas have the best prognosis of all breast cancer subtypes, being the most common breast cancers, they still contribute heavily to the global cancer burden. Moreover, initially successful treatment is often followed by tumor relapse. Luminal A patients tend to respond very well to endocrine therapy, and yet years later some of them develop metastases. Thus, to be able to help these patients, it is crucial to better understand the factors and players contributing to Luminal A tumor progression. Although the transformed cancer cells have always been the the obvious culprits and therefore the center of attention in scientists' efforts to fight against cancer, in more recent times, the non-transformed *normal* cells, within or surrounding the tumor, i.e., the tumor microenvironment (TME), have become a topic of research.

Within the tumor mass, the cancer cells do not exist on their own. They are usually surrounded by the cells making up the blood vessels (pericytes and endothelial cells), the immune cells, extracellular matrix (ECM), cytokines, chemokines and more, all of which are part of the so-called tumor microenvironment (Figure 2; (Rønnov-Jessen and Petersen, 1996; Soysal *et al*., 2015). The TME is also referred to as the tumor stroma. The environment, in which the tumor resides, can be very harsh, especially during anti-cancer treatments. Hypoxia and lack of nutrients due to limited blood supply, insults coming from targeted therapies, DNA damage-inducing chemo- and radiotherapy, and reactive oxygen species (ROS) lead to metabolic and oxidative stress (Brahimi-Horn *et al*., 2007; Nakamura and Takada, 2021). This level of stress in normal circumstances leads to cell death. And yet the cancer cells often survive, persist, and strive through it all, because they can rely on their partners in crime, the-tumor-supportive side of the TME (Hanahan and Coussens, 2012). While one part of the TME, for example the tumor-suppressive side of the immune system, is trying to eliminate the cancer cells, other TME components may come to their rescue (Quail and Joyce, 2013). Among the *rescuers* are the fibroblasts, which in the context of cancer are defined as CAFs, cancer-associated fibroblasts (Liao *et al*., 2019). Although some tumor-residing fibroblasts seem to have tumor-restraining functions (Wagner, 2016), especially at the initial stages of tumor development, most of them eventually help the cancer cells survive, proliferate, and metastasize.

This is why CAFs have become a hot topic of research in recent years (Kalluri, 2016; Sahai *et al*., 2020). Their involvement in breast cancer has been studied extensively (Hu *et al*., 2022) and yet there is still a lot left unknown. In the next few sections, I will introduce you to these somewhat enigmatic cells, their biology and role in cancer. Let me start first with answering the question: "What is a fibroblast?".

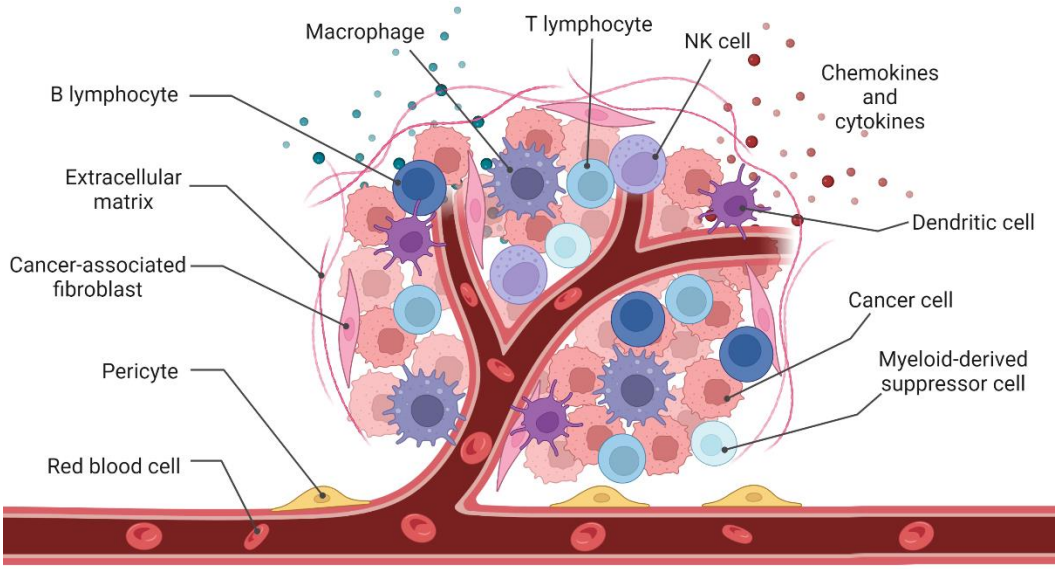

Figure 2. Components of the tumor microenvironment. The TME is a term coined to describe any cell or component (cytokine, chemokine, ECM) within the tumor or in close proximity to it. That includes (but is not limited to) the immune cells, the cells that make up the blood vessels (endothelial cells and pericytes), as well as the cancer-associated fibroblasts (CAFs). Adapted from "Tumor microenvironment", by BioRender.com (2022). Retrieved from https://app.biorender.com/biorender-templates.

1.3 Fibroblasts

Fibroblasts are spindle-shaped non-epithelial, non-immune cells of most likely mesenchymal origin (Kalluri, 2016). They were first described in 1858 by Rudolf Virchow as collagen-producing cells residing in the connective tissue (Virchow, 1858). Raghu Kalluri more recently described them as the cockroaches of the human body because of their resilience against severe stress (Kalluri, 2016). An illustration of that is the fact that they can be easily isolated for cell culture even from human post-mortem tissues (Bliss *et al*., 2012). They usually exist in an inert quiescent state, however, get activated during tissue injury. Once activated, they

assist with the wound healing process by synthesizing components of the ECM (extracellular matrix), such as collagen, fibronectin, and laminin. They also secrete ECM-degrading endopeptidases called MMPs (matrix metalloproteinases), which are necessary for the ECM turnover. In this activated state, they express αSMA (alpha smooth muscle actin) and are referred to as myofibroblasts because of their contractile phenotype (Darby *et al*., 2014). It is because of their contractility that the wound can contract and close. Once the wound has healed, they go back to their resting state or undergo apoptosis (Gabbiani, 2003). As major producers of ECM, the fibroblasts are important for maintenance of tissue integrity and homeostasis. However, there are also pathological conditions in which the hibernating fibroblasts are activated, such as acute and chronic inflammation, fibrosis, and cancer (Micallef *et al*, 2012; Kalluri, 2016). As already mentioned, in the context of cancer, the activated fibroblasts are called CAFs, cancer-associated fibroblasts. So, what exactly is a CAF?

1.4 Cancer-associated fibroblasts and their biomarkers

The consensus is that CAFs are permanently activated fibroblasts, which may have tumor-supportive and/or tumor-suppressive functions (Kalluri, 2016). To be able to identify them in a tumor biopsy, scientists have been on the search for CAF-specific biomarkers for decades. Their efforts, however, so far have been futile. Many of the markers historically used to isolate CAFs are in fact not unique to CAFs or even to the fibroblast lineage (Nurmik *et al*., 2020). Nevertheless, there are several biomarkers which have been used successfully by the scientific community to identify and study CAFs. A few of them are summarized in Table 1. To gain a better understanding about what a CAF is, let us examine some of the putative CAF biomarkers in more detail.

Table 1. Potential biomarkers of CAFs.

CAF marker	Description	Main functions	Expressed also by	References
αSMA/*ACTA2*	Microfilament component	Cell motility and contractility, wound healing, cell integrity	Myofibroblasts, smooth muscle cells, pericytes, cardiomyocytes	Lazard *et al*., 1993 Surowiak *et al*., 2007
Decorin/*DCN*	Matrix proteoglycan	Regulation of collagen fibrillogenesis, autophagy, proliferation, migration	Normal fibroblasts, vascular endothelial cells, smooth muscle cells	Li H *et al*., 2017 Niell *et al*., 2012
FAP	Type II integral membrane protein	Serine protease, ECM remodeling, fibrogenesis	Epithelial cells undergoing EMT, Bone marrow stem cells, $CD45^+$ immune cells	Huber *et al*., 2003 Li H *et al*., 2017 Kahounová *et al*., 2018
Fibronectin/*FN1*	ECM glycoprotein	Wound healing, ECM remodeling, cell adhesion and migration	Normal fibroblasts, hepatocytes, macrophages, endothelial cells, some epithelial cells	Erdogan *et al*., 2017
PDGFRα	Receptor tyrosine kinase	Cell differentiation, proliferation, survival, migration	Normal fibroblasts, pericytes, vascular smooth muscle cells, skeletal muscle cells, cardiomyocytes, tumor cells	Sharon *et al*., 2013
PDGFRβ	Receptor tyrosine kinase	Cell differentiation, proliferation, survival, migration	Normal fibroblasts, pericytes, vascular smooth muscle cells, skeletal muscle cells, cardiomyocytes, tumor cells	Paulsson *et al*., 2009
FSP-1/ *S100A4*	Calcium-binding protein	Cell motility, tissue fibrosis	Quiescent fibroblasts, epithelial cells undergoing EMT, macrophages, tumor cells	Strutz *et al*., 1995
Vimentin/*VIM*	Type III intermediate filament	Cytoskeleton formation, cell integrity, migration	All fibroblasts, other mesenchymal cells, epithelial cells undergoing EMT	Maehira *et al*., 2019
Collagens	ECM components	Wound healing, proliferation, migration, chemoresistance	Normal fibroblasts, MSCs, renal tubular epithelial cells	Lai *et al*., 2019 Nissen et al., 2019
MMPs	ECM components, proteases	Wound healing, ECM remodeling/degradation, cell migration, proliferation	Monocytes, keratinocytes, macrophages, normal fibroblasts	Sternlicht *et al*., 1999
GPR77	G-protein coupled receptor	Complement activation, pro-inflammatory signaling	Polymorphonuclear neutrophils	Su *et al*., 2018

1.4.1 αSMA

αSMA (alpha smooth muscle actin), encoded by *ACTA*, is an intracellular protein. It is a member of the actin family and as such is essential for cell integrity, motility, and contractility. The contractile/motile phenotype is impaired in fibroblasts upon inhibition of *ACTA2* expression (Rockey *et al*., 2013). αSMA is one of the go-to markers for the identification of CAFs, even though it is not exclusive to them (Nurmik *et al*., 2020). Other αSMA positive cells are the pericytes (Bergers and Song, 2005) and smooth muscle cells (Latif *et al*., 2015). As mentioned already, the wound healing fibroblasts also express αSMA and are called myofibroblasts because of their contractility (Darby *et al*., 2014). Similarly, CAFs which are αSMA^{high} are often referred to as myCAFs, or myofibroblastic CAFs, and can contract and remodel the ECM, making it easier for cancer cells to migrate. Expression of αSMA in the myCAFs is associated with TGFβ1. Blockade of TGFβ1 signaling with anti-TGFβ1 neutralization antibody results in ablation of the myCAF subpopulation in the bulk CAF population (Grauel *et al*., 2020; the concept of CAF subpopulations will be elaborated on in section 1.5). Furthermore, it has been demonstrated *in vitro* that TGFβ1 can induce *ACTA* expression in myofibroblasts, in resting and in growing fibroblasts (Desmoulière *et al*., 1993). Thus, myofibroblasts/fibroblasts may acquire αSMA-positive myCAF-like phenotype upon stimulation with TGFβ1 and lose it when TGFβ1 is neutralized. αSMA expression is negatively correlated with overall and relapse-free survival in breast cancer - the higher the content of αSMA myofibroblasts, the worse the prognosis (Surowiak *et al*., 2007). Another protein used as a CAF marker is FAP.

1.4.2 FAP

Fibroblast activation protein, or FAP, is a type II integral membrane glycoprotein. It is a serine protease with dipeptidyl peptidase and collagenase activity. As such, it participates in ECM remodeling and degradation during tissue repair (Park *et al*., 1999). In the early 2000s, it was estimated that FAP expression is high in more than 90% of all investigated carcinomas at the time (Huber *et al*., 2003). Its expression on the cell surface makes it a better candidate, than the intracellular αSMA, for isolation of viable CAFs via FACS (fluorescence-activated cell sorting). This feature has also made it the target of several anti-CAF drugs.

Not all CAFs though are FAP-positive. The expression of FAP by the CAFs varies between tumors and even within the same tumor, where both FAP-positive and FAP-negative CAF subpopulations have been identified (Li H *et al*., 2017). In ovarian cancer, high FAP expression has been associated with poor prognosis (Hussain *et al*., 2020). FAP is also expressed by other cell types such as epithelial cells undergoing EMT (Kahounová *et al*., 2018) and bone marrow stem cells (Bae *et al*., 2008).

1.4.3 Fibronectin

Another potential CAF biomarker is fibronectin, encoded by *FN1* (Ping *et al*., 2021). It is a high-molecular weight secreted glycoprotein. It has several isoforms resulting from alternative splicing of its pre-mRNA (ffrench-Constant, 1995; Kosmehl *et al*., 1996). Fibronectins bind to the transmembrane receptors integrins on the cell surface (Plow *et al*., 2000), and to several components of the ECM, e.g., collagens and fibrins (Pankov and Yamada, 2002). Because of its loss of expression in tumor cells, *FN1* is considered a tumor suppressor (Vaheri and Mosher, 1978). However, its expression in the TME, and particularly CAFs, has been shown to facilitate cancer cell migration, invasion, and metastasis (Erdogan *et al*., 2017; Lin *et al*., 2019; Miyazaki K *et al*., 2020). CL. Li *et al*. has demonstrated that stimulation with fibronectin induces EMT (epithelial-to-mesenchymal transition), migration and invasion in MCF7 breast cancer cells (Li CL *et al*., 2017). Similarly to the other putative CAF markers already discussed, fibronectin is also not exclusively expressed by fibroblasts. Among the other sources of fibronectin are macrophages (Alitalo *et al*., 1980; Gratchev *et al*., 2001) and endothelial cells (Andrews *et al*., 2018).

1.4.4 Vimentin

Vimentin, encoded by *VIM*, is a type III intermediate filament protein and an important component of the cytoskeleton network. It is expressed by all cells of mesenchymal origin and has often been used to identify fibroblasts and CAFs. Of all putative CAF biomarkers described so far, vimentin is probably the least specific (Nurmik *et al*., 2020). In addition to CAFs and fibroblasts in general, it is expressed also by macrophages (Cain *et al*., 1983; Mor-Vaknin *et al*., 2003), adipocytes (Roh

and Yoo, 2021) and epithelial cells undergoing EMT (Kalluri and Weinberg, 2009), to name a few. Vimentin plays an essential role in cell motility and adhesion (Ivashka *et al*., 2007). Richardson *et al*. has demonstrated that vimentin is required for invasion and metastasis in mouse models of lung adenocarcinoma (Richardson *et al*., 2018). Moreover, this group has shown that it is the CAFs that are vimentin-positive and not the lung cancer cells, and that the CAFs' motility depends on vimentin expression. They also observed that at the invasion front the vimentin-positive CAFs led the invasion of vimentin-negative lung tumor cells (Richardson *et al*., 2018). CAFs with high expression of vimentin correlate with poor prognosis in colorectal cancer (Ngan *et al*., 2007) and pancreatic ductal adenocarcinoma (Maehira *et al*., 2019).

So, what is a CAF? Considering the lack of CAF specific markers, the question what a CAF is remains hard to answer. In 2020, Sahai *et al.* published a consensus statement in Nature which included the agreement on what the definition of a CAF could be (Sahai *et al.*, 2020). To sum it up, a CAF *may be* any elongated mesenchymal cell derived from a tumor as long as it is **not**:

- Harboring any of the mutations of the tumor cells.
- An epithelial cell.
- An endothelial cell.
- A leukocyte.

The requirement that it must be mesenchymal means that in principle as long as the cell is non-transformed and negative for the above lineages, positivity for any of the aforementioned mesenchymal markers means that it is a CAF, with the caveat that once cultured any cell will lose some of its original characteristics (Sahai *et al*., 2020). What adds even more to the complexity is the fact that CAFs show high heterogeneity and plasticity (Sugimoto *et al*., 2006; Öhlund *et al*., 2014).

1.5 CAF heterogeneity and plasticity

Although the focus of this study is not directly on CAF heterogeneity, it is such an important aspect that it must be briefly commented on. The fact that no all-inclusive CAF markers could be discovered was perhaps the earliest indication of CAF diversity. FACS-based studies helped scientists identify multiple CAF subsets with distinct markers within the same tumor (Costa *et al*., 2018; Su *et al*., 2018). Now the development of single cell RNA-sequencing allows us to study the tumor stroma in detail not possible before (Bartoschek *et al*., 2018; Valdés-Mora *et al.*, 2021). It has reaffirmed the notion that CAFs within a tumor are a diverse population with multiple subclasses which could coexist (Kanzaki and Pietras, 2020; Biffi and Tuveson, 2021). Each subpopulation has its own distinctive markers, characteristics, and functions. Some of the CAF subpopulations described so far in breast cancer are summarized in Table 2.

In addition, CAFs demonstrate plasticity – they can undergo switch from one subset to another upon cues coming from the TME. For example, TGFβ1 can activate quiescent fibroblasts and convert them into myCAFs. Neutralization of TGFβ1 has been demonstrated to result in ablation of the myCAF subset which seems to be then converted into other CAF subpopulations, including inflammatory CAFs, termed iCAFs, and interferon-licensed CAFs, termed ilCAFs (Grauel *et al*., 2020). Thus, upon TGFβ1 blockade, the ECM-remodeling myCAFs are replaced by the immunomodulatory iCAFs and ilCAFs. The authors also show in the mouse 4T1 model of breast cancer that such a conversion to ilCAFs may support the success of anti-PD1 immunotherapy (Grauel *et al*., 2020).

Similar CAF plasticity has been observed in pancreatic cancer models as well. Biffi *et al*. have found that upon stimulation with IL-1, CAFs acquire inflammatory phenotype (iCAF) characterized by JAK/STAT and NF-κB signaling and the expression of inflammatory cytokines such as IL6 and LIF (Biffi *et al*., 2019). Treatment with TGFβ1 can antagonize the IL-1 effects and convert the iCAFs into myCAFs (Biffi *et al*., 2019), thus illustrating how CAF interconversion depends on tumor microenvironmental cues.

Table 2.CAF subpopulations in breast cancer.

Sample type	CAF subset	Defining markers	Putative function	References
Breast/lung cancer, patient samples	CD10+ GPR77+	$CD10^{+}$, $GPR77^{+}$, $IL6^{+}$	Chemotherapy resistance, cancer stemness	Su *et al*., 2018
Breast/ovarian cancer, patient samples	CAF-S1	FAP^{High}, αSMA^{High}, $CXCL12^{+}$, $IL6^{+}$	Immunosuppression, ECM production	Costa *et al*., 2018 Givel *et al*., 2018
	CAF-S2	Low expression of all markers	Contractility	
	CAF-S3	αSMA^{Low}, FSP-1^{+}, $PDGFR\beta^{+}$		
	CAF-S4	$CD29^{High}$, αSMA^{High}, FAP^{Low}		
Breast cancer, patient samples	iCAF (inflammatory)	$CXCL12^{+}$	Immunomodulation, immune evasion	Wu *et al*., 2020
	myCAF (myofibroblastic)	ACTA2, FAP, PDPN, COL1A1/2	ECM production/ remodeling	
MMTV-PyMT mouse tumors	vCAF (vascular)	αSMA^{High}, $PDGFR\beta^{High}$	Angiogenesis	Bartoschek *et al*., 2018
	mCAF (matrix)	αSMA^{Low}, $PDGFR\alpha^{High}$, Fibulin-1	ECM production	
	cCAF (cycling)	$PDGFR\beta^{High}$	Angiogenesis	
	dCAF (developmental)	$PDGFR\beta^{-}$, $SOX9^{+}$, $SCRG1^{+}$	Cell differentiation	
MMTV-PyMT mouse tumors	ECM-CAF	TNC+	ECM production	Valdés-Mora *et al.*, 2021
	immune-CAF (iCAF)	$Ly6C^{High}$, $C3^{+}$, $CXCL12^{+}$, $PDGFR\alpha^{High}$	Immunomodulation, JAK/STAT signature	
	Myofibroblastic CAF	αSMA^{High}, $MYLK^{+}$	Contractility	
4T1 mouse tumors	PDPN-CAF (pCAF) (6 subcluster):	PDPN and:		Friedman *et al.*, 2020
	1) immune reg E	CXCL12	Immunoregulation/ migration	
	2) immune reg L	SAA3		
	3) ECM	Fibrillin-1	ECM organization	
	4) wound healing	αSMA	Collagen synthesis	
	5) inflammatory A	CXCL1		
	6) inflammatory B	IL6		
	S100A4-CAF (sCAF) (2 subclusters):			
	1) protein folding	HSPD1, $SPP1^{Low}$, $S100A4^{High}$		
	2) antigen presenting	$SPP1^{High}$, $S100A4^{Low}$	Antigen presentation	

1.6 Cellular Origin of CAFs

The possible sources of CAFs are as diverse as the existing numerous CAF subpopulations may suggest. Cancer-associated fibroblasts can originate from multiple cell types (Figure 3), including tumor-infiltrating bone marrow-derived mesenchymal stem cells (MSCs) (Quante *et al*., 2011, Weber *et al*., 2015; Tan *et al*., 2019), adipose tissue-derived stem cells (Jotzu *et al*., 2011; Miyazaki Y *et al*., 2020), adipocytes (Bochet *et al*., 2013), pericytes (Hosaka *et al*., 2016; Ning *et al*., 2018) endothelial (Zeisberg *et al*., 2007; Yeon *et al*., 2018) and epithelial cells (Iwano *et al*., 2002), which have undergone endothelial-to-mesenchymal (EndMT) and epithelial-to-mesenchymal transition (EMT), respectively. CAF-like cells can also arise from cancer stem cells (CSCs; Nair *et al*., 2017) and hematopoietic stem cells (HSCs; McDonald, *et al*., 2015). Although CAFs can transdifferentiate from the aforementioned and other cell lineages, the general consensus is that their primary source is resident normal fibroblasts, which have become permanently activated (Mueller *et al*., 2007; Arina *et al*., 2016; Sahai *et al*., 2020). This phenotypic switch from a normal fibroblast (NF) into a CAF is triggered mainly by cytokines (such as TNFα and TGFβ1), growth factors, exosomes and other cues released by the tumor cells or the immune system.

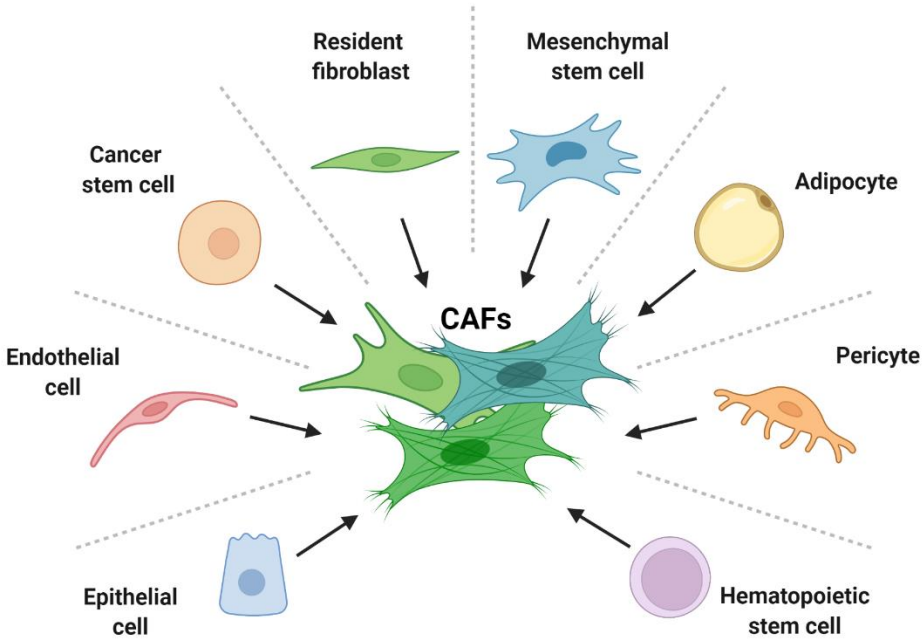

Figure 3. Cellular origin of cancer-associated fibroblasts. CAFs can originate from multiple precursors, such as hematopoietic stem cells, pericytes, adipocytes and mesenchymal stem cells. There is also evidence that they may be the result of epithelial and endothelial cells undergoing EMT and EndMT, respectively. Even cancer stem cells have been shown to be able to give rise to CAFs. The consensus, however, is that the majority of CAFs in the TME are resident fibroblasts, which have been permanently activated. Image created with BioRender.com.

1.7 Activation of Fibroblasts: The Phenotypic Switch

Normal fibroblasts (NFs) can be converted into CAFs with tumor-promoting properties via diverse mechanisms (Figure 4). Microenvironmental triggers such as chronic oxidative stress, characterized by the accumulation of reactive oxygen species (ROS), can induce the NF-to-CAF switch (Toullec *et al*., 2010; Costa *et al*., 2014; Arcucci *et al*., 2016). Persistently elevated ROS levels within the tumor microenvironment lead to chronic inflammation. The ROS act as chemoattractant for the immune cells which are then recruited to the tumor and secrete inflammatory cytokines such as IL-1, TNFα and TGFβ1, all of which can drive the conversion of resident fibroblasts into CAFs (Costa *et al*., 2014). Thus, the inflammatory response can stimulate CAF activation and contribute to tumor progression. Other TME changes that support the generation of CAFs are ECM

stiffening and increase in tissue mechanical force (Calvo *et al*., 2013). Interestingly, in that respect CAFs, as major remodelers of the ECM, can themselves contribute to sustaining their own activation.

Cancer therapies can also stimulate CAF activation or further increase it. For example, chemotherapy-treated breast cancer cells secrete IFNβ1 that can induce an anti-viral inflammatory response signature in patient-derived CAFs and reprogram them to support the recovery and survival of the cancer cells after chemotreatment (Maia *et al*., 2021). Another study has shown that chemotherapy can induce oxidative and metabolic stress, which activates the NF-κB (Nuclear factor kappa-light-chain-enhancer of activated B cells) and STAT3 (Signal transducer and activator of transcription 3) signaling pathways in normal fibroblasts and drives their transformation into IL6-secreting αSMA^{+} CAFs (Peiris-Pagès *et al*., 2015). Radiotherapy can also induce DNA damage and p53 activation in preexisting CAFs and drive them towards a pro-metastatic secretory phenotype, which promotes the survival and spread of colorectal cancer cells (Tommelein *et al*., 2018).

Another interesting mechanism of CAF activation has been studied in *Timp*-deficient mice. TIMPs (tissue inhibitors of metalloproteinases) inhibit the activity of the ECM remodelers MMPs (matrix metalloproteinases) and ADAMs (disintegrin and metalloproteinase domain containing proteins). Loss of *Timp* expression in mouse fibroblasts converts them into CAF-like cells characterized with increased αSMA expression and secretion of ADAM10-rich exosomes, which can enhance the motility of human breast cancer cells (Shimoda *et al*., 2014).

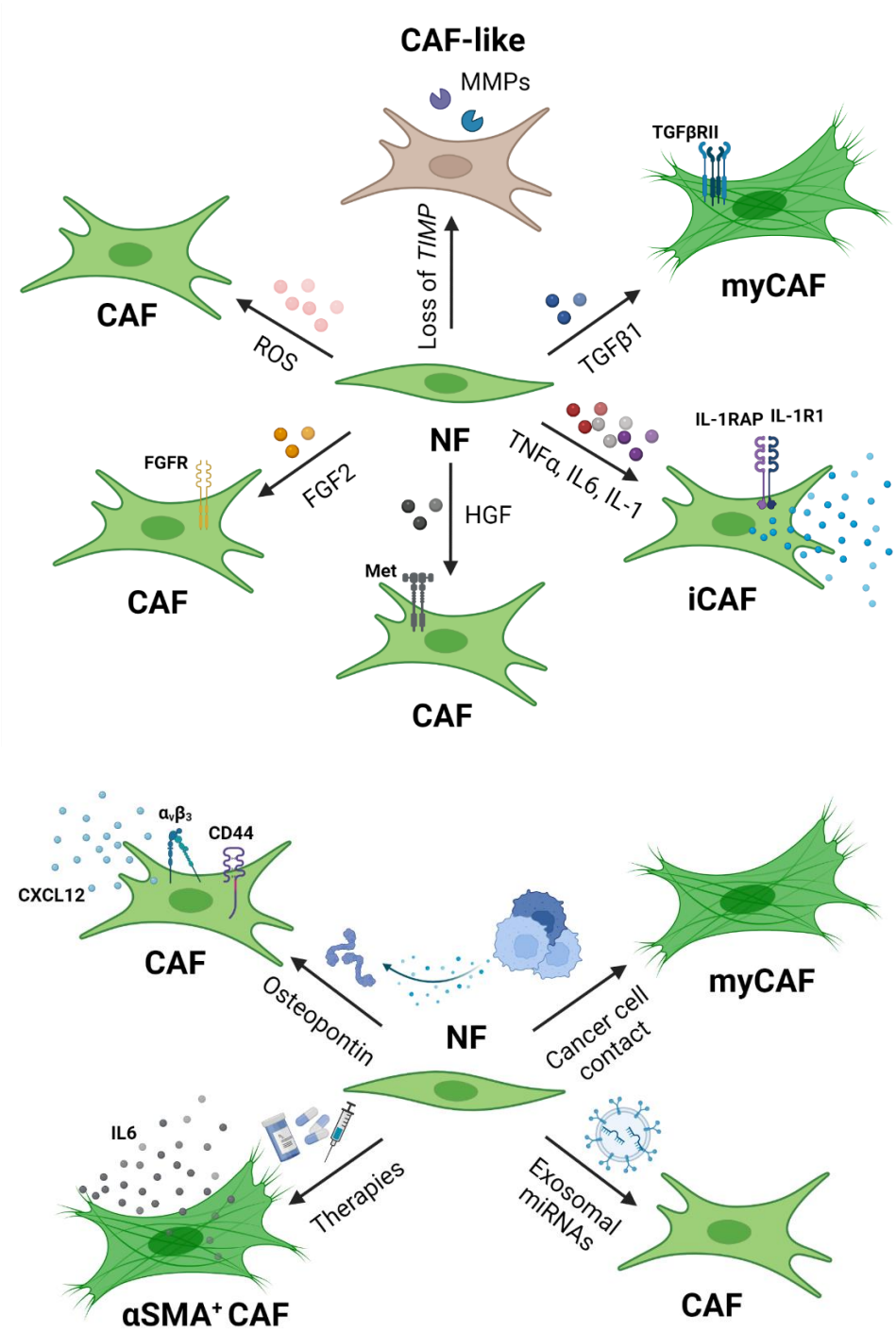

Figure 4. Conversion of normal fibroblasts into CAFs. Normal fibroblasts, resident in the tumor, can give rise to CAFs via various routes. Cytokines, chemokines and growth factors secreted by the cancer cells or immune cells, such as the tumor-associated macrophages (TAMs), can drive the phenotypic switch from a normal fibroblast (NF) into a CAF. Other factors, that the cancer cells secrete to drive this conversion, are exosomal miRNAs and osteopontin. Cancer therapies, reactive oxygen species (ROS), loss of *TIMP* expression and direct contacts with the cancer cells are other factors that can contribute to the NF-CAF conversion. Image created with BioRender.com.

As mentioned, the immune system also plays a role in CAF reprogramming. Immune cell-derived IL-1β, an inducer of the NF-κB pathway, can convert normal skin fibroblasts into pro-inflammatory CAFs with tumor-promoting functions (Erez *et al*., 2010). Tumor-associated macrophages (TAMs), especially the tumor-promoting M2 phenotype, have been shown to secrete factors capable of inducing CAF activation (Comito *et al*., 2014). In a positive feedback loop, the activated CAFs then can drive macrophage M2 polarization, and together support cancer progression, as demonstrated in prostate cancer (Comito *et al*., 2014). Furthermore, macrophages secrete TGFβ1 and TNFα, both of which have been implicated in fibroblast activation (Ueshima *et al*., 2018). Macrophages have also been shown to facilitate the transdifferentiation of MSCs to CAFs (Zhang *et al*., 2019).

Cancer cells themselves can *corrupt* the stroma and *enslave* it to serve their own needs. There is evidence that tumor cells can induce CAF activation by direct contacts with the stroma (Martinez-Outschoorn *et al*., 2010). They can also recruit and activate fibroblasts by secreting growth factors, such as FGF2 (fibroblast growth factor 2; Strutz *et al*., 2000), HGF (hepatocyte growth factor; Wu *et al*., 2013) and TGFβ1 (Lewis *et al*., 2004; Hawinkels *et al*., 2014; Biffi *et al*., 2019). They can also stimulate NF-to-CAF conversion by secretion of the TGFβ1 signaling modulator Wnt7a (Avgustinova *et al*., 2016), the CD44/ $\alpha_v\beta_3$ integrin-ligand osteopontin (Sharon *et al*., 2015; Butti *et al*., 2021) or exosomes loaded with miRNAs, such as the NF-κB activating miR-370-3p (Ren *et al*., 2021). Tumor cell-derived IL6 has also been reported as a promoter of CAF activation (Karakasheva *et al*., 2018). In addition, Lau *et al*. has demonstrated that ovarian metastatic cancer cells secrete TNFα, another activator of the NF-κB pathway, which then stimulates normal omental fibroblasts to acquire CAF characteristics. The stimulated fibroblasts then secrete TGFα and promote peritoneal metastasis by activating the EGFR (epidermal growth factor receptor) pathway in the cancer cells (Lau *et al*., 2017). Squamous cell carcinoma-derived TNFα has been also reported to increase the tumor-promoting potential of already existing CAFs, which then in turn could support cancer invasion (Chaudhry *et al*., 2013). To sum it up, CAF activation is often driven by secreted factors, predominantly, but not limited to, cytokines and growth factors, such as TNFα and TGFβ1, released usually by the

immune or cancer cells, which leads to enhancement of the CAF tumor-promoting activities and ultimately tumor progression.

1.8 The tumor-promoting functions of CAFs

In the previous section, I have briefly mentioned some of the ways in which CAFs support the tumor. Let me now elaborate on it. CAFs share some properties with their most common precursors, the resident normal fibroblasts. Similarly to them, they secrete growth factors, cytokines, chemokines and components of the ECM. A CAF in a sense resembles a wound-healing normal myofibroblast, which is "awaken" upon injury to remodel the ECM and restore tissue integrity (Gabbiani, 2003). However, while NFs go back to their resting state or undergo apoptosis, as soon as the wound has healed and homeostasis has been reestablished (Gabbiani, 2003), CAFs instead persist and continue to assist the tumor. This is fitting, considering that once Dvorak described a tumor as a wound, which does not heal. In 1986, he was among the first to point out the resemblance between the wound-healing process and the generation of the reactive tumor stroma (Dvorak 1986).

Decades later we have come to realize that the functions of CAFs go beyond those of the wound-healing myofibroblasts. CAFs support the tumor in a multitude of ways (Figure 5). Many of the factors, released by the cancer cells to hijack the fibroblasts, are in turn also produced by the CAFs, and can influence disease progression. CAF- derived TGFβ1 has been reported to promote EMT, migration, invasion (Yu *et al*., 2014), and metastasis in breast cancer models (Ren *et al*., 2018) and immune evasion in colon cancer (Tauriello *et al*., 2018). CAF-secreted FGF2 has been shown to increase the proliferation and migration of TNBC cells (Suh *et al*., 2020), while FGF5 has been recently implicated with resistance to HER2-targeted therapies (Fernández-Nogueira *et al*., 2020). CAFs seem to induce breast cancer metastatic potential also via secretion of osteopontin, and inhibition of CAF-derived osteopontin can prevent lung metastasis in a mouse model of breast cancer (Xu *et al*., 2016). CAF-derived but not cancer cell-derived IL6 has been demostrated to promote the progression from DCIS (ductal carcinoma *in situ*) to invasive breast cancer by inducing proliferation and invasion of the DCIS cells (Osuala *et al*., 2015). Moreover, luminal A breast

cancer MCF7 cells were able to form tumors in mice when coinjected with CAFs secreting high levels of IL6, but not when coinjected with IL6-low CAFs, demostrating that CAF-secreted IL6 could promote breast cancer growth and invasion *in vivo* (Studebaker *et al*., 2008).

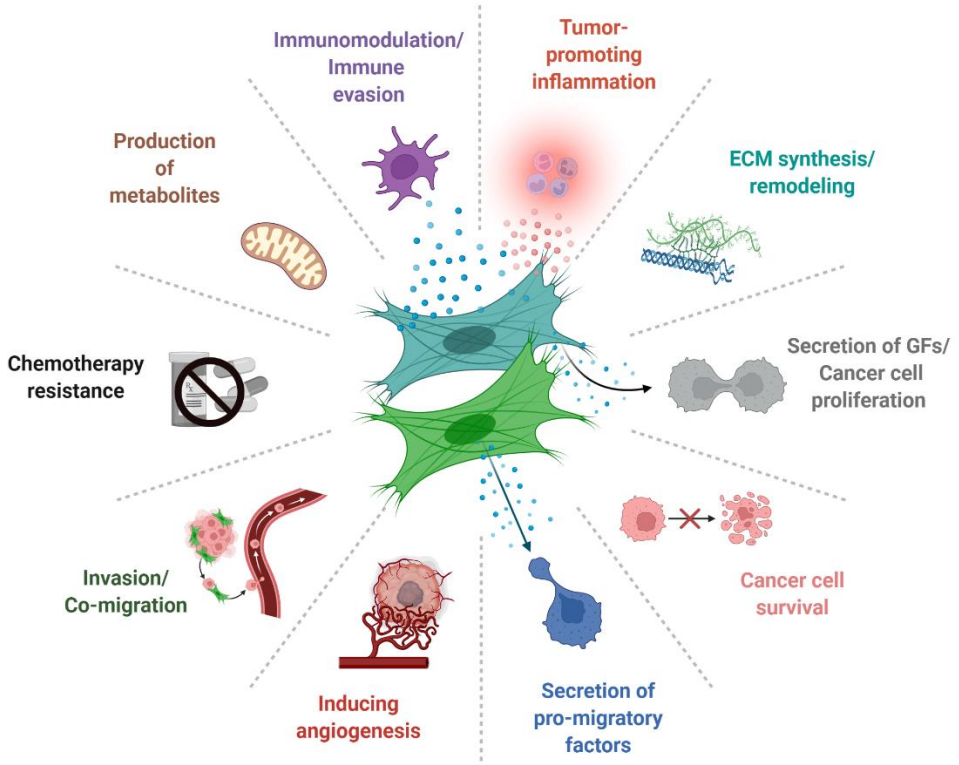

Figure 5. The tumor-supportive functions of CAFs. The cancer-associated fibroblasts can influence almost every hallmark of cancer and support tumor development and progression. They can modulate the immune system and contribute to the development of immunosuppressive TME. Thus, they can help the tumor escape the immune response (immune evasion). CAFs, as mesenchymal cells with enhanced secretory phenotype, can support the tumor cells via secretion of metabolites, tumor-promoting inflammatory cytokines, and growth factors. CAF-secreted proteins and/or exosomes have been shown to promote angiogenesis, tumor cell proliferation, migration and invasion. These tumor allies have been observed at the leading edge of the tumor invasion front, where they can remodel the ECM and make it easier for the cancer cells to migrate. Certain CAF subpopulations have also been demonstrated to support cancer cell survival and the development of chemoresistance, as well as resistance to other anti-cancer therapies. Image created with BioRender.com.

CAFs can also support tumor growth by producing and releasing metabolites, such as amino acids (Bertero *et al*., 2019), lactate and pyruvate (Becker *et al*., 2020). They can achieve this also by inducing angiogenesis, the formation of new blood vessels, via secretion of angiogenic mediators, such as VEGF (vascular endothelial growth factor; De Francesco et al., 2013) and Chitinase 3-like 1 (Watanabe *et al*., 2022). This is particularly important for the cancer cell survival in the otherwise nutrient-deprived TME (Olivares, *et al*., 2017).

Another way CAFs support tumor progression is by suppressing the anti-tumor immune response and promoting immune escape (Barrett and Puré, 2020; Mhaidly and Mechta-Grigoriou, 2021). The aforementioned dense and rigid ECM, resulting from the CAF deposition of fibronectin, laminins, and collagens serves as a barrier that limits the access of both drugs and immune cells to the tumor (Salmon *et al*., 2014). CAFs contribute to the creation of an immunosuppressive TME also by secreting immunosuppressive factors, such as TGFβ1 (Flavell *et al*., 2010; Mariathasan *et al*., 2018; Tauriello *et al*., 2018), IL10 (Mhaidly and Mechta-Grigoriou, 2021) and CCXL12 (Ene-Obong *et al*., 2013; Feig *et al*., 2013), and by recruiting immune cells with immunosuppressive functions (Yang *et al*., 2016; Kumar *et al*., 2017). For example, CAFs have been shown to recruit monocytes and induce their differentiation into immunosuppressive M2 macrophages in prostate (Comito *et al*., 2014) and breast cancer (Gok Yavuz *et al*., 2019). Moreover, Cheng *et al*. has demonstrated that CAFs, derived from hepatocellular carcinoma (HCC), can also recruit and activate neutrophils by secreting CXCL12, also known as SDF1a (stromal cell-derived factor 1a), and IL6, respectively (Cheng *et al*., 2018). The CAF-secreted IL6 then induces JAK/STAT3 signaling in the neutrophils, which results in their expression of PDL1. The PD-L1+ neutrophils can then inhibit the anti-tumor activity of T cells via the PD-1/PD-L1 pathway (Cheng *et al.*, 2018), a process described as T cell exclusion. To summarize, CAFs are major modulators of the anti-cancer immune response, and, as such, may be responsible for failure of targeted cancer immunotherapies. There are also indications that CAFs support angiogenesis, cancer cell migration, proliferation, survival, and metastasis.

1.8.1 Role of Cancer-Associated Fibroblasts in Metastasis

In Greek, *metastasis (μετάστασις)* means removal or migration, dislocation (Retsas, 2017). This term is used to describe the dissemination of cancer cells from the primary tumor to distant organs. Since metastasis is the main reason for recurrence and mortality in Luminal A breast cancer, and in solid tumors in general (Dillekås *et al*., 2019), it is important to explore how CAFs contribute to this process.

As the main producer of ECM components, CAFs can remodel the ECM in such a way that ECM tracks are generated for the migrating cancer cells. In this way, the CAFs ultimately supports tumor invasion and metastasis. For the formation of the invasive tracks CAFs rely on MMPs which degrade the rigid ECM where a path is needed (Li *et al*., 2016). The CAFs then can lead at the invasive front with the cancer cells following within the tracks left behind by the CAFs, a process described as fibroblast-led collective invasion (Gaggioli *et al*., 2007; Neri *et al*., 2015). When MMP inhibitors are used, the CAF-led invasion is prevented (Li *et al*., 2016). In addition to MMP-mediated ECM degradation, the CAFs seem to also require Rho-ROCK activity to exert the necessary force on the ECM, since Rho- or ROCK inhibitors can diminish CAF-led invasion (Gaggioli *et al*., 2007; Neri *et al*., 2015).

ECM degradation is essential for the creation of invasive tracks, and yet surprisingly, seemingly the opposite appears to be also important for metastasis. Matrix stiffness, which is also controlled by CAFs, e.g., by collagen deposition and crosslinking, has been shown to correlate with invasion in breast (Acerbi *et al*., 2015) and colorectal cancer (Bauer *et al*., 2020). Acerbi *et al*. has discovered that the more aggressive Basal-like and HER2 breast cancer subtypes have stiffer stroma than the less aggressive Luminal A and B subtypes (Acerbi *et al*., 2015). The stiffer the matrix, the higher the invasion capacity. In fact, the tumor matrix is estimated to be 1.5 times stiffer than normal ECM (Voutouri *et al*., 2014). Matrix stiffness matters because it promotes the formation of invadosomes (Kai *et al*., 2016), a collective term for podosomes and invapodopia, actin-rich protrusions formed at the leading edge of migrating cell. Invadosomes secrete ECM-degrading MMPs, and thus facilitate cell invasion (Linder et al., 2011).

Matrix stiffness can support metastasis also by inducing EMT in the cancer cells (Wei *et al*., 2015; Dong *et al*., 2019). In addition to ECM remodeling and degradation, EMT is another step leading to enhanced migratory capacity and invasion. EMT is characterized by the downregulation of epithelial and the upregulation of mesenchymal markers in the epithelial cancer cells, a process controlled by the EMT transcription factors from the TWIST, ZEB and SNAIL/SLUG families (Zhang and Weinberg, 2018). For example, during EMT of the cancer cells, the epithelial marker and tumor-suppressor E-cadherin is downregulated, its expression is lost entirely, or its adhesive activity is reduced, all of which may lead to loss of cell-to-cell adhesion and allow the cancer cells to dissociate from the main tumor mass and migrate (Mendonsa *et al*., 2018; Na *et al*., 2020). As mentioned already, CAF-secreted factors, such as TGFβ1, can promote EMT of the tumor cells (Yu *et al*., 2014). Another example is CAF-derived IL6 which has been implicated in EMT and migration in several cancer entities, including gastric cancer (Wu *et al*., 2017), esophageal adenocarcinoma (Ebbing *et al*., 2019), and bladder cancer (Goulet *et al*., 2019).

1.8.2 Role of CAFs in Autophagy and Therapy Resistance

Another cellular process worth exploring, because of its connection to metastasis, is autophagy (Babaei et al., 2021). From Greek, it means *self-eating* or *self-devouring*. The cell utilizes autophagy, or self-degradation, usually to eliminate misfolded proteins or damaged organelles. Autophagy allows for recycling of cellular components, which are engulfed inside an intracellular membrane vesicle (autophagosome) and transported to the lysosome for degradation and reuse. This could be of particular importance during nutrient deprivation or metabolic stress, when, to survive, the cell uses autophagy to provide itself with energy sources (Levine and Klionsky, 2004; Mathew *et al*., 2007). In the context of cancer and metastasis, autophagy is a double-edge sword. At the initial stages of metastasis, autophagy can be tumor-suppressive and inhibit dissemination. At the advanced stages, however, it can promote metastasis by allowing cancer cells to overcome environmental stresses such as hypoxia, metabolic and oxidative stress (Babaei *et al*., 2021; Rakesh *et al*., 2022).

Studies have associated autophagy with MDR (multidrug resistance) development, a phenomenon that usually occurs after a prolonged use of chemotherapy (Li YJ *et al*., 2017). MDR means that the tumor cells have lost chemosensitivity and are not affected by the chemotherapy anymore. Thus, MDR leads to refractory cancer and relapse. In in *vitro* and in *vivo* models of cancer, the use of pharmacological or genetic inhibition of autophagy has been shown to increase chemosensitivity and prevent tumor recurrence (Levy JM *et al*., 2014; Levy JMM *et al*., 2017; Chen M *et al*., 2021).

CAFs themselves may contribute to cancer cell survival during therapy and allow for subsequent relapse by inducing autophagy. Wang *et al*. have provided *in vitro* and *in vivo* evidence for the involvement of CAFs in radiotherapy resistance (Wang *et al*., 2017). They showed that CAFs secreted IGF1/2, CXCL12 and β-hydroxybutyrate, which were able to enhance autophagy in irradiated cancer cells. The autophagy had a protective effect against the radiation-induced DNA damage and allowed for tumor regrowth post radiation. An autophagy inhibitor and an anti-IGF2 neutralization antibody were able to prevent the CAF-promoted tumor relapse after radiotherapy (Wang *et al*., 2017).

Furthermore, a recent study has demonstrated that $GPR30^+$ CAFs can induce autophagy in ER^+ breast cancer cells and promote their resistance to tamoxifen (Liu *et al*., 2021). Tamoxifen treatment activated the G-protein coupled estrogen receptor (GPR30) in patient-derived CAFs, which led to the upregulation and secretion of high mobility group box 1 (HMGB1). The CAF-secreted HMGB1 then could induce autophagy and tamoxifen resistance in MCF7 luminal A breast cancer cells (Liu *et al*., 2021).

In addition to inducing drug resistance by supporting autophagy, CAFs also support the recovery of cancer cells after chemo- and radiotherapy (Boelens *et al*., 2014 ;Wang *et al*., 2017; Maia *et al*., 2021), likely not only by promoting the development of drug-resistant cells but also by supporting the survival of persistent and stem-like cancer cells (Su *et al*., 2018; Shen *et al*., 2020) . In addition, CAFs can reduce treatment efficacy by blocking drug transport to the tumor. They achieve this by producing a dense ECM which functions as a protective wall shielding the cancer cells and hindering drug delivery (Henke *et al*., 2020). Furthermore, CAFs secrete hyaluronan, a polysaccharide, that at elevated levels

causes high interstitial fluid pressure leading to compression and collapse of the blood vessels and hypoperfusion, which subsequently impedes with drug delivery (Jacobetz *et al*., 2013; Domen *et al*., 2021).

To sum up, upon their activation, the cancer-associated fibroblasts secrete factors which may contribute to cancer progression by promoting tumor-supportive processes such as migration, metastasis, autophagy, and drug resistance. Therefore, future anti-cancer therapies may target the CAFs and the factors they secrete in order to block the CAF-cancer crosstalk and prevent future tumor relapse. Before this is possible, despite the decades of CAF research, there is still a dire need to better understand the complexity of tumor-CAF communication by identifying novel CAF-derived factors and studying their multifaceted effects on cancer. This leads us to the aims of this PhD work.

2. STUDY AIMS

Breast cancer is a leading cause of cancer-related death in women world-wide. It is a heterogeneous disease with multiple subtypes. The most common subtype is Luminal A. Although this subtype is characterized with a relatively good prognosis and Luminal A patients respond rather well to standard endocrine therapies, years later refractory relapse may occur. There are indications in literature that the cancer-associated fibroblasts (CAFs), a major component of the tumor-microenvironment (TME) may be contributing to this, but the exact mechanisms are still under investigation. To be able to design drugs that target or even better prevent Luminal A relapse, looking deeper into what role the CAFs play in Luminal A progression is of utmost importance.

To this end, I worked with Luminal A-derived CAFs, both primary and immortalized, and with the classical in *vitro* models of the same breast cancer subtype, namely the MCF7 and T47D cell lines. The overall goal of my PhD thesis was to identify novel CAF-secreted factors which promote Luminal A breast cancer progression. As phenotypic assays, indicative of tumor progression, I investigated cancer cell migration, autophagy, and recovery after chemotherapy. CAFs are known to be derived from normal tumor resident or recruited fibroblasts, when the latter are activated by tumor- or TME-derived factors, such as the cytokines TNFα and TGFβ1. Therefore, the focus of my work was three-fold:

a) Luminal A-derived fibroblasts, from now on often referred to as CAFs, were stimulated with TNFα and TGFβ1 and the effect of the stimulation on the CAF secretome and full proteome was studied via HPLC-Mass Spectrometry.
b) The effect of the CAF CM, both before and after the cytokine-stimulation, on the MCF7 and/or T47D migratory phenotype, autophagy and ability to recover after chemotherapy was investigated.
c) Signaling pathways and transcription factors activated in the MCF7 cell in response to the CAF CM (CM from cytokine-stimulated versus unstimulated CAFs) was also investigated. For this purpose, RNA-Seq data-based computational tools, such as GSEA (Gene set enrichment analysis), PROGENy (Pathway RespOnsive GENes for activity inference) and DoRothEA (Discriminant Regulon Expression Analysis) were used.

In addition, various other protein expression assays, such as Western Blotting, ELISA/FLISA and RPPA (Reverse Phase Protein Array), and gene expression assays, such as RT-qPCR, were also utilized for further characterization and/or validation of the OMICS data. The goal was to better understand the complex CAF-Luminal A crosstalk. In the future, such understanding could be crucial for the development of new anti-cancer drugs for the treatment and/or prevention of refractory Luminal A breast cancer.

3. MATERIAL AND METHODS

3.1 Materials

3.1.1 Consumables

Article	Company
6-well companion plate	FALCON®.
6-well cell culture plate	Greiner Bio-One GmbH
6-well cell culture inserts 0.4 µm pore size, translucent PET membrane	FALCON®.
8er PCR-Strip (0.2 ml, Art. 968-888B)	Steinbrenner Laborsysteme GmbH
12-Well cell culture plate	Corning
96-Deep-well plates	Thermo Fisher Scientific
96-Well cell culture microplate µClear®, black, Cellstar®	Greiner Bio-One GmbH
96-Well cell culture plate Cellstar® (clear)	Greiner Bio-One GmbH
96-Well cell culture microplate Cellstar®, white, chimney well	Greiner Bio-One GmbH
96-Well High-binding FLISA microplate µClear® (black)	Greiner Bio-One GmbH
Amicon® Ultra-15 3K Centrifugal Filter Devices (Cat No UFC900324)	Merck Millipore
Amicon® Ultra-15 50K Centrifugal Filter Devices (Cat No UFC905024)	Merck Millipore
Cell culture flasks Cellstar ($25cm^2$, $75cm^2$, $150cm^2$)	Greiner Bio-One GmbH
Cell scrapers and spatulas	TPP Techno Plastic Products AG
Combitips Advanced (0.1 ml)	Eppendorf AG
Conical Tubes (15 ml and 50 ml) Falcon®	BD Falcon
Disposable Filter Tips for Micropipettes NEPTUNE (10-1000 µl)	Neptune Scientific
Disposable Filter Tips for Micropipettes TipOne®	Starlab
Disposable No-filter Tips for Micropipettes Kisker (10-1000 µl)	Steinbrenner Laborsysteme GmbH
Eppendorf tubes (1.5 ml, 2ml, 5ml)	Eppendorf AG
Liquidator96 tips	Steinbrenner Laborsysteme GmbH
MicroAmp® Optical 384-Well Reaction Plate with Barcode	Applied Biosystems
Multipette® Combitips	Eppendorf AG
Nitrocellulose-coated glass slides	Oncyte Avid, Grace-Biolabs
Optically clear Adhesive Seal Sheets (Cat No AB-1170)	Thermo Fisher Scientific
Serological Pipettes (5 ml, 10 ml, 25 ml, 50 ml)	Becton Dickinson
TPP® Petri dishes (10 Ø cm, 20 Ø cm)	TPP Techno Plastic Products AG
TPP® tissue culture flasks ($25\ cm^2$, $75\ cm^2$)	TPP Techno Plastic Products AG
Trans-Blot® Turbo™ Mini-size Transfer Stacks	Bio-Rad Laboratories
Wilhem Ulbrich™ (WU Mainz) Pasteur Capillary Pipettes, Long size (230 mm)	Thermo Fisher Scientific

3.1.2 Laboratory equipment

Equipment	Company
AB184-A3 High Precision Scale	Mettler Toledo
BP 4100S scale	Sartorius
Bacterial incubator (37°C)	Memmert
Biofuge Fresco benchtop centrifuge	Heraeus
BLAUBRAND® Neubauer counting chamber	Brand GmbH & CO KG
DigestPro MSi robotic system	INTAVIS Bioanalytical Instruments
EcoTemp TW8 Waterbath	JULABO GmbH
Fluorescence Microscope ImageXpress® Micro	Molecular Devices
Freezer (-20°C)	Bosch
Freezer (-80°C)	Sanyo Denki Germany GmbH, Eppendorf GmbH
Fridge (4°C)	Liebherr
GloMax® Discover Microplate Reader	Promega
Heraeus® BBD6220 CO_2 Incubator (cell culture incubator)	Thermo Fisher Scientific
Heraeus Multifuge 4 KR	Thermo Fisher Scientific
Heraeus Varifuge 3.0R Refrigerated Centrifuge	Heraeus
Infrared Odyssey scanner	LI-COR Biosciences GmbH
Light Microscope	Hund Wetzlar GmbH
Light Microscope Zeiss Axiovert 25	Carl Zeiss AG
Liquidator96	Steinbrenner Laborsysteme GmbH
Micropipettes PIPETMAN Classic (P2, P10, P20, P200, P1000)	Gilson
Mini-Protean® Tetra-System	Bio-Rad Laboratory
Multichannel Pipet Tranferpette® S-12 (20-200µl)	Brand GmbH & CO KG
Multipette® Plus Pipet	Eppendorf AG
NanoDrop™ spectrophotometer	Thermo Fisher Scientific
NeoLab-Rotator 2-1175/2-1177	neoLab
Pipetboy acu	Integra Biosciences
Q-Exactive-HF-X mass spectrometer	Thermo Fisher Scientific
QuantStudio™ 3D Digital PCR System	Applied Biosystems
RM 5 V-30 CAT roller mixer	Ingenieurbüro CAT
Safe 2020 Safety Cabinet (cell culture hood)	Thermo Fisher Scientific
Scanner	EPSON
ST 5 CAT rocking shaker	Ingenieurbüro CAT
Super-speed Bench-top Centrifuge 4K15 Sigma	Thermo Fisher Scientific
TapeStation 3.2	Agilent Technologies
Thermocycler GeneAmp® PCR System 9700	Applied Biosystems
Thermomixer comfort, 1.5 mL	Eppendorf AG
Trans-Blot® Turbo™ Transfer System	Bio-Rad Laboratories
VACUBOY® aspiration system	INTEGRA Biosciences
Vortex mixer Vortex-Genie 2	Scientific industries

3.1.3 Reagents

Reagent	Company
2x qPCR-Probe-MasterMix-low-ROX (SL-9813-smp)	Steinbrenner Laborsysteme GmbH
Bafilomycin A1 (J61835.MX)	VWR
Blocking buffer for Fluorescent Western Blocking	Rockland Antibodies & Assays
Bovine Serum Albumin (BSA)	Roche
CellTracker™ Green CMFDA Dye	Thermo Fisher Scientific
Chloroform	Sigma-Aldrich
Collagenase A	Roche
cOmplete Mini Protease Inhibitor Cocktail	Roche
Crystal violet	Sigma-Aldrich
Dimethyl sulfoxide (DMSO)	Sigma-Aldrich
Epirubicin HCl	Biomol GmbH
Ethanol, 100 %	VWR Chemicals
Gibco® 0.25 % Trypsin (EDTA) Solution	Thermo Fisher Scientific
Gibco® DMEM/F12	Thermo Fisher Scientific
Gibco® DPBS	Thermo Fisher Scientific
Gibco® FCS	Thermo Fisher Scientific
Gibco™ Opti-MEM	Thermo Fisher Scientific
Gibco® Penicillin/Streptomycin (P/S)	Thermo Fisher Scientific
Hoechst staining 33342 (Cat No 62249)	Thermo Fisher Scientific
Lipofectamine™ RNAiMAX Transfection Reagent	Invitrogen, Thermo Fisher Scientific
Methanol	Sigma-Aldrich
Mini-PROTEAN TGX Gels	Bio-Rad Laboratories
non-DEPC treated nuclease-free water Ambion®	Thermo Fisher Scientific
Paclitaxel	Biomol GmbH
PhosStop™ Phosphatase Inhibitor Cocktail	Roche
Pierce™ RIPA lysis buffer	Thermo Fisher Scientific
Protein ladder Precision Plus Protein™ Dual Color Standards	Bio-Rad Laboratories
Puromycin	Thermo Fisher Scientific
QIAzol™ lysis reagent	QIAGEN
RNase-free DNase Set (50)	QIAGEN
Roti-Load 1, Protein loading buffer (4x, reducing)	Carl Roth GmbH + Co. KG
Sodium Fluoride (NaF)	Sigma-Aldrich
Sodium orthovanadate (Na_3VO_4)	Sigma-Aldrich
Stop solution 2N Sulfuric Acid (DY994)	R&D Systems
Substrate reagent pack (ELISA, DY999)	R&D Systems
Torin 1 (T6045-1mL-TM)	BIOCAT
Triton X-100	Sigma-Aldrich
Tween®20	Sigma-Aldrich
Universal Probe Library (UPL) Probes	Roche

3.1.4 Solutions

Blocking buffer (ELISA, FLISA)	**DPBS with 1% BSA**
Blocking Buffer (RPPA)	Rockland blocking buffer+TBS (1:1) 10 mM NaF 1 mM Na3VO4
Blocking Buffer (WB)	Rockland blocking buffer+TBS (1:1) 5mM NaF 1mM Na_3VO_4
FCF stain (RPPA)	0.005% FCF 30% absolute EtOH 10% acetic acid in Milli-Q H_2O
Printing Buffer (RPPA)	10% glycerol 4% SDS 10 mM DTT 125 mM Tris–HCl pH 6.8
Protein Lysis Buffer	RIPA lysis buffer 1x Complete Mini Protease Inhibitor Cocktail 1x PhosSTOP Phosphatase Inhibitor Cocktail 1 mM Na_3VO_4 10 mM NaF.
10x TBS	1.5 M NaCl, 200mM Tris base, pH 7.6
1X TBST	0.1% Tween 20 in 1x TBS
10x SDS Running Buffer (WB)	1.92 M Glycine 250 mM Tris base 0.1% SDS
Washing Buffer (ELISA)	DPBS with 0.25% Tween 20
Transfer Buffer (WB)	20% Trans-BlotR Turbo™ 5x Transfer Buffer 20% EtOH 60% Milli-Q H2O

3.1.5 Kits

Product kit	Company	Cat #
miRNeasy Mini Kit	QIAGEN	217084
Pierce™ BCA protein Assay kit	Thermo Fisher Scientific	23227
RevertAid H Minus First Strand cDNA Synthesis kit	Thermo Fisher Scientific	K1631
Human IFN-beta DuoSet ELISA	R&D Systems	DY814-05
Nano-Glo® HiBiT Lytic Detection System	Promega	N3030
Trans-Blot® Turbo™ RTA Transfer PVDF Kit	Bio-Rad Laboratories	1704273

3.1.6. Human Recombinant Proteins

Recombinant Protein	Company	Cat #
IFNβ1	PeproTech	300-02BC
IL6	R&D Systems	206-IL
TGFβ1	PeproTech	100-21C
TNFα	PeproTech	300-01A

3.1.7 Antibodies

3.1.7.1 Neutralization Antibodies

NAb (human anti-)	Company	Cat #
IFNβ1	R&D Systems	AF814
IL6	R&D Systems	MAB206
TNFα	R&D Systems	MAB610-100

3.1.7.2 Antibodies used for FLISA

Antibody	Company	Cat #	Concentration/Dilution
Human IL6 Ab (Capture)	R&D Systems	MAB206	4 µg/mL
Human IL6 Biotinylated Ab (Detection)	R&D Systems	BAF206	0.2 µg/mL
Streptavidin AlexaFluor™-680	Invitrogen	S32358	1:5000

3.1.7.3 Antibodies used for Western Blot

Primary antibodies	Host	Company	Cat #	Dilution
αSMA	mouse	Abcam	ab7817	1:300
E-cadherin	mouse	Abcam	ab1416	1:50
Fibronectin	rabbit	Abcam	ab2413	1:1000
GAPDH	rabbit	Cell Signaling Technology	CST2118	1:1000
Laminin 5 (γ2 chain)	mouse	Merck Millipore	MAB19562	1:200
STAT1	rabbit	Cell Signaling Technology	CST9175	1:1000
pSTAT1(Y701)	mouse	BD Biosciences	BD 612232	1:500
STAT3	mouse	Cell Signaling Technology	CST4904	1:1000
pSTAT3(Y705)	rabbit	Cell Signaling Technology	CST9131	1:1000
Secondary antibodies	**Host**	**Company**	**Cat #**	**Dilution**
Anti-mouse Dylight 680	goat	Invitrogen	35518	1:10000
Anti-mouse Dylight 800	goat	Invitrogen	SA535521	1:10000
Anti-rabbit Dylight 680	goat	Invitrogen	35568	1:10000
Anti-rabbit Dylight 800	goat	Invitrogen	SA535571	1:10000

3.1.7.4 Antibodies used for RPPA

Protein target	Ab cat#	Protein target	Ab cat#	Protein target	Ab cat#
pak1	CST 2602	Phospho-S6 Ribosomal Protein_Ser235-236_D57-2-2E_XP	CST 4858	CREB _48H2	CST 9197
pak2	ab76293	S6 Ribosomal Protein_5G10	CST 2217	IkappaB-alpha	CST 9242
Phospho-FAK_Tyr397	CST 3283	Phospho-p70 S6 Kinase_Thr389_108D2	CST 9234	MEK4	ab 33912
Vimentin	CST 3932	Dishevelled 3_EP1991Y	ab 76081	phospho_Met	CST3129
CSNK1A1	CST_2655	Phospho-Stat3_Tyr705	CST 9131	Integrin beta 4	CST4707
CSNK1E	CST_12448	Phospho-c-Raf_Ser259	CST 9421	rhoa	CST 2117
EGFR	CST 2232	Phospho-PKCalpha_Ser657	Millipore 06-822	Rac1-2-3	CST 2465
beta-Catenin	CST 9562	P44/42	CST9102	E-cad	CST3195
FAK	CST 3285	pSMAD2	CST 3108	Integrin beta 1 (CD29)	CST4706
Phospho-beta-Catenin_Ser675	CST 9567	pSMAD3	CST 9520	Integrin alpha 6 (CD49f)	CST3750
Smad3_C67H9	CST 9523	CTNNBIP1_EPR6697_2	ab 129011	LaminA_C	CST 2032
LRP5_D80F2	CST 5731	Wnt16	ab 109437	SNAIL_SLUG	ab 63371
ERBB2	MS-730 neu Ab-17	Axin1_C7B12	CST 3323	Fibronectin	ab32419
c-Jun_60A8	CST 9165	Notch2_D67C8_XP	CST 4530	Stat3	BD 610189
c-Myc	ab32072	Jagged1_28H8	CST 2620	MEK1	BD 610122
Frizzled 6_EPR7279	ab 128916	Jagged2_C23D2	CST 2210	Ras, clone RAS10	Millipore 05-516
Phospho-p44/42 MAPK_ERK1-2_Thr202-Tyr204	CST 4370	Nicastrin	CST 5665	Met_L41G3	CST 3148
Phospho-MAP Kinase Kinase 1-2_MEK1-2_phosphoserine 217-220	CST 9154	Lunatic Fringe_D6V2V	CST66472	casein kinase IIbeta_6D5 (CSNK2B)	sc 12739
IKKß_D30C6	CST8943	Phospho-EGF Receptor_Tyr1086	CST 2220	Smad4	Millipore MAB1132
Phospho-Akt_Ser473	CST 9271	Phospho-HER2-ErbB2_Tyr1221-1222_6B12	CST 2243	DKK1_4D4	WH0022943M1
PI3 Kinase p110 beta_Y384	ab 32569	HER3_ErbB3_D22C5_XP	CST 12708	Smad2_L16D3	CST 3103
PI3 Kinase p85 alpha_ep380y	ab 40755	Phospho-HER3-ErbB3_Tyr1289_21D3	CST 4791	cyclin D1_M-20	CST 2926
TACE_D22H4	CST 6978	ErbB4	ab76303	JNK1_2C6	CST3708
GSK-3beta_27C10	CST 9315	HER4_ErbB4 Phospho_pY1284	CST 4757	IKKa_3G12	CST11930
PKCdelta_D10E2	CST 9616	Phospho-Src Family_Tyr416	CST 2101	Snail	CST 3895
Phospho-PKCalpha-beta II_Thr638-641	CST 9375	Src_32G6	CST 2123	CD44	CST5640
Phospho-NF-kappaB p65_Ser536_93H1	CST 3033	Smad2 (D43B4)	CST5339	AKT	CST 9272
p70 S6 Kinase_49D7	CST 2708				

3.1.8 Primers

Target gene	Forward primer (5' → 3')	Reverse primer (5' → 3')	UPL Probe #
ACTB	CCAACCGCGAGAAGATGA	CCAGAGGCGTACAGGGATAG	64
CDH1	CCCGGGACAACGTTTATTAC	GCTGGCTCAAGTCAAAGTCC	35
DDX58	ATGTGGGCAATGTCATCAAA	AAGCACTTGCTACCTCTTGCTC	13
FN1	GGGAGAATAAGCTGTACCATCG	TCCATTACCAAGACACACACACT	25
GAPDH	AGCCACATCGCTCAGACAC	GCCCAATACGACCAAATCC	60
IFIH1	TTTTGCAGATTCTTCTGTAGTTTCA	TGCTGTTATGTCCAAGACTTTCA	29
IFNAR1	TGACCAGAAATGAACTGTGTCAA	GACCTCAGGCTCCCAGTGTA	18
IFNB1	TTGCTCTGGCACAACAGGTA	TGGAGAAGCACAACAGGAGA	25
ISG15	GAGGCAGCGAACTCATCTTT	AGCATCTTCACCGTCAGGTC	76
LAMC2	CTACTTCGGGGACCCATTG	GGTTACAGTTGCAAGCTCGAC	3
MMP1	GCTAACCTTTGATGCTATAACTACGA	TTTGTGCGCATGTAGAATCTG	7
MMP13	CCAGTCTCCGAGGAGAAACA	AAAAACAGCTCCGCATCAAC	73
MMP2	ATAACCTGGATGCCGTCGT	AGGCACCCTTGAAGAAGTAGC	70
MMP3	CCAGGTGTGGAGTTCCTGAT	CATCTTTTGGCAAATCTGGTG	72
MMP9	GAACCAATCTCACCGACAGG	GCCACCCGAGTGTAACCATA	6
RELA	CGGGATGGCTTCTATGAGG	CTCCAGGTCCCGCTTCTT	48
SNAI1	TACAGCGAGCTGCAGGACT	ATCTCCGGAGGTGGGATG	11
SNAI2	TGGTTGCTTCAAGGACACAT	AATGCTCCATGGGGATGA	7
STAT1	ACTTCAGCAGCTTGACTCAAAA	ATCATTGGCAGCGTGCTC	1
STAT2	TTTGGGACTTTGGTTACCTGA	AGTTCCTCTGTCACACCTAGTGG	22
STAT3	CTCTGCCGGAGAAACAGG	CTGTCACTGTAGAGCTGATGGAG	1
TNF	CAGCCTCTTCTCCTTCCTGAT	GCCAGAGGGCTGATTAGAGA	29
TWIST1	AGCTACGCCTTCTCGGTCT	CCTTCTCTGGAAACAATGACATC	58
OAS1	GGTGGAGTTCGATGTGCTG	AGGTTTATAGCCGCCAGTCA	37

3.1.9 siRNAs

siRNA	Sequence	Company	Cat#
si*LAMC2* #2	#2: GCAGGUGUUUGAAGUGUAU	Dharmacon	J-012119-06
si*LAMC2* #3	#3: GGGUGGUGAUGGAGUAGUA	Dharmacon	J-012119-07
si*LAMC2*	Pool of several siRNA against *LAMC2*	siTOOLs Biotech	n/a
si*IFNAR1*	#1: GCGAAAGUCUUCUUGAGAU #2: UGAAACCACUGACUGUAUA #3: GAAAAUUGGUGUCUAUAGU #4: GAAGAUAAGGCAAUAGUGA	Dharmacon	J-020209-05 J-020209-06 J-020209-07 J-020209-08
si*RELA*	Pool of four siRNAs	Dharmacon	D-003533-04 D-003533-05 D-003533-06 D-003533-18
si*STAT1*	#1: GCACGAUGGGCUCAGCUUU #2: CUACGAACAUGACCCUAUC #3: GAACCUGACUUCCAUGCGG #4: AGAAAGAGCUUGACAGUAA	Dharmacon	J-003543-06 J-003543-07 J-003543-08 J-003543-09
si*STAT2*	#1: GGACUGAGUUGCCUGGUUA #2: GGACUGAGGAUCCAUUAUU #3: GACCCCUCCUGGCAAGUUA #4: GAUUUGCCCUGUGAUCUGA	Dharmacon	J-012064-05 J-012064-06 J-012064-07 J-012064-08
si*STAT3*	Pool of four siRNAs	Dharmacon	J-003544-07 J-003544-08 J-003544-09 J-003544-10
siCTRL (ON-TARGET plus)	#1: UGGUUUACAUGUCGACUAA #2: UGGUUUACAUGUUGUGUGA #3: UGGUUUACAUGUUUUCUGA #4: UGGUUUACAUGUUUUCCUA	Dharmacon	D-001810-10
siCTRL1	Pool of several non-targeting siRNAS	siTOOLs Biotech	n/a
siCTRL2	Pool of several non-targeting siRNAS	siTOOLs Biotech	n/a

3.1.10 Software.

Software/database	Version/URL
MaxQuant	ver. 1.6.3.3
Perseus	ver. 1.6.7.0
GraphPad Prism	ver. 9.3.1
GenePixPro	ver. 7.2.22
Image Studio Lite software	ver. 5.2
STAR	ver. 2.3.0e
featureCounts	ver. 1.5.1
Morpheus software	https://software.broadinstitute.org/morpheus
Heatmapper	http://www.heatmapper.ca
HTSeq count	ver. 0.6.0
R	ver. 3.5.3 (RPPA analysis) ver. 4.0.3 (RNA-seq analysis by Dr. Michels) ver. 4.1.0 (RNA-seq analysis by Dr. Vlachavas)
RStudio	ver. 1.3.959
DESeq2 package	ver. 1.28.1
apeglm package	ver. 1.10.0
BiomaRt	ver. 2.44.4
GSEA software from Broad institute	ver. 4.1.0
MSigDB database	ver. 7.2 ver. 7.5.1
ImajeJ	ver. 2.0.0-rc-65/1.52b
Java	ver. 1.8.0_172
Bioconductor software	https://www.bioconductor.org
PROGENy R package	ver. 1.16.0
R package DoRothEA	ver. 1.6.0
BioRender	https://biorender.com/

3.2 Methods

3.2.1 Cell Culture

3.2.1.1 Maintenance and generation

Luminal A breast cancer MCF7 and T47D cells (ATCC) and primary and immortalized carcinoma-associated fibroblast lines were cultured under standard conditions (37ºC, 5% CO_2) in Gibco™ DMEM/F12 (Dulbecco's Modified Eagle's Medium-F12, Thermo Fisher Scientific) supplemented with 10% fetal calf serum (FCS) and 1% P/S. The primary CAF cultures were maintained for no more than 15 passages. The rest of the cell lines were split no more than 20 times before discarded and replaced by freshly thawed new lower passages. The cell lines were authenticated and regularly tested for mycoplasma contamination. When the cell lines had reached 80% confluence, unless used for CM collection, they were split under sterile conditions under a laminar air-flow hood.

The E6/E7 immortalized and LAMC2 overexpression CAF1 cell lines were generated before and after the start of my PhD, respectively, by the Stable Isogenic Cell Lines department of the DKFZ Genomics and Proteomics Core Facility. Briefly, the immortalized CAF1 cell line was generated as follows. The primary CAF1 cells were immortalized by lentiviral infection with a construct (rwpLX305_TATA_E6_E7_closed_HA_IRES_Puro) expressing the HPV E6/E7 (Halbert *et al.,* 1991) fused to an IRES-Puro selection maker under control of a CMV-promoter. The lentiviral particles were generated as follows. HEK293FT cells were co-transfected with rwpLX305_TATA_E6_E7_closed_HA_IRES_Puro and 2nd generation viral packaging plasmids VSV.G (Addgene #14888) and psPAX2 (Addgene #12260). The virus containing supernatant was removed and cleared by centrifugation. To remove remaining cellular debris the supernatant was passed through a 0.45µm filter. The primary CAF1 cells were transduced with lentiviral particles at 70% confluency in the presence of polybrene. Twenty-four hours after transduction the virus containing medium was replaced with selection medium for the respective expression constructs (1µg/mL puromycin; Merck, Germany).

For the generation of the LAMC2 oe (overexpression) cell line, the following protocol was used. For functional analysis, the ORF of human LAMC2 lacking a

stop codon was PCR-amplified from cDNA using LAMC2 specific primers flanked with attB-recombination sites (in bold) for the gateway recombination system:

LAMC2-F_**GGGGACAAGTTTGTACAAAAAAGCAGGCTTA**accATGCCTGCGCTCT

LAMC2-R_GG**GACCACTTTGTACAAGAAAGCTGGGTTCTGT**TGCTCAAGAGCCTGGG

After purification, the PCR-products were recombined by gateway BP reaction into the universal entry pDONR221. The inserts of the resulting clones were validated by Sanger sequencing and served as a template for site specific LR recombination into the lentiviral expression vectors (Core Facility Cellular Tools, DKFZ):

rwpLX305_GW_HA_IRES_Puro

OR

rwpLX305_GW_HA_IRES_Neo

These vectors add an immunogenic HA and an IRES sequence coupled to either a neomycin resistance or puromycin resistance marker to the c-terminus of the protein. After validation by Sanger sequencing the expression constructs were ready for the generation of lentiviral particles. For generation of lentiviral particles, HEK293FT cells (Thermo Fisher Scientific, Germany) were co-transfected with the LAMC2 expression constructs and 2nd generation viral packaging plasmids VSV.G (Addgene #14888) and psPAX2 (Addgene #12260). Next, 48h after transfection, virus containing supernatant was removed and cleared by centrifugation (5min/500g). The supernatant was passed through a 0.45µm filter to remove remaining cellular debris. CAF cells were transduced with lentiviral particles at 70% confluency in the presence of 10 µg/ml polybrene (Merck, Germany). Twenty-four hours after transduction virus containing medium was replaced with selection medium for the respective expression constructs.

The GFP LC3-HiBiT cell lines were also generated by the Stable Isogenic Cell Lines department as described in Will *et al*. (Will *et al*., 2022). In addition to the clones listed in Table 3, two more MCF7 clones (MCF7 K7 and K3) and HeLa clones (HeLa K7 and K10) were tested. All GFP LC3-HiBiT cell lines were maintained in 10% FCS 1% P/S 2 µg/mL puromycin DMEM/F12. CM without puromycin was used for the short (less than 24h) autophagy flux assays.

Table 3. Cell Lines.

Cell line	Source	Annotation	Derived from	Characteristics	Media
MCF7	ATCC HTB-22	MCF7	Breast adenocarcinoma, pleural effusion	Luminal A BC cell line	10% FCS 1% P/S DMEM/F12
T47D	ATCC HTB-133	T47D	Breast ductal carcinoma, pleural effusion	Luminal A BC cell line	
H8/CAF	Patient material	CAF1 primary	Luminal A BC	Primary CAF cell line	
H8/CAF imm	Generated by Core Facility Cellular Tools	**CAF1**	Luminal A BC	E6/E7 immortalized H8/CAF	
H8/CAF LAMC2 oe	Generated by Core Facility Cellular Tools	LAMC2 oe CAF1	Luminal A BC	LAMC overexpressing E6/E7 immortalized H8/CAF	10% FCS 1% P/S DMEM/F12 with 10 mg/mL Genetecin
H4/CAF	Patient material	**CAF2**	Luminal A BC	Primary CAF cell line	10% FCS 1% P/S DMEM/F12
H3/CAF	Patient material	CAF3	Luminal A BC	Primary CAF cell line	
NCT1	Patient material	CAF4	Most likely TNBC	Primary CAF cell line	
GFP LC3-HiBiT MCF7 K9	Provided by Dr. Rainer Will	GFP LC3-HiBiT MCF7	Breast adenocarcinoma, pleural effusion	MCF7 with tagged LC3	10% FCS 1% P/S DMEM/F12 with 2µg/mL Puromycin
GFP LC3-HiBiT HeLa K5	Provided by Dr. Rainer Will	GFP LC3-HiBiT HeLa	Cervical adenocarcinoma	HeLa with tagged LC3	

3.2.1.2 Stimulations

The various stimulations with cytokines and neutralization antibodies used in this study were performed by me and are described in the corresponding figure legends. For stimulation of CAF1 and CAF2 cells, the fibroblasts were seeded in 15-cm dishes in full growth media (10% FCS 1% P/S DMEM/F12) and allowed to grow to 80-100% confluence. Then they were stimulated for 24 hours with human recombinant TNFα and TGFβ purchased from PeproTech. The concentrations used were 10ng/mL TNFα and 2ng/mL TGFβ1 in 0% FCS 1%P/S DMEM/F12. Only for the recovery assays, 2.5% FCS media was used instead. For estimation of IFNβ1 levels after TNFα stimulation, $2x10^6$ MCF7 cells were seeded in 15cm dishes and allowed to reach 80% confluence. Then they were stimulated with TNFα (in 0%FCS) the same way as the CAFs.

3.2.1.3 Conditioned media (CM)

Collection: After the end of 24-hour stimulation, the CM was collected into 50mL falcons. Cell debris was removed by centrifugation (1,500 rpm for 5 minutes in Heraeus Multifuge 4 KR at 4°C). The debris-free CM was aliquoted and stored at -80°C until needed.

Heat Inactivation: The CAF CM was heat inactivated at 95°C for 5 minutes and allowed to reach RT before being added to the breast cancer cells.

*Fractionation***:** Amicon® Ultra-15 50K Centrifugal Filter Devices (Cat No UFC905024, Merck Millipore) were used to fractionate the CAF CM. The manufacturer's instructions were followed. The filter devices were sterilize by UV for 30 min. Then 8mL CM was added to them. The CM-filled devices were centrifuged at 4,000 x g for 15 minutes at 4°C. Two CM fractions were obtained: one containing proteins with molecular weight above 50 kDa (top fraction) and one with proteins smaller than 50kDa (the bottom faction). The top fraction was about 40-fold concentrated, so prior to using for the scratch assays, I diluted it back to its original concentration. I achieved that by adding enough 0% FCS 1% P/S DMEM/F12 media to make it up to 8 mL, the volume the CM had prior to the fractionation. The fractionated CM was used the same day for scratch assays.

3.2.1.4 siRNA transfections

All siRNA transfections used for this study were performed by me. Briefly, cells were seeded in 15-cm dishes, 6-well or 96-well plates in full growth media (10% FCS, 1% P/S DMEM/F12) and allowed to reach 60-80% confluence. Then they were transfected with siRNAs targeting the mRNA of interest or with non-targeting negative control siRNAs. Briefly, the day of the transfection the P/S-containing media was aspirated. The cells were washed with DPBS to remove any remaining antibiotic. Media without P/S (1%FCS DMEM/F12) was added to the cells at the appropriate volume for the Petri dish/well. The siRNAs were diluted in Gibco™ Opti-MEM, so that their final concentration in the Petri dish/well would be 30nM for the siRNAs purchased from Dharmacon or 3nM for the siPOOLs siRNAs purchased from siTOOLs Biotech. Lipofectamine®RNAimax (Invitrogen) was also diluted in Gibco™ Opti-MEM according to the manufacturers' instructions. The

siRNA mix and the Lipofectamine mix were combined, mixed by pipetting and incubated for 5 min at RT, then added dropwise to the cells. Cells without transfection (1%FCS DMEM-F12 only) were used as controls. To allow sufficient time for proper knockdown to occur, the cells were used for further experiments or CM collection two-three days after the addition of the transfection reagents. For CM collection, the transfection reagent-containing media was aspirated, the cells were washed with DPBS and fresh 0% FCS 1%P/S DMEM/F12 was added to be collected later as CM. Once not needed anymore, the transfected cells were subjected to RNA isolation. The successful knockdown of targets was verified by RT-qPCR.

3.2.1.5 STAT1 and STAT3 signaling

For evaluation of STAT signaling in the MCF7 cells in response to treatment with CAF CM, I performed the following. First, I seeded MCF7 cells in 6-well plates (150,000 cells/well) and allowed them to reach 60-80% confluence, which typically took 2 days. Then the cells were starved O/N. The next day the cells were incubated with CAF CM and the different controls for 20 minutes before being lysed on ice in Pierce™ RIPA lysis buffer (Thermo Fisher Scientific) supplemented with PhosStop™ Phosphatase Inhibitor Cocktail (Roche), protease inhibitor cocktail (Roche), 1mM Na_3VO_4 and 10mM NaF. Then I performed protein extraction and western blotting, as described below. For evaluation of the induction of STAT1 and STAT3 signaling, the primary anti-total and anti-phospho STAT1/3 antibodies listed in section *3.1.6.4 Antibodies used for Western Blot* were used.

3.2.2 Protein work

3.2.2.1 Protein extraction from cell lysates and western blotting

To collect total protein from cell lysates, I performed protein extraction with RIPA buffer as follows. Immediately after media removal, the cultured cells were washed once with cold DPBS and lysed with cold Pierce™ RIPA lysis buffer (Thermo Fisher Scientific) supplemented with PhosStop™ Phosphatase Inhibitor Cocktail (Roche), protease inhibitor cocktail (Roche), 1mM Na_3VO_4 and 10mM NaF. The protein concentration was determined by Pierce® BCA Protein Assay (Thermo Fisher Scientific), following the manufacturer's instructions. The protein samples were lysed, denatured (5min at 95°C), and then resolved by SDS-PAGE

on 4-20% gradient Mini PROTEAN TGX pre-cast gels (Bio-Rad) and semi-dry transferred to a PVDF membrane (Bio-Rad) using Trans-Blot® Turbo™ Transfer System (Bio-Rad). Each membrane was incubated in Blocking buffer (Rockland supplemented with 50% (v/v) 1xTBS, 5mM NaF and 1mM Na_3VO_4) for 1h at RT and then probed O/N at 4°C with primary antibodies diluted in blocking buffer. The next day, the blots were washed three times with TBS-T (0.1% Tween® 20 in 1xTBS (150mM NaCl, 20mM Tris base, pH 7.6)) and incubated with the respective anti-mouse and anti-rabbit secondary antibodies conjugated to DyLight™ 680 or 800 (Thermo Scientific) (1:10,000 (v/v) in TBS-T, 1h incubation at RT), washed again and scanned with Odyssey Infrared Scanner (Li-COR). The blots were then reprobed for 2h at RT with anti-GAPDH (endogenous loading control), washed, incubated with secondary Ab and imaged again.

3.2.2.2 Protein extraction from CAF CM

In order to extract proteins from the CAF CM to use it later for mass spectrometry analysis or WB, I performed methanol/chloroform extraction as described in Wessel and Flügge with adjustments (Wessel and Flügge, 1984).

First, the CM was concentrated 40-fold with Amicon® Ultra-15 3K Centrifugal Filter Devices (Cat No UFC900324, Merck Millipore) following the manufacturers' instructions. To achieve this concentration the CM-filled filter devices were centrifuged at 4,000 x g at 4°C for 1h. Immediately at the end of the centrifugation, the concentrated CM was pipetted out of the filter device (the top fraction) and used for protein extraction.

The protein extraction was performed at RT as follows. Four parts of absolute methanol and one part of chloroform were added to one part concentrated CM and vortexed until only one phase was present. Three volumes of sterile nuclease-free water was added. The mixture was vortexed thoroughly and centrifuged at full speed for 1min at RT in benchtop centrifuge. The upper organic phase was pipetted out carefully without disturbing the interphase. The interphase contained the proteins. The upper phase was discarded. Three parts of absolute methanol were added to the interphase and lower phase. The mixture was vortexed thoroughly and centrifuged as before for 1min at full speed at RT. The supernatant was pipetted out. The pellet, which contained the extracted proteins,

was allowed to air dry and then dissolved in RIPA buffer supplemented with PhosStop™ Phosphatase Inhibitor Cocktail (Roche), protease inhibitor cocktail (Roche), 1mM Na_3VO_4 and 10mM NaF. The protein concentration was determined by Pierce® BCA Protein Assay (Thermo Fisher Scientific), following the manufacturer's instructions. The sample was either submitted for secretome analysis via mass spectrometry or lysed and denatured for Western blotting (WB protocol described above).

3.2.2.3 HPLC-Mass spectrometry analysis

To study the effect of the stimulation on the CAF protein expression and secretion, I collected in biological triplicates total protein lysates from the cytokine-stimulated immortalized CAF1 cells and extracted protein from their corresponding CM, as described above. I measured the protein concentration and submitted all samples to the DKFZ Genomics and Proteomics Core Facility, where HPLC-MS-based CAF secretome and full proteome analyses were performed. The secretome and full proteome samples were analyzed separately as follows. Unfractionated samples (10ug) were subjected to in-gel digestion using DigestPro MSi robotic system (INTAVIS Bioanalytical Instruments) as described in Shevchenko *et al*. (Shevchenko *et al*., 2006). The peptides were then separated on a 20-cm long column filled with C18 material (Waters), and the eluting peptides were analyzed online by a coupled Q-Exactive-HF-X mass spectrometer (Thermo Fisher Scientific) in data-depend acquisition (DDA) mode for 120 minutes. At each time point the most abundant peptides were selected and isolated for MS2 spectrum acquisition at a resolution of 15,000 and a cycle time of 60 seconds.

The data analysis was performed by Martin Schneider at the core facility. Briefly, the data analysis was carried out by MaxQuant (version 1.6.3.3, Tyanova *et al*., 2016a) using the human database extracted from Uniprot.org under default settings. Identification FDR cutoffs were 0.01 on peptide level and 0.01 on protein level. Match between runs option was enabled to transfer peptide identifications across raw files based on accurate retention time and m/z.

The quantification and statistics were performed by Martin Schneider as follows. Quantification was done using a label free quantification (LFQ) approach based on the MaxLFQ algorithm (Cox *et al*., 2014). A minimum of two quantified

peptides per protein was required for protein quantification. For the statistical analysis, the Perseus software package (version 1.6.7.0; Tyanova *et al*., 2016b) was used under default parameters. Statistics were performed with LFQ values, filtering was set to 100% in at least one condition. Besides LFQ, no further normalization was applied. Values were imputed via downshifted normal distribution, two-sample *t*-tests were performed with a significance level of 0.1 and a permutation-based FDR cutoff of 0.05. Proteins were annotated via the preprocessed set of annotations from UniProt provided by Perseus. Enrichment analysis was performed via Fisher's exact test. The heatmaps shown in Figure 15 and Figure 20 were created by me using the Morpheus software of the Broad Institute (https://software.broadinstitute.org/morpheus, accessed on the dates specified in the figure legends). The volcano plots (Figure 16 and Figure 21) and the bar graphs (Figure 22-24) were generated by me using GraphPad Prism (version 9.3.1).

3.2.2.4 RPPA

I extracted protein from immortalized CAF1 cells stimulated with TNFα and/or TGFβ1 (10ng/mL and 2ng/mL, respectively, in 0% FCS 1%P/S DMEM/F12) or left unstimulated (same volume of solvent, i.e sterile nuclease-free H_20) for 24h. I also collected protein lysates from MCF7 and T47D cells treated for 24h with CM collected from 24 hour-stimulated or unstimulated immortalized CAF1 cells. I repeated these steps twice to obtain three biological replicates for each condition. Then I determined the protein concentration of all samples by BCA (Pierce™ BCA protein Assay kit, Thermo Fisher). RPPA (Reverse Phase Protein Array) was performed on the protein samples by Dr. Simone Borgoni, Nooraldeen Tarade and Lukas Beumers (a Postdoc and PhD students, respectively) at the division of Molecular Genome Analysis, DKFZ. The array was performed as described previously (Sonntag *et al*., 2014). To sum it up, the protein lysates were diluted to a concentration of 1.4 µg/µl, mixed with 4x RPPA printing buffer, and denatured for 5min at 95°C. The processed lysates were then pipetted in 384-well plates. In addition, a pool of four samples was made. A dilution series of the pool was generated and also pipetted in the 384-well plate, to serve later as an internal control. The plates were then centrifuged at 200 x g for 2min. The Aushon 2470 contact printer with a 12-pin (185-µm) configuration was used to spot all samples

in technical triplicates on nitrocellulose-coated glass slides (Oncyte Avid, Grace-Biolabs). For each spot, 1.6 nl of sample was printed. The printed slides were kept at 4°C short-term or stored at -20°C, if not used soon. The following day, two of the sample-spotted slides were stained with Fast Green FCF total protein staining. The FCF stained slides would be later used for normalization of the target signal to the total protein. All sample-spotted slides were then blocked for 2h at RT with blocking buffer (Rockland supplemented with 50% (v/v) 1xTBS, 10mM NaF and 1mM Na_3VO_4), and then incubated with primary antibodies O/N at 4°C. Only primary antibodies, which were previously validated by Western blot and determined to show high specificity were used. The next day, the slides were washed 3x 5min with TBS-T and incubated with secondary antibodies (1:12,000 dilution) for 1h at RT protected from direct light. Next, the slides were washed 2x 5min with TBS-T and 2x 5min with Milli-Q H_20. The slides were allowed to dry before scanning them with Odyssey Infrared Scanner (Li-COR). The processing of the raw data was performed by Dr. Simone Borgoni. Signal intensities of all spots were quantified with GenePixPro 7.2.22 (Molecular Devices). Preprocessing of the GPR raw data files, quality control, background correction and technical replicates merging were performed with the RPPanalyzer R-package (Mannsperger *et al*., 2010; von der Heyde *et al*., 2014) using R (version 3.5.3). I performed *t*-test analysis and generated heatmaps using the Morpheus software by the Broad Institute (https://software.broadinstitute.org/morpheus).

3.2.2.5 IL6 FLISA

To evaluate the levels of IL6 in the CAF CM post stimulation with TNFα+/-TGFβ1, I performed the following assay. A 96-well high-binding plate was coated O/N at 4°C with capture antibody (Cat # MAB206, R&D systems) diluted in DPBS (4 µg/mL; 100 µl/well). The next day the capture Ab solution was aspirated and the wells were washed three times with washing buffer (0.05% Tween 20 in DPBS, 200 µl/well). After each wash, the remaining buffer was completely removed by blotting the plate upside down against a stack of clean paper towels. Blocking buffer (1% BSA in Milli-Q H_2O, 200 µl/well) was added to the plate and incubated for 2 hours at RT. Meanwhile IL6 standards (Cat # 206-IL, R&D systems) were prepared by two-fold serial dilution in blocking buffer (0.25 ng/mL-32 ng/mL). At the end of the 2h-incubation, the blocking buffer was aspirated and the wells

washed three times as described above. IL6 standards and CAF CM were added to the plate (100 µl/well, one sample or standard per well, in duplicates). The plate was sealed and incubate at RT for 2 hours, after which the samples were aspirated, and the wells were washed as already described three times. Detection antibody (Cat # BAF206, R&D systems) diluted in washing buffer (0.2 µg/mL) was added to the wells (100 µl/well), and the plate was sealed and incubated at RT. After 2 hours, the detection Ab solution was aspirated, and the wells were washed again (3x). Alexa 680-conjugated streptavidin (Cat# S32358, Invitrogen) diluted 1:5000 in washing buffer was added to the wells (100µl/well). The plate was covered in aluminum foil to protect it from direct light and incubated for 1 hour at RT. The plate was then aspirated and washed three times with washing buffer followed by one wash with Milli-Q H_2O (200 µl/well). Then the plate was aspirated, dried by centrifugation (upside down for 1 min at 200 x g) and imaged with the Odyssey Scanner (settings: 700nm, 84 µM, offset of 4.0 and intensity of 9). The fluorescent signal intensities from each condition were analyzed using the Image Studio Lite software (version 5.2). GraphPad Prism was used to generate a standard curve using the signal intensity values measured for the standards (intensity versus concentration, non-linear fit). From this graph, the concentration of IL6 in the CAF CM was interpolated for each sample by using GraphPad Prism.

3.2.2.6 IFNβ1 ELISA

To determine the level of IFNβ1 present in the CAF CM and the MCF7 CM post stimulation with TNFα, I performed an ELISA. For this purpose, a kit was purchased from R&D Systems (Cat # DY814-05; Lot # P215632) and the assay was performed according to the manufacturer's instructions as follows. A 96-well high-binding plate was coated with capture Ab diluted in DPBS (4 µg/mL working concentration, 100 µl/well), sealed and incubated O/N at RT. The next day, each well was aspirated and washed three times with washing buffer (0.05% Tween 20 in DPBS, 400 µl/well). After each wash, the remaining buffer was completely removed by blotting the plate upside down against a stack of clean paper towels. Blocking buffer (1% BSA in DPBS) was added to the plate (300 µl/well), which was then incubated at RT for 2h. Then the washing steps were repeated as already described. IFNβ1 standards prepared by two-fold serial dilution (concentration range 3.905 pg/mL-500 pg/mL in 1% BSA in DPBS) and CM samples were added

to the plate (100 µl/well, one sample or standard per well, in duplicates). The plate was sealed and incubated at RT for 2 hours, after which the washing steps were repeated. Next, detection antibody (250 ng/mL in blocking buffer) was added to each well (100 µL/well). The plate was incubated for 2h at RT. The washing was repeated again as described above. Streptavidin-HRP diluted 1:40 in blocking buffer was added to the plate (100 µl/well). The plate was covered and incubated for 20 minutes at RT and away from direct light. The washes were repeated. Then 100µl of Substrate solution (1:1 mixture of H_2O_2 and Tetramethylbenzidine, Cat # DY999) was added to each well. The plate was incubated for 20 minutes at RT away from direct light. At the end of the 20 minutes, Stop solution (2N H_2SO_4, Cat# DY994, R&D Systems) was added to each well (50µl/well) and the plate was gently shaken on a rocker to allow for thorough mixing. The optical density of each well was determined using a plate reader (GloMax, Promega) set at 450nm with wavelength correction set to 560nm to correct for optical imperfections in the plate. GraphPad Prism was used to generate a standard curve using the optical density values measured for the standards (optical density versus concentration, non-linear fit). From this graph, the concentration of IFNβ1 in the CM was interpolated for each sample with the help of GraphPad Prism analysis tools.

3.2.3 RNA work

3.2.3.1 RNA isolation, cDNA synthesis and qPCR analysis

To analyze gene expression for individual genes of interest, I performed RNA isolation, cDNA synthesis and qPCR analysis. Briefly, cells were lysed using QIAzol™ Lysis Reagent (QIAGEN) and either further processed immediately or stored at -80ºC. Phenol-chloroform total RNA extraction was performed using RNeasy® Mini Kit (QIAGEN) following the manufacturer's instructions. The RNA concentration was determined with NanoDrop. Then mRNA reverse transcription was performed using RevertAid H Minus First Strand cDNA Synthesis Kit (Thermo Fisher Scientific). The manufacturer's instructions were followed. Briefly, per cDNA reaction 500-1000ng of total mRNA was used. All RNA samples were first brought to the same concentration by diluting them with sterile nuclease-free H_20 up to a volume of 11µl. Then 1µl of oligo(dT)18 Primer was added per reaction for a total volume of 12µl (11µl mRNA-H2O mix + 1µl oligo(dT)). The reactions were incubated in a thermocycler (GeneAmp® PCR System 9700, Applied Biosystems)

for 5 min at 70ºC followed by a brief incubation at 4ºC. Meanwhile a master mix was prepared as indicated in Table 4. The enzymes were added last to the mix.

Table 4. First Strand cDNA synthesis master mix.

Component	µl/1 rxn	µl/10rxns
5X Reaction Buffer	4	40
10mM dNTP mix	2	20
RiboLock RNase Inhibitor (20 units/ul)	1	10
RevertAid H Minus Reverse Transcriptase	1	10

Per reaction, 8µl of the master mix were added. After a brief centrifugation in a picofuge, the samples were incubated again in the thermocycler. Table 5 below summarizes the thermocycler profile used for the reverse transcription. At the end of the reverse transcription, the synthesized cDNA was either used immediately for qPCR analysis or stored at -20ºC.

Table 5. Thermocycler profile for cDNA synthesis.

Temperature	Duration
37ºC	**5 min**
42ºC	**60 min**
70ºC	**40 cycles, 10 min each**
4ºC	**final hold**

Standard qPCR analysis (see Table 6 for master mix content) was performed for the genes of interest. Expression levels of two housekeeping genes (*ACTB* and *GAPDH*) were used for normalization. Table 7 lists the temperature profile used for the qPCR assay.

Table 6. qPCR master mix (individual genes).

Component	1Rxn	15 Rxns
2x qPCR-Probe-MasterMix-low-ROX	5.5 µl	82.5 µl
Primer left	0.11 µl	1.65 µl
Primer right	0.11 µl	1.65 µl
UPL Probe	0.11 µl	1.65 µl
H_20	0.17 µl	2.55 µl

Table 7. Thermal profile for the qPCR assay.

Step	Temperature	Duration	# Cycles
	50°C	2 min	1
Initial denaturation	95°C	15 min	1
Denaturation	95°C	15 sec	45
Annealing	60°C	1 min	

3.2.3.2 RNA-Seq

Two sets of RNA-Seq data are shown in this thesis: 1) CAF1/CAF2 versus MCF7/T47D breast cancer cell lines characterization and 2) MCF7 cells treated with CM from cytokine-stimulated CAF1 cells versus MCF7 cells treated with CM from unstimulated CAF1 cells.

The first set of RNA data was generated by Dr. Mireia Berdiel-Acer (CAF data), Dr. Simone Borgoni and Dr. Emre Sofyali (MCF7 and T47D data) with the help of the DKFZ High Throughput Sequencing Core Facility. For this purpose, the HiSeq 4000 platform (Illumina) and stranded Tru-SeqRNA paired end sequencing kit (Illumina) were used. Then quality control was performed. The data was analyzed by Dr. Birgitta Michels. Briefly, the reads were mapped to the human genome hg38 using STAR (version 2.3.0e). Reverse strand read counts were determined with featureCounts (version 1.5.1). The reads were mapped to ENSEMBL IDs and gene symbols. Exonic gene lengths and TPMs (Transcript Per kilobase Million reads) were calculated in R. To avoid infinite values, a count of one was added to each TPM value and the resulting values were then log2 transformed. I used the TPM data to generate the heatmap comparing CAF1 and CAF2 cells to the BC cells. For this purpose, I used the Morpheus software of the Broad Institute (https://software.broadinstitute.org/morpheus). The RNA-Seq data for the CAF2 cells, but not for the CAF1 cells have already been published in Berdiel-Acer *et al*., a paper of which I am one of the co-authors (Berdiel-Acer *et al*., 2021).

The second dataset was generated by me with help by others as follows. I stimulated immortalized CAF1 cells with 10ng/mL TNFα and 2ng/mL TGFβ1 in 0%FCS 1%P/S DMEM/F12. Nuclease-free water was used for the unstimulated control group. After 24 hours, I collected the CM and froze it at -80°C until further use. I seeded MCF7 cells in 10-cm dishes and the following day treated them for 24 hours with thawed CM collected from the stimulated or unstimulated immortalized CAF1 fibroblasts. After the 24-hour treatment, I lysed the cells and isolated their total RNA using the miRNeasy Mini Kit (Qiagen) and quantified it with Nanodrop. Then I submitted the RNA samples to the High Throughput Sequencing Core Facility at the DKFZ for RNA quality control, library preparation and sequencing. The following steps were performed by the core facility. First the RNA

quantity was determined by Qubit. The RNA quality was analyzed with TapeStation 3.2 (Agilent Technologies). All samples had a RIN (RNA Integrity Number) of 10. SASIs (Sample Assurance Spike-Ins), uniquely barcoded PhiX PCR-products, were added to each sample for contamination control. The library was prepared using the TruSeq Stranded total RNA kit (Illumina). Single-read 50bp RNA sequencing was performed using a HiSeq 4000 instrument (Illumina). Phred +33 Quality score encoding was used. Between 59 Million and 76 Million total reads per sample were obtained. Quality of the data was monitored using FastQC Analysis. Dr. Birgitta Michels (a Postdoc at the Division of Molecular Genome Analysis) performed quality score filtering, poly-A trimming, artifact removal, removal of N containing reads, and clearing of rRNA contamination using a pipeline provided by the HUSAR platform, DKFZ. Then she performed genomic mapping to human genome 38 using STAR (version 2.3; Dobin *et al*., 2013), and determined the number of reads per gene using HTSeq count (version 0.6.0; Anders *et al*., 2015) and the gencode annotations (release 24).

Dr. Birgitta Michels performed a differential expression analysis comparing gene read counts from the two groups of MCF7 cells in R (version 4.0.3; R Core Team, 2014, R Foundation for Statistical Computing, Vienna, Austria; https://www.R-project.org) and RStudio (version1.3.959) using the DESeq2 package (version 1.28.1; Love *et al*., 2014). The apeglm package was used for log fold change shrinkage (version 1.10.0; Zhu *et al*., 2018). BiomaRt (version 2.44.4; Durinck, *et al*., 2005; Durinck, *et al*., 2009) was used to obtain corresponding gene names to the ensemble gene ids provided by HT-Seq Count. I used GraphPad Prism (version 9.3.1) to generate the volcano plot in Figure 28.

Dr. Birgitta Michels also performed GSEA using the preranked tool of the GSEA software from Broad institute (version 4.1.0; Subramanian *et al*., 2005; Liberzon *et al*., 2015). The Hallmarks (Liberzon *et al*., 2015) and the TFT_Legacy subset of TFT (Xie *et al*., 2005) datasets from the MSigDB collection (version 7.2; Subramanian *et al*., 2005; Liberzon *et al*., 2015) were used as grp files. Rnk files were generated from gene names and the log2 fold changes of the differential expression analysis comparing the two groups of MCF7 cells. No collapsing was performed for gene symbols. Default options were used for all other parameters.

To acquire additional information on signaling pathways and transcription factors activated in the MCF7 cells post treatment with CM collected from cytokine-activated vs unstimulated immortalized CAF1s, Dr. Efstathios-Iason Vlachavas (a Postdoc at the Division of Molecular Genome Analysis) also performed complete RNA-Seq analysis using R (R version 4.1.0) and the Bioconductor software (https://www.bioconductor.org). First to identify putative differentially activated pathways between the two MCF7 groups, he implemented the PROGENy (Pathway RespOnsive GENes, Schubert *et al*., 2018) R package (version 1.16.0). This analysis was based on the derived differential moderated statistics from the DeSeq2 pipeline (top 100 most responsive genes for each pathway). Additionally, he also performed transcription factor activity analysis using the R package DoRothEA (Discriminant Regulon Expression Analysis, version 1.6.0; Garcia-Alonso *et al*., 2019). For this analysis he used the default settings as suggested (using A to C confidence assignments) and the VIPER algorithm (Alvarez *et al*., 2016). TF activity was additionally run per sample basis, to also illustrate the relative TF activities per sample and the respective heterogeneity.

3.2.4 Phenotypic Assays

3.2.4.1 Scratch migration assay

MCF7 and T47D monocultures were seeded in 96-well plates at a confluence of 30,000 cells/well in 100μl standard media (10% FCS 1% P/S DMEM-F12). Cells were allowed to grow to a 90-100% confluence, and then starved O/N in 1%FCS media. The next day, the cells were stained with Cell Tracker™ Green CMFDA (Invitrogen C2925, stock concentration of 10mM in DMSO). For the staining 1:5000 dilution in starvation media was used. The cells were incubated with the dye for 30 min at 37ºC, 5% CO_2. Then the media was changed again to fresh starvation media (100μl/well) and left for another 30-45 min in the cell incubator, time necessary for the metabolization of the dye. A scratch was introduced in the middle of each well semi-manually by using a 96-well multichannel pipette (Liquidator96, Steinbrenner). The wells were then washed twice with DPBS (100μl/well) to remove any floating cell debris. After the last wash, the various conditions to be tested were added, e.g. CAF-conditioned media (CM) collected from different CAF cell lines, DMEM/F12 (negative control), hrTNFα at various concentrations, etc., as specified in the figures and their legends. All media

contained 0%FCS and 1% P/S. The plates were imaged immediately (0h time point) with a fluorescence microscope ImageXpress®Micro (Molecular Devices). Images were taken again after 20-21h. The images were analyzed using the MRI Wound Healing Tool in ImageJ, and the gap closure was assessed by comparing the scratch surface areas at 0h and 21h post CM addition.

3.2.4.2 Autophagy Flux Assay

To investigate whether the interferon beta-containing CAF2 CM, which was collected post TNFα or double stimulation, had any effect on MCF7 cells in terms of autophagy, I performed an autophagy flux assay as follows. GFP LC3-HiBiT MCF7 cells were seeded in a solid white non-transparent 96-well plate (Greiner Bio-One GmbH, Cat# 655083) at a confluence of 4,000 cells/well in 100 µl/well standard media supplemented with puromycin (10% FCS 1% P/S, 2 µg/mL puromycin DMEM/F12) and allowed to attach O/N. The next day the media was removed with a multichannel pipet and replaced by starvation media with puromycin (1%FCS 1% P/S, 2 µg/mL puromycin DMEM/F12). The following day, the starvation media was discarded, and the conditions indicated in Table 8 were added (50 µl/well) in at least 4 technical replicates. Note that the conditions containing Torin or Bafilomycin were added the following day 3h prior to detecting the autophagy flux. These are the positive and negative control, respectively. According to Will *et al.* the effects of the inducer (Torin) and inhibitor (Bafilomycin) of autophagy are well-detectable within three-four hours after addition (Will *et al*., 2022). The plate was returned to the incubator (37°C, 5% CO_2) for O/N (14-16 hours) incubation with the conditions. The next day an autophagy flux assay was performed on the cells using the Nano-Glo® HiBiT Lytic Detection System kit (Promega, Cat # N3030). The manufacturer's instructions were followed, as well as the autophagy flux protocol described in Will *et al*. (Will *et al*., 2022). To summarize the steps, first, the HiBiT Lytic buffer, which the night before had been taken out of the freezer and put in the fridge to thaw, was now taken out of the fridge and equilibrated to RT for at least 3 hours before use. Thirteen-fifteen hours after the conditions were added to the cells, the plate was taken out of the incubator. Torin and Bafilomycin controls were added. The plate was returned to the incubator for another 3 hours. At the end of the 3-hour incubation with Torin/Bafilomycin or, in other words, 14-16 hours post addition of all other

conditions, the plate was taken out of the cell culture incubator and allowed to equilibrate to RT for 30 minutes. The total volume of reagent mixture necessary for the plate was calculated, so that there would be enough to add to all wells (50µl/well). Right before use, the reagent mixture was prepared by diluting LgBiT Protein and HiBiT Lytic Substrate together in HiBiT Lytic buffer for 1:100 and 1:50 dilution, respectively. The mixture of all three components was mixed well by inversion and then added to the cell culture plate (50 µl/well), including to three wells which contained only media (no cells) to be used as background control. The plate was covered in aluminum foil to protect it from direct light. To ensure proper mixing, the plate was placed on rocking shaker (ST 5 CAT, Ingenieurbüro CAT) for 10 min at medium speed. The luminescence was measured using GloMax plate reader (Promega) with integration time of 0.5 seconds. Background noise was subtracted from each reading, and the average of at least 4 technical replicates was plotted for each condition using GraphPad Prism. The assay was repeated with GFP LC3-HiBiT HeLa cells as a positive control.

Table 8. Conditions tested in autophagy flux assay.

Condition	Concentration/Molarity	Rationale
0% FCS 1% P/S DMEM/F12	Not applicable	Base line
Human recombinant IFNβ1	50 pg/mL	Control
Human recombinant IFNβ1 + IFNβ1 NAb	50 pg/mL + 0.2 µg/mL	Control
Torin in 0% FCS 1% P/S DMEM/F12	250 nM	Positive control
CAF2 CM collected post no stimulation	Not applicable	Control
CAF2 CM collected post TNFα stimulation	Not applicable	To study effect of CM
CAF2 CM collected post TGFβ1 stimulation	Not applicable	Control
CAF2 CM collected post double stimulation (TNFα+TGFβ)	Not applicable	To study effect of CM
IFNβ1 NAb added to CAF2 CM collected post TNFα stimulation	0.2 µg/mL	Control
Bafilomycin added to CAF2 CM collected post TNFα stimulation	100nM	Negative control

3.2.4.3 Recovery Assays

To evaluate whether the stimulation with TNFα increased the CAFs' ability to induce the recovery of breast cancer cells after chemotherapy, I performed two kinds of recovery assays – with indirect CAF2-MCF7/T47D cocultures and with CAF2 CM.

Indirect cocultures: MCF7 and T47D monocultures were seeded in 6-well companion plates at a confluence of 250,000 cells/well in 10%FCS 1%P/S DMEM/F12, and allowed to attach O/N. The breast cancer cells were then treated with 4nM paclitaxel in 2.5% FCS 1%P/S DMEM/F12. The next day CAF2 cells were seeded in cell culture inserts (20,000 cells/insert in 10%FCS 1% P/S DMEM/F12) and allowed to attach O/N. After attachment, the CAFs were stimulated for 24h with TNFα (10ng/mL in 0% FCS 1%P/S DMEM/F12) or solvent (sterile nuclease-free H_2O). After 3 days of chemotherapy, the drug was taken off the breast cancer cells by gently aspirating the media and carefully washing 3x with DPBS. These washes are important to ensure removal of any remaining paclitaxel. It was important to do this step carefully to avoid detachment of the chemo-treated cells. Fresh 2.5% FCS 1%P/S DMEM/F12 was added to the MCF7 and T47D cells. The media of the CAF2 cells, which at this point have been prestimulated with TNFα for 24h, was also aspirated and, after the cells were washed 3x with DPBS, changed to 2.5% FCS 1% P/S DMEM/F12. The washes were done, so that residual TNFα could be removed. The unstimulated CAF2 cells were treated (washed 3x etc.) the exact same way The CAF-containing inserts were then added on top of the chemo-pretreated and washed breast cancer cells in the companion plate. Chemo-pretreated breast cancer cell monocultures were also maintained for comparison. In this way, the MCF7 and T47D cells were allowed to recover from the paclitaxel treatment for 15 days either in indirect coculture with stimulated or unstimulated CAF2 cells or as monocultures. During that period, the media in both inserts and companion plates was changed every three-four days. To avoid detachment of the fragile recovering breast cancer cells, the media change was performed gently. At day 15 post the end of the chemotherapy, the inserts with CAF2 fibroblasts were discarded. The companion plates containing the recovered breast cancer cells were kept and processed immediately as follows. The media was carefully removed by pipetting with

Pipetboy. The cells were washed once with DPBS and fixed with 100% methanol (1mL/well) for 10 minutes. Then the methanol was replaced with crystal violet staining (0.2% crystal violet in Milli-Q H_2O; 2mL/well). After one hour the staining was removed by pipetting and the residual stain was carefully washed with Milli-Q H_2O at least 2-3 times. The stained plates were allowed to dry O/N and then scanned with EPSON scanner.

Recovery Assay with CAF2 CM: $1x10^6$ CAF2 cells were seeded in 15-cm cell culture Petri dishes in full-growth media (10% FCS 1%P/S DMEM/F12) and allowed to reach 80-100% confluence. They were then treated with TNFα (PeproTech, 10ng/mL in 2.5% FCS 1%P/S DMEM/F12) or sterile nuclease free H_20 (the solvent, in which the TNFα stock was diluted; this is the unstimulated condition). The CM was collected 24 hours later. The fibroblasts were washed with DPBS 3x to remove any residual TNFα. Fresh 2.5% FCS 1%P/S DMEM/F12 was added to them. Any potential debris was removed from the collected CM by centrifugation. The CM was aliquoted and stored at -80°C until needed. Another 24h after the addition of the fresh media, the CM (CM post TNFα 24+24h) was collected, processed as described before and stored at -80°C. MCF7 and T47D monocultures were seeded in 12-well dishes at a confluence of 20,000 cells/well in 10% FCS 1% P/S DMEM/F12. The next day the cells were treated with either 70nM epirubicin or 4nM paclitaxel in 2.5% FCS 1%P/S DMEM/F12. Three days later the chemotherapy-containing media was carefully aspirated, and the cells were washed gently 3x with DPBS. After the last wash, thawed CAF2 CM (collected as described above) was added to them. As a control 2.5% FCS 1% P/S DMEM/F12 was used. The cells were allowed to recover from the chemo-treatment for 15 days during which the media was refreshed every 4-5 days. After the 15 days, the cells were fixed and stained as described above but with lesser volumes of reagents needed per well (500 µl/well). The plates were allowed to dry O/N and then scanned with EPSON.

3.2.5 Graphical Illustrations

Graphs were generated with GraphPad Prism (version 9.3.1). Illustrations were created with BioRender.com. Heatmaps were created using the Morpheus software of the Broad Institute (https://software.broadinstitute.org/morpheus) and Heatmapper (http://www.heatmapper.ca/; Babicki *et al*., 2016). Venn diagrams were created with the Bioinformatics and Evolutionary Genomics online tool (https://bioinformatics.psb.ugent.be/webtools/Venn/).

3.2.6 Statistical Analysis

Unless otherwise stated, the data was presented as mean ± SD. For direct comparisons of two groups, a two-tailed unpaired Student's *t*-test was used. For multiple comparisons, ANOVA followed by Bonferroni's post-hoc correction was performed. *P*-values less than 0.05 were considered statistically significant, unless otherwise stated.

4. RESULTS

4.1 Luminal A breast cancer-derived fibroblasts express mesenchymal and CAF-like markers

In this study, I used fibroblasts derived from luminal A patients in combination with MCF7 and T47D cell lines to establish an *in vitro* system mimicking the breast cancer-TME (tumor microenvironment) interaction. The first step was to verify the CAF origin of the fibroblasts. (As discussed at length in the introduction, there are no CAF-specific markers. A few though have been proven to be reliable CAF and/or mesenchymal markers and have been selected here to verify the origin of my CAF cell lines.) Cancer-associated fibroblasts are known to express a variety of putative CAF markers, such as αSMA (alpha smooth-muscle actin, encoded by *ACTA*), decorin (encoded by *DCN*) and FAP (fibroblast activation protein alpha, encoded by *FAP*), as well as common fibroblast/mesenchymal markers, such as FN1 (fibronectin-1, encoded by *FN1*), PDGFRα/β (platelet-derived growth factor receptor α/β, encoded by *PDGFRA*/*PDGFRB*), FSP-1 (fibroblast-specific protein 1, encoded by *S100A4*) and vimentin (encoded by *VIM*), while expressing low levels of common epithelial markers such as E-cadherin (encoded by *CDH1*)(Nurmik *et al*., 2020). CAFs are also expected to express higher levels of N-cadherin (encoded by *CDH2*) and extracellular matrix components (e.g. collagens and MMPs) in comparison to cancer cells of epithelial origin, such as the MCF7 and T47D cell lines. To confirm the mesenchymal/CAF origin of the patient-derived fibroblasts, I thus first checked for the expression of the above markers at RNA and/or protein levels (Figure 6). RNA-seq (Figure 6A), as well as WB (Figure 6B) and RPPA (Figure 6C) analyses showed that indeed our CAF cell lines, regardless of their immortalization status, expressed higher levels of putative CAF and common mesenchymal markers in comparison to the luminal A breast cancer cell lines MCF7 and T47D.

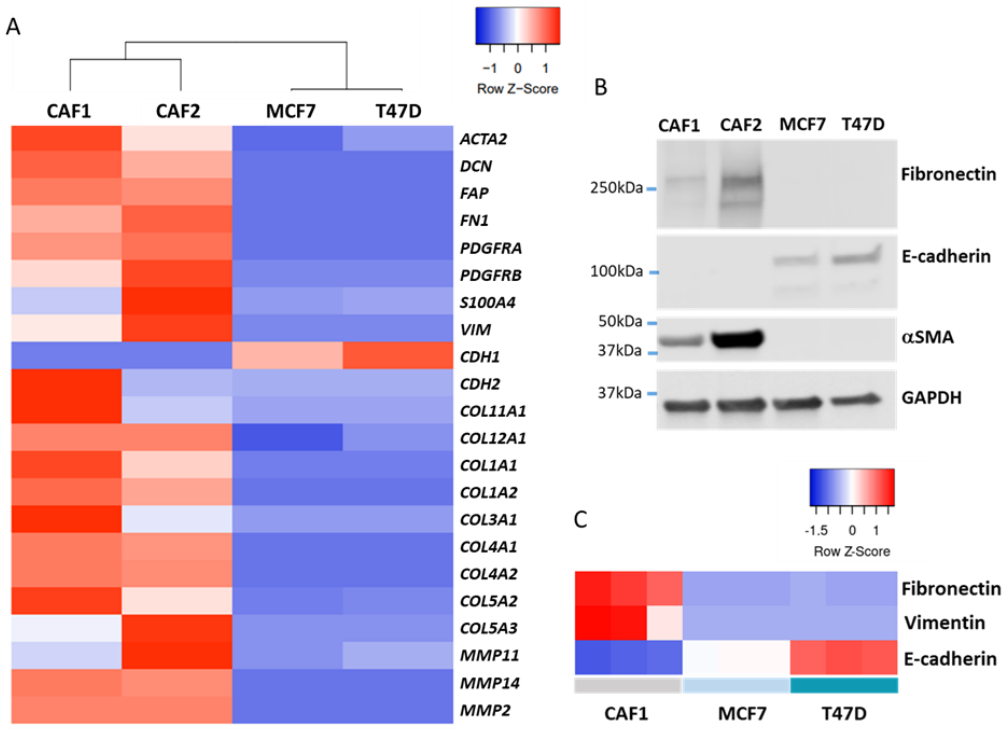

Figure 6. **Patient-derived CAFs express common mesenchymal and CAF markers.** (A) RNA-seq data. Heatmap of the TPM (transcripts per million) values for selected CAF and mesenchymal markers in primary CAF cell lines in comparison to the luminal breast cancer cell lines MCF7 and T47D. For the clustering, Euclidean distances and average linkage were used. Blue and red represent lower and higher TPM values, respectively, within each row. (B) Western blot analysis of the expression of common CAF markers in the E6/E7 immortalized CAF1 and the primary CAF2 cells in comparison to the luminal breast cancer cell lines MCF7 and T47D. E-cadherin was used as an epithelial marker, and GAPDH – as a loading control. Representative data are shown from three biological replicates per cell line. (C) Heatmap of the protein expression levels of fibroblast and epithelial markers as assessed via RPPA (reverse phase protein array) in the E6/E7 immortalized CAF1 cell line and the epithelial MCF7 and T47D cells. Three biological replicates per cell line. Blue and red represent lower and higher protein expression, respectively, within each row. The heatmaps in (A) and (C) were generated using Heatmapper (http://www.heatmapper.ca/, accessed on March 25th, 2022).

The stimulation with the cytokines TNFa, TGFβ1, and the two cytokines in combination did not seem to have a major effect on the levels of expression of CAF-like markers (Figure 7), although for the CAF1 cell line, which at basal levels showed lower expression of fibronectin in comparison to the CAF2 cell line (Figure 6A, 6B), the stimulation with TGFβ1 alone resulted in upregulation of fibronectin as detected via RPPA (Figure 7A). The same elevated expression was not observed for the CAF2 cells (Figure 7B).

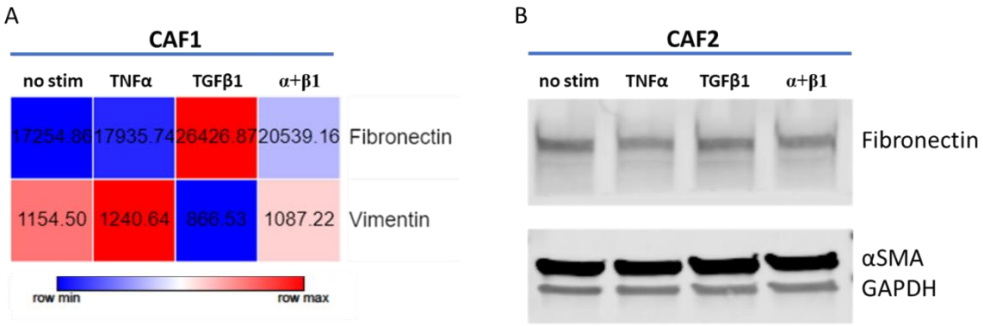

Figure 7. **Effect of the stimulation on the expression of CAF-like markers.** (A) RPPA (reverse phase protein array) analysis was performed on total protein lysates of immortalized CAF1 cells after 24-hour stimulation with TNFα (10ng/mL), TGFβ1 (2ng/mL) or both. No stimulation samples (no stim) were used for comparison. For each condition, the average of 3 biological replicates is depicted. Blue and red represent lower and higher protein expression, respectively, within each row, and the number in the middle of each square is the corresponding normalized protein expression value.
The heatmap was generated using the Morpheus software of the Broad Institute (https://software.broadinstitute.org/morpheus, accessed on February 28th, 2022). (B) WB analysis of primary CAF2 cells stimulated with TNFα (10ng/mL), TGFβ1 (2ng/mL), or both cytokines for 24h versus their unstimulated counterparts (no stim). GAPDH was used as a loading control.

4.2 CAF CM induces migration in MCF7 and T47D Luminal A breast cancer cells

Having characterized the patient-derived cells as CAFs, I next tested the effect of the CAF conditioned medium on the migration of MCF7 and T47D cells, classical luminal A breast cancer models. To assess the ability of CAF-secreted factors to induce breast cancer cell migration, scratch assays were performed with CAF conditioned medium (CM) from three different primary CAF cell lines - the E6/E7 immortalized CAF1 and the primary CAF2 and CAF3. The cancer cells migrated faster with the CAF CM than with the control DMEM/F12 medium (Figure 8), indicating that the CAFs, regardless of their immortalization status, secreted factors with pro-migratory properties.

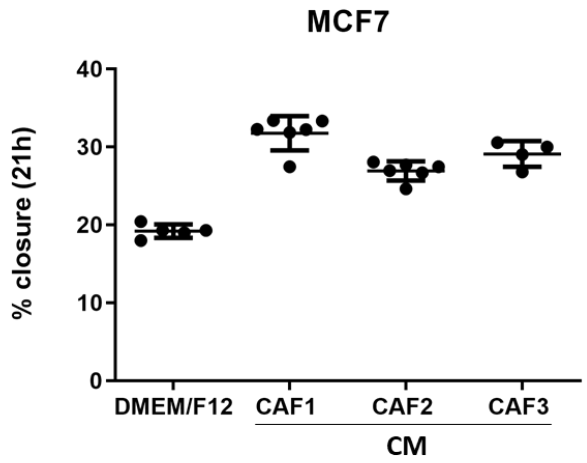

Figure 8. **CM from patient-derived CAFs confers higher migratory potential on MCF7 cells**. MCF7 cells were seeded in a 96-well plate and allowed to reach 100% confluence. A scratch/wound was introduced manually in the middle of each well. The detached cells were removed via washes with DPBS. Fresh DMEM/F12 media or CM (conditioned medium) from three independent CAF cell lines (E6/E7 immortalized CAF1 and primary CAF2 and -3) was added to the scratched MCF7 monocultures. Images of the wound were taken immediately and 21h later. The area of the wound at both timepoints was calculated using Image J. The percentage wound closure was determined for each well. The dots in the plot represent technical replicates, and the error bars - standard deviation.

4.3 CM of cytokine - stimulated CAFs induces more pronounced Luminal A migration

Previous findings suggest that cytokine-activated stroma (e.g., MSCs and fibroblasts), in comparison to unstimulated stroma, can confer more pronounced metastatic properties on luminal A BC cells (Lerrer *et al.*, 2017). Therefore, the scratch assay was repeated with CM from cytokine-activated E6/E7 immortalized CAF1 cells, as well as CM from the corresponding unstimulated fibroblasts. DMEM/F12 media was used as a control. While the CM from unstimulated CAFs in comparison to DMEM/F12 was again able to induce higher migratory potential in the cancer cells, the MCF7 and T47D cells migrated to the highest extent in the presence of CM from CAF1s which had been stimulated with TNFα and TGFβ1 (Figure 9A). The effect was not due to residual TNFα remaining in the CM post the stimulation, as shown in an additional scratch assay in which TNFα neutralization antibody was added to the CM prior to incubation with the tumor cells (Figure 9B).

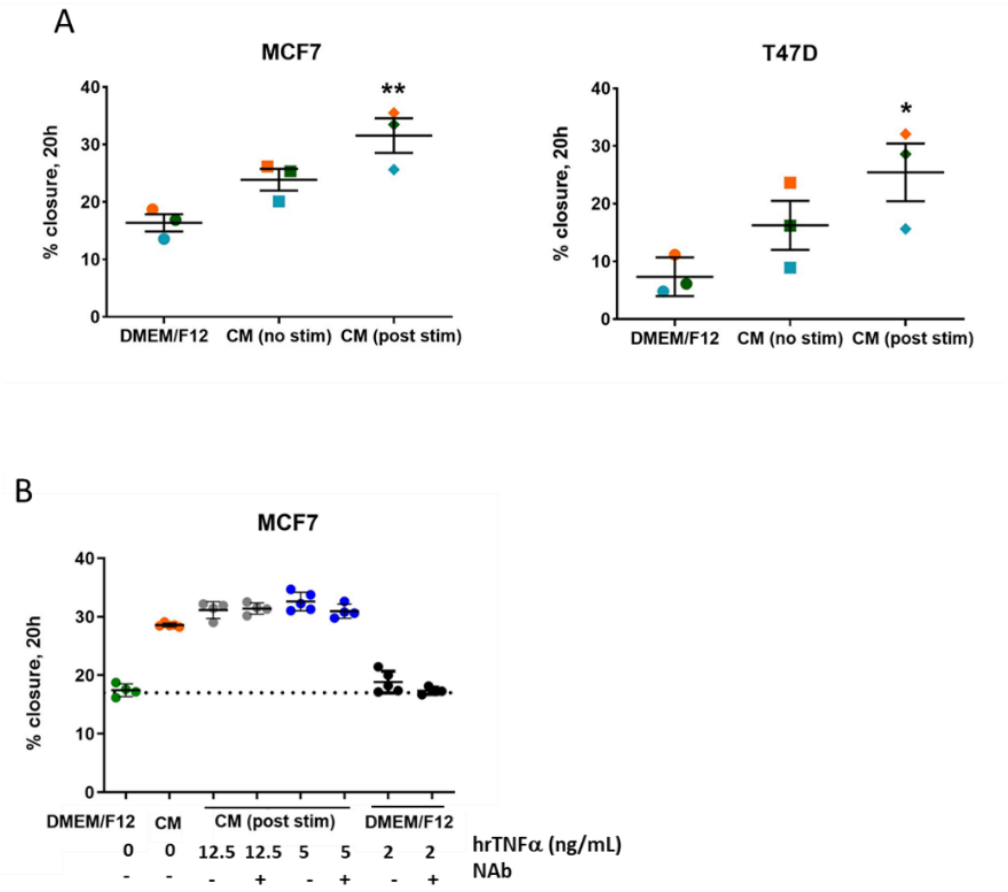

Figure 9. **(A) CM from cytokine-stimulated CAFs conferred even higher migratory potential on MCF7 and T47D cells.** MCF7 and T47D monocultures were seeded in a 96-well plate and allowed to reach 100% confluence. A scratch/wound was introduced manually in the middle of each well. The detached cells were removed via washes with DPBS. Fresh DMEM/F12 media, CM from unstimulated (no stim) or prestimulated CAF1 cells (post stim; 10ng/ml TNFα and 2ng/mL TGFβ1 for 24h) was added to the scratched monocultures. Images of the wound were taken immediately and after 20h. The area of the wound at both timepoints was calculated using Image J. The percentage wound closure was determined for each well. Each symbol represents a biological replicate (n=3) and is the average of 5 technical replicates. The error bars are SEM.Statistical analysis was performed using a one-way ANOVA test followed by Bonferroni correction. * $p \leq 0.05$, ** $p \leq 0.01$. **(B) The effect the CM from stimulated CAF1s on the MCF7 migration was not due to residual hrTNFα**. The scratch assay was performed as described above. CAF1 CM collected after stimulation with TGFβ1 (2ng/mL) and two different concentrations of TNFα (12.5 or 5 ng/mL) was used. CM from unstimulated CAF1 cells and TNFα-spiked DMEM/F12 were also included as controls. In order to assess whether the MCF7 migration was caused by the TNFα remaining in the CM post stimulation, TNFα neutralization Ab (NAb) was added to the CM. The wound closure was determined using ImageJ. Each dot represents a technical replicate. The error bars are standard deviation.

4.4 CM from cytokine-activated CAFs induces STAT3 signaling in Lum A cancer cells

So far, I had observed that the CM from cytokine-activated immortalized CAF1 cells could confer a stronger migratory phenotype on the MCF7 and T47D cells, even more so than the CM from unstimulated CAFs (Figure 9A). However, the reason why was unclear. To gain insights into what pathways or proteins may play a role in the observed CM-induced phenotype, total protein lysates from MCF7 and T47D cells treated with CM from unstimulated and stimulated CAF1 cells, as well as with DMEM/F12 (negative control), were analyzed via reverse phase protein array (RPPA). The relative expression of 77 proteins involved in major cancer pathways was compared between each condition within each cell line (Figure 10A). Of all comparisons, very few passed the statistical significance test, with pSTAT3 (Y705) being the only protein significantly upregulated in both breast cancer cell lines in response to the treatment with CM from stimulated CAF1s (Figure 10B). Phosphorylation at residue Y705 of STAT3 suggested activation of the STAT3 pathway in the MCF7 and T47D cells upon exposure to factors secreted by the cytokine-activated but not by the unstimulated CAF1 fibroblasts.

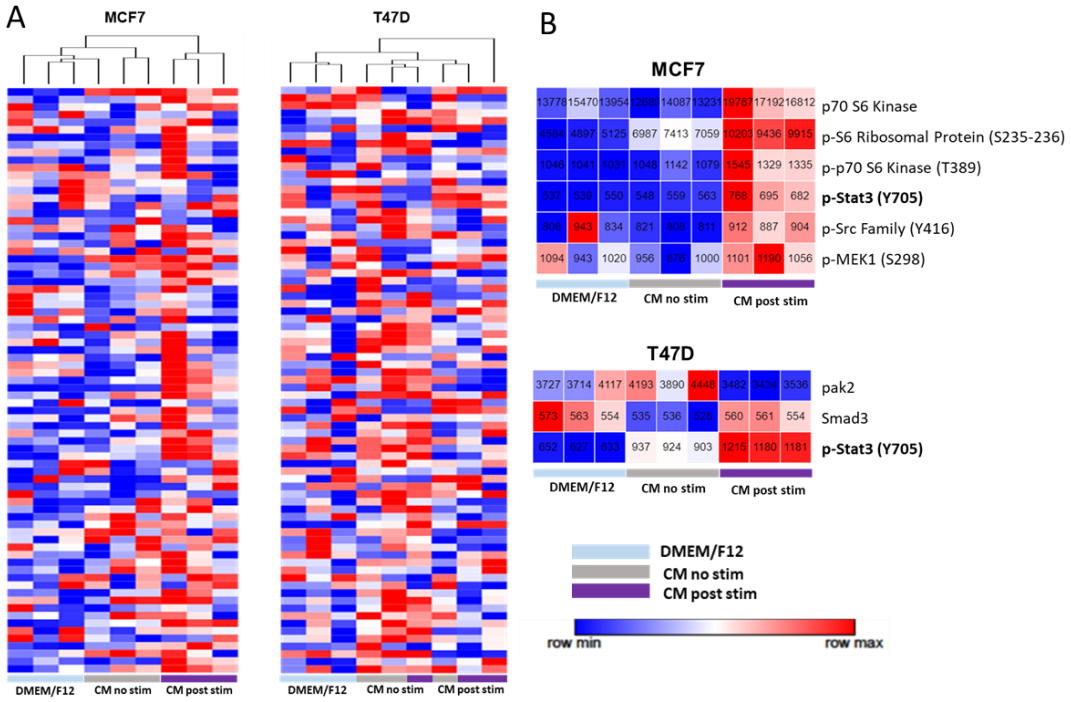

Figure 10. **RPPA analysis reveals induction of STAT3 signaling in the breast cancer cells upon treatment with cytokine-activated CAF CM.** MCF7 and T47D cells were treated for 24h with CM from unstimulated or cytokine-stimulated E6/E7 immortalized CAF1 cells (CM collected post TNFα(10ng/mL) and TGFβ1 (2ng/mL) stimulation). Treatment with DMEM/F12 was used as a control. (A) Heatmaps of the expression level of 77 proteins as assessed via RPPA (reverse phase protein array). For the clustering, Euclidean distances and average linkage were used. Blue and red represent lower and higher protein levels, respectively, within each row. Each rectangle is a biological replicate. (B) Heatmap of all proteins with significantly different expression between the CM no and CM post stimulation conditions as assessed via RPPA. The statistical significance was determined using a two-tailed t-test assuming unequal variance. Each square is a biological replicate. The number in the middle of each square is the corresponding normalized protein expression value.
All heatmaps were generated using the Morpheus software of the Broad Institute (https://software.broadinstitute.org/morpheus, accessed on March 2nd, 2022).

4.5 CAF-secreted IL6 induces STAT3 signaling in MCF7 cells

TNFα is known to induce secretion of IL6 (Tanabe *et al*., 2010). Thus, IL6 was the obvious candidate for induction of phenotypes in the cancer cells. Moreover, it has been reported to elicit STAT3 signaling (Toth *et al*., 2011). Hence, I hypothesized that IL6 presence in the CM post stimulation could thus explain the increase of pSTAT3 (Y705) observed in the cancer cells upon treatment with CM from TNFα+TGFβ1-stimulated CAFs (Figure 10B). Therefore, I next investigated whether IL6/STAT3 signaling played a role also in the migratory phenotype of MCF7 cells. First, I tested whether the CAFs indeed secreted IL6, and whether TNFα contributed to this secretion. Indeed, I could detect IL6 in CAF CM via FLISA, and the levels of secreted IL6 increased upon stimulation with TNFα (Figure 11A). Then, with a WB (Figure 11B), I confirmed that STAT3 signaling was activated in the MCF7 cells upon treatment with stimulated CAF1 CM, and that this was brought about by factors secreted by the CAF1s in response mainly to the TNFα. The responsible secreted factor was most likely IL6, since adding IL6 neutralization antibody to the CM attenuated its ability to induce STAT3 phosphorylation (Figure 11B). However, in an MCF7 migration assay, an IL6 neutralization Ab failed to abrogate the effect of the stimulated CAF1 CM, therefore showing that the increase in migration was most likely not due to CAF-secreted IL6 (Figure 11C).

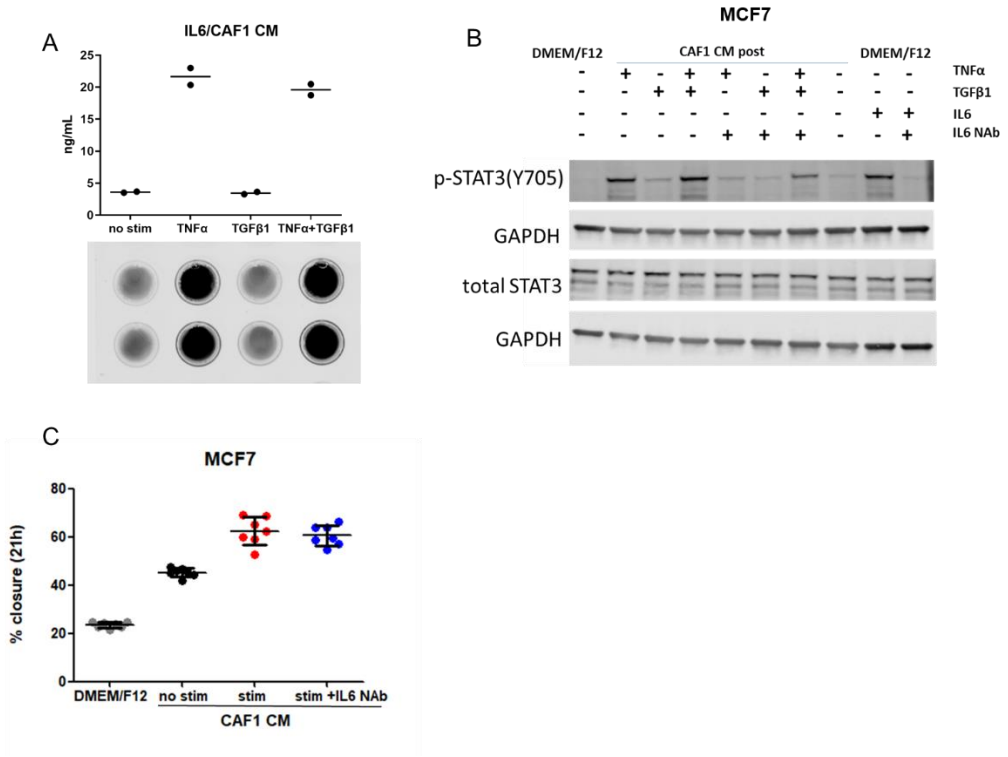

Figure 11. **Investigation of STAT3 signaling in the MCF7 cells post treatment with CAF1 CM. (A) IL6 FLISA.** IL6 was secreted at higher levels by the CAF1s upon treatment with TNFα or the double stimulation. **(B) Western blot.** MCF7 cells were treated for 20 min with CAF1 CM -/+ IL6 neutralization antibody (enough to neutralize 40ng/mL IL6). The STAT3 signaling was activated in the MCF7s treated with CM post TNFα or double stimulation. The STAT3 phosphorylation was at least partially due to IL6, since it could be diminished by addition of IL6 NAb. **(C) Migration assay**. Adding IL6 neutralization Ab (NAb) to the CAF1 CM did not affect its ability to induce migratory phenotype in the MCF7 cells.

4.6 The pro-migratory CAF-secreted factors are most likely of a protein origin

Now that I had eliminated the obvious candidate, namely IL6, I proceeded to investigate whether the factor(s) responsible for the migratory phenotype was/were of a protein nature to begin with. To this aim, heat inactivation of the conditioned medium was performed prior to using it for the scratch assays. When heat inactivated CM was used, the effect of the CM on the migration was diminished proving that the responsible factors were most likely proteins (Figure 12).

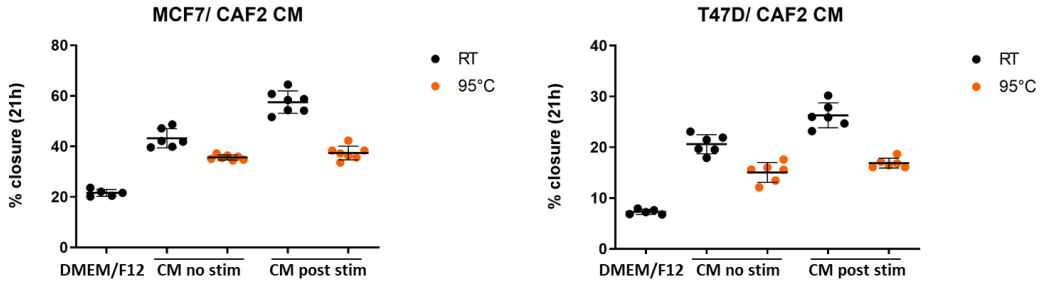

Figure 12. **Heat inactivation of the CAF conditioned medium attenuated the ability of the CM to induce migration.** MCF7 and T47D cells treated with heat inactivated CM migrated to a lesser extent than when treated with corresponding intact CM. Each dot represents a technical replicate. The error bars represent the standard deviation. The experiment was repeated 3 times for each cell line. Similar results were obtained also when CAF1 CM was used. Representative data shown.

4.7 CAF-secreted high molecular weight proteins are the drivers of the breast cancer migration

Next, to identify whether low or high molecular weight proteins drove the migratory phenotype, the CM was fractionated using size exclusion filters with 50kDa cut-off. Both CM fractions, as well as the respective control CM (no fractionation), were used to repeat the scratch assays. The data suggested that the CAF-secreted proteins conferring higher migratory phenotype on the breast cancer cells were of molecular weight greater than 50 kDa (Figure 13).

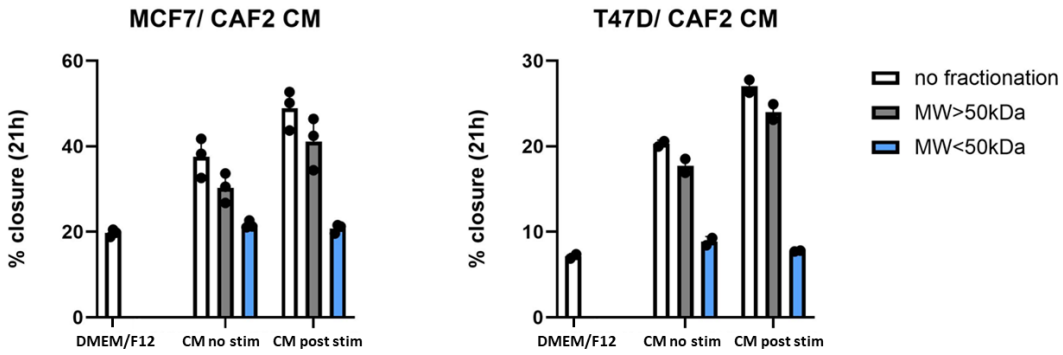

Figure 13. **The CAF-secreted proteins responsible for the observed higher breast cancer migration were of molecular size above 50 kDa.** MCF7 and T47D cells treated with fractionated CM migrated similarly as to when treated with the intact CM (white bars) only when the higher molecular weight fraction (MW>50 kDa, gray bars) was used. The lower molecular weight fraction (MW<50kDa, blue bars) did not induce migration. Each dot is a biological replicate and the average of 5 technical replicates. The error bars are SEM.

4.8 Mass spectrometry analysis of CAF1 CM

When E6/E7 immortalized CAF1 cells were used, single stimulations with only TNFα or only TGFβ1 were not sufficient to induce the observed CM effect on the MCF7 migration. Only the double stimulation led to the secretion of proteins able to confer a higher migratory phenotype on the cancer cells (Figure 14A). To identify the protein factors, which the CAF1s secreted upon stimulation, a mass spectrometry-based approach was used (Figure 14A). Briefly, conditioned medium from CAF1s untreated or treated with single and double stimulations was collected and concentrated, the proteins were extracted from the CM and submitted to the DKFZ Genomics and Proteomics Core Facility for analysis via label-free mass spectrometry, which allowed for relative quantitation of the secreted proteins (Figure 14B).

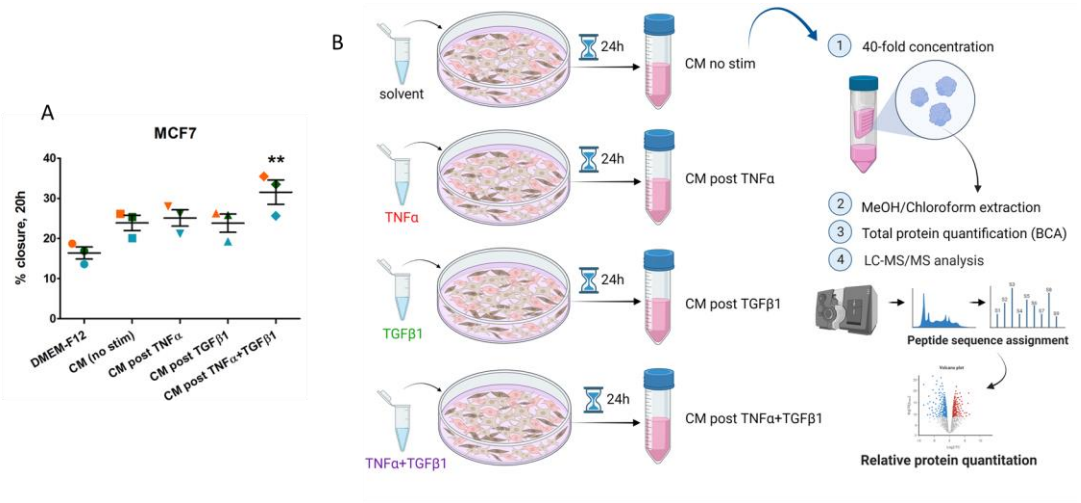

Figure 14. **Mass spectrometry analysis of CAF1 CM: rationale and workflow. (A) Scratch assays** showed that only CM from immortalized CAF1 fibroblasts stimulated with both cytokines significantly enhanced the migratory potential of MCF7 cells. Each dot is a biological replicate and the average of 5 technical replicates. Statistical analysis was performed using a one-way ANOVA test followed by Bonferroni correction. Values were compared to the negative control DMEM-F12. ** $p \leq 0.01$. **(B) Secretome analysis workflow**. Fibroblasts were stimulated with solvent (nuclease-free water), TNFα alone (10ng/mL), TGFβ1 alone (2 ng/mL), or both. The CM was collected 24h later and processed for HPLC-MS secretome analysis. Stim stands for stimulation, and CM for conditioned medium. Image created with BioRender.

In total 4170 peptides corresponding to 484 proteins could be identified in the CAF1 CM via mass spectrometry. Of those 483 proteins could be quantified, and 377 were detected in more than one sample out of the 12 analyzed. These 377 proteins were used for further expression analysis with the Morpheus software (https://software.broadinstitute.org/morpheus). Pearson correlation hierarchical clustering (Figure 15) of all samples showed that the effect of the double stimulation on the secretome was closely related to the impact of the stimulation with TNFα alone. The biological replicates clustered relatively well with each other. A group of proteins seemingly upregulated only in response to the double stimulation could be identified (Figure 15, enlarged part of the heatmap). Among these proteins were collagens and proteoglycans, major components of the extracellular matrix.

Next, two-sample *t*-tests were performed by Martin Schneider at the Proteomics core facility to determine which secreted proteins were significantly upregulated or downregulated due to the different stimulations. Any protein with a log2 fold change higher than 2 or less than -2 was considered differentially expressed, if the adjusted *p* value was less than 0.05. The volcano plots in Figure 16A-C illustrate the effect of the stimulations on the expression of the detected CAF1-secreted proteins. Comparison of the lists of upregulated proteins in each condition (Figure 16D) suggested that the effects of the double stimulation (Figure 16A) were brought about mainly by the TNFα (Figure 16B), while TGFβ1 had a minor role in affecting the CAF1 secretome (Figure 16C). This was in agreement with the results from the hierarchical clustering (Figure 15). Stimulation with TNFα alone led to the upregulation of 21 proteins. The double stimulation resulted in the overexpression of 24 proteins, while the TGFβ1 – of only 6 proteins (Figure 16D). Of the 24 proteins upregulated in response to the double stimulation, six were significantly overexpressed exclusively only when the double stimulation was used (Figure 16D, Table 9).

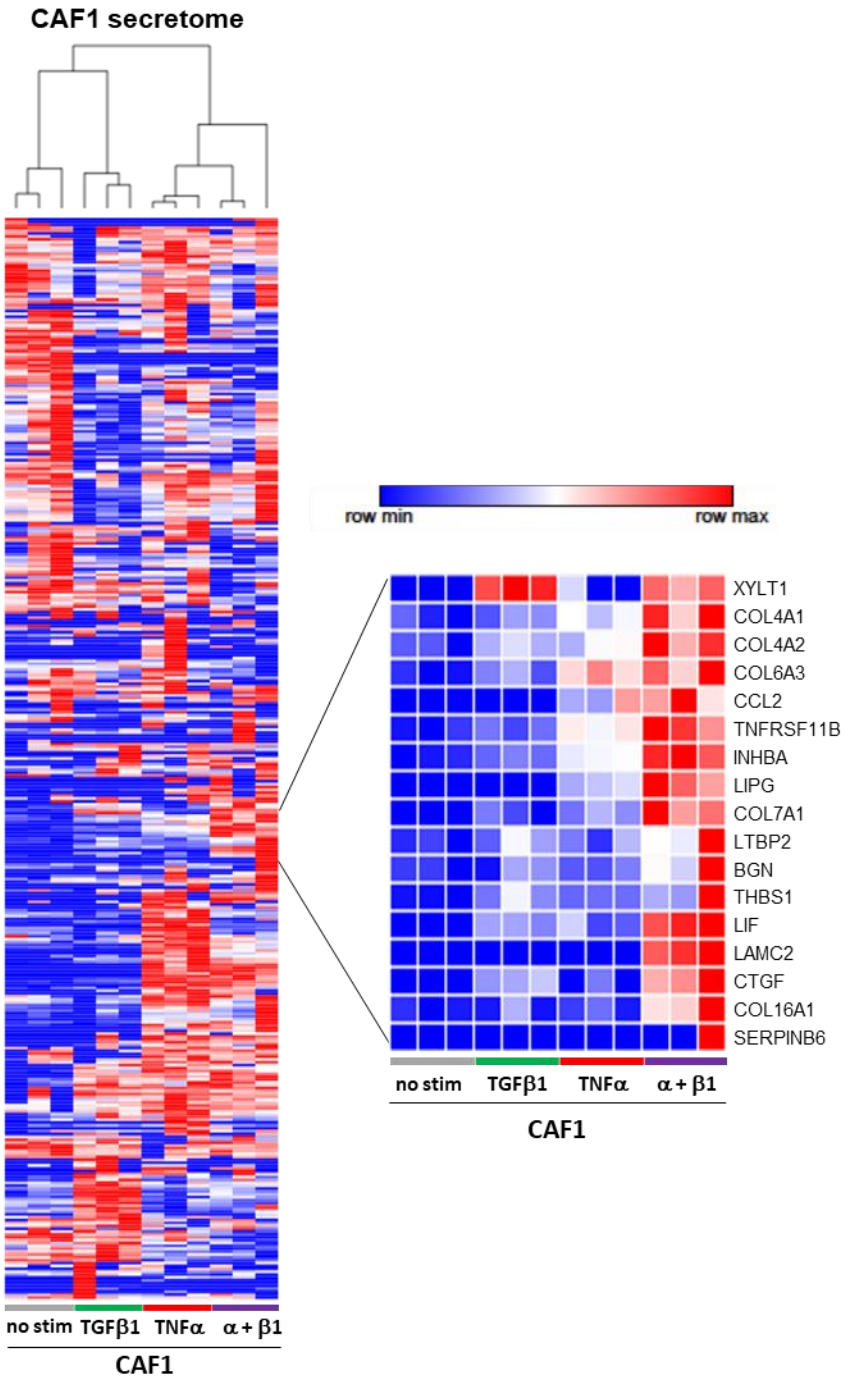

Figure 15. **Heatmap portraying the effect of the various cytokine stimulations on the CAF1 secretome.** The dendrogram shows the Pearson correlation hierarchical clustering (average linkage) of the samples. The comparison is based on similarities in protein expression measured in LFQ values as detected via label-free mass spectrometry analysis of the CAF1 CM. Each row represents one protein (377 proteins in total). Blue and red represent lower and higher LFQ values, respectively, within each row/protein. Three biological replicates per each condition. On the right is the portion of the heatmap which represents mainly proteins upregulated only upon the double stimulation (red only in the α+β1 condition). The heatmap was generated using the Morpheus software of the Broad Institute https://software.broadinstitute.org/morpheus, accessed on February 18th, 2022.

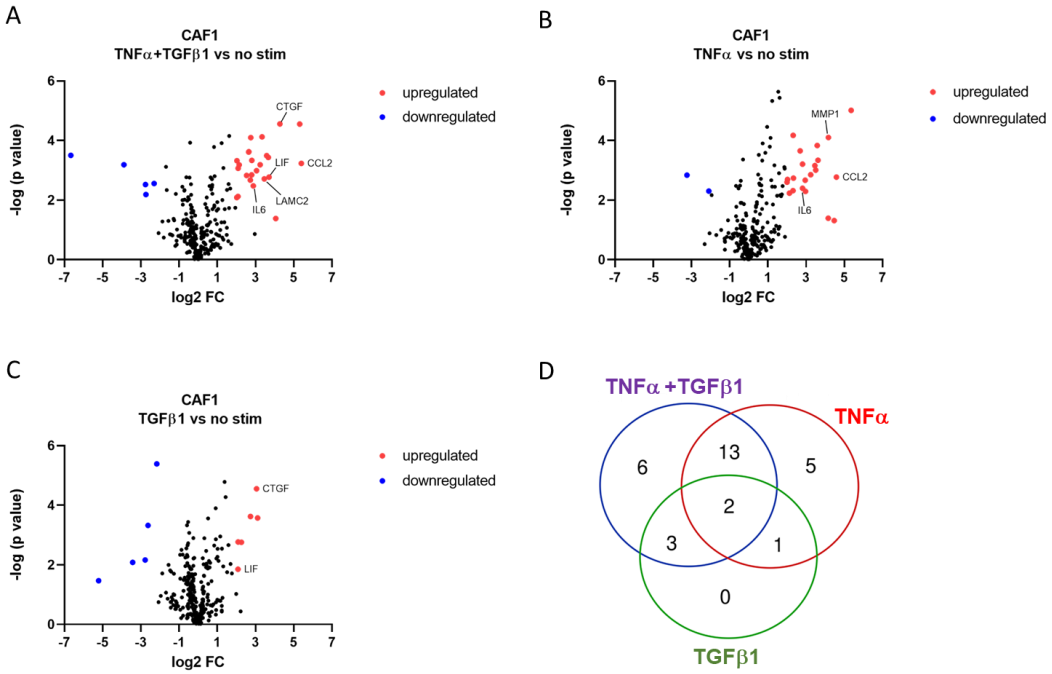

Figure 16. **The stimulation changes the CAF1 secretome. (A-C) Volcano plots** showing the secreted proteins differentially expressed between the 24h-stimulated and the unstimulated CAF1 cells as detected via Mass spectrometry analysis of the corresponding CAF1 CM. The significantly upregulated and downregulated proteins (adjusted *p* value <0.05, log2 fold change >2 or <-2, respectively) are illustrated in red and blue, respectively. The volcano plot in (A) shows the effect of the double stimulation (TNFα+TGFβ1), while the plots in (B) and (C) – the effect of the single stimulations, TNFα alone and TGFβ1 alone, respectively. The black dots are the proteins, which are not significantly changed. **(D) Venn diagram** of the significantly upregulated CAF1-secreted proteins (adjusted *p*-value <0.05, log2 fold change >2, the red dots in A-C) in response to the three different stimulations. There are six proteins, which are significantly upregulated only when the double stimulation is used.

Table 9. CAF1-secreted proteins significantly upregulated only upon double stimulation as determined by Mass spectrometry analysis of the CAF1 CM.

Protein	***Gene***	***Log2 FC***	***q value***	***# Unique peptides***
Laminin -γ2	*LAMC2*	3.456	0.0056	11
Lipase G	*LIPG*	2.796	0.0058	4
Collagen alpha-1 (VII)	*COL7A1*	2.749	0.0000	16
Inhibin Beta A chain	*INHBA*	2.648	0.0000	20
TNFRSF11B	*TNFRSF11B*	2.146	0.0067	15
Cystatin C	*CST3*	2.017	0.0061	3

4.9 Further analysis of the involvement of laminin gamma 2 in the breast cancer migration

Based on the CAF1 secretome analysis via mass spectrometry, I could identify 6 proteins, which were significantly upregulated only upon the double stimulation (Table 1; log2 FC >2, *q* value <0.05). Of those proteins, I initially chose to focus on the glycoprotein laminin-γ2 encoded by *LAMC2*. Among the proteins detected with a significant number of unique peptides, LAMC2 had the highest log2 fold change. I was also able to detect it with a WB, and to show once again that its expression was higher upon the stimulation with the cytokines (Figure 17A). Based on the above findings, I hypothesized that upon activation with TNFα and TGFβ1, the CAF1 fibroblasts secreted laminin-γ2, which then could induce migration of the breast cancer cells (Figure 17B).

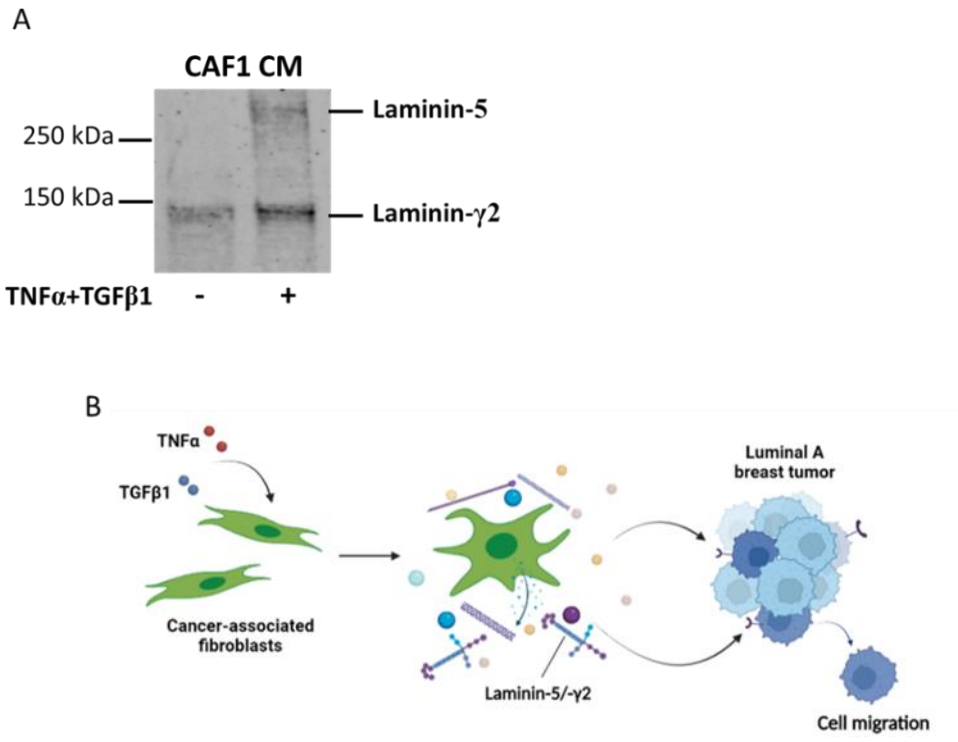

Figure 17. **(A) Detection of laminin-γ2 in the CM as confirmed by WB**. CM was collected from unstimulated and pre-stimulated CAF1 cells and concentrated. The total protein was isolated via a methanol/chloroform extraction and SDS-PAGE was performed. **(B) Proposed mechanism.** Upon stimulation with TNFα and TGFβ1, the CAF1s secrete laminin-γ2, which then can lead to increased breast cancer cell migration. Image created with BioRender.

To test the hypothesis that LAMC2 is the factor responsible for the breast cancer migration, I knocked down *LAMC2* in the CAF1 cells prior to stimulating them with the cytokines. The CM was then collected and used to repeat the migration assay with the MCF7 cells (Figure 18A). The KD was successful and importantly, it was able to abrogate the effect of the stimulation (Figure 18B). The MCF7 cells treated with the CM from the *LAMC2* KD CAFs did not migrate as much as the MCF7 cells treated with CM from the CAFs transfected with control siRNAs (Figure 18B). Further analysis, though, with siRNAs against *LAMC2* from a second vendor (Figure 18C), a second batch of siRNAs from our usual vendor (Figure 18D), as well as CM from *LAMC2* overexpression CAF1 cell line (Figure 18E), showed no relation between the observed MCF7 migration (Figure 18C-E) and the level of expression of *LAMC2* by the fibroblasts (Figure 18F-H).

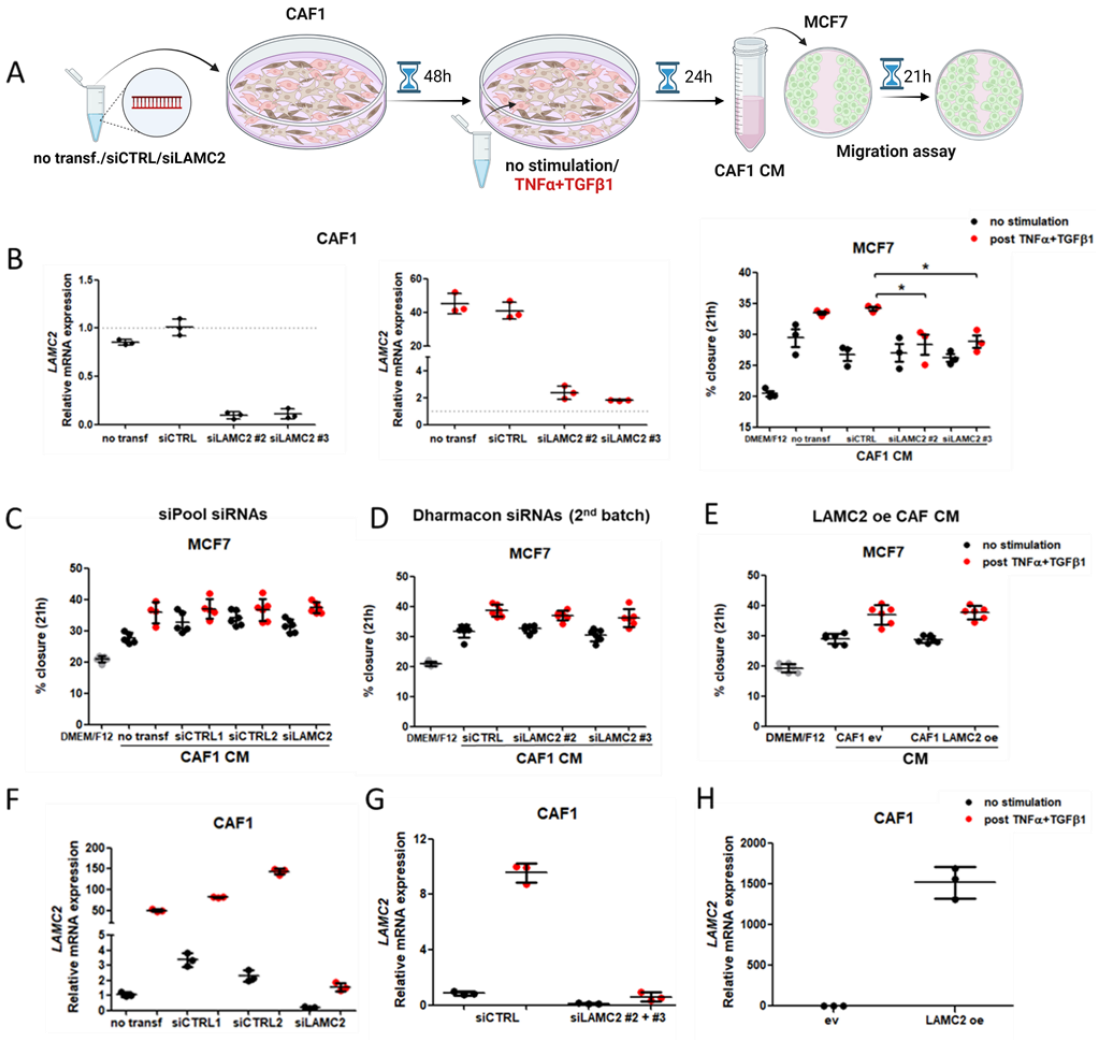

Figure 18. **Target validation. (A) Experimental scheme.** Created with BioRender. **(B) Initially siRNA-mediated knock-down of *LAMC2* in the fibroblasts** (on the left) **reduced the ability of the CM to induce MCF7 cell migration** (on the right). Each dot in the graph on the right represents a biological replicate and is the mean of 5 technical replicates. Each condition was compared to all others. Statistical analysis was performed using a one-way ANOVA test followed by Bonferroni correction, * $p \leq 0.05$. Statistical significance shown only for the most relevant comparisons. The error bars represent the standard deviation from the mean value of three biological replicates. **(C-H) Further validation** with siRNAs purchased from a different vendor (siPools, **C**), a second batch of siRNAs from the initial vendor (Dharmacon, **D**)**,** as well as CM from *LAMC2* overexpressing CAFs **(E)** suggested LACM2 was not essential for the observed migration**.** The error bars represent standard deviation. **(F) siPool siRNA-mediated and (G) second batch Dharmacon siRNA-mediated knockdown efficiency. (H) Validation of LAMC2 overexpression in the LAMC2 oe CAF1 cell line.**

4.10 The stimulation with TNFα alone is sufficient to increase the secretion of pro-migratory proteins by primary CAFs

As suggested by the MCF7 migration results in Figure 14A, the stimulations with only TNFα or only TGFβ1 were not sufficient to activate the E6/E7 immortalized CAF1 cell line. Only the double stimulation, in comparison to the no stimulation, was able to lead to the secretion of factors that then induced higher migratory potential on the MCF7 cells. I wanted to verify whether that was also true for other primary CAF cell lines, which have not been immortalized, as well as for the precursor CAF1 cells (primary CAF1s) from which the E6/E7 immortalized CAF1 cell line had been created. The migration assay was performed with CM from unstimulated, TNFα-, TGFβ1- and TNFα+TGFβ1- stimulated primary CAF cell lines (Figure 19). As expected, in terms of its ability to induce migration, the CM from TGFβ1-stimulated primary CAFs performed as efficiently as the CM from unstimulated primary CAFs. However, surprisingly, higher migratory phenotype was conferred on the MCF7 cells in the presence of CM from primary CAFs, which have been prestimulated with only TNFα or both cytokines (TNFα+TGFβ1). Thus, in contrast to the data generated with CM from E6/E7 immortalized CAF1 cells (Figure 14A), the stimulation with TNFα alone appeared to be sufficient to induce the secretion of pro-migratory factors when the source was a truly primary CAF cell lines (Figure 19).

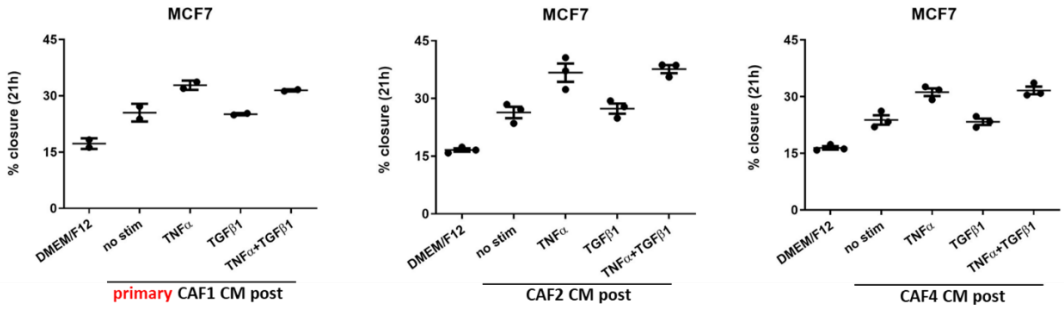

Figure 19. **Scratch assay with CM collected from three primary CAF cell lines**. Stimulation with TNFα is sufficient to increase the CAF CM ability to induce MCF7 migration. Each dot represents a biological replicate and is the average of 5 technical replicates. The error bars are SEM.

4.11 Total proteome analysis reveals induction of IFN signaling in the CAFs in response to TNFα

To complement the CAF1 secretome data, and to gain more insight into the effect of the stimulation on the CAFs, in addition to the CAF1 CM, I submitted for label-free mass spectrometry analysis also the corresponding immortalized CAF1 full protein lysates. In total 76,452 peptides corresponding to 5,445 proteins could be identified in the CAF proteome. Of those 5,441 proteins could be quantified. Pearson correlation hierarchical clustering (average linkage) of the 500 most variant proteins was performed using the Morpheus software (Figure 20A). As observed with the CM samples (Figure 15), the CAFs treated with the double stimulation clustered closer to the samples treated with TNFα alone. The enlarged portion of the heatmap shows the list of proteins seemingly upregulated in both the double and TNFα alone stimulations (Figure 20A). A comparison of this list with the interferon-α and -γ response molecular gene signatures (obtained from the Molecular Signature Database, version 7.5.1) suggested upregulation of interferon signaling in the CAFs in response to the TNFα/double stimulation (Figure 20B). Of 57 proteins potentially up in the CAFs post treatment with TNFα or double stimulation, 36 were encoded by genes known to be upregulated in response to interferon-α and/or -γ. However, interferons were not detected in either of the two mass spec analyses most likely due to their low abundance and small molecular size.

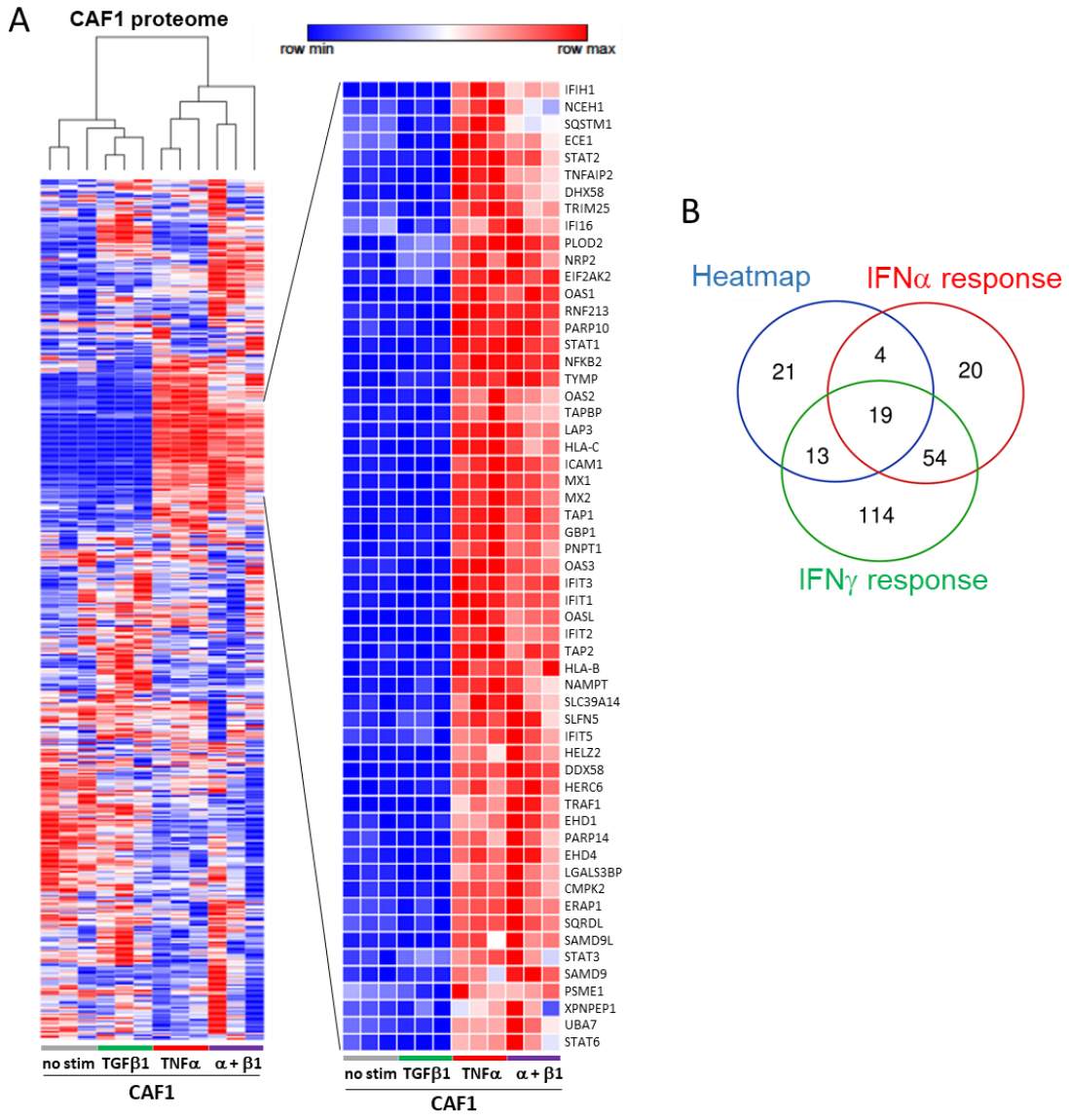

Figure 20. **Effect of the various cytokine stimulations on the CAF1 proteome. (A) Heatmap of the 500 most variant CAF1 proteins.** The dendrogram shows the hierarchical clustering of the samples based on Pearson correlation (average linkage) of LFQ values as detected via label free mass spectrometry analysis of stimulated and unstimulated CAF1 protein lysates. Blue and red represent lower and higher LFQ values, respectively, within each row/protein. Three biological replicates per condition were analyzed. On the right is the portion of the heatmap which represents mainly proteins upregulated only upon the double and TNFα stimulations (red only in the α+β1 and the TNFα conditions). The heatmap was generated using the Morpheus software of the Broad Institute (https://software.broadinstitute.org/morpheus, accessed on February 16th, 2022)**. (B) Venn diagram** illustrating the overlap between 1) the proteins seemingly upregulated in the CAF1 cells in response to the TNFα and the double stimulation (the proteins listed in the heatmap, blue circle in the Venn diagram), 2) the interferon-α (red) and 3) interferon-γ (green) response molecular gene signatures. The signatures were taken from the hallmark gene set collection of the Molecular Signatures Database (MSigDB, https://www.gsea-msigdb.org, accessed on February 18th, 2022).

To evaluate the statistical significance of the observed changes in protein expression due to the different stimulations, Student's *t*-tests were performed. Proteins with a log2 fold change higher than 2 or less than -2 were considered upregulated or downregulated, respectively. The second requirement was that the adjusted *p* value had to be less than 0.05. The volcano plots in Figure 21A-C illustrate the results from the *t*-tests. Overall, very few proteins were downregulated regardless of which stimulation was used. Similarly to the CM analysis (Figure 16D), the response to the double stimulation again seemed to be driven mainly by TNFα (Figure 21). The effect of TGFβ1 was rather minor with only 6 proteins upregulated in response to it (Figure 21C). Fifty of the 62 proteins upregulated due to the double stimulation were also overexpressed in response to the TNFα alone stimulation (Figure 21D). There were only 11 proteins which were overexpressed exclusively when the double stimulation was used (Figure 21D). Many of the proteins upregulated by TNFα or the double stimulation, e. g. OAS1, IFIH1, DDX58, IFIT1, ISG15 and ISG20, are encoded by the interferon stimulated genes (ISGs), suggesting that IFN signaling was activated in response to the stimulation (Figure 21A-B).

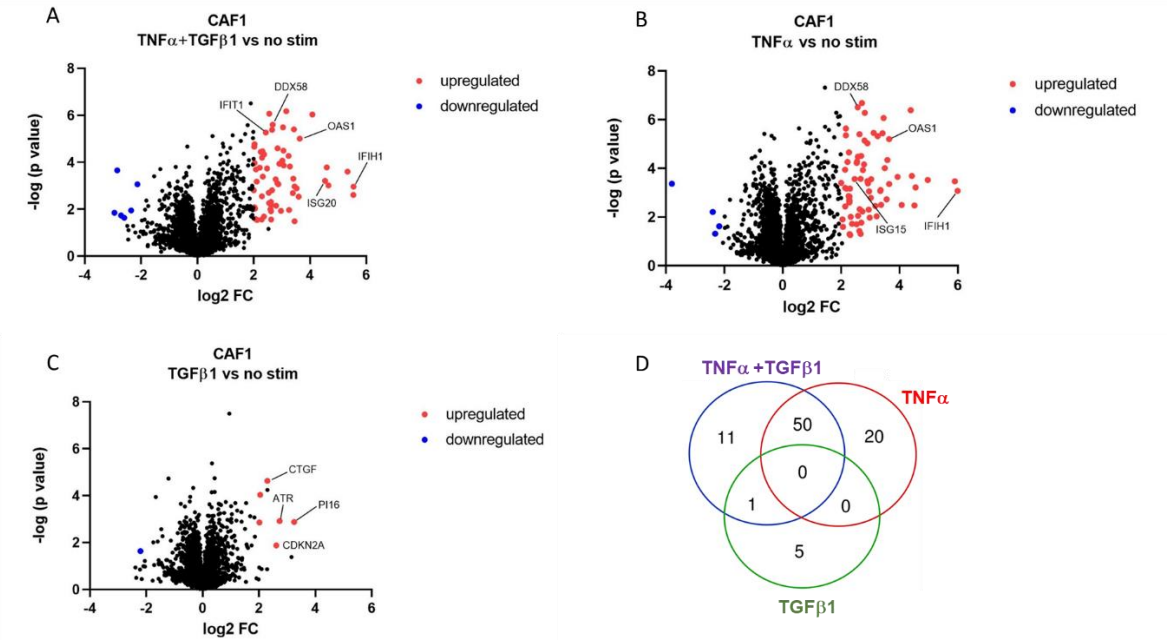

Figure 21. **The stimulation changes the CAF1 proteome. (A-C) Volcano plots** representing the proteins differentially expressed between the 24h-stimulated and the unstimulated CAF1 cells as detected via Mass spec analysis of the corresponding total protein lysates. The significantly upregulated and downregulated proteins (adjusted p value <0.05, log2 fold change >2 or <-2, respectively) are illustrated in red and blue, respectively. The volcano plot in (A) illustrates the impact of the double stimulation (TNFα+TGFβ1), while the plots in (B) and (C) - of the single stimulations, TNFα and TGFβ1, respectively. The black dots represent the proteins which expression is not significantly affected by the stimulations. **(D) Venn diagram** of the significantly upregulated CAF1 proteins (adjusted p-value <0.05, log2 fold change >2, namely the red dots in A-C) in response to the three different stimulations.

Next, to find out the pathways enriched in the CAFs in response to the stimulations, Fisher exact test was performed by Martin Schneider from the DKFZ core facility. This test allowed for comparison of the list of significantly upregulated proteins in each condition to proteins known to be involved in signaling pathways according to publicly available databases, such as GOBP (Gene Ontology Biological Process) and Reactome. Thus, it was revealed that the double stimulation (Figure 22) and the stimulation with TNFα alone (Figure 23) both led to induction of interferon signaling and anti-viral/inflammatory response. The stimulation with TGFβ1 alone affected a relatively smaller set of pathways and seemed to play a role mainly in ECM organization and collagen synthesis (Figure 24).

Overall, the results from the mass spectrometry analysis of the CAF proteome showed that TNFα alone was sufficient to induce the expression of the proteins encoded by the so-called ISG genes (interferon-stimulated genes). Also, the effects of the double stimulation on protein expression and signaling were mainly driven by the TNFα and pointed towards activation of interferon signaling.

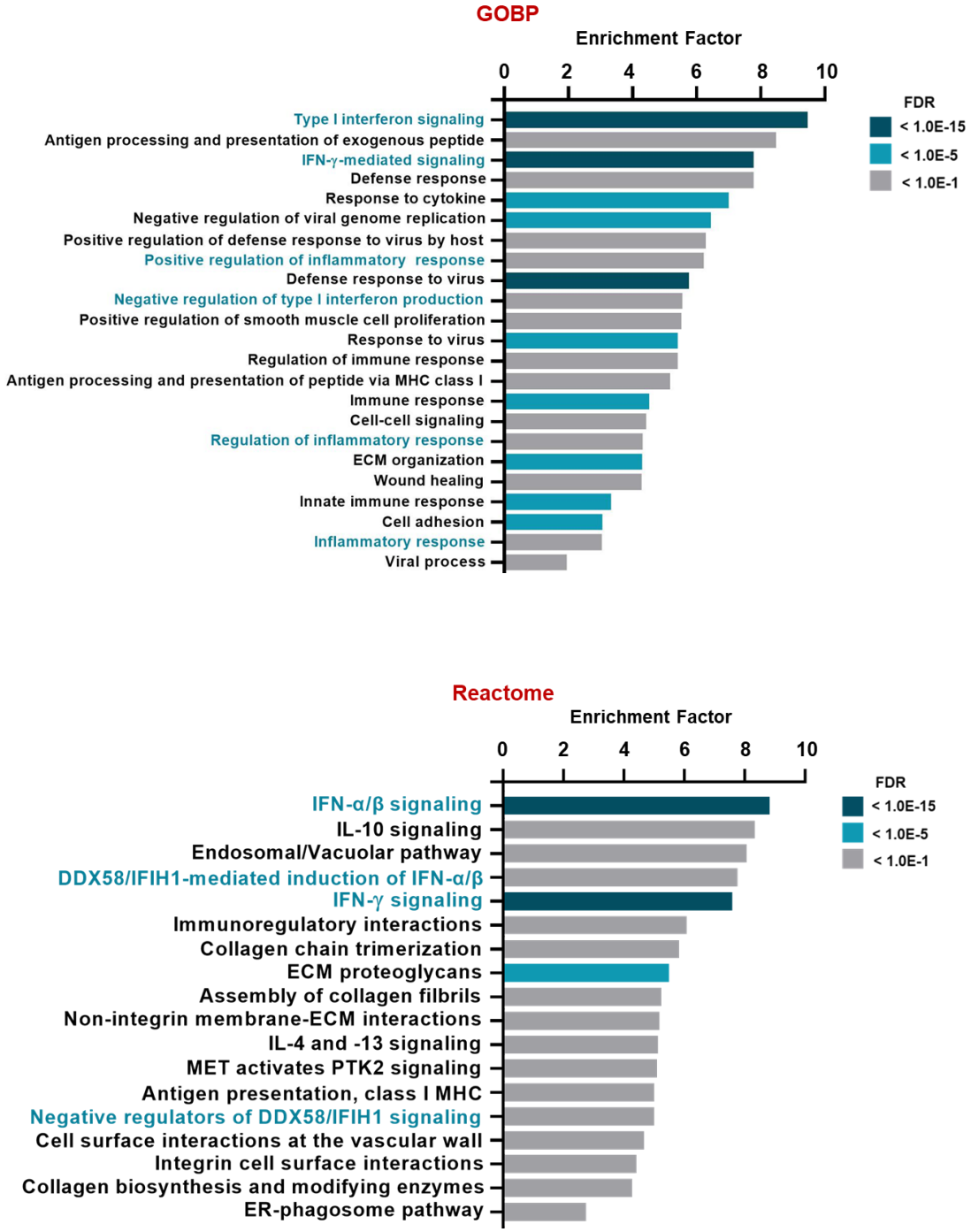

Figure 22. **Pathway enrichment analysis** (Fisher exact test) for proteins expressed differentially between **CAF1s treated with the double stimulation and their untreated counterparts**. Based on data collected via label free mass spectrometry analysis of the CAF1 full proteome post 24h-stimulation with 10 ng/mL TNFα and 2 ng/mL TGFβ1. Marked in turquoise are all the pathways or terms related to interferon signaling. FDR: false discovery rate.

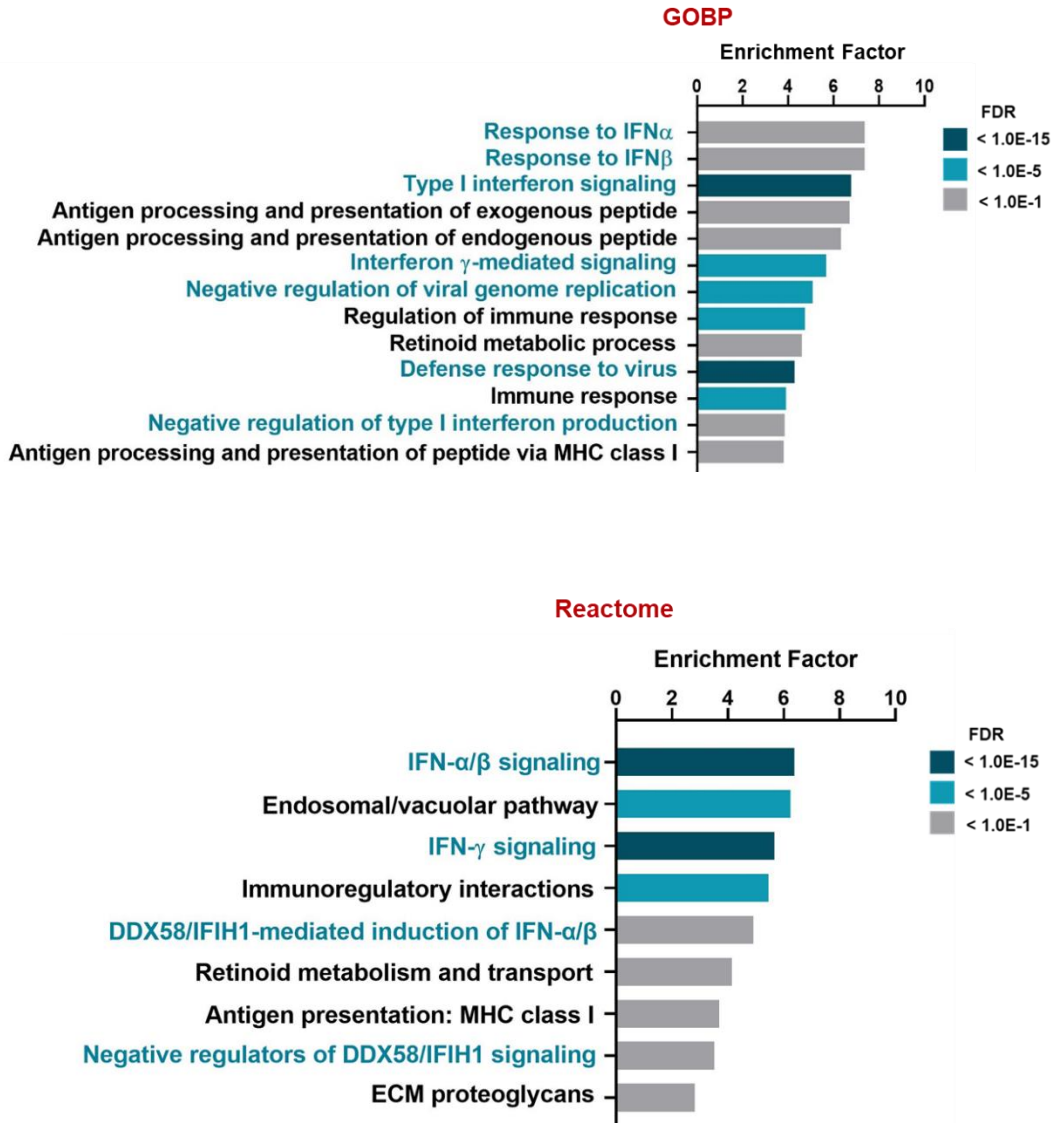

Figure 23. **Pathway enrichment analysis** (Fisher exact test) for proteins expressed differentially between **CAF1s treated with TNFα and their untreated counterparts**. Based on data collected via label free mass spectrometry analysis of the CAF1 full proteome post 24h- stimulation with 10 ng/mL TNFα. Marked in turquoise are all the pathways or terms related to interferon signaling. FDR: false discovery rate.

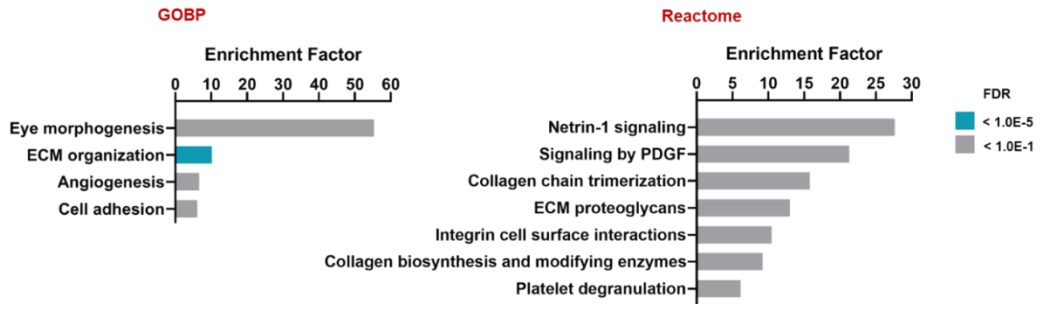

Figure 24. **Pathway enrichment analysis** (Fisher exact test) for proteins expressed differentially between **CAF1 cells treated with TGFβ1 and their untreated counterparts.** Based on data collected via label free mass spectrometry analysis of the CAF1 full proteome post 24h- stimulation with 2ng/mL TGFβ1. FDR: false discovery rate.

4.12 IFN signaling is induced in MCF7 cells upon treatment with CM from stimulated CAFs

To investigate the effect of the CAF1 CM on the MCF7 cells in terms of gene expression changes, RNA-sequencing was performed. Briefly, I treated MCF7 cells with CM from stimulated (TNFα+TGFβ1) and non-stimulated CAFs and to compare the two groups, I isolated total RNA and submitted it to the DKFZ sequencing core facility (Figure 25A). The treatment with cytokine-stimulated CAF1 CM resulted in upregulation of interferon signaling in the MCF7 cells, as shown by Gene set enrichment analysis (GSEA) performed by Dr. Birgitta Michels (Figure 25B). In support of that, a PROGENy (Pathway RespOnsive GENes) pathway enrichment analysis performed by Dr. Efstathios-Iason Vlachavas, also showed that JAK/STAT signaling was upregulated significantly in the MCF7, when they were treated with CM from stimulated CAF1s (versus when treated with CM from unstimulated CAF1s) (Figure 25C).

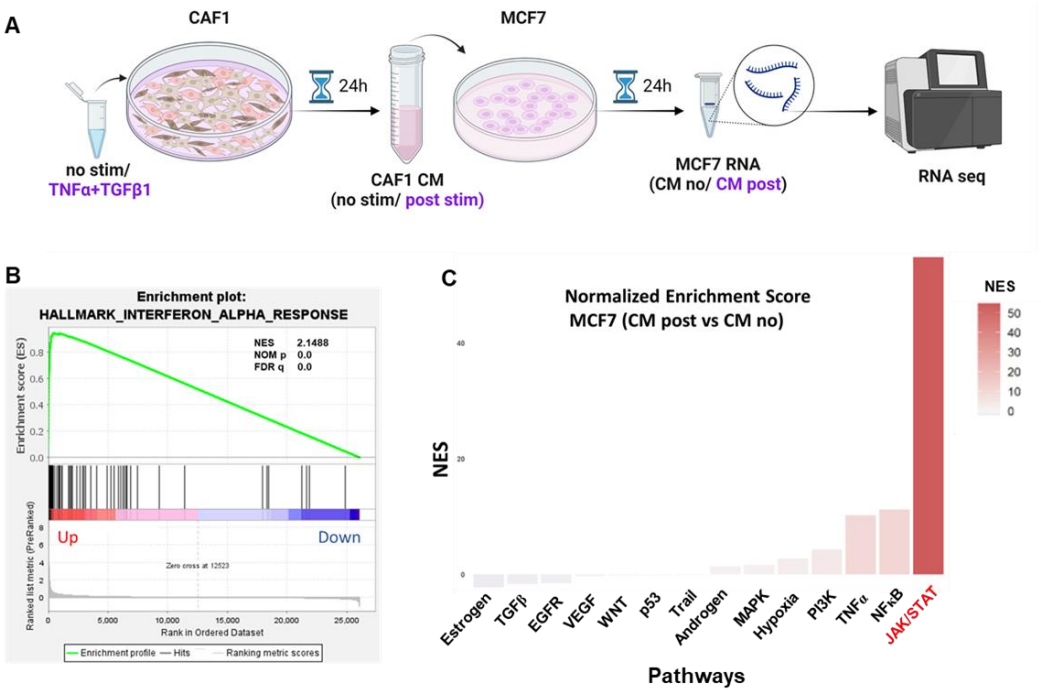

Figure 25. **RNA-seq analysis of MCF7 cells treated with CM from cytokine-activated fibroblasts (CM post) reveals upregulation of the interferon-JAK/STAT signaling pathway. (A) Experimental scheme.** CAF1s were stimulated with TNFα and TGFβ1 for 24h. CAF CM was collected and used to treat MCF7 cells for 24h, prior to isolating their RNA and submitting it for RNA-seq. Image created with BioRender. **(B) Gene set enrichment analysis.** Interferon alpha/beta signaling pathway was upregulated in the MCF7 cells upon treatment with CM post in comparison to MCF7s treated with CM from unstimulated CAFs. The GSEA was performed by Dr. Birgitta Michels. **(C) PROGENy normalized enrichment score (NES) analysis**. The JAK/STAT signaling was the most significantly activated pathway in the MCF7 cells treated with CM post. The NES analysis was performed by Dr. Efstathios-Iason Vlachavas.

The full results of the GSEA are summarized in Table 10, which lists the name of all gene sets found to be significantly upregulated (FDR *q*-value <0.05) in the MCF7 cells post treatment with CM from TNFα+TGFβ1-activated CAF1 cells in comparison to their counterparts treated instead with CM from unstimulated CAF1 cells. The size of each gene set, and the degree of enrichment (NES, normalized enrichment score) are also indicated. The IL6/JAK/STAT3 signaling gene signature was enriched in the MCF7 cells treated with CM from stimulated CAFs (Table 10), in agreement with the RPPA data (Figure 10B), as well as with data obtained with Western blot (Figure 11A), Moreover, STAT3 was among the upregulated transcription factor gene sets (Table 10). Furthermore, not only the inflammatory and interferon gamma/alpha responses but also several of the associated IRF (interferon regulatory factor)/ISRE (interferon-sensitive response element) gene sets were significantly enriched in the MCF7 cells treated with CM post (Table 10). Thus, the data presented so far suggested that the induction of interferon signaling in the CAFs observed after treatment with TNFα alone or TNFα+TGFβ1 double stimulation (Figure 20-23), could be relayed to the breast cancer cells via CAF-secreted factors, most likely interferons.

Table 10. Gene sets enriched in the MCF7 cells post treatment with CM from TNFα+TGFβ1-stimulated CAF1 cells (in comparison to MCF7 cells treated with CM from unstimulated CAF1s).
The GSEA was performed by Dr. Birgitta Michels.

Gene Set Name	Size	NES	NOM *p*-value	FDR q-value
HALLMARK_INTERFERON_GAMMA_RESPONSE	191	2.1878	0.0000	0.00E+00
HALLMARK_INTERFERON_ALPHA_RESPONSE	97	2.1488	0.0000	0.00E+00
HALLMARK_ALLOGRAFT_REJECTION	174	1.9006	0.0000	0.00E+00
HALLMARK_INFLAMMATORY_RESPONSE	184	1.8830	0.0000	0.00E+00
HALLMARK_IL6_JAK_STAT3_SIGNALING	82	1.8597	0.0000	2.84E-04
HALLMARK_COMPLEMENT	183	1.8591	0.0000	2.37E-04
HALLMARK_TNFA_SIGNALING_VIA_NFKB	188	1.7818	0.0000	6.22E-04
HALLMARK_KRAS_SIGNALING_UP	187	1.7083	0.0000	2.28E-03
HALLMARK_COAGULATION	122	1.6204	0.0023	1.06E-02
STTTCRNTTT_IRF_Q6	181	1.9491	0.0000	0.00E+00
IRF2_01	121	1.8917	0.0000	8.91E-04
IRF_Q6	237	1.8727	0.0000	5.94E-04
ISRE_01	238	1.8665	0.0000	6.69E-04
ICSBP_Q6	242	1.8473	0.0000	1.07E-03
IRF7_01	247	1.8320	0.0000	1.20E-03
STAT3_01	21	1.7563	0.0015	1.30E-02
IRF1_01	234	1.7447	0.0000	1.59E-02

Interferon α/β signaling is known to be relayed via the STAT1/2 transcription factors (TFs), which once activated, can bind to IRF9, thus forming the ISGF3 (interferon-stimulated gene factor 3) complex. This complex is then translocated to the nucleus where it binds the ISRE promoter and induces the expression of interferon-stimulated genes (ISGs). Further computational analyses (Figure 26) were performed by Dr. Efstathios-Iason Vlachavas to investigate the activation level of these transcription factors (relative to other TFs) in the MCF7 cells after they had been exposed to stimulated versus unstimulated CAF1 CM. To this end, he applied the DoRothEA (**D**iscriminant **R**egulon **E**xpression **A**nalysis) analysis tool (Garcia-Alonso *et al*., 2019). Indeed, STAT2 was the TF with highest normalized enrichment score (Figure 26A). STAT1, IRF1, -2, and -9 were also among the transcription factors with upregulated activity (Figure 26A). TF activity analysis was additionally run per sample basis, to also illustrate the relative TF activities per sample and the respective heterogeneity (Figure 26B). This representation (Figure 26B) also inferred upregulation of STAT1, IRF1, -2, and -9 activity. These findings are in agreement with the aforementioned GSEA results (Table 10).

It is worth mentioning that all three enrichment analyses, namely GSEA (Table 10), PROGENy (Figure 25C), and DoRothEA (Figure 26A/B), consistently suggested upregulation of the TNFα/NF-κB signaling pathway and an increased activity of its associated transcription factors, RELA and NF-κB in the CM post-treated MCF7 cells (which have been treated with CM from cytokine-stimulated CAFs). This was not surprising considering that the CM potentially contained residual human recombinant TNFα remaining from the stimulation, as well as TNFα expressed and secreted by the CAFs. In a way, the fact that the expected activation of the NF-κB pathway was detected by the different computational analyses could serve as evidence for their validity.

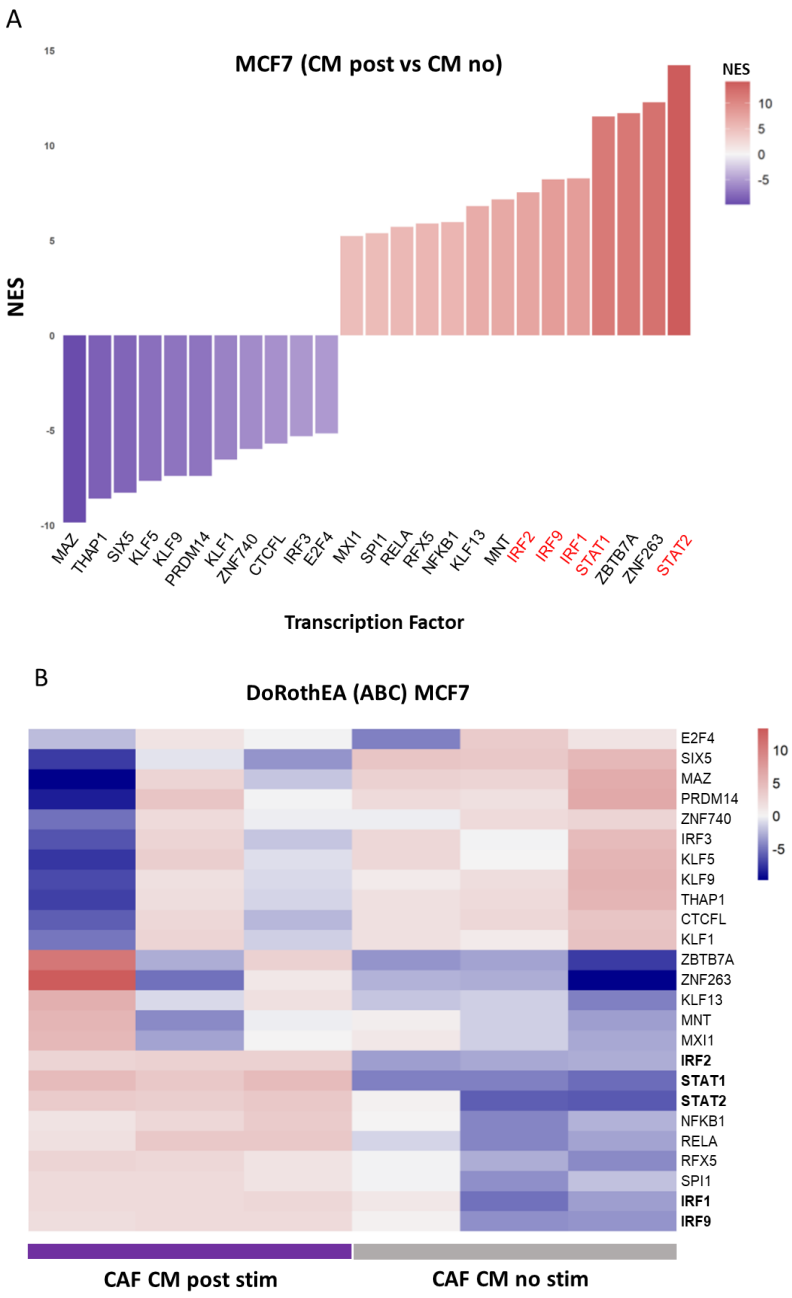

Figure 26. **Upregulation of STAT1/2 activity in MCF7 cells post treatment with CM from TNFα+TGFβ1-stimulated CAF1 cells.** DoRothEA analysis was performed to identify the most regulated TFs in the MCF7 cells upon treatment with CM from stimulated CAFs versus CM from unstimulated CAFs. **(A) Top 25 differentially activated TFs.** The depicted values in the y-axis represent the relative activity, with red and blue values showing activation and repression, respectively**. (B) Heatmap of the TF activities per sample.** Top 25 TFs with the highest absolute value of activity are shown. Samples with relatively high activity of the highlighted TF are marked in red and samples with relatively low activity are marked in blue**.** Three biological replicates per condition. ABC refers to the confidence levels (A being the highest). The analysis was performed and the plots were generated by Dr. Efstathios-Iason Vlachavas.

To confirm the findings from the computational analyses described so far, I investigated the expression levels of individual genes in the MCF7 RNA-seq data. Using the Morpheus software, I generated a heatmap of the 500 most variant genes (Figure 27A). The biological replicates (three per condition) clustered well together (Euclidean distances, average linkage). A group of genes (Figure 27A, the enlarged heatmap portion on the right) appeared to be overexpressed in the MCF7 cells, which had been treated with CM from TNFα+TGFβ1-stimulated CAF1 cultures. Next, I used a Venn diagram to overlap the list of these genes with the publicly available interferon-α and -γ response gene sets (MSigDB, https://www.gsea-msigdb.org, accessed on February 18th, 2022). Of the 76 genes which were up in the CM post-treated MCF7 cells, 47, meaning more than half, were implicated in interferon signaling (Figure 27B), thus confirming the results of the GSEA (Figure 25B, Table 10).

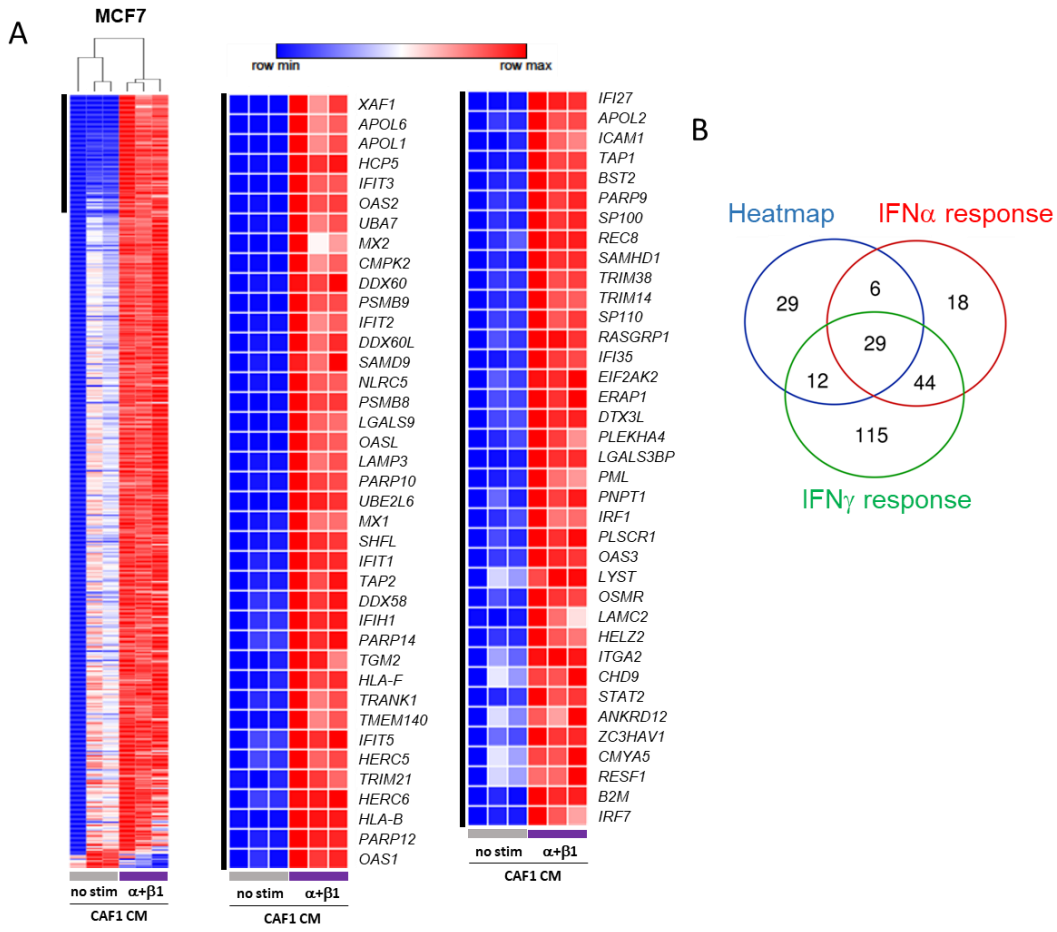

Figure 27. **The treatment with CAF CM collected post stimulation results in upregulation of interferon signaling in the MCF7 cells. (A) Heatmap of the 500 most variant genes** in MCF7 cells treated with CM from unstimulated and prestimulated immortalized CAF1 cells as evaluated via RNA-seq. The dendrogram shows the hierarchical clustering of the samples based on Euclidean distances (average linkage). Blue and red represent lower and higher expression, respectively, within each row/gene. Three biological replicates per condition were analyzed. On the right is enlarged the portion of the heatmap which represents genes with higher expression (red) in the MCF7 treated with CM from cytokine-stimulated CAFs (α+β1). The heatmap was generated using the Morpheus software of the Broad Institute (https://software.broadinstitute.org/morpheus, accessed on February 17th, 2022)**. (B) Venn diagram** illustrating the overlap between 1) the genes seemingly upregulated in the MCF7 cells in response to the CM from TNFα+TGFβ1-treated CAFs (the genes listed in the enlarged portion of the heatmap, blue circle in the Venn diagram), 2) the interferon-α (red) and 3) interferon-γ (green) response molecular gene signatures. The signatures were obtained from the hallmark gene set collection of the Molecular Signatures Database (MSigDB, https://www.gsea-msigdb.org, accessed on February 18th, 2022).

Although the heatmap gave good indication of the genes potentially upregulated in the MCF7 cells upon treatment with CM from cytokine-activated CAF1 fibroblasts, it did not provide information on statistical significance. Therefore, I used again the information from the DESeq2 analysis, which had been performed by Dr. Birgitta Michels on the MCF7 RNA-seq data (and had served already as input for the GSEA shown in Figure 25A and Table 10). This analysis allowed for the identification of the differentially expressed genes (DEGs) between the two sets examined, namely the MCF7 cells treated with stimulated versus unstimulated CAF1 CM. The genes with log2 fold change larger than 2 and adjusted *p* value smaller than 0.05 were defined as significantly upregulated. There were no significantly downregulated genes (log2FC<-2, adjusted $p<0.05$). The results from the DESeq2 analysis are summarized in a volcano plot (Figure 28A) with some of the upregulated genes indicated: *OAS2*, *IFIH1*, *DDX58* and *-60*, *IFIT1*, *-2*, and-*3*. Since these genes belonged to the ISG (interferon-stimulated gene) signature, next I overlapped the list of the MCF7 DEGs (Table 11) with the IFNα/γ response gene sets from the Molecular Signatures Database (ver. 7.5.1). More than half of the upregulated genes (i.e., 32) turned out to be involved in response to interferon signaling - 19 genes in IFNα, and 29 in IFNβ response (Figure 28B).

To sum up, according to the mass spectrometry analysis of the CAF1 proteome, the double stimulation clearly induced interferon signaling in the fibroblasts. Via secreted factors, the stromal cells could then relay the interferon signaling to the breast cancer cells, as revealed by RNA-seq analysis of the CAF1 CM-treated MCF7 cells.

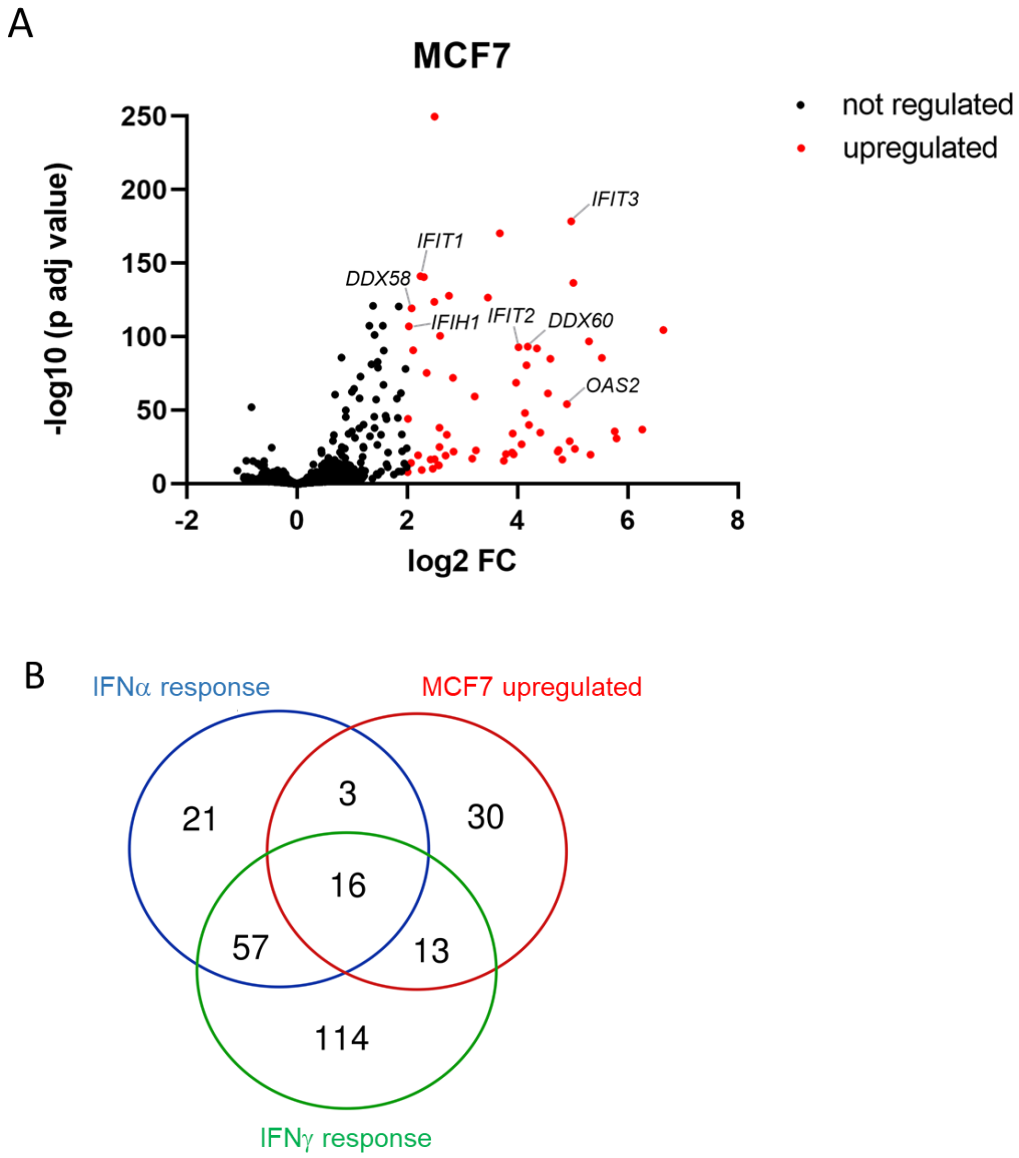

Figure 28. **RNA-seq analysis of the differentially expressed genes between MCF7 cells treated with CM from TNFα+TGFβ1-stimulated CAF1 cells and MCF7s treated with CM from unstimulated CAF1 cells**. (A) **Volcano plot** showing the differentially expressed genes as determined by DESeq2. Colored in red are the significantly upregulated genes (*p* adjusted <0.05 and log2 fold change >2), and in black – the genes which are not significantly changed. (B) **Venn diagram** showing the overlap between the genes upregulated in the MCF7 cells in response to the treatment with CM from stimulated CAF1 cells (red circle in B, red dots in A) and the interferon α (blue) and -γ (green) response molecular gene signatures. The signatures were obtained from the hallmark gene set collection of the Molecular Signatures Database (MSigDB, https://www.gsea-msigdb.org, accessed on February 18th, 2022).

Table 11. List of differentially expressed genes in MCF7 cells in response to treatment with CAF1 CM collected post stimulation (in comparison to MCF7 cells treated with CM from unstimulated CAF1 cells)

Gene	Log2 FC	*p* adj value	Gene	Log2 FC	*p* adj value
XAF1	6.65	3.77E-105	*NLRC5*	3.68	4.36E-171
IFI44	6.26	1.61E-37	*PSMB8*	3.47	2.36E-127
IFI44L	5.80	1.99E-31	*CIITA*	3.25	2.23E-23
TRIM22	5.76	3.68E-36	*GBP3*	3.22	6.30E-60
APOL6	5.53	2.50E-86	*CEACAM1*	3.18	9.07E-18
GBP1	5.32	2.36E-20	*CCL5*	2.84	1.74E-22
APOL1	5.30	2.11E-97	*LGALS9*	2.83	9.97E-73
CD74	5.04	2.15E-24	*OASL*	2.76	1.35E-128
HCP5	5.02	3.28E-137	*BISPR*	2.72	4.83E-34
IFIT3	4.97	4.20E-179	*KLHDC7B*	2.70	7.58E-20
PSMB8-AS1	4.95	1.46E-29	*LAMP3*	2.60	3.79E-101
OAS2	4.90	8.14E-55	*LCN2*	2.59	1.13E-25
APOL3	4.81	4.48E-17	*IRF1-AS1*	2.59	1.00E-38
RSAD2	4.75	1.45E-23	*GSDMC*	2.58	4.05E-13
BTN3A2	4.73	1.59E-22	*ENSG00000272941*	2.57	2.31E-13
UBA7	4.60	1.25E-85	*PARP10*	2.50	2.21E-250
BATF2	4.55	4.15E-62	*PLAT*	2.50	3.10E-17
MX2	4.41	2.05E-35	*UBE2L6*	2.49	2.08E-124
CMPK2	4.35	9.58E-93	*ETV7*	2.46	6.73E-11
PLAAT4	4.21	1.49E-40	*ODF3B*	2.42	4.62E-17
DDX60	4.19	5.58E-94	*MX1*	2.35	5.86E-76
PSMB9	4.16	2.40E-81	*SHFL*	2.30	2.82E-141
DHX58	4.14	8.91E-49	*CCR1*	2.26	5.03E-10
CFB	4.07	2.10E-27	*IFIT1*	2.24	6.55E-142
IFIT2	4.02	1.46E-93	*IL15RA*	2.20	4.38E-20
DDX60L	3.98	2.75E-69	*TAP2*	2.11	2.20E-91
BTN3A3	3.93	1.48E-20	*DDX58*	2.08	4.37E-120
SAMD9	3.91	7.27E-35	*SECTM1*	2.07	8.67E-15
BTN3A1	3.90	7.88E-22	*IFIH1*	2.03	9.28E-108
SERPING1	3.79	7.31E-21	*MLKL*	2.01	8.84E-45
HLA-DRA	3.75	2.58E-16	*CASP10*	2.01	1.30E-08

4.13 Cytokine-stimulated CAFs secrete IFNβ1 and induce STAT1 signaling in MCF7 cells

The pathway enrichment (Figure 25C) and the TF activity (Figure 26) analyses based on MCF7 RNA-seq data strongly suggested upregulation of STAT signaling in the breast cancer cells in response to the CM from stimulated CAF1 cells. I proceeded to check for STAT1 signaling in the MCF7 cells upon treatment with CM from two independent CAF cell lines (Figure 29A). Treatment with CM post double stimulation as well as treatment with CM post TNFα alone led to STAT1 phosphorylation in the MCF7 cells (Figure 29A). STAT1 signaling is known to be activated in response to interferon β. A qPCR showed that indeed *IFNB1* was upregulated in the CAFs upon treatment with TNFα (Figure 29B). With an ELISA, I confirmed that interferon-β1 was also secreted at detectable levels by the TNFα-stimulated fibroblasts, but not by the MCF7 cells, even if the latter were themselves treated with TNFα (Figure 29C).

4.14 Knockdown of *IFNAR1* does not abrogate the effect of the CM on the MCF7 migration

To check whether interferon/STAT1 signaling played a role in the observed migratory phenotype, I knocked down *IFNAR1* (codes for the interferon alpha/beta receptor) in the MCF7 cells prior to performing the migration assay. Although the knockdown was successful (Figure 29D), it had no effect on the migration (Figure 29E). I thus concluded that although STAT signaling did not seem to play a role in the CM-induced MCF7 migration, it was worth exploring other phenotypes with which it could be associated.

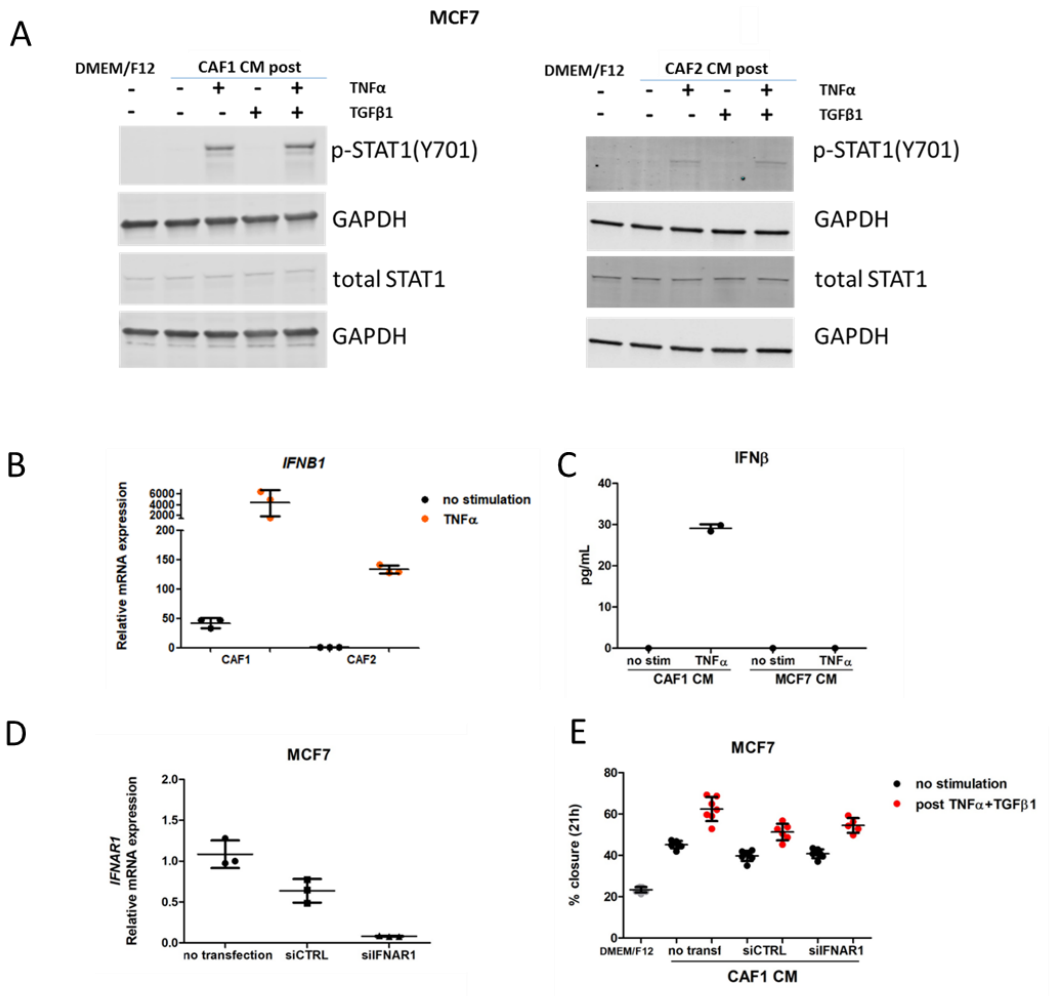

Figure 29**. Investigation of STAT1 signaling in the MCF7 cells post treatment with CAF CM. (A) Western blot.** MCF7 cells were treated for 20 min with CM from two independent CAF cell lines (immortalized CAF1, left, and primary CAF2, right). The STAT1 signaling was activated in the MCF7 cells treated with the CM collected post TNFα or double stimulation. **(B) qPCR analysis of *IFNB1* expression in CAFs upon stimulation with TNFα.** The CAFs expressed higher levels of *IFNB1* in response to the stimulation (10ng/mL TNFα). **(C) Interferon β ELISA.** IFNβ1 is secreted at detectable levels by the CAFs upon treatment with TNFα, while it is undetectable in the MCF7 CM even upon treatment with TNFα. **(D) Efficiency of siRNA mediated knockdown of *IFNAR1* in MCF7 cells. (E) Migration assay.** The increase in migration is not due to signaling via the IFNα/β receptor since knockdown of *IFNAR1* had no effect on the observed migratory phenotype. The error bars represent standard deviation.

The overall aim of my project was to identify factors driving further Luminal A breast cancer progression. My data so far showed that the CAFs secreted interferon β1 upon treatment with TNFα and that this interferon β1-containing CM then induced STAT1 phosphorylation in the MCF7 cells (Figure 29). Moreover, RNA-sequencing of the CM-treated MCF7s also revealed enrichment (Figure 25B) and activation (Figure 25C, Figure 26) of the interferon/STAT1/2 signaling. Interferon β1/STAT1 signaling has been shown to induce autophagy (Ambjorn *et al*., 2013). Tumor cells, which are not actively proliferating, but are instead undergoing autophagy or are in cell cycle arrest will be resistant to chemotherapy and therefore could later give rise to metastasis (Legrier *et al*., 2016). Therefore, I investigated two more phenotypes in the breast cancer cells: 1) autophagy and 2) recovery after chemotherapy in the presence of CAF-secreted factors.

4.15 The interferon-containing CAF CM does not induce autophagy, but rather inhibits it

Interferon β1 has been reported to be an inducer of autophagy. Since the stimulation with TNFα resulted in increased secretion of interferon β1 by the fibroblasts (Figure 29C), I hypothesized that their conditioned medium could potentially induce autophagy in the breast cancer cells. To check for this, I performed LC3-HiBiT autophagy flux assays with three independent stably transfected GFP LC3-HiBiT MCF7 clones (provided by Dr. Rainer Will). Representative data from one of the clones is presented in Figure 30A. Torin and Bafilomycin, an inducer and an inhibitor of autophagy, respectively, were used as controls. The assay relies on the detection of luminescence. LC3 is a cytosolic protein, which during autophagy is incorporated into the membrane of autophagosomes (Tanida, Ueno and Kominami, 2008; Figure 30C). HiBiT is a small tag that allows to assess the autophagic flux using a commercially available bioluminescence-based kit (Promega). An increase in autophagy will lead to degradation of HiBiT (Figure 30C) and a concomitant decrease in luminescent signal, and vice versa. The positive and negative controls showed that in principle, the assay worked well, but neither the CM used, nor recombinant IFNβ1 induced autophagy (Figure 30A). For the recombinant IFNβ1, levels similar to those detected in the conditioned medium were used (i.e., 50 pg/mL). Since MCF7 cells

express very low levels of Beclin1, a major player in autophagy, while HeLa cells express higher levels, the latter cell line was used as an additional experimental system, to serve as a positive control for the assay. The autophagy flux assay was performed with three independent GFP LC3-HiBiT HeLa clones (provided by Dr. Rainer Will). The data generated with the HeLa clones (Figure 30B) were very similar to the data from the MCF7 clones (Figure 30A), thus proving that the levels of interferon in our CM were not sufficient to induce autophagy, regardless of the cell-specific differences in Beclin 1 expression levels. A further explanation could be that our CM was a complex system, which potentially contained several factors with opposing functions, both inducers and inhibitors of autophagy. My data suggested that our CAF CM was rather richer in inhibitors of autophagy than in inducers of this phenotype.

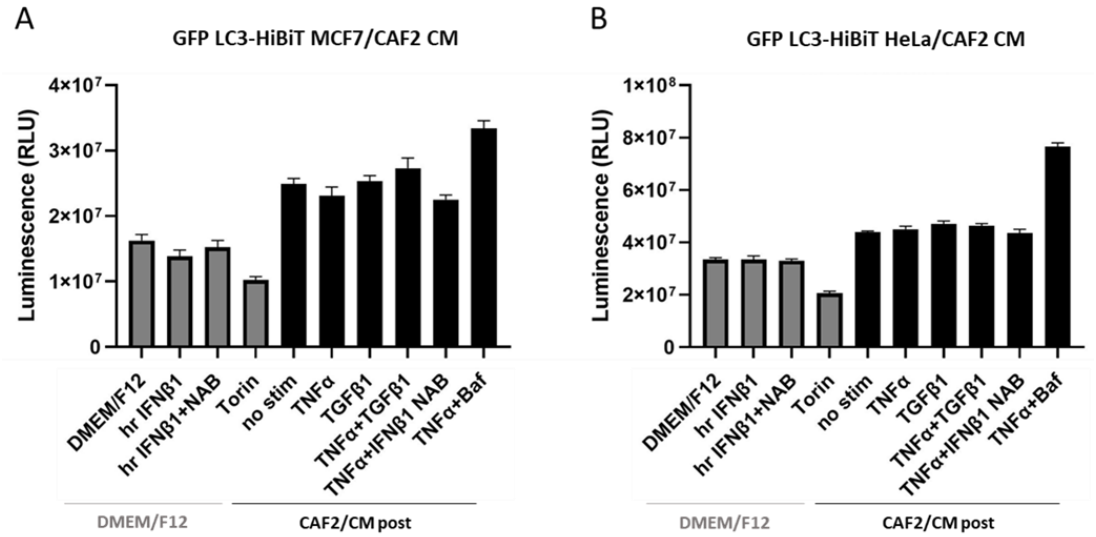

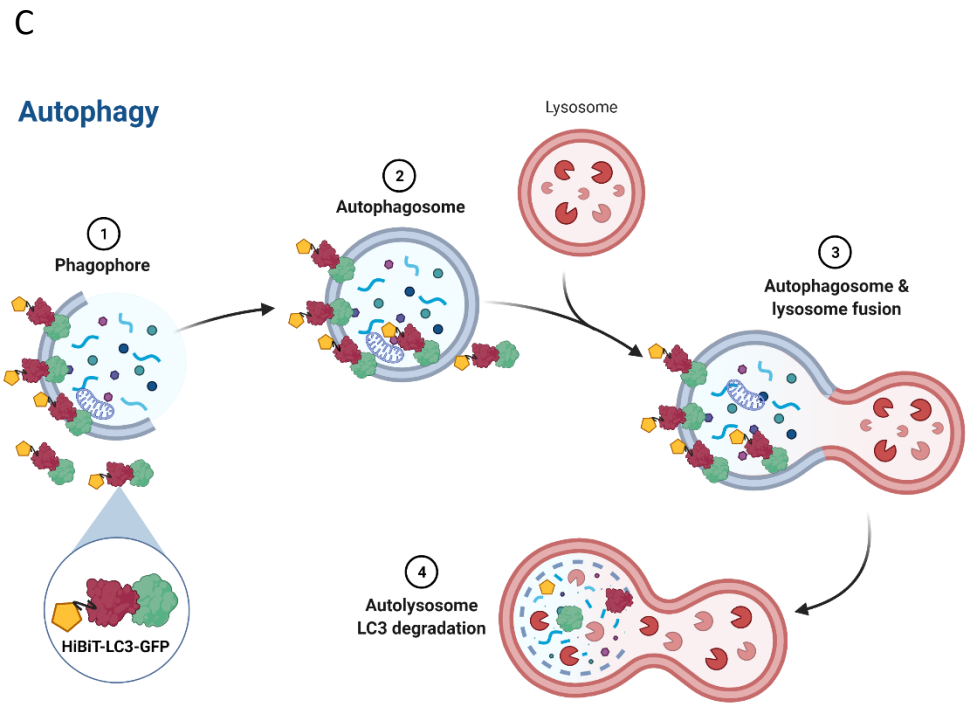

Figure 30. **Effect of the CAF CM on autophagy in MCF7 (A) and HeLa (B) cells.** An autophagy flux assay was performed to estimate the effect of the CAF2 CM on the autophagy of MCF7 cells stably transfected to express GFP LC3-HiBiT. HeLa GFP LC3-HiBiT cells were used as a positive control. Torin (250nM) and Bafilomycin (100nM), an inducer and an inhibitor of autophagy, respectively, were also used as controls. The assay was performed with three independent clones for each cell line. Each column is the average of at least 4 technical replicates. Representative data (one clone per cell line) shown. (C) Autophagy leads to degradation of LC3 and loss of HiBiT. Adapted from “Autophagy Process", by BioRender.com (2022). Retrieved from: https://app.biorender.com/biorender-templates.

4.16 There is no positive effect of the stimulation with TNFα on the CAF ability to support tumor regrowth after chemotherapy

Interferon signaling has been reported to play an essential role in resistance to chemotherapy. Previous data from our lab and others suggests that CAFs expressing higher levels of the ISG genes could potentially support the recovery of cancer cells after chemo-treatment to a greater extent than ISG low CAFs (Maia *et al*., 2021). Since stimulation with TNFα led to higher ISGs expression (Figure 20, Figure 21), I hypothesized that TNFα-stimulated CAFs would better support the recovery of paclitaxel- or epirubicin-treated breast cancer cells than unstimulated CAFs. To test this hypothesis, I treated MCF7 and T47D breast cancer cells with chemotherapy for 3 days and then allowed the cells to recover for 15 days in the presence of either unstimulated or TNFα-pretreated CAF2 cells (indirect cocultures) or the corresponding CAF2 CM. Cancer cells in monocultures and DMEM/F12 medium instead of CAF2 CM were used as controls. Both indirect coculturing with unstimulated CAFs and treatment with their respective CM (CM no stimulation) led to faster recovery of the cancer cells (Figure 31, Figure 32). There was no advantage of using prestimulated CAFs or their CM (Figure 31, Figure 32). In fact, the CM from 24h-stimulated CAFs reduced the ability of the cancer cells to regrow (Figure 32) probably due to the anti-proliferative properties of TNFα. In support of this possibility is the fact that when the recombinant TNFα was washed away and fresh CM was collected 24h later (24+24h CM), this CAF CM with lower TNFα concentration was able to help the cancer cells recover better than the corresponding 24h CAF CM, which still contained the residual recombinant TNFα (Figure 32). Overall, prestimulating the CAFs with TNFα, despite resulting in induction of the ISG signature expression, an effect which lasted even 24h after removal of the recombinant TNFα (Figure 33), did not increase their ability to support tumor regrowth post paclitaxel or epirubicin treatment (Figure 31, Figure 32).

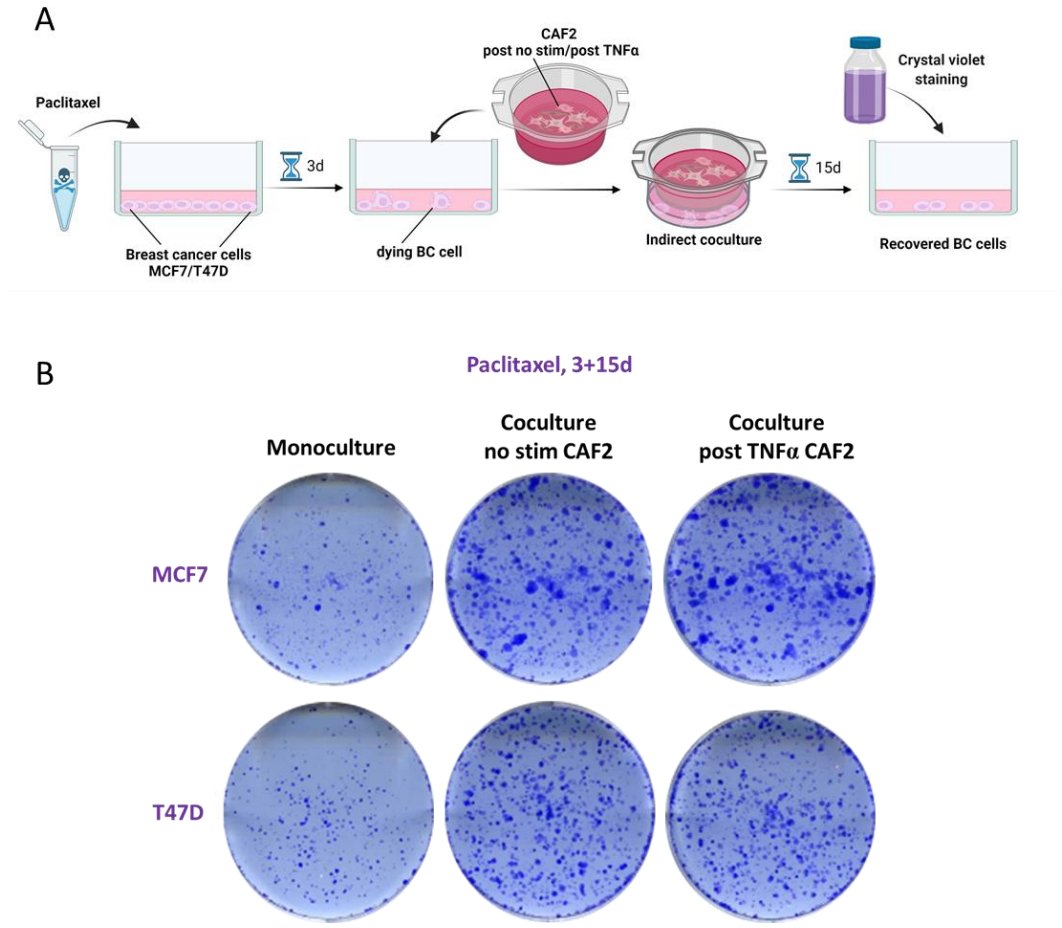

Figure 31. **CAF2 cells support the recovery and regrowth of breast cancer after chemotherapy. (A) Schematic of the experimental set up**. MCF7 and T47D monocultures were seeded in 6 well plates and treated with paclitaxel (4nM) for 3 days. Primary CAF2 cells were seeded in transwells with a permeable membrane allowing for exchange of soluble factors. The CAFs were prestimulated with human recombinant TNFα (10 ng/mL) for 24h. The CAFs were washed at the end of the stimulation to remove any remaining recombinant TNFα. At the end of the chemotreatment, the cancer cells were washed (to remove any residual drug) and allowed to recover for 15 days either alone or in indirect cocultures with unstimulated or prestimulated CAFs. The recovered cells were fixed with methanol and stained with crystal violet. The scheme was created with BioRender.com. **B) Recovery of breast cancer cells after paclitaxel treatment.** The assay was performed as described in the schematic. Representative images of the recovered crystal violet stained cancer cells. N=3 for each condition.

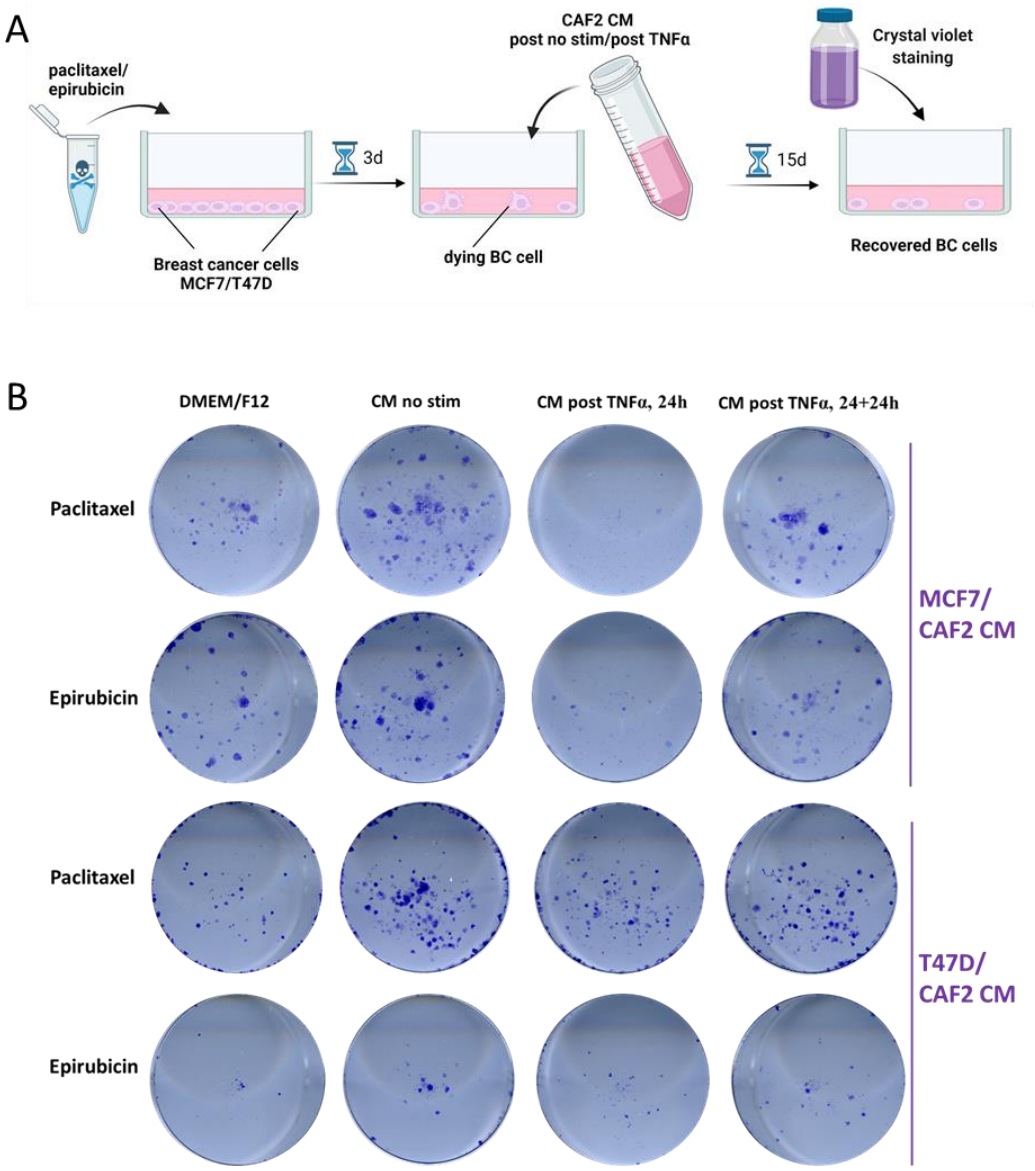

Figure 32. **CAF2-secreted factors are sufficient to support breast cancer recovery and regrowth after chemotherapy.** (**A) Schematic of the experimental set up** (generated with BioRender.com). MCF7 and T47D monocultures seeded in 12-well plates were treated with pacitaxel (4nM) or epirubicin (70nM) for 3 days. Meanwhile CAF2 monocultures were stimulated with TNFα (10ng/mL) for 24h. CAF2 conditioned medium was collected at the end of the stimulation (CM post TNFα, 24h). The fibroblasts were washed to ensure removal of any residual TNFα prior to addition of fresh media without stimulation. CAF2 CM was collected again another 24h later (CM post TNFα, 24+24h). After the chemotreatment, the breast cancer cells were washed and allowed to recover in DMEM/F12 (negative control) or CM from unstimulated or prestimulated CAF2 cells. After 15 days of recovery, the breast cancer cells were fixed with methanol, stained with crystal violet and imaged. **(B) Unstimulated CAF2 CM accelerates the regrowth of breast cancer cells after chemotherapy.** Recovery assays were performed as aforementioned. Representative images of the recovered crystal violet stained cancer cells. N=3 for each condition.

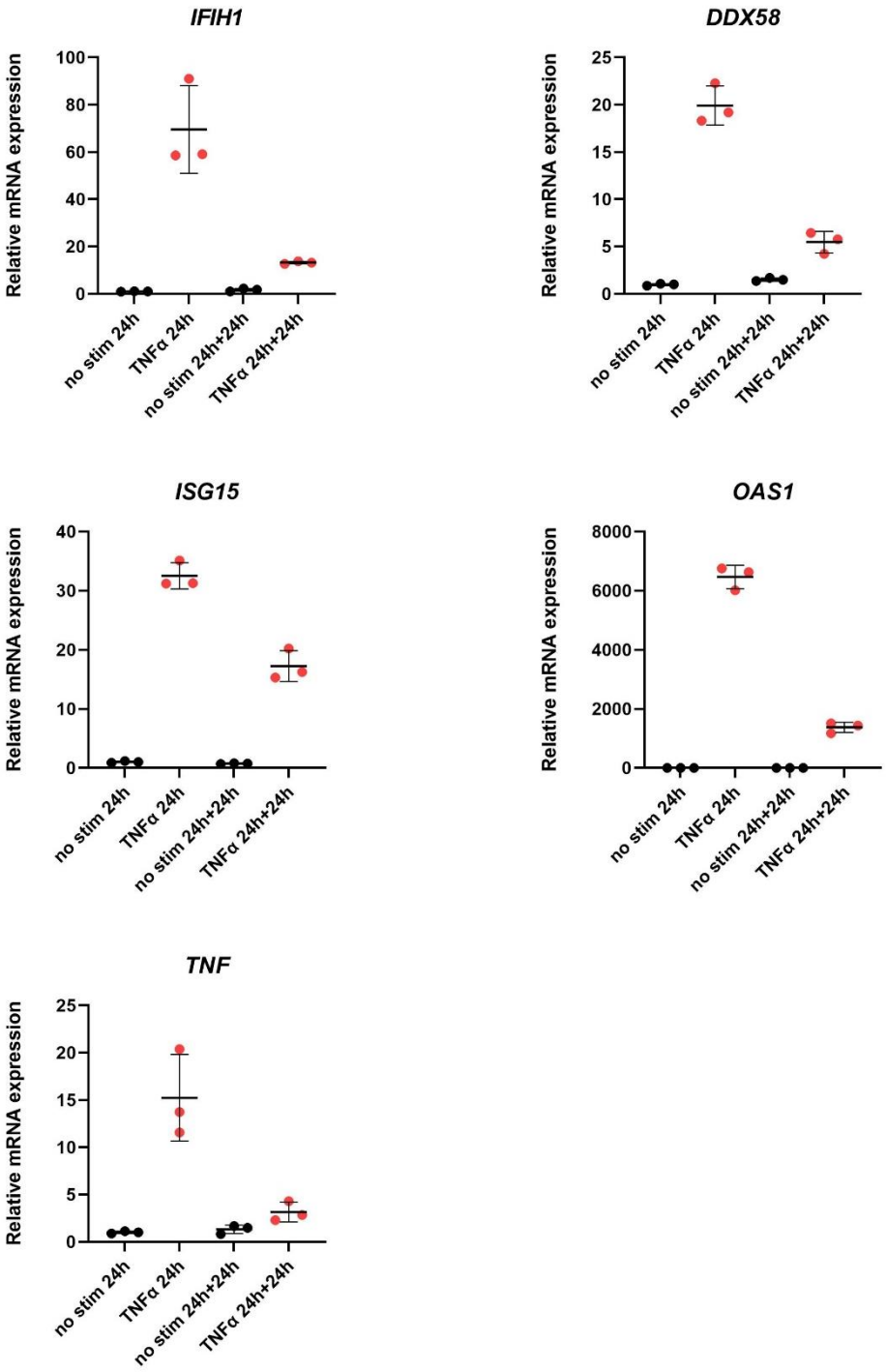

Figure 33. **Stimulation of CAF2 cells with TNFα results in induction of the ISG signature. The ISGs expression is sustained even 24h after withdrawal of the TNFα.** CAF2 monocultures (in duplicates) were stimulated with human recombinant TNFα (10 ng/ml) for 24h. At the end of the stimulation, either the cells were lysed immediately and their total RNA isolated (TNFα 24h), or kept for another 24h in TNFα-free media before being also processed for RNA isolation (TNFα 24h+24h). Unstimulated CAF2 cells were used as a control. The relative expression of several interferon-stimulated genes and *TNF* was determined via qPCR. The error bars represent the standard deviation.

4.17 TNFα induces IFN signaling in the CAFs due to a NF-κB/IFN signaling crosstalk

A potential crosstalk between the TNFα/NF-κB and IFNβ1/STAT signaling pathways has been already described in literature (Figure 34). To test its validity in our system, a series of siRNA-mediated knockdown experiments was performed in the CAF2 fibroblasts and the results are summarized in Figure 35. As expected, stimulation with TNFα led to upregulation of several interferon-stimulated genes, namely *IFIH1*, *DDX58*, *ISG15*, *OAS1* and *IFNB1,* as well as *TNF*, one of the early response genes of the NF-κB pathway. This effect of the stimulation on the ISG signature and *TNF* expression was significantly attenuated upon silencing of *RELA*, which codes for the p65 component of the NF-κB complex. This and the fact that *IFNAR1* knockdown negatively affected *TNF* expression provided evidence of the NF-κB-interferon signaling crosstalk in the tested fibroblasts. Moreover, knockdown of *IFNAR1* also partially reduced the effect of the stimulation on the ISG upregulation, which suggested the presence of a positive feedback loop – binding of IFNβ1 to its receptor led to upregulation of *IFNB1* and the downstream ISG genes. STAT2 seems to be the TF with the most essential role in this crosstalk. Of the three STATs examined, only silencing of *STAT2* resulted in a decreased effect of the TNFα stimulation on the ISGs and *TNF* upregulation. This finding, based on my earlier computational analyses, could potentially be true also for the CAF CM post-treated MCF7 cells, in which STAT2 was the transcription factor with the highest enrichment score (Figure 26A). This suggests that in the cells under investigation, STAT2 does not necessarily form heterodimers with STAT1 to induce ISG expression, but supports the notion that STAT2 homodimers in conjunction with IRF9 could be the relevant factor. Altogether, the qPCR data supports the existence of a crosstalk between TNFα/NF-κB and IFNβ1/STAT pathways in our TNFα-stimulated fibroblasts.

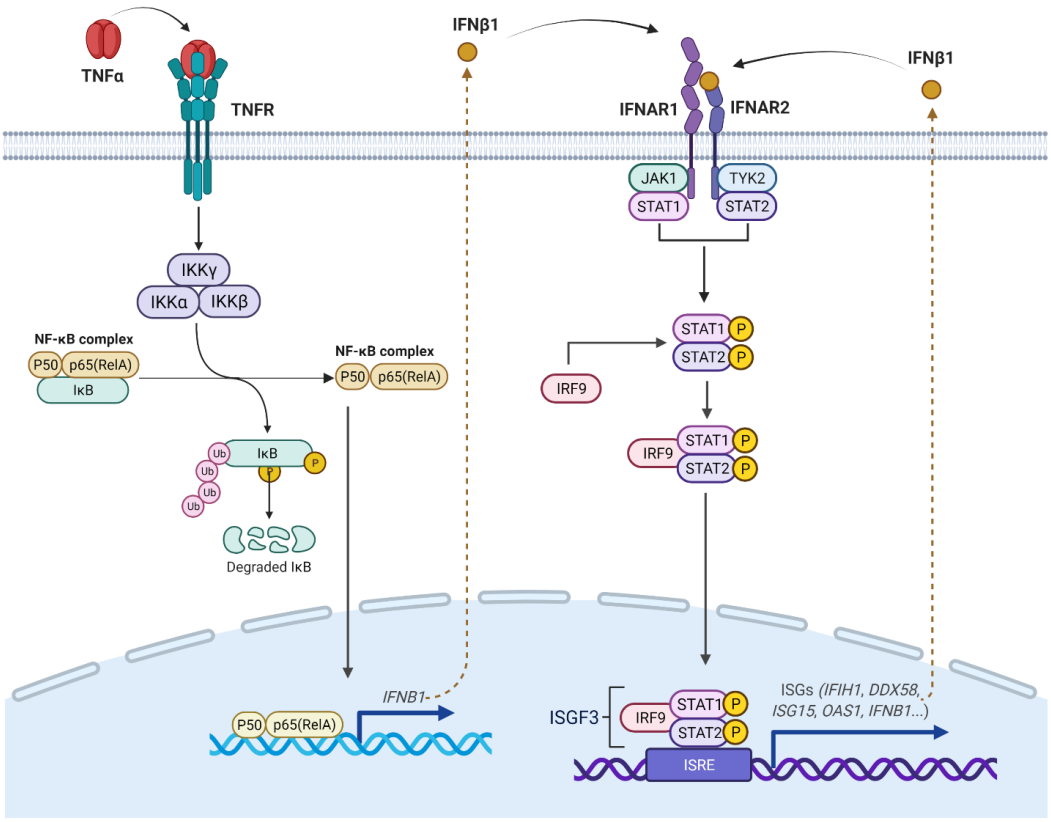

Figure 34. **Crosstalk between the NF-κB and the IFNβ1/STAT signaling pathways.** Binding of TNFα to its receptor ultimately leads to degradation of IkB (inhibitor of NF-κB) and activation of the NF-κB complex. The latter is translocated to the nucleus where it serves as a transcripition factor. It leads to the expression of several targets, including *IFNB1*. As a result, interferon β1 is secreted by the cell and can function in an auto- or paracrine fashion. It binds to its receptor IFNAR1/2, thus eliciting the JAK/STAT signaling. Phosphorylated STAT1/2 heterodimers bind to IRF9 to form the ISGF3 (interferon-stimulated gene factor 3) transcription factor complex. Once in the nucleus, ISGF3 binds to ISRE (interferon-sensitive response element) and induces the expression of the ISGs (interferon-stimulated genes). Image created with BioRender.com.

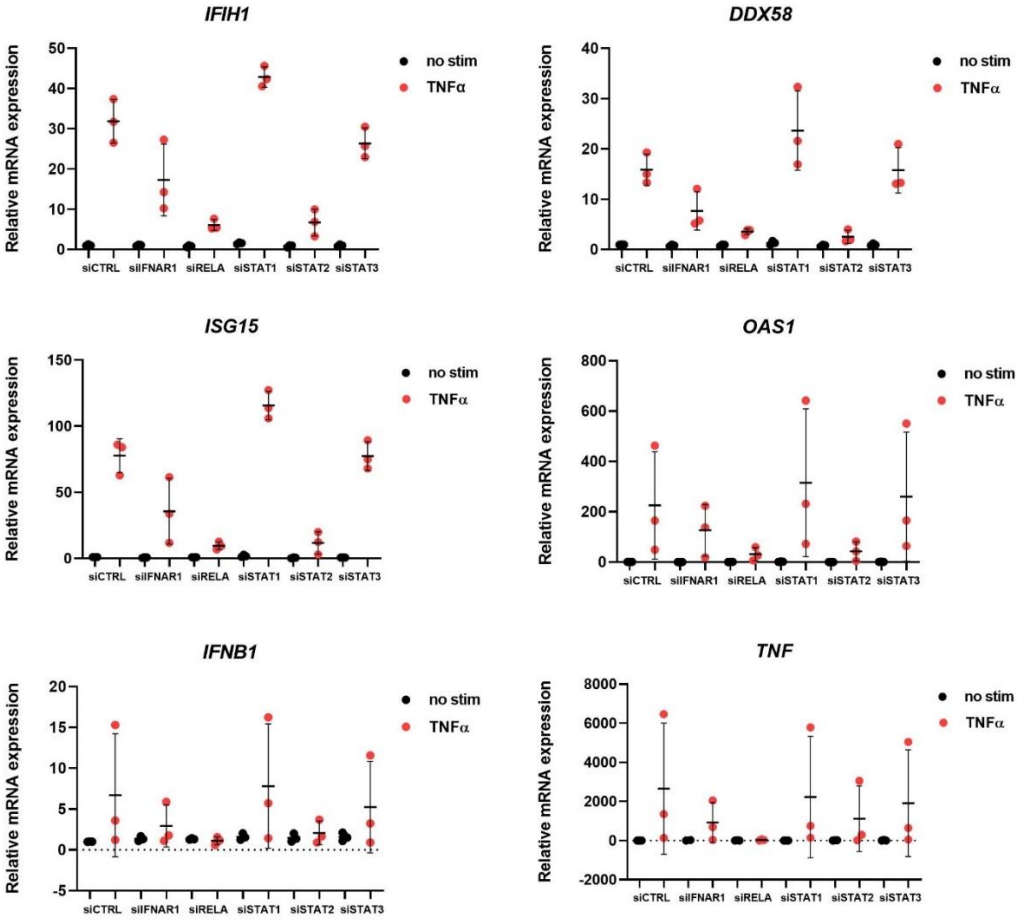

Figure 35. **Validation of the crosstalk between the NF-κB and the IFNβ1/STAT signaling pathways in TNFα-treated cancer-associated fibroblasts.** CAF2 cells were transfected with siRNA pools targeting major components of the two pathways. Then they were stimulated with 10ng/ml TNFα for 24h. Transfected but unstimuated CAF2 cultures were used as controls. The CAFs were lysed and their total RNA was isolated and used for analysis of the expression of ISGs (interferon-stimulated genes), *IFNB1* and *TNF* via qPCR. Each dot is a biological replicate and the average of 3 technical replicates. The error bars are SEM.

5. DUSCUSSION

In this study I examined several of the ways the tumor microenvironment, here represented by primary breast cancer-associated fibroblasts, may support Luminal A breast cancer progression. Although this subtype is characterized by a rather good prognosis, it still contributes heavily to the global cancer burden. Roughly 40% of all breast tumors are Luminal A, making this subtype the most common. Moreover, the initial good response to hormonal therapy can be followed years later by metastasis of cancer cells which have developed resistance (or persistence). The endocrine treatment which is commonly-used for this subtype targets predominantly the Luminal A cancer cells but not the surrounding tumor-supporting fibroblasts (CAFs). CAFs do not express the estrogen receptor and are therefore not dependent on estrogen signaling. Thus, the endocrine therapy will not affect them. Considering that the CAFs are a major component of the tumor stroma with well-documented contribution to cancer progression (Kalluri, 2016; Chen Y *et al*., 2021; Hu *et al*., 2022), there is clearly a need for development of therapeutic strategies targeting the CAF-breast cancer crosstalk. If we could identify the exact cues that the CAFs relay to the cancer cells to make them more metastatic or resistant, that will bring us one step closer to discovering more permanent therapeutic solutions for patients affected by Luminal A breast cancer.

5.1 Primary versus immortalized CAFs as sources of pro-migratory factors

In this study primary CAF cell lines derived from breast cancer biopsies were used. Primary cells can be more biologically relevant in comparison to commercially available cell lines that have been maintained in culture for a long time. This is because with every passage, the probability of selecting for a certain cell subpopulation (e.g., one that is more proliferative) over another increases. Most commercially available cell lines have undergone many such selection rounds and may not represent the original state of the tissue they were derived from. Primary cells, though, have undergone fewer passages by definition and therefore are more representative of their tissue or organ of origin. They have one big disadvantage though – they can be passaged only a limited number of times before they start undergoing senescence or cannot be considered primary

anymore. Therefore, scientists often opt for immortalization of their primary cell lines for larger scale experiments that require a more substantial number of cells. This is also why I used E6/E7 immortalized CAF1 cells to generate most of the OMICS data presented here. Hypotheses based on this data were later validated in the primary CAF2 cells. Conditioned medium from unstimulated CAFs, regardless of their immortalization status, could increase the migratory potential of otherwise low-migratory luminal A breast cancer cell lines. However, one striking difference between the immortalized and the primary CAFs was observed. In order to be stimulated to secrete factors able to induce tumor cell migration even to a greater extent than their unstimulated counterparts, the immortalized CAFs had to be activated with both TNFα and TGFβ1. In comparison, the primary CAFs required stimulation with only TNFα to have the same impact (compare Figure 14A to Figure 19). This discrepancy could suggest that the immortalization had affected the basal levels of TGFβ1 signaling in the CAFs. Indeed Lee *et al*. have provided evidence that E7 can interact with the Smad complex and prevent its binding to DNA, thereby essentially attenuating TGFβ1-induced transcription (Lee *et al*., 2002). While the primary CAFs did not require activation with recombinant TGFβ1, their E6/E7 immortalized counterparts did, since their innate TGFβ1 pathway was most likely repressed by the E7 protein. Treatment with TGFβ1 potentially was able to partially overcome the E7 effect and elicit low levels of TGFβ1 signaling. Meanwhile in the primary CAFs, the basal TGFβ1 signaling was not affected and thus did not require further activation with exogenous TGFβ1. This explanation, however, is hypothetical and requires further investigation to be confirmed or rejected. The discrepancies between results obtained with immortalized cell lines versus the corresponding primary cells illustrates how findings made with the former should always be validated with the latter. Discoveries based only on artificially immortalized cell lines should be taken with caution, and the possible side effects from the immortalization should be considered.

5.2 TNFα plays a double role in breast cancer

Most studies investigating the role of TNFα in cancer have focused on how it affects the transformed tumor cells and the immune system. Although there are many publications on the effect of TNFα on normal fibroblasts (Costa *et al*., 2014;

Lau *et al*., 2017; Ueshima *et al*., 2018), a lot fewer findings have been made on how this pro-inflammatory cytokine works on the cancer-associated fibroblasts. The basis of my work had been the finding made by Lerrer *et al*. that mesenchymal stem cells (MSCs) treated with high levels of TNFα and TGFβ1 secrete factors that support MCF7 cell migration (Lerrer *et al.*, 2017). Since MSCs recruited to the tumor site are considered to be one of the sources of cancer-associated fibroblasts, the next logical step was to explore what the effect of these cytokines was when used directly on CAFs. It turned out that concentrations five times lower than the ones used by Lerrer were sufficient to induce secretion of pro-migratory factors by the immortalized CAFs, which then led to increased MCF7 and T47D cell migration (Figure 9A). In the case of primary CAFs, however, stimulation with TNFα alone was enough to achieve the same effect (Figure 19). Since TNFα itself is known to promote breast cancer cell migration (Wolczyk *et al.*, 2016), it was important to examine its role in my *in vitro* system. Because the CAF CM I collected after stimulation with the cytokines could still contain residual human recombinant TNFα and potentially also TNFα secreted by the CAFs, it was possible that the TNFα itself was responsible for the observed effect of the CM on MCF7 migration. With the use of a TNFα neutralization antibody I was able to exclude this scenario and confirm that the migration of cancer cells was indeed due to CAF-secreted factors other than TNFα (Figure 9B). Thus, although in my experimental set up this cytokine could not directly affect the cancer cells in terms of migration, it acted on the CAFs and instructed them to produce other pro-metastatic factors which then could facilitate MCF7 and T47D migration.

The link between EMT (epithelial to mesenchymal transition), migration and metastasis is well-known (Saitoh, 2018; Aiello and Kang, 2019). Thus, although not a major point of interest in this study, it must be commented on. The untreated MCF7 and T47D cells show no or low expression of the classic EMT markers (Saitoh, 2018), such as *TWIST1/2*, *SNAI1/2,* and *ZEB1/2* to name a few. Changes in these genes in individual cells post treatment with CAF CM are thus hard to detect in the bulk cell population, in which only a very small percentage of the cells, if any, would have acquired complete EMT. For non-migratory epithelial cells, such as the breast cancer cell lines used in this study, even just a partial EMT, during which the cells express simultaneously both epithelial and mesenchymal markers,

may be enough to render them more mesenchymal-like and migratory. Evidence in support of how partial EMT may contribute to cancer progression has been reviewed in Aiello and Kang (2019), who argue that complete EMT in cancer is rare, and that cancer cells rather exist in different states along a spectrum of epithelial towards mesenchymal phenotypes.

The notion of partial EMT is supported by data generated by me together with Christina Schniederjohann (a Bachelor student whom I co-supervised at the division of Molecular Genome Analysis, DKFZ). MCF7 and T47D cultures treated with CM from TNFα+TGFβ1-stimulated CAF1 cells migrated to a higher extent in comparison to their untreated counterparts (Figure 9A). In addition, they were also characterized with higher levels of expression of the mesenchymal markers *FN1* and *MMP13*, while the transcription of *TWIST1*, *SNAI1/2* and *CDH1* was not significantly affected (Figure S1). The upregulation of *FN1* in the cancer cells upon CM treatment was also confirmed at the protein level (Figure S2). However, at protein level, in comparison to the no CM control, both CM from cytokine-stimulated and unstimulated CAFs led to induction of FN1 expression (Figure S2). Since treatment with TNFα has been shown to lead to increased MMP secretion and activity in MCF7 cells, in particular MMP9 (Wolczyk *et al*., 2016), the observed *MMP13* overexpression in the cancer cells may be partially due to residual human recombinant TNFα present in the CM of the cytokine-activated CAFs. To test this, neutralization antibody against TNFα could be added to the CM prior to treating the cancer cells with it and then checking whether the CM still induces *MMP13* transcription. Interestingly the CAFs themselves also upregulated their expression of *MMP1*, *MMP3*, *MMP9* and *MMP13* in response to the stimulation. The induction of *MMPs* in the CAFs was clearly driven by TNFα while TGFβ1 appeared to either have no effect when used alone or rather have the opposite effect when in combination with TNFα (Figure S3). The partial EMT undergone in the cancer cells, as demonstrated by the increase in *FN1* and *MMP13* levels, in combination with the overexpression of *MMPs* in the CAFs, may partially explain the increase in migratory capacity observed in the MCF7 and T47D cells. To test this hypothesis, inhibitors of MMP activity could be utilized to check whether they would prevent the increase in MCF7 and T47D migration, otherwise induced by the CM of cytokine-activated CAFs.

While the residual hrTNFα had no direct effect on the migration of MCF7 breast cancer cells, but potentially drove them into partial EMT, it seemed to affect their cell numbers. The MCF7 cells appeared to increase in cell numbers at a slower rate in the presence of CAF CM collected post TNFα stimulation, in comparison to when CM post no stimulation was used (Figure S4). This effect may be due to the residual human recombinant TNFα, or TNFα produced by the CAFs, or another factor the CAFs secrete upon stimulation with TNFα. Further investigation would be required to make a definitive conclusion. The potential anti-proliferative effect of TNFα has been observed in some breast cancer cell lines, but not in others (Cruceriu *et al.*, 2020). In fact, depending on the cell line and the concentration of TNFα, this cytokine can lead to either apoptosis or survival (Cruceriu *et al.*, 2020). The potential anti-proliferative and pro-apoptotic effect of TNFα on MCF7 cells has been reported before (Jeoung *et al*., 1995; Donato and Klostergaard, 2004), and seems to be dependent on the expression of the apoptosis regulator Bcl2. Burow *et al*. have demonstrated that MCF7 variant cell lines maintained in different laboratories show different levels of susceptibility to TNFα-induced apoptosis – Bcl2-low MCF7 cells were more sensitive than Bcl2-high MCF7 variants (Burow *et al*., 1998). Bcl2 expression correlated with resistance to TNFα-mediated apoptosis. This is in accordance with my own observations – although so far, Bcl2 expression has not been investigated, the MCF7 cells maintained in the laboratory of our collaborators (Ben-Baruch lab, Tel Aviv University) seem to be more resistant to potential TNFα toxicity than the MCF7 (obtained from ATCC) cultures I used in my study. Such a discrepancy between findings generated with the ‘same’ cell line in different labs should be considered when attempting to replicate a study. Nevertheless, the consensus seems to be that despite its pro-survival and pro-tumorigenic effects, TNFα in certain cases can act as an anti-cancer agent by inducing tumor cell apoptosis. This dual role of TNFα in cancer should be carefully examined on an individual patient basis. Information about TNFα levels in the patient’s plasma and tumor and its possible effects on the TME, including CAFs, and the transformed cells should be taken into account, when deciding on the best therapeutic options. Some of the TNFα effects discussed in this work are summarized in Figure 36.

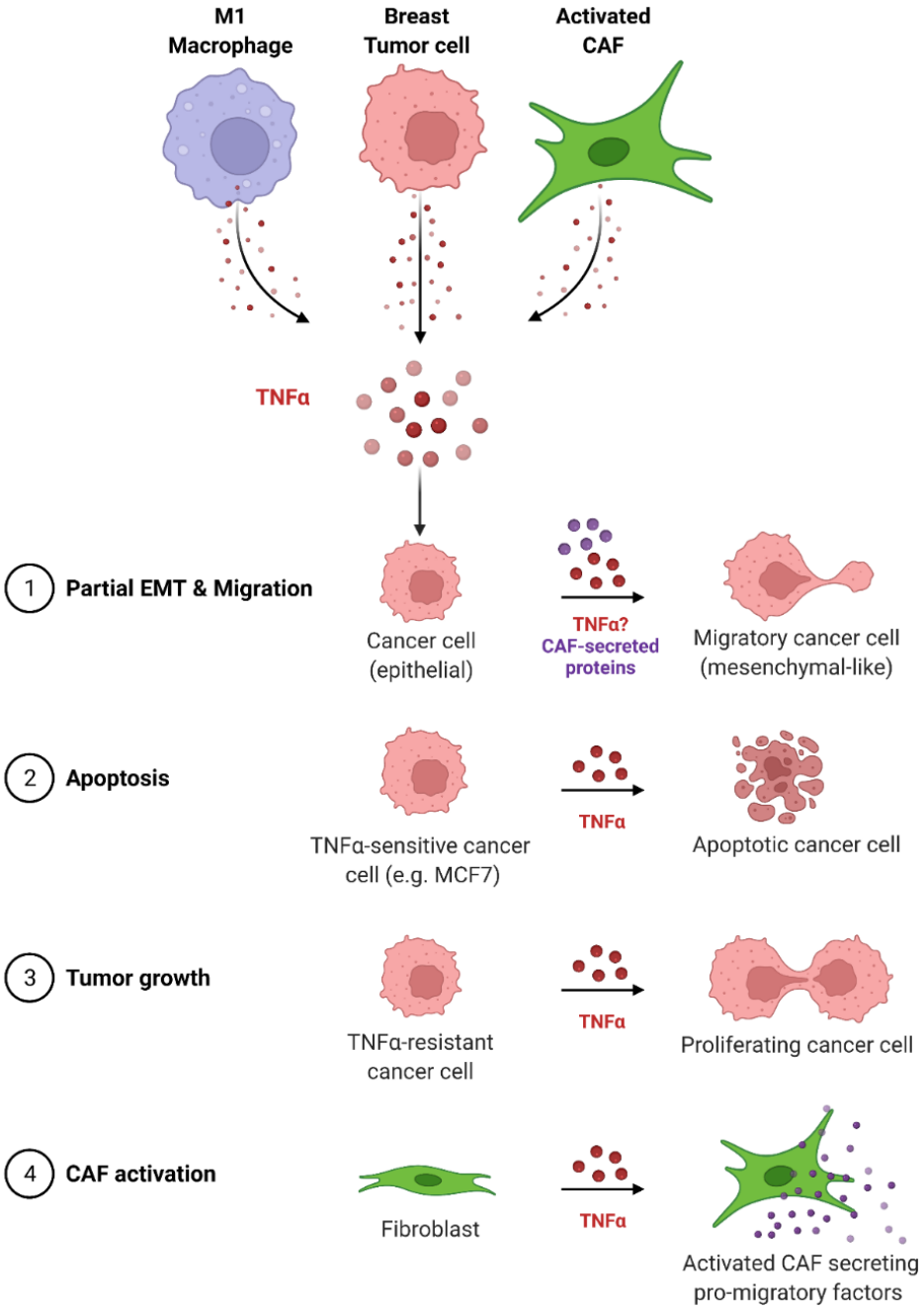

Figure 36. **The role of TNFα in breast cancer.** The pro-inflammatory cytokine TNFα is secreted in the TME primarily by the M1 macrophages (Shapouri-Moghaddam *et al*., 2018), but breast cancer cells and CAFs can also be sources of it. TNFα can act directly on the tumor cells by inducing their partial EMT, migration and growth. In some cases, though, it could also induce breast cancer cell apoptosis. In this work I showed that TNFα can influence Luminal A breast cancer progression also indirectly by activating the tumor-resident fibroblasts. The TNFα- stimulated CAFs secrete higher levels of pro-migratory and pro-metastatic factors, and thus could play a role in tumor relapse. Image created with Biorender.

5.3 TNFα as a breast cancer prognostic marker

Several studies have reported elevated TNFα levels in breast cancer. As early as in 1994, Miles *et al*. investigated the TNFα expression in benign and malignant breast tissues. With immunohistochemistry they showed that TNFα was expressed at higher levels in the invasive breast carcinomas than in the benign tissues, and that TNFα expression was confined to the tumor stroma (Miles *et al*., 1994). In 1997, Sheen-Chen *et al*. compared the serum TNFα levels in blood samples collected from 40 patients with invasive breast cancer and 30 age-matched healthy control subjects. Not only the concentration of TNFα was higher in the breast cancer patients but also the higher the levels, the more advanced the stage of the disease was (Sheen-Chen *et al.*, 1997). In a study of 112 breast carcinoma patients and 45 age-matched healthy individuals, Tripsianis *et al.* showed that TNFα concentration was higher in invasive tumors, in the advanced stage and in patients with metastases in more than three lymph nodes (Tripsianis *et al*., 2014). Moreover, they found that higher TNFα and IL6 serum levels correlated with shorter survival and increased risk of death. The risk was highest when both cytokines were highly expressed suggesting that the co-expression of TNFα and IL6 could be used as a prognostic factor for the disease outcome (Tripsianis *et al*., 2014). In my *in vitro* studies, stimulation with human recombinant TNFα resulted in increased secretion of IL6 by the CAFs (Figure 11B), which was expected considering that TNFα activates the NF-κB pathway, thus ultimately leading to IL6 secretion (Tak and Firestein, 2001). Although there was no direct effect of IL6 (Figure 11C) or TNFα (Figure 9B) on MCF7 migration, as demonstrated by the use of the respective neutralization antibodies, the presence of these cytokines in the CAF CM could indicate that the TNFα-activated CAFs could contribute to creating a pro-metastatic environment that ultimately leads to increased breast cancer cell migration and dissemination.

5.4 TNFα as a therapeutic target

In vitro and *in vivo* findings suggest that blocking soluble TNFα with antibodies could represent a novel therapeutic strategy for treatment of cancer. Etanercept (Enbrel®) is a soluble TNFR2 fused with the Fc domain of human IgG. It binds both soluble and transmembrane TNFα thus preventing it from binding its

receptors on the cell surface. Shirmohammadi *et al*. demonstrated that etanercept inhibited the growth and invasive properties of MDA MB 231 breast cancer cells (Shirmohammadi *et al*., 2020). These changes were accompanied by decreased NF-κB activity and enhanced apoptosis. Etanercept however, was less effective when the breast cancer cells were exposed to macrophage-secreted factors. The macrophage secretome could reactivate the NF-κB signaling in the tumor cells, thus making them less susceptible to the drug, a clear illustration of how the TME could diminish the efficacy of anti-cancer therapies (Shirmohammadi *et al*., 2020). Another group showed that etanercept could partially protect mice from chemically induced tumors (Sobo-Vujanovic *et al*., 2016). Furthermore, Mercogliano *et al*. used etanercept to overcome TNFα-induced trastuzumab resistance in *in vitro* and *in vivo* models of HER2-positive breast cancer, thus providing a rationale for administration of TNFα blockers in combination with standard therapy to patients with TNFα-high tumors (Mercogliano *et al*., 2017). In a phase II clinical study, seven patients with refractory metastatic breast cancer were treated with etanercept for at least 12 weeks. The drug was well-tolerated and led to a decrease in serum IL6 and CCL2 levels. Two patients diagnosed with estrogen receptor-positive lobular carcinoma as the primary cancer and having already developed secondary lesions prior to the study, achieved brief disease stabilization. In one of the patients the stabilization lasted for 16.4 weeks (Madhusudan *et al*., 2004).

Infliximab (Remicade®), a monoclonal anti-TNFα antibody, has also been tested in a clinical study of advanced solid tumors. The drug was well tolerated and resulted in decreased plasma IL6 and CCL2 concentrations. From the 41 patients treated with the TNFα blocker, seven achieved disease stabilization ranging from 10 to 50+ weeks (Brown *et al*., 2008). More recently, infliximab and certolizumab (Cimzia®), another anti-TNFα antibody, were evaluated in combination with immunotherapy for the treatment of advanced melanoma (Montfort *et al*., 2021). In this phase I clinical trial, TICIMEL, 14 patients were treated with nivolumab (anti-PD-1) and ipilimumab (anti-CTLA-4). Six of them also received infliximab, and the remaining eight patients - certolizumab. The drug combinations were safe with manageable side effects. Although the study had a limited patient number, the results were promising. In the infliximab-immunotherapy group, one complete and two partial responses were observed.

One patient in the certolizumab-immunotherapy cohort had to be excluded from the analysis. The remaining seven patients in this group all achieved objective response – three partial and four complete responses. At the one-year follow up, one of the infliximab and four of the certolizumab patients were still responders. Whether or not the tri-therapies are more effective than immunotherapy alone remains to be elucidated, but the high response rate with certolizumab highly encourages further investigation. The second phase of TICIMEL is still ongoing.

In this thesis, I have shown that stimulation with TNFα activates the CAFs and promotes their secretion of pro-migratory and potentially pro-metastatic factors. My findings, as well as the clinical data discussed here, suggest that targeting TNFα can potentially be a promising avenue for the treatment of Luminal A refractory cancer.

5.5 Therapeutic CAF-targeted strategies for treatment of cancer

Although none of the aforementioned studies have addressed the effect of TNFα blockers on the cancer-associated fibroblasts, it is fair to assume that they will be affected as well. Verjee *et al*. demonstrated that TNFα blockade could inhibit the contractility of myofibroblasts and convert them into more normal-like fibroblasts (Verjee *et al*., 2013), suggesting that TNFα inhibitors could be used to treat fibrosis. Anti-TNFα agents are already FDA (Food and Drug Administration) approved for treatment of Crohn's disease, rheumatoid arthritis, psoriasis, and other autoimmune and inflammatory diseases (Gerriets *et al*., 2021). Since TNFα is a double-edged sword, which, as demonstrated in this thesis, leads to CAF activation, but potentially also to breast cancer cell death, there may be a need for the development of inhibitors of TNFα signaling that specifically target CAFs. This could perhaps be partially achieved with bispecific antibodies (BsAbs) targeting, for example, FAP and TNFR1, thus blocking the TNFα from binding to its receptor specifically in the FAP^+ CAF population. Still, even such antibodies might have some off-target effects since, as discussed in the introduction, FAP is not exclusively expressed by CAFs. Some bone marrow derived stromal cells (BMSCs) are also FAP-positive. In addition, this approach will obviously not work on the CAF subpopulations which do not express FAP. Alternatively anti-

GPR77/TNFR1 BsAbs may be used to block TNFα signaling in the $CD10^{+}GPR77^{+}$ CAF subset, which was first observed by Su *et al.* in 2018. The CAFs isolated from breast cancer biopsies used in my studies, however, were GPR77-negative and relatively FAP-low (Table S1; compare *FAP* TPM values to *FN1* TPM values), so neither of the proposed BsAbs would be effective against their TNFα-induced activation.

This raises the question about what constitutes a cancer-associated fibroblast. It used to be considered that most CAFs express FAP, but now there is evidence that this is not always the case. In fact, the era of single-cell RNA sequencing has made it easier for researchers to identify different CAF subtypes within a tumor as well as between different tumor entities. For example, Li et al. has demonstrated the existence of two CAF subpopulations in colorectal cancer, and only one of them was FAP-positive (Li *et al*., 2017). This CAF intrinsic heterogeneity could explain why anti-FAP cancer therapies have not been successful in the clinics so far. Talabostat, a small molecule FAP inhibitor, and sibrotuzumab, an anti-FAP mAb, both have failed to demonstrate efficacy in Phase II clinical trials in metastatic colorectal cancer (Narra *et al.,* 2007; Hofheinz *et al*., 2003). Clearly there is a need for the development of strategies that address the issue of CAF heterogeneity and lack of specific and exclusive CAF markers.

Several other approaches to target CAFs have been described in literature (Chen and Song, 2019). CAFs could be depleted using anti-FAP CAR-T cells (Bughda *et al.*, 2021), anti-GPR77 mAb (Su *et al*., 2018), DNA vaccines targeting FAP (Duperett *et al*, 2018), or anti-FAP mAbs conjugated to toxins, such as FAP5-DM1 (Ostermann *et al*., 2008) and αFAP-PE38 (Fang *et al*., 2016). CAF depletion, however, may result in ablation also of tumor suppressive CAF subpopulations, and therefore may lead to tumor progression. A better alternative could be CAF normalization, i.e., conversion of activated CAFs into quiescent normal fibroblasts. This has been achieved in models of pancreatic cancer by reprogramming the tumor stroma with calcipotriol (Sherman *et al*., 2014) or ATRA (all trans retinoic acid) (Froeling *et al*., 2011), which are vitamin D and vitamin A analogues, respectively.

Since CAFs can relay their pro-tumorigenic effects via secretion of proteins, another strategy is to target protein synthesis by inhibiting the mTOR pathway

specifically in the CAFs (Duluc *et al*., 2015). CAFs secrete ECM components, which can contribute to cancer cell migration and metastasis. Therefore, another approach is to use SMO (smoothened) inhibitors which lead to decreased ECM production (Olive *et al*., 2009). ECM components which have pro-metastatic properties, can be eliminated, or reduced with agents, such as MMP inhibitors (Chiappori *et al*., 2007), collagenases, hyaluronidase (Provenzano *et al*., 2012) and inhibitors of collagen/hyaluronan production (Chauhan *et al*., 2013).

The aforementioned anti-CAF therapies have not shown promising results as anti-cancer treatments in the clinics so far. The majority of them attempt to target the CAFs as a whole, which could be both challenging (because of the CAF heterogeneity) and undesirable (because it will eliminate also the anti-tumorigenic CAFs). There is now a shift away from therapies targeting the common CAF features and functionality and towards therapies that target directly the specific signaling pathways induced in or by them which contributing to tumor progression (Wu et al., 2021). The exact pathways may vary between cancer entities and even between patients diagnosed with the same tumor subtype. In this thesis, I identified a crosstalk between the TNFα/NF-κB and IFNβ1-STAT signaling pathways in CAFs and investigated whether it could play a role in promoting breast cancer progression.

5.6 Non-canonical STAT2 signaling

Canonical interferon-β1-induced signaling requires participation of both STAT1 and STAT2 transcription factors. Binding of IFNβ1 to the IFNAR1/2 transmembrane receptor results in activation of the associated JAK1 and TYK2 kinases which in turn autophosphorylate. This enables them to transphosphorylate tyrosine residues on the intracellular portion of the receptor. These phosphotyrosines act as docking sites for the SH2 domains of cytoplasmic STAT1 and STAT2, scaffolding them to the JAK1/TYK2 kinases allowing for their activation through phosphorylation. Phospho-STAT1 and phospho-STAT2 form stable heterodimers which dissociate from the receptor. Together with cytoplasmic IRF9, they form the ISGF3 complex, which once translocated to the nucleus, can bind to the ISRE DNA sequence motif and induce the transcription of the ISG genes (*OAS1*, *IFIH1*, *ISG15*, *DDX58* etc.)

My data from TNFα-stimulated CAFs supports the existence of a non-canonical STAT1-independent IFNβ1 signaling. If the pathway was dependent on the presence of both STAT1 and STAT2, knockdown of either would have prevented its ultimate outcome - the increased expression of the ISGs. Instead, my data suggests that only STAT2 is indispensable, since silencing of *STAT2* but not of *STAT1* resulted in failure to induce *OAS1*, *IFIH1*, *ISG15* and *DDX58* transcription (Figure 35). Such non-canonical type I interferon signaling has been already described before (Fink and Grandvaux, 2013). Several possible scenarios have been reported (Figure 37). For example, phospho-STAT2 can form a functional dimer with phospho-STAT6, and together they can associate with IRF9 to form a complex capable of binding to ISRE (Wan *et al.*, 2008). In addition, the formation of alternative STAT1-independent ISGF3-like complexes consisted of IRF9 and phopho-STAT2 or unphosphorylated STAT2 homodimers has been observed (Lou *et al*., 2009; Fink *et al*., 2013; Blaszczyk *et al*., 2015; Nan *et al*., 2018).

My data cannot rule out possible involvement of STAT6 in the interferon signaling observed in TNFα-stimulated CAF2 cultures. In fact, RNA-seq data, generated previously in our lab by Dr. Mireia Berdiel-Acer and analyzed by Dr. Birgitta Michels, shows that the CAFs, and especially the CAF2 cells, express *STAT6* at transcript levels relatively similar to those for *STAT2* (Table S2). Silencing of *STAT6* prior to the stimulation will be necessary to find out whether it is as essential as STAT2 for the upregulation of the ISG signature. If the expression of the ISGs turns out to not be dependent on STAT6, it would be fair to assume that it relies only on STAT2 homodimers, especially considering that the transcript levels of the other untested STATs (*STAT4*, *STAT5A* and *STAT5B*) are rather low in the CAFs according to the RNA-seq data (Table S2). In addition, interference with *IRF9* expression could also be used to confirm its involvement in the pathway as part of the ISGF3-like complex.

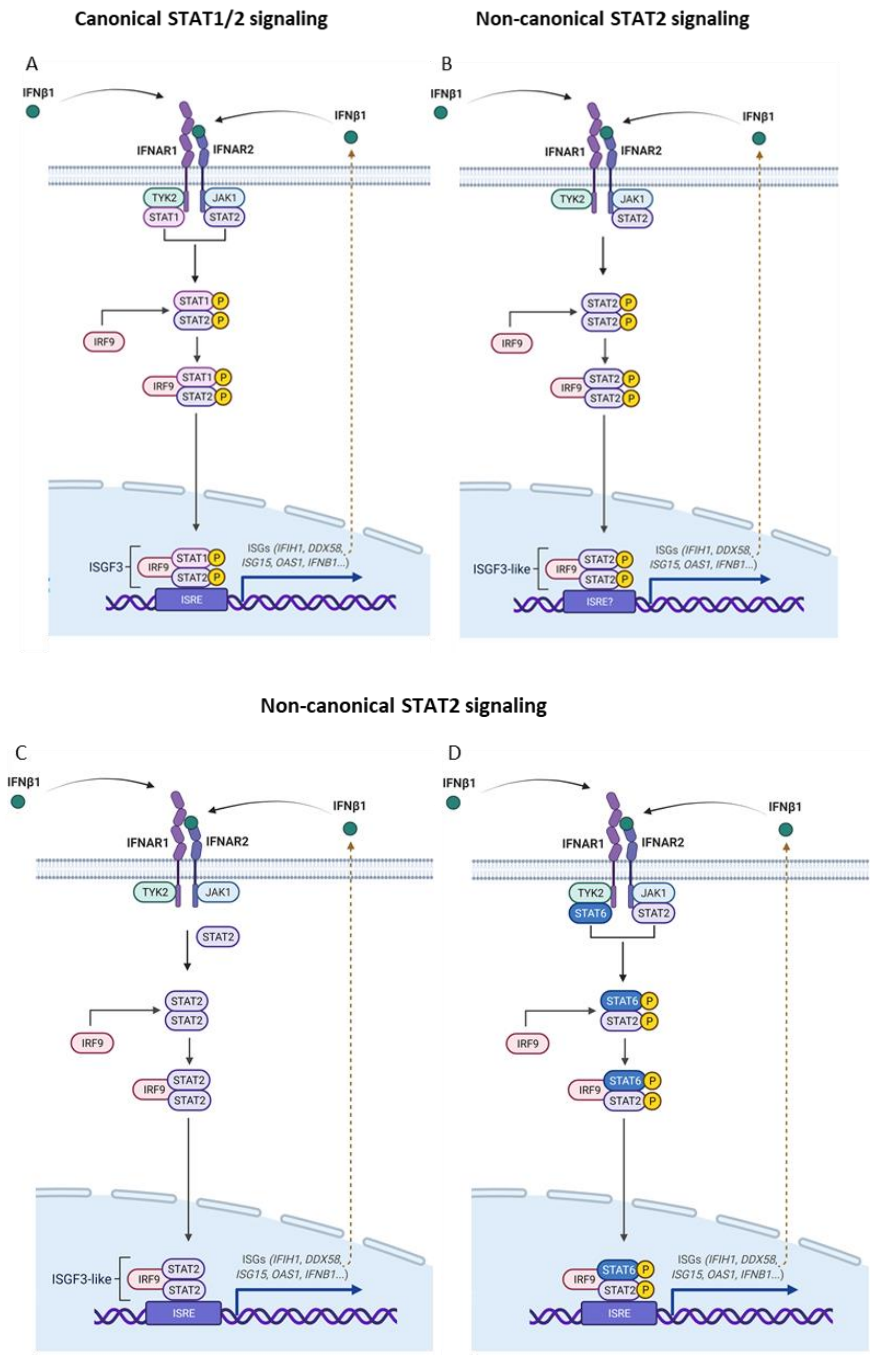

Figure 37. **Canonical and non-canonical IFNβ1/STAT signaling.** (A) In canonical IFNβ1/STAT signaling, STAT1 and STAT2 get phosphorylated upon IFNβ1 binding to its receptor and form a heterodimer. Phospho-STAT1/2 then can associate with IRF9 to form the ISGF3 complex which is translocated to the nucleus. There it binds the ISRE and induces the transcription of the ISG genes. (B-D) In the non-canonical STAT1-independent IFNβ1 signaling several scenarios are possible. STAT2, phosphorylated (B) or unphosphorylated (C), can form homodimers which can associate with IRF9 to form an ISGF3-like complex. Alternatively, phospho-STAT2 can also form a heterodimer with phospho-STAT6 (D) and together they can form a complex with IRF9, which again can induce the transcription of the ISG genes. Image created with Biorender.

5.7 TNFα-IFNβ1 synergism

In this study I have identified potential synergism between the pathways induced by tumor necrosis factor-α and interferon-β1 in breast cancer-associated fibroblasts. Evidence for the crosstalk between the NF-κB and interferon-JAK/STAT signaling pathways can be found in literature as well (Reis *et al*., 1989; Bartee *et al*., 2008; Yarilina and Ivashkiv, 2010). Upon stimulation of the CAFs with TNFα, the NF-κB pathway was activated, as demonstrated by the secretion of IL6 (Figure 11A). The activation of the NF- κB pathway ultimately led to upregulation of *IFNB1* expression (Figure 29B, Figure 35). IFNβ1 was then secreted (Figure 29C) and could bind its receptor, thus activating the JAK/STAT signaling pathway, which led to the elevated expression of the ISGs, including *IFNB1* (Figure 35). Silencing of *IFNAR1* or *STAT2* partially abolished *IFNB1* upregulation in response to TNFα. The effect on *IFNB1* expression was even more pronounced when *RELA*, coding for a major component of the NF-κB complex, was silenced. This confirmed that indeed the NF-κB pathway, and not the JAK/STAT pathway, was responsible for this initial burst in *IFNB1* expression. Interfering with the latter pathway though (siIFNAR1/siSTAT2) reduced the overall effect of the stimulation on *IFNB1* mRNA levels, showing that both pathways contributed to the *IFNB1* upregulation (Figure 35).

A positive feedback loop existed in both pathways. IFNβ1 activated the JAK/STAT pathway which resulted in *IFNB1* transcription. Similarly, stimulation of the NF-κB pathway with TNFα resulted in *TNF* upregulation (Figure 32). Thus, both cytokines could be present long after the addition of the stimulation. This seemed to result in sustained JAK/STAT signaling, as demonstrated by maintenance of elevated ISGs expression levels that lasted for at least 24h post TNFα withdrawal, or a total of 48h since the initiation of the stimulation (Figure 32).

5.8 The STING pathway and cancer

The synergy of action of TNFα and IFNβ1 can be quite essential for initiating a rapid inflammatory response against a viral infection. Moreover, due to the positive feedback, the pathways that these cytokines activate, can sustain the anti-viral state for a prolonged period. In the context of cancer and chemotherapy,

the main source of the inflammatory triggers is not usually of viral origin. Instead, it is rather of self-origin - dsDNA released in the cytosol of dying cancer cells. dsDNA is usually found in the nucleus, not in the cytosol. Therefore, once in this unusual location, the misplaced dsDNA is sensed as foreign by the cGAS-STING (stimulator of interferon genes) pathway which leads to the activation of type I interferon response, as well as NF-κB signaling (Balka and Nardo, 2020). The cGAS-STING signaling is essential for the sensing of foreign viral nucleic acids and initiation of the anti-viral response. Its effect on tumor progression has been explored for years. Mouse studies show that STING activation can act as a switch which turns on the anti-tumor immune response and thus leads to tumor regression (Corrales *et al*., 2015). STING agonists have been developed and are currently in preclinical and clinical trials as monotreatment and in combination with chemotherapy or other immunotherapy approaches (Amouzegar *et al*., 2021).

Whether or not the STING pathway is involved in the development of chemoresistance in our in vitro model remains to be clarified but is highly probable. It may be interesting to know what its exact effect is when the immune system is not included in the equation, which is the case in our CAF-tumor system, and possibly mimics what happens in severely immunocompromised cancer patients. In this scenario, silencing the STING pathway in the chemotreated breast cancer cells should prevent the upregulation of the ISG signature in the tumor cells, which would then secrete less IFNβ1. Perhaps that would result in failure of the breast cancer cell to induce the antiviral state in the CAFs cocultured with them, and thus less tumor recovery post chemotherapy would be observed. The CAFs which have been stimulated with TNFα though would still show high ISG expression independently from the STING pathway, and rather due to the crosstalk between the NF-κB and IFNβ1/STAT signaling pathways.

5.9 Interferon/JAK/STAT, NF-κB and chemoresistance

While there seems to be an agreement in the scientific community on the possibility of exploiting the STING pathway as an anti-tumor therapeutic target, no consensus has been reached so far on whether interferon signaling could be similarly manipulated for the benefit of cancer patients. It is fair to assume that in the recovery assays shown here (Figure 31-32), there are two main sources of

interferon-β1: 1) the dying cancer cells, in which the STING pathway has been potentially activated, and 2) the CAFs, which have been pre-stimulated with TNFα, and their respective CM. Regardless of the source of IFNβ1, the interferon/JAK/STAT pathway can be activated in both the tumor (Figure 25) and the stroma (Figure 23), here represented by the MCF7 and CAF1 cell lines, respectively. Thus, both entities can acquire an antiviral state and potentially relay it to each other. While in previous studies the initiation of interferon signaling in the CAFs seems to be important for their ability to support tumor regrowth after chemotherapy (Maia *et al*., 2021), here the picture seems to be more complicated. Stimulation of the CAFs with TNFα initiated the expression of the ISG signature (Figure 33) and yet neither these CAFs, nor their CM could support the recovery of the chemotreated cancer cells better than their unstimulated counterparts (Figure 31-32). This raises the question of whether the interplay between the NF-κB and STAT signaling is the reason for these perplexing observations. Could the inflammatory response, when sustained over a long period, become damaging towards the cancer cells rather than protective? This is quite probable, especially considering that it can result in TNFα production, at least in the CAFs, as my qPCR data suggests (Figure 33). The CAF-secreted TNFα may inhibit MCF7 proliferation or induce MCF7 cell death, which is supported by the fact that CM from TNFα -stimulated CAFs resulted in a decrease in MCF7 nuclei counts (Figure S4). Whether the TNFα, of endogenous and exogenous origin, is responsible for the inability of the CM from stimulated CAFs to support tumor recovery post chemotherapy can be tested by adding TNFα neutralization antibody to the CM prior to using it on the cancer cells. If the TNFα indeed is harmful to the cancer cells, the neutralization antibody should prevent its toxicity, and the CM from TNFα-stimulated CAFs should then be able to support the recovery of the cancer cells just as CM from unstimulated CAFs does. Furthermore, since this stimulated CAF CM will also contain components secreted due to the induction of interferon signaling, it may even further increase recovery but only if first treated with TNFα neutralization antibody. The exact identity of the CAF-secreted factors which lead to the chemoresistant (or -persistent) breast cancer phenotype remains to be elucidated in future studies.

Another important aspect to consider is that not all cancer cells that recovered after the chemotherapy are necessarily permanently resistant to it. To check whether they are indeed resistant, additional experiments, in which the recovered cells are re-treated with the same chemodrug, need to be performed. If truly resistant, comparison with their non-resistant counterparts, through an RNA-seq analysis for example, may give us insights into what pathways may have driven the development of the drug resistance and how soluble CAF factors may have contributed. Since pathways have known signals that elicit them, once the former is known, the latter can be confirmed by CAF secretome analysis via targeted mass spectrometry or other approaches (ELISA, FLISA, or WB). Perturbation of the suspected pathways and CAF-secreted factors can be used to validate their role in inducing chemoresistance.

6. CONCLUSIONS & OUTLOOK

Luminal A breast cancer, albeit with good initial response to standard endocrine therapies, still often results in tumor relapse and ultimately, years after diagnosis, may be the cause of death. It is believed that the tumor-microenvironment (TME) contributes to Luminal A progression, but the exact mechanisms are still a matter of research. Here, in this thesis, I investigated the role of cancer-associated fibroblasts, a major component of the TME, in the progression of Luminal A breast cancer. To mimic some of the TME factors to which the CAFs are physiologically exposed, I used human recombinant TNFα and TGFβ1, cytokines known to induce conversion of CAF precursors into CAFs, as well as NF and CAF activation.

My first major finding was that upon cytokine-activation, CAF secretion of pro-migratory factors appeared to be increased, as demonstrated by the effect of the CAF CM on Luminal A breast cancer migration. Both MCF7 and T47D cells, classical models of this cancer subtype, migrated to a greater extent when treated with CM of cytokine-stimulated CAFs in comparison to CM collected from unstimulated CAFs. To achieve such an effect on Lum A migration, the E6/E7 immortalized CAFs required activation with both TNFα and TGFβ1, while for primary CAF cultures the stimulation with TNFα alone was sufficient. Perhaps this was due to differences in endogenous TGFβ1 signaling.

Next, I attempted to identify the exact CAF-secreted pro-migratory factors. I was able to show that the Lum A migration was most likely due to high molecular weight proteins. To identify the exact identity of the responsible secreted proteins, I utilized secretome analysis via label-free HPLC-MS, run in the DDA (data-dependent acquisition) mode. This approach did not produce promising findings, as far as the identity of the pro-migratory factors was concerned. Perhaps, using DIA (data-independent acquisition) settings in the future may help increase the list of potential targets.

The mass spec analysis of the CAF full proteome gave further insights into the effect of the stimulation on the CAFs. It revealed that the TNFα stimulation resulted in the activation of interferon signaling in the CAFs. RNA-seq analysis of CM-treated MCF7 breast cancer cells showed that the CAFs were able to relay the TNFα-activated IFN signaling to the cancer cells. I then demonstrated that CAF-secreted IFNβ1 was perhaps the responsible mediator. In *vitro* validation of the RNA-seq findings showed that indeed the CM from TNFα-stimulated CAFs could induce JAK/STAT signaling in the cancer cells. However, I found no connection between the migratory phenotype and the interferon-induced JAK/STAT signaling. This signaling pathway, contrary to previous findings, also did not appear to induce MCF7 autophagy or increase the ability of the CAFs to support Lum A recovery post chemotherapy.

I could demonstrate however, that, in the CAFs, there was a crosstalk between the TNFα-activated NF-κB pathway and the interferon-beta JAK/STAT2 signaling, and that this signaling appeared to be STAT1-independent. Further investigation is required to find out whether STAT2 works alone as a homodimer or in combination with another STAT, and what are the consequences of STAT activation in the CAFs for the cancer cells.

Finally, I demonstrated that TNFα seemed to play a double role in Luminal A breast cancer. On one side it appeared to be anti-tumorigenic by itself or perhaps by eliciting the secretion of anti-proliferative factors by the CAFs. On the other side, it was able to activate the primary CAFs and drive them to secrete pro-migratory factors. My data is in agreement with already published work of the double role of TNFα in cancer. Although no in *vivo* data is presented here due to lack of promising Luminal A mouse models, my in *vitro* findings are in accordance with the published

clinical data, suggesting that perhaps the levels of TNFα in the plasma or tumor of Luminal A breast cancer patients could be indicative of worse prognosis. Perhaps in the future TNFα blockers could prevent Luminal A metastasis and relapse. However, due to the double role of TNFα in cancer, demonstrated here and in literature, such therapeutic steps should perhaps be made in a CAF-targeted manner. Otherwise, we may run into the problem of unwillingly inducing Lum A proliferation or recovery after chemotherapy once the anti-cancer effects of TNFα are lifted.

To sum up, in my PhD thesis work I was able to investigate the complex CAF-tumor crosstalk and study several of the factors and pathways which may play a role in Luminal A progression. I was able to identify TNFα as an important player in this crosstalk and to make recommendation for the use of TNFα blockers for the prevention of Luminal A metastasis, with the caveat that further investigation is needed to avoid unwanted side-effects and possible increased cancer cell proliferation.

REFERENCES

1. Acerbi I, Cassereau L, Dean I, Shi Q, Au A, Park C, Chen YY, Liphardt J, Hwang ES, Weaver VM. Human breast cancer invasion and aggression correlates with ECM stiffening and immune cell infiltration. Integr Biol (Camb). 2015 Oct;7(10):1120-34. PMID: 25959051.
2. Aiello NM, Kang Y. Context-dependent EMT programs in cancer metastasis. J Exp Med. 2019 May 6;216(5):1016-1026. PMID: 30975895.
3. Alitalo K, Hovi T, Vaheri A. Fibronectin is produced by human macrophages. J Exp Med. 1980 Mar 1;151(3):602-13. PMID: 7359083.
4. Alvarez MJ, Shen Y, Giorgi FM, Lachmann A, Ding BB, Ye BH, Califano A. Functional characterization of somatic mutations in cancer using network-based inference of protein activity. Nat Genet. 2016 Aug;48(8):838-47. PMID: 27322546.
5. Ambjørn M, Ejlerskov P, Liu Y, Lees M, Jäättelä M, Issazadeh-Navikas S. IFNB1/interferon-β-induced autophagy in MCF-7 breast cancer cells counteracts its proapoptotic function. Autophagy. 2013 Mar;9(3):287-302. PMID: 23221969.
6. Amouzegar A, Chelvanambi M, Filderman JN, Storkus WJ, Luke JJ. STING Agonists as Cancer Therapeutics. Cancers (Basel). 2021 May 30;13(11):2695. PMID: 34070756.

7. Anders S, Pyl PT, Huber W. HTSeq--a Python framework to work with high-throughput sequencing data. Bioinformatics. 2015 Jan 15;31(2):166-9. PMID: 25260700.
8. Andrews RN, Caudell DL, Metheny-Barlow LJ, Peiffer AM, Tooze JA, Bourland JD, Hampson RE, Deadwyler SA, Cline JM. Fibronectin Produced by Cerebral Endothelial and Vascular Smooth Muscle Cells Contributes to Perivascular Extracellular Matrix in Late-Delayed Radiation-Induced Brain Injury. Radiat Res. 2018 Oct;190(4):361-373. PMID: 30016219.
9. Arcucci A, Ruocco MR, Granato G, Sacco AM, Montagnani S. Cancer: An Oxidative Crosstalk between Solid Tumor Cells and Cancer Associated Fibroblasts. Biomed Res Int. 2016;2016:4502846. PMID: 27595103.
10. Arina A, Idel C, Hyjek EM, Alegre ML, Wang Y, Bindokas VP, Weichselbaum RR, Schreiber H. Tumor-associated fibroblasts predominantly come from local and not circulating precursors. Proc Natl Acad Sci U S A. 2016 Jul 5;113(27):7551-6. PMID: 27317748.
11. Avgustinova A, Iravani M, Robertson D, Fearns A, Gao Q, Klingbeil P, Hanby AM, Speirs V, Sahai E, Calvo F, Isacke CM. Tumour cell-derived Wnt7a recruits and activates fibroblasts to promote tumour aggressiveness. Nat Commun. 2016 Jan 18;7:10305. PMID: 26777421.
12. Babaei G, Aziz SG, Jaghi NZZ. EMT, cancer stem cells and autophagy; The three main axes of metastasis. Biomed Pharmacother. 2021 Jan;133:110909. PMID: 33227701.
13. Babicki S, Arndt D, Marcu A, Liang Y, Grant JR, Maciejewski A, Wishart DS. Heatmapper: web-enabled heat mapping for all. Nucleic Acids Res. 2016 Jul 8;44(W1):W147-53. PMID: 27190236.
14. Bae S, Park CW, Son HK, Ju HK, Paik D, Jeon CJ, Koh GY, Kim J, Kim H. Fibroblast activation protein alpha identifies mesenchymal stromal cells from human bone marrow. Br J Haematol. 2008 Sep;142(5):827-30. PMID: 18510677.
15. Barrett R, Puré E. Cancer-associated fibroblasts: key determinants of tumor immunity and immunotherapy. Curr Opin Immunol. 2020 Jun;64:80-87. PMID: 32402828.
16. Bartee E, Mohamed MR, Lopez MC, Baker HV, McFadden G. The addition of tumor necrosis factor plus beta interferon induces a novel synergistic antiviral state against poxviruses in primary human fibroblasts. J Virol. 2009 Jan;83(2):498-511. PMID: 18971273.
17. Bartoschek M, Oskolkov N, Bocci M, Lövrot J, Larsson C, Sommarin M, Madsen CD, Lindgren D, Pekar G, Karlsson G, Ringnér M, Bergh J, Björklund Å, Pietras K. Spatially and functionally distinct subclasses of

breast cancer-associated fibroblasts revealed by single cell RNA sequencing. Nat Commun. 2018 Dec 4;9(1):5150. PMID: 30514914.
18. Bauer J, Emon MAB, Staudacher JJ, Thomas AL, Zessner-Spitzenberg J, Mancinelli G, Krett N, Saif MT, Jung B. Increased stiffness of the tumor microenvironment in colon cancer stimulates cancer associated fibroblast-mediated prometastatic activin A signaling. Sci Rep. 2020 Jan 9;10(1):50. Erratum in: Sci Rep. 2020 Apr 30;10(1):7606. PMID: 31919369.
19. Becker LM, O'Connell JT, Vo AP, Cain MP, Tampe D, Bizarro L, Sugimoto H, McGow AK, Asara JM, Lovisa S, McAndrews KM, Zielinski R, Lorenzi PL, Zeisberg M, Raza S, LeBleu VS, Kalluri R. Epigenetic Reprogramming of Cancer-Associated Fibroblasts Deregulates Glucose Metabolism and Facilitates Progression of Breast Cancer. Cell Rep. 2020 Jun 2;31(9):107701. PMID: 32492417.
20. Berdiel-Acer M, Maia A, Hristova Z, Borgoni S, Vetter M, Burmester S, Becki C, Michels B, Abnaof K, Binenbaum I, Bethmann D, Chatziioannou A, Hasmann M, Thomssen C, Espinet E, Wiemann S. Stromal NRG1 in luminal breast cancer defines pro-fibrotic and migratory cancer-associated fibroblasts. Oncogene. 2021 Apr;40(15):2651-2666. PMID: 33692466.
21. Bergers G, Song S. The role of pericytes in blood-vessel formation and maintenance. Neuro Oncol. 2005 Oct;7(4):452-64. PMID: 16212810.
22. Bertero T, Oldham WM, Grasset EM, Bourget I, Boulter E, Pisano S, Hofman P, Bellvert F, Meneguzzi G, Bulavin DV, Estrach S, Feral CC, Chan SY, Bozec A, Gaggioli C. Tumor-Stroma Mechanics Coordinate Amino Acid Availability to Sustain Tumor Growth and Malignancy. Cell Metab. 2019 Jan 8;29(1):124-140.e10. PMID: 30293773.
23. Biffi G, Oni TE, Spielman B, Hao Y, Elyada E, Park Y, Preall J, Tuveson DA. IL1-Induced JAK/STAT Signaling Is Antagonized by TGFβ to Shape CAF Heterogeneity in Pancreatic Ductal Adenocarcinoma. Cancer Discov. 2019 Feb;9(2):282-301. PMID: 30366930.
24. Biffi G, Tuveson DA. Diversity and Biology of Cancer-Associated Fibroblasts. Physiol Rev. 2021 Jan 1;101(1):147-176. PMID: 32466724.
25. Blaszczyk K, Olejnik A, Nowicka H, Ozgyin L, Chen YL, Chmielewski S, Kostyrko K, Wesoly J, Balint BL, Lee CK, Bluyssen HA. STAT2/IRF9 directs a prolonged ISGF3-like transcriptional response and antiviral activity in the absence of STAT1. Biochem J. 2015 Mar 15;466(3):511-24. PMID: 25564224.
26. Bliss LA, Sams MR, Deep-Soboslay A, Ren-Patterson R, Jaffe AE, Chenoweth JG, Jaishankar A, Kleinman JE, Hyde TM. Use of postmortem

human dura mater and scalp for deriving human fibroblast cultures. PLoS One. 2012;7(9):e45282. PMID: 23028905.
27. Bochet L, Lehuédé C, Dauvillier S, Wang YY, Dirat B, Laurent V, Dray C, Guiet R, Maridonneau-Parini I, Le Gonidec S, Couderc B, Escourrou G, Valet P, Muller C. Adipocyte-derived fibroblasts promote tumor progression and contribute to the desmoplastic reaction in breast cancer. Cancer Res. 2013 Sep 15;73(18):5657-68. PMID: 23903958.
28. Boelens MC, Wu TJ, Nabet BY, Xu B, Qiu Y, Yoon T, Azzam DJ, Twyman-Saint Victor C, Wiemann BZ, Ishwaran H, Ter Brugge PJ, Jonkers J, Slingerland J, Minn AJ. Exosome transfer from stromal to breast cancer cells regulates therapy resistance pathways. Cell. 2014 Oct 23;159(3):499-513. PMID: 25417103.
29. Brahimi-Horn MC, Chiche J, Pouysségur J. Hypoxia and cancer. J Mol Med (Berl). 2007 Dec;85(12):1301-7. PMID: 18026916.
30. Brandão M, Pondé NF, Poggio F, Kotecki N, Salis M, Lambertini M, de Azambuja E. Combination therapies for the treatment of HER2-positive breast cancer: current and future prospects. Expert Rev Anticancer Ther. 2018 Jul;18(7):629-649. PMID: 29781317.
31. Brown ER, Charles KA, Hoare SA, Rye RL, Jodrell DI, Aird RE, Vora R, Prabhakar U, Nakada M, Corringham RE, DeWitte M, Sturgeon C, Propper D, Balkwill FR, Smyth JF. A clinical study assessing the tolerability and biological effects of infliximab, a TNF-alpha inhibitor, in patients with advanced cancer. Ann Oncol. 2008 Jul;19(7):1340-1346. PMID: 18325912.
32. Bughda R, Dimou P, D'Souza RR, Klampatsa A. Fibroblast Activation Protein (FAP)-Targeted CAR-T Cells: Launching an Attack on Tumor Stroma. Immunotargets Ther. 2021 Aug 5;10:313-323. PMID: 34386436.
33. Burow ME, Weldon CB, Tang Y, Navar GL, Krajewski S, Reed JC, Hammond TG, Clejan S, Beckman BS. Differences in susceptibility to tumor necrosis factor alpha-induced apoptosis among MCF-7 breast cancer cell variants. Cancer Res. 1998 Nov 1;58(21):4940-6. PMID: 9810003.
34. Butti R, Nimma R, Kundu G, Bulbule A, Kumar TVS, Gunasekaran VP, Tomar D, Kumar D, Mane A, Gill SS, Patil T, Weber GF, Kundu GC. Tumor-derived osteopontin drives the resident fibroblast to myofibroblast differentiation through Twist1 to promote breast cancer progression. Oncogene. 2021 Mar;40(11):2002-2017. PMID: 33603163.
35. Cain H, Kraus B, Krauspe R, Osborn M, Weber K. Vimentin filaments in peritoneal macrophages at various stages of differentiation and with

altered function. Virchows Arch B Cell Pathol Incl Mol Pathol. 1983;42(1):65-81. PMID: 6132490.

36. Calvo F, Ege N, Grande-Garcia A, Hooper S, Jenkins RP, Chaudhry SI, Harrington K, Williamson P, Moeendarbary E, Charras G, Sahai E. Mechanotransduction and YAP-dependent matrix remodelling is required for the generation and maintenance of cancer-associated fibroblasts. Nat Cell Biol. 2013 Jun;15(6):637-46. PMID: 23708000.
37. Chaudhry SI, Hooper S, Nye E, Williamson P, Harrington K, Sahai E. Autocrine IL-1β-TRAF6 signalling promotes squamous cell carcinoma invasion through paracrine TNFα signalling to carcinoma-associated fibroblasts. Oncogene. 2013 Feb 7;32(6):747-58. PMID: 22450746.
38. Chauhan VP, Martin JD, Liu H, Lacorre DA, Jain SR, Kozin SV, Stylianopoulos T, Mousa AS, Han X, Adstamongkonkul P, Popović Z, Huang P, Bawendi MG, Boucher Y, Jain RK. Angiotensin inhibition enhances drug delivery and potentiates chemotherapy by decompressing tumour blood vessels. Nat Commun. 2013;4:2516. PMID: 24084631.
39. Cheang MC, Chia SK, Voduc D, Gao D, Leung S, Snider J, Watson M, Davies S, Bernard PS, Parker JS, Perou CM, Ellis MJ, Nielsen TO. Ki67 index, HER2 status, and prognosis of patients with luminal B breast cancer. J Natl Cancer Inst. 2009 May 20;101(10):736-50. PMID: 19436038.
40. Chen M, Gowd V, Wang M, Chen F, Cheng KW. The apple dihydrochalcone phloretin suppresses growth and improves chemosensitivity of breast cancer cells via inhibition of cytoprotective autophagy. Food Funct. 2021 Jan 7;12(1):177-190. PMID: 33291138.
41. Chen X, Song E. Turning foes to friends: targeting cancer-associated fibroblasts. Nat Rev Drug Discov. 2019 Feb;18(2):99-115. PMID: 30470818.
42. Chen Y, McAndrews KM, Kalluri R. Clinical and therapeutic relevance of cancer-associated fibroblasts. Nat Rev Clin Oncol. 2021 Dec;18(12):792-804. PMID: 34489603.
43. Cheng Y, Li H, Deng Y, Tai Y, Zeng K, Zhang Y, Liu W, Zhang Q, Yang Y. Cancer-associated fibroblasts induce PDL1+ neutrophils through the IL6-STAT3 pathway that foster immune suppression in hepatocellular carcinoma. Cell Death Dis. 2018 Apr 1;9(4):422. PMID: 29556041.
44. Chiappori AA, Eckhardt SG, Bukowski R, Sullivan DM, Ikeda M, Yano Y, Yamada-Sawada T, Kambayashi Y, Tanaka K, Javle MM, Mekhail T, O'bryant CL, Creaven PJ. A phase I pharmacokinetic and pharmacodynamic study of s-3304, a novel matrix metalloproteinase

inhibitor, in patients with advanced and refractory solid tumors. Clin Cancer Res. 2007 Apr 1;13(7):2091-9. PMID: 17404091.

45. Comito G, Giannoni E, Segura CP, Barcellos-de-Souza P, Raspollini MR, Baroni G, Lanciotti M, Serni S, Chiarugi P. Cancer-associated fibroblasts and M2-polarized macrophages synergize during prostate carcinoma progression. Oncogene. 2014 May 8;33(19):2423-31. PMID: 23728338.
46. Corrales L, Glickman LH, McWhirter SM, Kanne DB, Sivick KE, Katibah GE, Woo SR, Lemmens E, Banda T, Leong JJ, Metchette K, Dubensky TW Jr, Gajewski TF. Direct Activation of STING in the Tumor Microenvironment Leads to Potent and Systemic Tumor Regression and Immunity. Cell Rep. 2015 May 19;11(7):1018-30. PMID: 25959818.
47. Costa A, Scholer-Dahirel A, Mechta-Grigoriou F. The role of reactive oxygen species and metabolism on cancer cells and their microenvironment. Semin Cancer Biol. 2014 Apr;25:23-32. PMID: 24406211.
48. Costa A, Kieffer Y, Scholer-Dahirel A, Pelon F, Bourachot B, Cardon M, Sirven P, Magagna I, Fuhrmann L, Bernard C, Bonneau C, Kondratova M, Kuperstein I, Zinovyev A, Givel AM, Parrini MC, Soumelis V, Vincent-Salomon A, Mechta-Grigoriou F. Fibroblast Heterogeneity and Immunosuppressive Environment in Human Breast Cancer. Cancer Cell. 2018 Mar 12;33(3):463-479.e10. PMID: 29455927.
49. Coukell AJ, Faulds D. Epirubicin. An updated review of its pharmacodynamic and pharmacokinetic properties and therapeutic efficacy in the management of breast cancer. Drugs. 1997 Mar;53(3):453-82. PMID: 9074845.
50. Cox J, Hein MY, Luber CA, Paron I, Nagaraj N, Mann M. Accurate proteome-wide label-free quantification by delayed normalization and maximal peptide ratio extraction, termed MaxLFQ. Mol Cell Proteomics. 2014 Sep;13(9):2513-26. PMID: 24942700.
51. Cruceriu D, Baldasici O, Balacescu O, Berindan-Neagoe I. The dual role of tumor necrosis factor-alpha (TNF-α) in breast cancer: molecular insights and therapeutic approaches. Cell Oncol (Dordr). 2020 Feb;43(1):1-18. PMID: 31900901.
52. Dai X, Li T, Bai Z, Yang Y, Liu X, Zhan J, Shi B. Breast cancer intrinsic subtype classification, clinical use and future trends. Am J Cancer Res. 2015 Sep 15;5(10):2929-43. PMID: 26693050.
53. Darby IA, Laverdet B, Bonté F, Desmoulière A. Fibroblasts and myofibroblasts in wound healing. Clin Cosmet Investig Dermatol. 2014 Nov 6;7:301-11. PMID: 25395868.

54. De Francesco EM, Lappano R, Santolla MF, Marsico S, Caruso A, Maggiolini M. HIF-1α/GPER signaling mediates the expression of VEGF induced by hypoxia in breast cancer associated fibroblasts (CAFs). Breast Cancer Res. 2013;15(4):R64. PMID: 23947803.
55. Desmoulière A, Darby IA, Gabbiani G. Normal and pathologic soft tissue remodeling: role of the myofibroblast, with special emphasis on liver and kidney fibrosis. Lab Invest. 2003 Dec;83(12):1689-707. PMID: 14691287.
56. Desmoulière A, Geinoz A, Gabbiani F, Gabbiani G. Transforming growth factor-beta 1 induces alpha-smooth muscle actin expression in granulation tissue myofibroblasts and in quiescent and growing cultured fibroblasts. J Cell Biol. 1993 Jul;122(1):103-11. PMID: 8314838.
57. Dillekås H, Rogers MS, Straume O. Are 90% of deaths from cancer caused by metastases? Cancer Med. 2019 Sep;8(12):5574-5576. PMID: 31397113.
58. Dobin A, Davis CA, Schlesinger F, Drenkow J, Zaleski C, Jha S, Batut P, Chaisson M, Gingeras TR. STAR: ultrafast universal RNA-seq aligner. Bioinformatics. 2013 Jan 1;29(1):15-21. PMID: 23104886.
59. Domen A, Quatannens D, Zanivan S, Deben C, Van Audenaerde J, Smits E, Wouters A, Lardon F, Roeyen G, Verhoeven Y, Janssens A, Vandamme T, van Dam P, Peeters M, Prenen H. Cancer-Associated Fibroblasts as a Common Orchestrator of Therapy Resistance in Lung and Pancreatic Cancer. Cancers (Basel). 2021 Feb 27;13(5):987. PMID: 33673405.
60. Donato NJ, Klostergaard J. Distinct stress and cell destruction pathways are engaged by TNF and ceramide during apoptosis of MCF-7 cells. Exp Cell Res. 2004 Apr 1;294(2):523-33. PMID: 15023539.
61. Dong Y, Zheng Q, Wang Z, Lin X, You Y, Wu S, Wang Y, Hu C, Xie X, Chen J, Gao D, Zhao Y, Wu W, Liu Y, Ren Z, Chen R, Cui J. Higher matrix stiffness as an independent initiator triggers epithelial-mesenchymal transition and facilitates HCC metastasis. J Hematol Oncol. 2019 Nov 8;12(1):112. PMID: 31703598.
62. Duluc C, Moatassim-Billah S, Chalabi-Dchar M, Perraud A, Samain R, Breibach F, Gayral M, Cordelier P, Delisle MB, Bousquet-Dubouch MP, Tomasini R, Schmid H, Mathonnet M, Pyronnet S, Martineau Y, Bousquet C. Pharmacological targeting of the protein synthesis mTOR/4E-BP1 pathway in cancer-associated fibroblasts abrogates pancreatic tumour chemoresistance. EMBO Mol Med. 2015 Jun;7(6):735-53. PMID: 25834145.
63. Duperret EK, Trautz A, Ammons D, Perales-Puchalt A, Wise MC, Yan J, Reed C, Weiner DB. Alteration of the Tumor Stroma Using a Consensus

DNA Vaccine Targeting Fibroblast Activation Protein (FAP) Synergizes with Antitumor Vaccine Therapy in Mice. Clin Cancer Res. 2018 Mar 1;24(5):1190-1201. PMID: 29269377.

64. Durinck S, Moreau Y, Kasprzyk A, Davis S, De Moor B, Brazma A, Huber W. BioMart and Bioconductor: a powerful link between biological databases and microarray data analysis. Bioinformatics. 2005 Aug 15;21(16):3439-40. PMID: 16082012.
65. Durinck S, Spellman PT, Birney E, Huber W. Mapping identifiers for the integration of genomic datasets with the R/Bioconductor package biomaRt. Nat Protoc. 2009;4(8):1184-91. PMID: 19617889.
66. Dvorak HF. Tumors: wounds that do not heal. Similarities between tumor stroma generation and wound healing. N Engl J Med. 1986 Dec 25;315(26):1650-9. PMID: 3537791.
67. Ebbing EA, van der Zalm AP, Steins A, Creemers A, Hermsen S, Rentenaar R, Klein M, Waasdorp C, Hooijer GKJ, Meijer SL, Krishnadath KK, Punt CJA, van Berge Henegouwen MI, Gisbertz SS, van Delden OM, Hulshof MCCM, Medema JP, van Laarhoven HWM, Bijlsma MF. Stromal-derived interleukin 6 drives epithelial-to-mesenchymal transition and therapy resistance in esophageal adenocarcinoma. Proc Natl Acad Sci U S A. 2019 Feb 5;116(6):2237-2242. Erratum in: Proc Natl Acad Sci U S A. 2021 Sep 14;118(37). PMID: 30670657.
68. Ene-Obong A, Clear AJ, Watt J, Wang J, Fatah R, Riches JC, Marshall JF, Chin-Aleong J, Chelala C, Gribben JG, Ramsay AG, Kocher HM. Activated pancreatic stellate cells sequester CD8+ T cells to reduce their infiltration of the juxtatumoral compartment of pancreatic ductal adenocarcinoma. Gastroenterology. 2013 Nov;145(5):1121-32. PMID: 23891972.
69. Erdogan B, Ao M, White LM, Means AL, Brewer BM, Yang L, Washington MK, Shi C, Franco OE, Weaver AM, Hayward SW, Li D, Webb DJ. Cancer-associated fibroblasts promote directional cancer cell migration by aligning fibronectin. J Cell Biol. 2017 Nov 6;216(11):3799-3816. PMID: 29021221.
70. Erez N, Truitt M, Olson P, Arron ST, Hanahan D. Cancer-Associated Fibroblasts Are Activated in Incipient Neoplasia to Orchestrate Tumor-Promoting Inflammation in an NF-kappaB-Dependent Manner. Cancer Cell. 2010 Feb 17;17(2):135-47. Erratum in: Cancer Cell. 2010 May 18;17(5):523. Arron, Sarah Tuttleton [added]. PMID: 20138012.
71. Fang J, Xiao L, Joo KI, Liu Y, Zhang C, Liu S, Conti PS, Li Z, Wang P. A potent immunotoxin targeting fibroblast activation protein for

treatment of breast cancer in mice. Int J Cancer. 2016 Feb 15;138(4):1013-23. PMID: 26334777.

72. Feig C, Jones JO, Kraman M, Wells RJ, Deonarine A, Chan DS, Connell CM, Roberts EW, Zhao Q, Caballero OL, Teichmann SA, Janowitz T, Jodrell DI, Tuveson DA, Fearon DT. Targeting CXCL12 from FAP-expressing carcinoma-associated fibroblasts synergizes with anti-PD-L1 immunotherapy in pancreatic cancer. Proc Natl Acad Sci U S A. 2013 Dec 10;110(50):20212-7. PMID: 24277834.
73. Fernández-Nogueira P, Mancino M, Fuster G, López-Plana A, Jauregui P, Almendro V, Enreig E, Menéndez S, Rojo F, Noguera-Castells A, Bill A, Gaither LA, Serrano L, Recalde-Percaz L, Moragas N, Alonso R, Ametller E, Rovira A, Lluch A, Albanell J, Gascon P, Bragado P. Tumor-Associated Fibroblasts Promote HER2-Targeted Therapy Resistance through FGFR2 Activation. Clin Cancer Res. 2020 Mar 15;26(6):1432-1448. PMID: 31699826.
74. ffrench-Constant C. Alternative splicing of fibronectin--many different proteins but few different functions. Exp Cell Res. 1995 Dec;221(2):261-71. PMID: 7493623.
75. Fink K, Grandvaux N. STAT2 and IRF9: Beyond ISGF3. JAKSTAT. 2013 Oct 1;2(4):e27521. PMID: 24498542.
76. Fink K, Martin L, Mukawera E, Chartier S, De Deken X, Brochiero E, Miot F, Grandvaux N. IFNβ/TNFα synergism induces a non-canonical STAT2/IRF9-dependent pathway triggering a novel DUOX2 NADPH oxidase-mediated airway antiviral response. Cell Res. 2013 May;23(5):673-90. Erratum in: Cell Res. 2014 Apr;24(4):509. PMID: 23545780.
77. Flavell RA, Sanjabi S, Wrzesinski SH, Licona-Limón P. The polarization of immune cells in the tumour environment by TGFbeta. Nat Rev Immunol. 2010 Aug;10(8):554-67. PMID: 20616810.
78. Friedman G, Levi-Galibov O, David E, Bornstein C, Giladi A, Dadiani M, Mayo A, Halperin C, Pevsner-Fischer M, Lavon H, Mayer S, Nevo R, Stein Y, Balint-Lahat N, Barshack I, Ali HR, Caldas C, Nili-Gal-Yam E, Alon U, Amit I, Scherz-Shouval R. Cancer-associated fibroblast compositions change with breast cancer progression linking the ratio of $S100A4^{+}$ and $PDPN^{+}$ CAFs to clinical outcome. Nat Cancer. 2020 Jul;1(7):692-708. PMID: 35122040.
79. Froeling FE, Feig C, Chelala C, Dobson R, Mein CE, Tuveson DA, Clevers H, Hart IR, Kocher HM. Retinoic acid-induced pancreatic stellate cell quiescence reduces paracrine Wnt-β-catenin signaling to slow tumor

progression. Gastroenterology. 2011 Oct;141(4):1486-97, 1497.e1-14. PMID: 21704588.

80. Gabbiani G. The myofibroblast in wound healing and fibrocontractive diseases. J Pathol. 2003 Jul;200(4):500-3. PMID: 12845617.
81. Gaggioli C, Hooper S, Hidalgo-Carcedo C, Grosse R, Marshall JF, Harrington K, Sahai E. Fibroblast-led collective invasion of carcinoma cells with differing roles for RhoGTPases in leading and following cells. Nat Cell Biol. 2007 Dec;9(12):1392-400. PMID: 18037882.
82. Gao JJ, Swain SM. Luminal A Breast Cancer and Molecular Assays: A Review. Oncologist. 2018 May;23(5):556-565. PMID: 29472313.
83. Garcia-Alonso L, Holland CH, Ibrahim MM, Turei D, Saez-Rodriguez J. Benchmark and integration of resources for the estimation of human transcription factor activities. Genome Res. 2019 Aug;29(8):1363-1375. Erratum in: Genome Res. 2021 Apr;31(4):745. PMID: 31340985.
84. Gerriets V, Goyal A, Khaddour K. Tumor Necrosis Factor Inhibitors. 2021 Jul 18. In: StatPearls [Internet]. Treasure Island (FL): StatPearls Publishing; 2022 Jan–. PMID: 29494032.
85. Givel AM, Kieffer Y, Scholer-Dahirel A, Sirven P, Cardon M, Pelon F, Magagna I, Gentric G, Costa A, Bonneau C, Mieulet V, Vincent-Salomon A, Mechta-Grigoriou F. miR200-regulated CXCL12β promotes fibroblast heterogeneity and immunosuppression in ovarian cancers. Nat Commun. 2018 Mar 13;9(1):1056. PMID: 29535360.
86. Gok Yavuz B, Gunaydin G, Gedik ME, Kosemehmetoglu K, Karakoc D, Ozgur F, Guc D. Cancer associated fibroblasts sculpt tumour microenvironment by recruiting monocytes and inducing immunosuppressive PD-1^{+} TAMs. Sci Rep. 2019 Feb 28;9(1):3172. PMID: 30816272.
87. Goulet CR, Champagne A, Bernard G, Vandal D, Chabaud S, Pouliot F, Bolduc S. Cancer-associated fibroblasts induce epithelial-mesenchymal transition of bladder cancer cells through paracrine IL-6 signalling. BMC Cancer. 2019 Feb 11;19(1):137. PMID: 30744595.
88. Gratchev A, Guillot P, Hakiy N, Politz O, Orfanos CE, Schledzewski K, Goerdt S. Alternatively activated macrophages differentially express fibronectin and its splice variants and the extracellular matrix protein betaIG-H3. Scand J Immunol. 2001 Apr;53(4):386-92. PMID: 11285119.
89. Grauel AL, Nguyen B, Ruddy D, Laszewski T, Schwartz S, Chang J, Chen J, Piquet M, Pelletier M, Yan Z, Kirkpatrick ND, Wu J, deWeck A, Riester M, Hims M, Geyer FC, Wagner J, MacIsaac K, Deeds J, Diwanji R, Jayaraman P, Yu Y, Simmons Q, Weng S, Raza A, Minie B, Dostalek M, Chikkegowda P, Ruda V, Iartchouk O, Chen N, Thierry R, Zhou J,

Pruteanu-Malinici I, Fabre C, Engelman JA, Dranoff G, Cremasco V. TGFβ-blockade uncovers stromal plasticity in tumors by revealing the existence of a subset of interferon-licensed fibroblasts. Nat Commun. 2020 Dec 9;11(1):6315. PMID: 33298926.

90. Halbert CL, Demers GW, Galloway DA. The E7 gene of human papillomavirus type 16 is sufficient for immortalization of human epithelial cells. J Virol. 1991 Jan;65(1):473-8. PMID: 1845902..
91. Hanahan D, Coussens LM. Accessories to the crime: functions of cells recruited to the tumor microenvironment. Cancer Cell. 2012 Mar 20;21(3):309-22. PMID: 22439926.
92. Harbeck N, Penault-Llorca F, Cortes J, Gnant M, Houssami N, Poortmans P, Ruddy K, Tsang J, Cardoso F. Breast cancer. Nat Rev Dis Primers. 2019 Sep 23;5(1):66. PMID: 31548545.
93. Hawinkels LJ, Paauwe M, Verspaget HW, Wiercinska E, van der Zon JM, van der Ploeg K, Koelink PJ, Lindeman JH, Mesker W, ten Dijke P, Sier CF. Interaction with colon cancer cells hyperactivates TGF-β signaling in cancer-associated fibroblasts. Oncogene. 2014 Jan 2;33(1):97-107. PMID: 23208491.
94. Henke E, Nandigama R, Ergün S. Extracellular Matrix in the Tumor Microenvironment and Its Impact on Cancer Therapy. Front Mol Biosci. 2020 Jan 31;6:160. PMID: 32118030.
95. Hennigs A, Riedel F, Gondos A, Sinn P, Schirmacher P, Marmé F, Jäger D, Kauczor HU, Stieber A, Lindel K, Debus J, Golatta M, Schütz F, Sohn C, Heil J, Schneeweiss A. Prognosis of breast cancer molecular subtypes in routine clinical care: A large prospective cohort study. BMC Cancer. 2016 Sep 15;16(1):734. PMID: 27634735.
96. Hofheinz RD, al-Batran SE, Hartmann F, Hartung G, Jäger D, Renner C, Tanswell P, Kunz U, Amelsberg A, Kuthan H, Stehle G. Stromal antigen targeting by a humanised monoclonal antibody: an early phase II trial of sibrotuzumab in patients with metastatic colorectal cancer. Onkologie. 2003 Feb;26(1):44-8. PMID: 12624517.
97. Horwitz SB. Taxol (paclitaxel): mechanisms of action. Ann Oncol. 1994;5 Suppl 6:S3-6. PMID: 7865431.
98. Hosaka K, Yang Y, Seki T, Fischer C, Dubey O, Fredlund E, Hartman J, Religa P, Morikawa H, Ishii Y, Sasahara M, Larsson O, Cossu G, Cao R, Lim S, Cao Y. Pericyte-fibroblast transition promotes tumor growth and metastasis. Proc Natl Acad Sci U S A. 2016 Sep 20;113(38):E5618-27. PMID: 27608497.
99. Hu D, Li Z, Zheng B, Lin X, Pan Y, Gong P, Zhuo W, Hu Y, Chen C, Chen L, Zhou J, Wang L. Cancer-associated fibroblasts in breast cancer:

Challenges and opportunities. Cancer Commun (Lond). 2022 May;42(5):401-434. PMID: 35481621.

100. Huber MA, Kraut N, Park JE, Schubert RD, Rettig WJ, Peter RU, Garin-Chesa P. Fibroblast activation protein: differential expression and serine protease activity in reactive stromal fibroblasts of melanocytic skin tumors. J Invest Dermatol. 2003 Feb;120(2):182-8. PMID: 12542520.
101. Hussain A, Voisin V, Poon S, Karamboulas C, Bui NHB, Meens J, Dmytryshyn J, Ho VW, Tang KH, Paterson J, Clarke BA, Bernardini MQ, Bader GD, Neel BG, Ailles LE. Distinct fibroblast functional states drive clinical outcomes in ovarian cancer and are regulated by TCF21. J Exp Med. 2020 Aug 3;217(8):e20191094. PMID: 32434219.
102. Ivaska J, Pallari HM, Nevo J, Eriksson JE. Novel functions of vimentin in cell adhesion, migration, and signaling. Exp Cell Res. 2007 Jun 10;313(10):2050-62. PMID: 17512929.
103. Iwano M, Plieth D, Danoff TM, Xue C, Okada H, Neilson EG. Evidence that fibroblasts derive from epithelium during tissue fibrosis. J Clin Invest. 2002 Aug;110(3):341-50. PMID: 12163453.
104. Jacobetz MA, Chan DS, Neesse A, Bapiro TE, Cook N, Frese KK, Feig C, Nakagawa T, Caldwell ME, Zecchini HI, Lolkema MP, Jiang P, Kultti A, Thompson CB, Maneval DC, Jodrell DI, Frost GI, Shepard HM, Skepper JN, Tuveson DA. Hyaluronan impairs vascular function and drug delivery in a mouse model of pancreatic cancer. Gut. 2013 Jan;62(1):112-20. PMID: 22466618.
105. Jeoung DI, Tang B, Sonenberg M. Effects of tumor necrosis factor-alpha on antimitogenicity and cell cycle-related proteins in MCF-7 cells. J Biol Chem. 1995 Aug 4;270(31):18367-73. PMID: 7629160.
106. Johnson KS, Conant EF, Soo MS. Molecular Subtypes of Breast Cancer: A Review for Breast Radiologists. Journal of Breast Imaging. 2021 Jan/Feb;3(1):12-24.
107. Jotzu C, Alt E, Welte G, Li J, Hennessy BT, Devarajan E, Krishnappa S, Pinilla S, Droll L, Song YH. Adipose tissue derived stem cells differentiate into carcinoma-associated fibroblast-like cells under the influence of tumor derived factors. Cell Oncol (Dordr). 2011 Feb;34(1):55-67. PMID: 21327615.
108. Kahounová Z, Kurfürstová D, Bouchal J, Kharaishvili G, Navrátil J, Remšík J, Šimečková Š, Študent V, Kozubík A, Souček K. The fibroblast surface markers FAP, anti-fibroblast, and FSP are expressed by cells of epithelial origin and may be altered during epithelial-to-mesenchymal transition. Cytometry A. 2018 Jul;93(9):941-951. PMID: 28383825.

109. Kai F, Laklai H, Weaver VM. Force Matters: Biomechanical Regulation of Cell Invasion and Migration in Disease. Trends Cell Biol. 2016 Jul;26(7):486-497. PMID: 27056543.
110. Kalluri R. The biology and function of fibroblasts in cancer. Nat Rev Cancer. 2016 Aug 23;16(9):582-98. PMID: 27550820.
111. Kalluri R, Weinberg RA. The basics of epithelial-mesenchymal transition. J Clin Invest. 2009 Jun;119(6):1420-8. doi: 10.1172/JCI39104. Erratum in: J Clin Invest. 2010 May 3;120(5):1786. PMID: 19487818.
112. Kanzaki R, Pietras K. Heterogeneity of cancer-associated fibroblasts: Opportunities for precision medicine. Cancer Sci. 2020 Aug;111(8):2708-2717. PMID: 32573845.
113. Karakasheva TA, Lin EW, Tang Q, Qiao E, Waldron TJ, Soni M, Klein-Szanto AJ, Sahu V, Basu D, Ohashi S, Baba K, Giaccone ZT, Walker SR, Frank DA, Wileyto EP, Long Q, Dunagin MC, Raj A, Diehl JA, Wong KK, Bass AJ, Rustgi AK. IL-6 Mediates Cross-Talk between Tumor Cells and Activated Fibroblasts in the Tumor Microenvironment. Cancer Res. 2018 Sep 1;78(17):4957-4970. PMID: 29976575.
114. Kosmehl H, Berndt A, Katenkamp D. Molecular variants of fibronectin and laminin: structure, physiological occurrence and histopathological aspects. Virchows Arch. 1996 Dec;429(6):311-22. PMID: 8982375.
115. Kumar V, Donthireddy L, Marvel D, Condamine T, Wang F, Lavilla-Alonso S, Hashimoto A, Vonteddu P, Behera R, Goins MA, Mulligan C, Nam B, Hockstein N, Denstman F, Shakamuri S, Speicher DW, Weeraratna AT, Chao T, Vonderheide RH, Languino LR, Ordentlich P, Liu Q, Xu X, Lo A, Puré E, Zhang C, Loboda A, Sepulveda MA, Snyder LA, Gabrilovich DI. Cancer-Associated Fibroblasts Neutralize the Anti-tumor Effect of CSF1 Receptor Blockade by Inducing PMN-MDSC Infiltration of Tumors. Cancer Cell. 2017 Nov 13;32(5):654-668.e5. PMID: 29136508.
116. Lai SL, Tan ML, Hollows RJ, Robinson M, Ibrahim M, Margielewska S, Parkinson EK, Ramanathan A, Zain RB, Mehanna H, Spruce RJ, Wei W, Chung I, Murray PG, Yap LF, Paterson IC. Collagen Induces a More Proliferative, Migratory and Chemoresistant Phenotype in Head and Neck Cancer via DDR1. Cancers (Basel). 2019 Nov 9;11(11):1766. PMID: 31717573.
117. Latif N, Sarathchandra P, Chester AH, Yacoub MH. Expression of smooth muscle cell markers and co-activators in calcified aortic valves. Eur Heart J. 2015 Jun 1;36(21):1335-45. PMID: 24419809.
118. Lau TS, Chan LK, Wong EC, Hui CW, Sneddon K, Cheung TH, Yim SF, Lee JH, Yeung CS, Chung TK, Kwong J. A loop of cancer-stroma-cancer

interaction promotes peritoneal metastasis of ovarian cancer via TNFα-TGFα-EGFR. Oncogene. 2017 Jun 22;36(25):3576-3587. PMID: 28166193.

119. Lazard D, Sastre X, Frid MG, Glukhova MA, Thiery JP, Koteliansky VE. Expression of smooth muscle-specific proteins in myoepithelium and stromal myofibroblasts of normal and malignant human breast tissue. Proc Natl Acad Sci U S A. 1993 Feb 1;90(3):999-1003. PMID: 8430113.
120. Lee DK, Kim BC, Kim IY, Cho EA, Satterwhite DJ, Kim SJ. The human papilloma virus E7 oncoprotein inhibits transforming growth factor-beta signaling by blocking binding of the Smad complex to its target sequence. J Biol Chem. 2002 Oct 11;277(41):38557-64. PMID: 12145312.
121. Legrier ME, Bièche I, Gaston J, Beurdeley A, Yvonnet V, Déas O, Thuleau A, Château-Joubert S, Servely JL, Vacher S, Lassalle M, Depil S, Tucker GC, Fontaine JJ, Poupon MF, Roman-Roman S, Judde JG, Decaudin D, Cairo S, Marangoni E. Activation of IFN/STAT1 signalling predicts response to chemotherapy in oestrogen receptor-negative breast cancer. Br J Cancer. 2016 Jan 19;114(2):177-87. PMID: 26695443.
122. Lehmann BD, Jovanović B, Chen X, Estrada MV, Johnson KN, Shyr Y, Moses HL, Sanders ME, Pietenpol JA. Refinement of Triple-Negative Breast Cancer Molecular Subtypes: Implications for Neoadjuvant Chemotherapy Selection. PLoS One. 2016 Jun 16;11(6):e0157368. PMID: 27310713.
123. Lerrer S, Liubomirski Y, Bott A, Abnaof K, Oren N, Yousaf A, Körner C, Meshel T, Wiemann S, Ben-Baruch A. Co-Inflammatory Roles of TGFβ1 in the Presence of TNFα Drive a Pro-inflammatory Fate in Mesenchymal Stem Cells. Front Immunol. 2017 May 11;8:479. PMID: 28553282.
124. Levine B, Klionsky DJ. Development by self-digestion: molecular mechanisms and biological functions of autophagy. Dev Cell. 2004 Apr;6(4):463-77. PMID: 15068787.
125. Levy JM, Thompson JC, Griesinger AM, Amani V, Donson AM, Birks DK, Morgan MJ, Mirsky DM, Handler MH, Foreman NK, Thorburn A. Autophagy inhibition improves chemosensitivity in BRAF(V600E) brain tumors. Cancer Discov. 2014 Jul;4(7):773-80. PMID: 24823863.
126. Levy JMM, Towers CG, Thorburn A. Targeting autophagy in cancer. Nat Rev Cancer. 2017 Sep;17(9):528-542. PMID: 28751651.
127. Lewis MP, Lygoe KA, Nystrom ML, Anderson WP, Speight PM, Marshall JF, Thomas GJ. Tumour-derived TGF-beta1 modulates myofibroblast differentiation and promotes HGF/SF-dependent invasion of squamous carcinoma cells. Br J Cancer. 2004 Feb 23;90(4):822-32. PMID: 14970860.

128. Li CL, Yang D, Cao X, Wang F, Hong DY, Wang J, Shen XC, Chen Y. Fibronectin induces epithelial-mesenchymal transition in human breast cancer MCF-7 cells via activation of calpain. Oncol Lett. 2017 May;13(5):3889-3895. PMID: 28521486.
129. Li H, Courtois ET, Sengupta D, Tan Y, Chen KH, Goh JJL, Kong SL, Chua C, Hon LK, Tan WS, Wong M, Choi PJ, Wee LJK, Hillmer AM, Tan IB, Robson P, Prabhakar S. Reference component analysis of single-cell transcriptomes elucidates cellular heterogeneity in human colorectal tumors. Nat Genet. 2017 May;49(5):708-718. Erratum in: Nat Genet. 2018 Dec;50(12):1754. PMID: 28319088.
130. Li YJ, Lei YH, Yao N, Wang CR, Hu N, Ye WC, Zhang DM, Chen ZS. Autophagy and multidrug resistance in cancer. Chin J Cancer. 2017 Jun 24;36(1):52. PMID: 28646911.
131. Li J, Jia Z, Kong J, Zhang F, Fang S, Li X, Li W, Yang X, Luo Y, Lin B, Liu T. Carcinoma-Associated Fibroblasts Lead the Invasion of Salivary Gland Adenoid Cystic Carcinoma Cells by Creating an Invasive Track. PLoS One. 2016 Mar 8;11(3):e0150247. PMID: 26954362.
132. Liao Z, Tan ZW, Zhu P, Tan NS. Cancer-associated fibroblasts in tumor microenvironment - Accomplices in tumor malignancy. Cell Immunol. 2019 Sep;343:103729. PMID: 29397066.
133. Liberzon A, Birger C, Thorvaldsdóttir H, Ghandi M, Mesirov JP, Tamayo P. The Molecular Signatures Database (MSigDB) hallmark gene set collection. Cell Syst. 2015 Dec 23;1(6):417-425. PMID: 26771021.
134. Lin TC, Yang CH, Cheng LH, Chang WT, Lin YR, Cheng HC. Fibronectin in Cancer: Friend or Foe. Cells. 2019 Dec 20;9(1):27. PMID: 31861892.
135. Linder S, Wiesner C, Himmel M. Degrading devices: invadosomes in proteolytic cell invasion. Annu Rev Cell Dev Biol. 2011;27:185-211. PMID: 21801014.
136. Liu L, Liu S, Luo H, Chen C, Zhang X, He L, Tu G. GPR30-mediated HMGB1 upregulation in CAFs induces autophagy and tamoxifen resistance in ERα-positive breast cancer cells. Aging (Albany NY). 2021 Jun 28;13(12):16178-16197. PMID: 34182538.
137. Lou YJ, Pan XR, Jia PM, Li D, Xiao S, Zhang ZL, Chen SJ, Chen Z, Tong JH. IRF-9/STAT2 [corrected] functional interaction drives retinoic acid-induced gene G expression independently of STAT1. Cancer Res. 2009 Apr 15;69(8):3673-80. Erratum in: Cancer Res. 2009 May 15;69(10):4553. PMID: 19351818.
138. Love MI, Huber W, Anders S. Moderated estimation of fold change and dispersion for RNA-seq data with DESeq2. Genome Biol. 2014;15(12):550. PMID: 25516281.

139. Madhusudan S, Foster M, Muthuramalingam SR, Braybrooke JP, Wilner S, Kaur K, Han C, Hoare S, Balkwill F, Talbot DC, Ganesan TS, Harris AL. A phase II study of etanercept (Enbrel), a tumor necrosis factor alpha inhibitor in patients with metastatic breast cancer. Clin Cancer Res. 2004 Oct 1;10(19):6528-34. PMID: 15475440.
140. Maehira H, Miyake T, Iida H, Tokuda A, Mori H, Yasukawa D, Mukaisho KI, Shimizu T, Tani M. Vimentin Expression in Tumor Microenvironment Predicts Survival in Pancreatic Ductal Adenocarcinoma: Heterogeneity in Fibroblast Population. Ann Surg Oncol. 2019 Dec;26(13):4791-4804. PMID: 31583548.
141. Maia A, Gu Z, Koch A, Berdiel-Acer M, Will R, Schlesner M, Wiemann S. IFNβ1 secreted by breast cancer cells undergoing chemotherapy reprograms stromal fibroblasts to support tumour growth after treatment. Mol Oncol. 2021 May;15(5):1308-1329. PMID: 33476079.
142. Mannsperger HA, Gade S, Henjes F, Beissbarth T, Korf U. RPPanalyzer: Analysis of reverse-phase protein array data. Bioinformatics. 2010 Sep 1;26(17):2202-3. PMID: 20634205.
143. Mariathasan S, Turley SJ, Nickles D, Castiglioni A, Yuen K, Wang Y, Kadel EE III, Koeppen H, Astarita JL, Cubas R, Jhunjhunwala S, Banchereau R, Yang Y, Guan Y, Chalouni C, Ziai J, Şenbabaoğlu Y, Santoro S, Sheinson D, Hung J, Giltnane JM, Pierce AA, Mesh K, Lianoglou S, Riegler J, Carano RAD, Eriksson P, Höglund M, Somarriba L, Halligan DL, van der Heijden MS, Loriot Y, Rosenberg JE, Fong L, Mellman I, Chen DS, Green M, Derleth C, Fine GD, Hegde PS, Bourgon R, Powles T. TGFβ attenuates tumour response to PD-L1 blockade by contributing to exclusion of T cells. Nature. 2018 Feb 22;554(7693):544-548. PMID: 29443960.
144. Martinez-Outschoorn UE, Pavlides S, Whitaker-Menezes D, Daumer KM, Milliman JN, Chiavarina B, Migneco G, Witkiewicz AK, Martinez-Cantarin MP, Flomenberg N, Howell A, Pestell RG, Lisanti MP, Sotgia F. Tumor cells induce the cancer associated fibroblast phenotype via caveolin-1 degradation: implications for breast cancer and DCIS therapy with autophagy inhibitors. Cell Cycle. 2010 Jun 15;9(12):2423-33. PMID: 20562526.
145. Mathew R, Karantza-Wadsworth V, White E. Role of autophagy in cancer. Nat Rev Cancer. 2007 Dec;7(12):961-7. PMID: 17972889.
146. McDonald LT, Russell DL, Kelly RR, Xiong Y, Motamarry A, Patel RK, Jones JA, Watson PM, Turner DP, Watson DK, Soloff AC, Findlay VJ, LaRue AC. Hematopoietic stem cell-derived cancer-associated fibroblasts are novel contributors to the pro-tumorigenic

microenvironment. Neoplasia. 2015 May;17(5):434-48. PMID: 26025666.
147. Mendonsa AM, Na TY, Gumbiner BM. E-cadherin in contact inhibition and cancer. Oncogene. 2018 Aug;37(35):4769-4780. PMID: 29780167.
148. Mercogliano MF, De Martino M, Venturutti L, Rivas MA, Proietti CJ, Inurrigarro G, Frahm I, Allemand DH, Deza EG, Ares S, Gercovich FG, Guzmán P, Roa JC, Elizalde PV, Schillaci R. TNFα-Induced Mucin 4 Expression Elicits Trastuzumab Resistance in HER2-Positive Breast Cancer. Clin Cancer Res. 2017 Feb 1;23(3):636-648. PMID: 27698002.
149. Mhaidly R, Mechta-Grigoriou F. Role of cancer-associated fibroblast subpopulations in immune infiltration, as a new means of treatment in cancer. Immunol Rev. 2021 Jul;302(1):259-272. PMID: 34013544.
150. Micallef L, Vedrenne N, Billet F, Coulomb B, Darby IA, Desmoulière A. The myofibroblast, multiple origins for major roles in normal and pathological tissue repair. Fibrogenesis Tissue Repair. 2012 Jun 6;5(Suppl 1):S5. PMID: 23259712.
151. Miles DW, Happerfield LC, Naylor MS, Bobrow LG, Rubens RD, Balkwill FR. Expression of tumour necrosis factor (TNF alpha) and its receptors in benign and malignant breast tissue. Int J Cancer. 1994 Mar 15;56(6):777-82. PMID: 8119765.
152. Miyazaki K, Togo S, Okamoto R, Idiris A, Kumagai H, Miyagi Y. Collective cancer cell invasion in contact with fibroblasts through integrin-α5β1/fibronectin interaction in collagen matrix. Cancer Sci. 2020 Dec;111(12):4381-4392. PMID: 32979884.
153. Miyazaki Y, Oda T, Mori N, Kida YS. Adipose-derived mesenchymal stem cells differentiate into pancreatic cancer-associated fibroblasts in vitro. FEBS Open Bio. 2020 Nov;10(11):2268-2281. PMID: 32931156.
154. Moasser MM. The oncogene HER2: its signaling and transforming functions and its role in human cancer pathogenesis. Oncogene. 2007 Oct 4;26(45):6469-87. PMID: 17471238.
155. Montfort A, Filleron T, Virazels M, Dufau C, Milhès J, Pagès C, Olivier P, Ayyoub M, Mounier M, Lusque A, Brayer S, Delord JP, Andrieu-Abadie N, Levade T, Colacios C, Ségui B, Meyer N. Combining Nivolumab and Ipilimumab with Infliximab or Certolizumab in Patients with Advanced Melanoma: First Results of a Phase Ib Clinical Trial. Clin Cancer Res. 2021 Feb 15;27(4):1037-1047. PMID: 33272982.
156. Mor-Vaknin N, Punturieri A, Sitwala K, Markovitz DM. Vimentin is secreted by activated macrophages. Nat Cell Biol. 2003 Jan;5(1):59-63. PMID: 12483219.

157. Mueller L, Goumas FA, Affeldt M, Sandtner S, Gehling UM, Brilloff S, Walter J, Karnatz N, Lamszus K, Rogiers X, Broering DC. Stromal fibroblasts in colorectal liver metastases originate from resident fibroblasts and generate an inflammatory microenvironment. Am J Pathol. 2007 Nov;171(5):1608-18. PMID: 17916596.
158. Na TY, Schecterson L, Mendonsa AM, Gumbiner BM. The functional activity of E-cadherin controls tumor cell metastasis at multiple steps. Proc Natl Acad Sci U S A. 2020 Mar 17;117(11):5931-5937. PMID: 32127478.
159. Nair N, Calle AS, Zahra MH, Prieto-Vila M, Oo AKK, Hurley L, Vaidyanath A, Seno A, Masuda J, Iwasaki Y, Tanaka H, Kasai T, Seno M. A cancer stem cell model as the point of origin of cancer-associated fibroblasts in tumor microenvironment. Sci Rep. 2017 Jul 28;7(1):6838. PMID: 28754894.
160. Nakamura H, Takada K. Reactive oxygen species in cancer: Current findings and future directions. Cancer Sci. 2021 Oct;112(10):3945-3952. PMID: 34286881.
161. Nan J, Wang Y, Yang J, Stark GR. IRF9 and unphosphorylated STAT2 cooperate with NF-κB to drive IL6 expression. Proc Natl Acad Sci U S A. 2018 Apr 10;115(15):3906-3911. PMID: 29581268.
162. Narra K, Mullins SR, Lee HO, Strzemkowski-Brun B, Magalong K, Christiansen VJ, McKee PA, Egleston B, Cohen SJ, Weiner LM, Meropol NJ, Cheng JD. Phase II trial of single agent Val-boroPro (Talabostat) inhibiting Fibroblast Activation Protein in patients with metastatic colorectal cancer. Cancer Biol Ther. 2007 Nov;6(11):1691-9. PMID: 18032930.
163. Navab R, Strumpf D, Bandarchi B, Zhu CQ, Pintilie M, Ramnarine VR, Ibrahimov E, Radulovich N, Leung L, Barczyk M, Panchal D, To C, Yun JJ, Der S, Shepherd FA, Jurisica I, Tsao MS. Prognostic gene-expression signature of carcinoma-associated fibroblasts in non-small cell lung cancer. Proc Natl Acad Sci U S A. 2011 Apr 26;108(17):7160-5. PMID: 21474781.
164. Neill T, Schaefer L, Iozzo RV. Decorin: a guardian from the matrix. Am J Pathol. 2012 Aug;181(2):380-7. PMID: 22735579.
165. Neri S, Ishii G, Hashimoto H, Kuwata T, Nagai K, Date H, Ochiai A. Podoplanin-expressing cancer-associated fibroblasts lead and enhance the local invasion of cancer cells in lung adenocarcinoma. Int J Cancer. 2015 Aug 15;137(4):784-96. PMID: 25648219.
166. Ngan CY, Yamamoto H, Seshimo I, Tsujino T, Man-i M, Ikeda JI, Konishi K, Takemasa I, Ikeda M, Sekimoto M, Matsuura N, Monden M.

Quantitative evaluation of vimentin expression in tumour stroma of colorectal cancer. Br J Cancer. 2007 Mar 26;96(6):986-92. PMID: 17325702.

167. Ning X, Zhang H, Wang C, Song X. Exosomes Released by Gastric Cancer Cells Induce Transition of Pericytes Into Cancer-Associated Fibroblasts. Med Sci Monit. 2018 Apr 18;24:2350-2359. PMID: 29668670.
168. Nissen NI, Karsdal M, Willumsen N. Collagens and Cancer associated fibroblasts in the reactive stroma and its relation to Cancer biology. J Exp Clin Cancer Res. 2019 Mar 6;38(1):115. PMID: 30841909.
169. Nurmik M, Ullmann P, Rodriguez F, Haan S, Letellier E. In search of definitions: Cancer-associated fibroblasts and their markers. Int J Cancer. 2020 Feb 15;146(4):895-905. PMID: 30734283.
170. Öhlund D, Elyada E, Tuveson D. Fibroblast heterogeneity in the cancer wound. J Exp Med. 2014 Jul 28;211(8):1503-23. PMID: 25071162.
171. Olivares O, Mayers JR, Gouirand V, Torrence ME, Gicquel T, Borge L, Lac S, Roques J, Lavaut MN, Berthezène P, Rubis M, Secq V, Garcia S, Moutardier V, Lombardo D, Iovanna JL, Tomasini R, Guillaumond F, Vander Heiden MG, Vasseur S. Collagen-derived proline promotes pancreatic ductal adenocarcinoma cell survival under nutrient limited conditions. Nat Commun. 2017 Jul 7;8:16031. PMID: 28685754.
172. Olive KP, Jacobetz MA, Davidson CJ, Gopinathan A, McIntyre D, Honess D, Madhu B, Goldgraben MA, Caldwell ME, Allard D, Frese KK, Denicola G, Feig C, Combs C, Winter SP, Ireland-Zecchini H, Reichelt S, Howat WJ, Chang A, Dhara M, Wang L, Rückert F, Grützmann R, Pilarsky C, Izeradjene K, Hingorani SR, Huang P, Davies SE, Plunkett W, Egorin M, Hruban RH, Whitebread N, McGovern K, Adams J, Iacobuzio-Donahue C, Griffiths J, Tuveson DA. Inhibition of Hedgehog signaling enhances delivery of chemotherapy in a mouse model of pancreatic cancer. Science. 2009 Jun 12;324(5933):1457-61. PMID: 19460966.
173. Ostermann E, Garin-Chesa P, Heider KH, Kalat M, Lamche H, Puri C, Kerjaschki D, Rettig WJ, Adolf GR. Effective immunoconjugate therapy in cancer models targeting a serine protease of tumor fibroblasts. Clin Cancer Res. 2008 Jul 15;14(14):4584-92. PMID: 18628473.
174. Osuala KO, Sameni M, Shah S, Aggarwal N, Simonait ML, Franco OE, Hong Y, Hayward SW, Behbod F, Mattingly RR, Sloane BF. Il-6 signaling between ductal carcinoma in situ cells and carcinoma-associated fibroblasts mediates tumor cell growth and migration. BMC Cancer. 2015 Aug 13;15:584. PMID: 26268945.
175. Pankov R, Yamada KM. Fibronectin at a glance. J Cell Sci. 2002 Oct 15;115(Pt 20):3861-3. PMID: 12244123.

176. Park JE, Lenter MC, Zimmermann RN, Garin-Chesa P, Old LJ, Rettig WJ. Fibroblast activation protein, a dual specificity serine protease expressed in reactive human tumor stromal fibroblasts. J Biol Chem. 1999 Dec 17;274(51):36505-12. PMID: 10593948.
177. Paulsson J, Sjöblom T, Micke P, Pontén F, Landberg G, Heldin CH, Bergh J, Brennan DJ, Jirström K, Ostman A. Prognostic significance of stromal platelet-derived growth factor beta-receptor expression in human breast cancer. Am J Pathol. 2009 Jul;175(1):334-41. PMID: 19498003.
178. Peiris-Pagès M, Sotgia F, Lisanti MP. Chemotherapy induces the cancer-associated fibroblast phenotype, activating paracrine Hedgehog-GLI signalling in breast cancer cells. Oncotarget. 2015 May 10;6(13):10728-45. PMID: 25915429.
179. Perou CM, Sørlie T, Eisen MB, van de Rijn M, Jeffrey SS, Rees CA, Pollack JR, Ross DT, Johnsen H, Akslen LA, Fluge O, Pergamenschikov A, Williams C, Zhu SX, Lønning PE, Børresen-Dale AL, Brown PO, Botstein D. Molecular portraits of human breast tumours. Nature. 2000 Aug 17;406(6797):747-52. PMID: 10963602.
180. Pickup M, Novitskiy S, Moses HL. The roles of TGFβ in the tumour microenvironment. Nat Rev Cancer. 2013 Nov;13(11):788-99. PMID: 24132110.
181. Ping Q, Yan R, Cheng X, Wang W, Zhong Y, Hou Z, Shi Y, Wang C, Li R. Cancer-associated fibroblasts: overview, progress, challenges, and directions. Cancer Gene Ther. 2021 Sep;28(9):984-999. Erratum in: Cancer Gene Ther. 2021 Jun 28. PMID: 33712707.
182. Plow EF, Haas TA, Zhang L, Loftus J, Smith JW. Ligand binding to integrins. J Biol Chem. 2000 Jul 21;275(29):21785-8. PMID: 10801897.
183. Provenzano PP, Cuevas C, Chang AE, Goel VK, Von Hoff DD, Hingorani SR. Enzymatic targeting of the stroma ablates physical barriers to treatment of pancreatic ductal adenocarcinoma. Cancer Cell. 2012 Mar 20;21(3):418-29. PMID: 22439937.
184. Quail DF, Joyce JA. Microenvironmental regulation of tumor progression and metastasis. Nat Med. 2013 Nov;19(11):1423-37. PMID: 24202395.
185. Quante M, Tu SP, Tomita H, Gonda T, Wang SS, Takashi S, Baik GH, Shibata W, Diprete B, Betz KS, Friedman R, Varro A, Tycko B, Wang TC. Bone marrow-derived myofibroblasts contribute to the mesenchymal stem cell niche and promote tumor growth. Cancer Cell. 2011 Feb 15;19(2):257-72. PMID: 21316604.

186. Rakesh R, PriyaDharshini LC, Sakthivel KM, Rasmi RR. Role and regulation of autophagy in cancer. Biochim Biophys Acta Mol Basis Dis. 2022 Jul 1;1868(7):166400. PMID: 35341960.
187. Reis LF, Ho Lee T, Vilcek J. Tumor necrosis factor acts synergistically with autocrine interferon-beta and increases interferon-beta mRNA levels in human fibroblasts. J Biol Chem. 1989 Oct 5;264(28):16351-4. PMID: 2550437.
188. Ren Y, Jia HH, Xu YQ, Zhou X, Zhao XH, Wang YF, Song X, Zhu ZY, Sun T, Dou Y, Tian WP, Zhao XL, Kang CS, Mei M. Paracrine and epigenetic control of CAF-induced metastasis: the role of HOTAIR stimulated by TGF-ß1 secretion. Mol Cancer. 2018 Jan 11;17(1):5. PMID: 29325547.
189. Ren Z, Lv M, Yu Q, Bao J, Lou K, Li X. MicroRNA-370-3p shuttled by breast cancer cell-derived extracellular vesicles induces fibroblast activation through the CYLD/Nf-κB axis to promote breast cancer progression. FASEB J. 2021 Mar;35(3):e21383. PMID: 33629796.
190. Retsas S. Cancer and the arts: metastasis-as perceived through the ages. ESMO Open. 2017 Jul 29;2(3):e000226. PMID: 29209528.
191. Richardson AM, Havel LS, Koyen AE, Konen JM, Shupe J, Wiles WG 4th, Martin WD, Grossniklaus HE, Sica G, Gilbert-Ross M, Marcus AI. Vimentin Is Required for Lung Adenocarcinoma Metastasis via Heterotypic Tumor Cell-Cancer-Associated Fibroblast Interactions during Collective Invasion. Clin Cancer Res. 2018 Jan 15;24(2):420-432. PMID: 29208669.
192. Rockey DC, Weymouth N, Shi Z. Smooth muscle α actin (Acta2) and myofibroblast function during hepatic wound healing. PLoS One. 2013 Oct 29;8(10):e77166. PMID: 24204762.
193. Roh E, Yoo HJ. The Role of Adipose Tissue Lipolysis in Diet-Induced Obesity: Focus on Vimentin. Diabetes Metab J. 2021 Jan;45(1):43-45. PMID: 33508908.
194. Rønnov-Jessen L, Petersen OW, Bissell MJ. Cellular changes involved in conversion of normal to malignant breast: importance of the stromal reaction. Physiol Rev. 1996 Jan;76(1):69-125. PMID: 8592733.
195. Sahai E, Astsaturov I, Cukierman E, DeNardo DG, Egeblad M, Evans RM, Fearon D, Greten FR, Hingorani SR, Hunter T, Hynes RO, Jain RK, Janowitz T, Jorgensen C, Kimmelman AC, Kolonin MG, Maki RG, Powers RS, Puré E, Ramirez DC, Scherz-Shouval R, Sherman MH, Stewart S, Tlsty TD, Tuveson DA, Watt FM, Weaver V, Weeraratna AT, Werb Z. A framework for advancing our understanding of cancer-associated fibroblasts. Nat Rev Cancer. 2020 Mar;20(3):174-186. PMID: 31980749.

196. Saitoh M. Involvement of partial EMT in cancer progression. J Biochem. 2018 Oct 1;164(4):257-264. PMID: 29726955.
197. Salmon H, Franciszkiewicz K, Damotte D, Dieu-Nosjean MC, Validire P, Trautmann A, Mami-Chouaib F, Donnadieu E. Matrix architecture defines the preferential localization and migration of T cells into the stroma of human lung tumors. J Clin Invest. 2012 Mar;122(3):899-910. PMID: 22293174.
198. Schick J, Ritchie RP, Restini C. Breast Cancer Therapeutics and Biomarkers: Past, Present, and Future Approaches. Breast Cancer (Auckl). 2021 Mar 24;15:1178223421995854. PMID: 33994789.
199. Shapouri-Moghaddam A, Mohammadian S, Vazini H, Taghadosi M, Esmaeili SA, Mardani F, Seifi B, Mohammadi A, Afshari JT, Sahebkar A. Macrophage plasticity, polarization, and function in health and disease. J Cell Physiol. 2018 Sep;233(9):6425-6440. PMID: 29319160.
200. Sharon Y, Alon L, Glanz S, Servais C, Erez N. Isolation of normal and cancer-associated fibroblasts from fresh tissues by Fluorescence Activated Cell Sorting (FACS). J Vis Exp. 2013 Jan 14;(71):e4425. PMID: 23354290.
201. Sharon Y, Raz Y, Cohen N, Ben-Shmuel A, Schwartz H, Geiger T, Erez N. Tumor-derived osteopontin reprograms normal mammary fibroblasts to promote inflammation and tumor growth in breast cancer. Cancer Res. 2015 Mar 15;75(6):963-73. PMID: 25600648.
202. Shen S, Vagner S, Robert C. Persistent Cancer Cells: The Deadly Survivors. Cell. 2020 Nov 12;183(4):860-874. PMID: 33186528.
203. Sheen-Chen SM, Chen WJ, Eng HL, Chou FF. Serum concentration of tumor necrosis factor in patients with breast cancer. Breast Cancer Res Treat. 1997 May;43(3):211-5. PMID: 9150900.
204. Sherman MH, Yu RT, Engle DD, Ding N, Atkins AR, Tiriac H, Collisson EA, Connor F, Van Dyke T, Kozlov S, Martin P, Tseng TW, Dawson DW, Donahue TR, Masamune A, Shimosegawa T, Apte MV, Wilson JS, Ng B, Lau SL, Gunton JE, Wahl GM, Hunter T, Drebin JA, O'Dwyer PJ, Liddle C, Tuveson DA, Downes M, Evans RM. Vitamin D receptor-mediated stromal reprogramming suppresses pancreatitis and enhances pancreatic cancer therapy. Cell. 2014 Sep 25;159(1):80-93. PMID: 25259922.
205. Shevchenko A, Tomas H, Havlis J, Olsen JV, Mann M. In-gel digestion for mass spectrometric characterization of proteins and proteomes. Nat Protoc. 2006;1(6):2856-60. PMID: 17406544.
206. Shimoda M, Principe S, Jackson HW, Luga V, Fang H, Molyneux SD, Shao YW, Aiken A, Waterhouse PD, Karamboulas C, Hess FM, Ohtsuka T,

Okada Y, Ailles L, Ludwig A, Wrana JL, Kislinger T, Khokha R. Loss of the Timp gene family is sufficient for the acquisition of the CAF-like cell state. Nat Cell Biol. 2014 Sep;16(9):889-901. PMID: 25150980.

207. Shirmohammadi E, Ebrahimi SS, Farshchi A, Salimi M. The efficacy of etanercept as anti-breast cancer treatment is attenuated by residing macrophages. BMC Cancer. 2020 Sep 3;20(1):836. Erratum in: BMC Cancer. 2020 Nov 20;20(1):1126. PMID: 32883235.
208. Schubert M, Klinger B, Klünemann M, Sieber A, Uhlitz F, Sauer S, Garnett MJ, Blüthgen N, Saez-Rodriguez J. Perturbation-response genes reveal signaling footprints in cancer gene expression. Nat Commun. 2018 Jan 2;9(1):20. PMID: 29295995.
209. Silwal-Pandit L, Vollan HK, Chin SF, Rueda OM, McKinney S, Osako T, Quigley DA, Kristensen VN, Aparicio S, Børresen-Dale AL, Caldas C, Langerød A. TP53 mutation spectrum in breast cancer is subtype specific and has distinct prognostic relevance. Clin Cancer Res. 2014 Jul 1;20(13):3569-80. Erratum in: Clin Cancer Res. 2015 Mar 15;21(6):1502. PMID: 24803582.
210. Sobo-Vujanovic A, Vujanovic L, DeLeo AB, Concha-Benavente F, Ferris RL, Lin Y, Vujanovic NL. Inhibition of Soluble Tumor Necrosis Factor Prevents Chemically Induced Carcinogenesis in Mice. Cancer Immunol Res. 2016 May;4(5):441-51. PMID: 26896171.
211. Sonntag J, Schlüter K, Bernhardt S, Korf U. Subtyping of breast cancer using reverse phase protein arrays. Expert Rev Proteomics. 2014 Dec;11(6):757-70. PMID: 25400094.
212. Soysal SD, Tzankov A, Muenst SE. Role of the Tumor Microenvironment in Breast Cancer. Pathobiology. 2015 Sep;82(3-4):142-52. PMID: 26330355.
213. Sternlicht MD, Lochter A, Sympson CJ, Huey B, Rougier JP, Gray JW, Pinkel D, Bissell MJ, Werb Z. The stromal proteinase MMP3/stromelysin-1 promotes mammary carcinogenesis. Cell. 1999 Jul 23;98(2):137-46. PMID: 10428026.
214. Strutz F, Okada H, Lo CW, Danoff T, Carone RL, Tomaszewski JE, Neilson EG. Identification and characterization of a fibroblast marker: FSP1. J Cell Biol. 1995 Jul;130(2):393-405. PMID: 7615639.
215. Strutz F, Zeisberg M, Hemmerlein B, Sattler B, Hummel K, Becker V, Müller GA. Basic fibroblast growth factor expression is increased in human renal fibrogenesis and may mediate autocrine fibroblast proliferation. Kidney Int. 2000 Apr;57(4):1521-38. PMID: 10760088.
216. Studebaker AW, Storci G, Werbeck JL, Sansone P, Sasser AK, Tavolari S, Huang T, Chan MW, Marini FC, Rosol TJ, Bonafé M, Hall BM. Fibroblasts

isolated from common sites of breast cancer metastasis enhance cancer cell growth rates and invasiveness in an interleukin-6-dependent manner. Cancer Res. 2008 Nov 1;68(21):9087-95. PMID: 18974155.

217. Su S, Chen J, Yao H, Liu J, Yu S, Lao L, Wang M, Luo M, Xing Y, Chen F, Huang D, Zhao J, Yang L, Liao D, Su F, Li M, Liu Q, Song E. $CD10^{+}GPR77^{+}$ Cancer-Associated Fibroblasts Promote Cancer Formation and Chemoresistance by Sustaining Cancer Stemness. Cell. 2018 Feb 8;172(4):841-856.e16. PMID: 29395328.
218. Sugimoto H, Mundel TM, Kieran MW, Kalluri R. Identification of fibroblast heterogeneity in the tumor microenvironment. Cancer Biol Ther. 2006 Dec;5(12):1640-6. PMID: 17106243.
219. Suh J, Kim DH, Lee YH, Jang JH, Surh YJ. Fibroblast growth factor-2, derived from cancer-associated fibroblasts, stimulates growth and progression of human breast cancer cells via FGFR1 signaling. Mol Carcinog. 2020 Sep;59(9):1028-1040. PMID: 32557854.
220. Sung H, Ferlay J, Siegel RL, Laversanne M, Soerjomataram I, Jemal A, Bray F. Global Cancer Statistics 2020: GLOBOCAN Estimates of Incidence and Mortality Worldwide for 36 Cancers in 185 Countries. CA Cancer J Clin. 2021 May;71(3):209-249. PMID: 33538338.
221. Subramanian A, Tamayo P, Mootha VK, Mukherjee S, Ebert BL, Gillette MA, Paulovich A, Pomeroy SL, Golub TR, Lander ES, Mesirov JP. Gene set enrichment analysis: a knowledge-based approach for interpreting genome-wide expression profiles. Proc Natl Acad Sci U S A. 2005 Oct 25;102(43):15545-50. PMID: 16199517.
222. Surowiak P, Murawa D, Materna V, Maciejczyk A, Pudelko M, Ciesla S, Breborowicz J, Murawa P, Zabel M, Dietel M, Lage H. Occurence of stromal myofibroblasts in the invasive ductal breast cancer tissue is an unfavourable prognostic factor. Anticancer Res. 2007 Jul-Aug;27(4C):2917-24. PMID: 17695471.
223. Tak PP, Firestein GS. NF-kappaB: a key role in inflammatory diseases. J Clin Invest. 2001 Jan;107(1):7-11. PMID: 11134171.
224. Tan HX, Cao ZB, He TT, Huang T, Xiang CL, Liu Y. TGFβ1 is essential for MSCs-CAFs differentiation and promotes HCT116 cells migration and invasion via JAK/STAT3 signaling. Onco Targets Ther. 2019 Jul 5;12:5323-5334. PMID: 31308702.
225. Tanabe K, Matsushima-Nishiwaki R, Yamaguchi S, Iida H, Dohi S, Kozawa O. Mechanisms of tumor necrosis factor-alpha-induced interleukin-6 synthesis in glioma cells. J Neuroinflammation. 2010 Mar 6;7:16. PMID: 20205746.

226. Tanida I, Ueno T, Kominami E. LC3 and Autophagy. Methods Mol Biol. 2008;445:77-88. PMID: 18425443.
227. Tauriello DVF, Palomo-Ponce S, Stork D, Berenguer-Llergo A, Badia-Ramentol J, Iglesias M, Sevillano M, Ibiza S, Cañellas A, Hernando-Momblona X, Byrom D, Matarin JA, Calon A, Rivas EI, Nebreda AR, Riera A, Attolini CS, Batlle E. TGFβ drives immune evasion in genetically reconstituted colon cancer metastasis. Nature. 2018 Feb 22;554(7693):538-543. PMID: 29443964.
228. Team, R Core. R: A language and environment for statistical computing. MSOR connections. 2014;1: n. pag.
229. Tommelein J, De Vlieghere E, Verset L, Melsens E, Leenders J, Descamps B, Debucquoy A, Vanhove C, Pauwels P, Gespach CP, Vral A, De Boeck A, Haustermans K, de Tullio P, Ceelen W, Demetter P, Boterberg T, Bracke M, De Wever O. Radiotherapy-Activated Cancer-Associated Fibroblasts Promote Tumor Progression through Paracrine IGF1R Activation. Cancer Res. 2018 Feb 1;78(3):659-670. PMID: 29217764.
230. Toth KG, McKay BR, De Lisio M, Little JP, Tarnopolsky MA, Parise G. IL-6 induced STAT3 signalling is associated with the proliferation of human muscle satellite cells following acute muscle damage. PLoS One. 2011 Mar 9;6(3):e17392. PMID: 21408055.
231. Toullec A, Gerald D, Despouy G, Bourachot B, Cardon M, Lefort S, Richardson M, Rigaill G, Parrini MC, Lucchesi C, Bellanger D, Stern MH, Dubois T, Sastre-Garau X, Delattre O, Vincent-Salomon A, Mechta-Grigoriou F. Oxidative stress promotes myofibroblast differentiation and tumour spreading. EMBO Mol Med. 2010 Jun;2(6):211-30. PMID: 20535745.
232. Tripsianis G, Papadopoulou E, Anagnostopoulos K, Botaitis S, Katotomichelakis M, Romanidis K, Kontomanolis E, Tentes I, Kortsaris A. Coexpression of IL-6 and TNF-α: prognostic significance on breast cancer outcome. Neoplasma. 2014;61(2):205-12. PMID: 24299316.
233. Tyanova S, Temu T, Cox J. The MaxQuant computational platform for mass spectrometry-based shotgun proteomics. Nat Protoc. 2016 Dec;11(12):2301-2319. PMID: 27809316.
234. Tyanova S, Temu T, Sinitcyn P, Carlson A, Hein MY, Geiger T, Mann M, Cox J. The Perseus computational platform for comprehensive analysis of (prote)omics data. Nat Methods. 2016 Sep;13(9):731-40. PMID: 27348712.
235. Ueshima E, Fujimori M, Kodama H, Felsen D, Chen J, Durack JC, Solomon SB, Coleman JA, Srimathveeravalli G. Macrophage-secreted TGF-β_1 contributes to fibroblast activation and ureteral stricture after

ablation injury. Am J Physiol Renal Physiol. 2019 Jul 1;317(7):F52-F64. PMID: 31017012.

236. Vaheri A, Mosher DF. High molecular weight, cell surface-associated glycoprotein (fibronectin) lost in malignant transformation. Biochim Biophys Acta. 1978 Sep 18;516(1):1-25. PMID: 361081.
237. Valdés-Mora F, Salomon R, Gloss BS, Law AMK, Venhuizen J, Castillo L, Murphy KJ, Magenau A, Papanicolaou M, Rodriguez de la Fuente L, Roden DL, Colino-Sanguino Y, Kikhtyak Z, Farbehi N, Conway JRW, Sikta N, Oakes SR, Cox TR, O'Donoghue SI, Timpson P, Ormandy CJ, Gallego-Ortega D. Single-cell transcriptomics reveals involution mimicry during the specification of the basal breast cancer subtype. Cell Rep. 2021 Apr 13;35(2):108945. PMID: 33852842.
238. van Maaren MC, de Munck L, Strobbe LJA, Sonke GS, Westenend PJ, Smidt ML, Poortmans PMP, Siesling S. Ten-year recurrence rates for breast cancer subtypes in the Netherlands: A large population-based study. Int J Cancer. 2019 Jan 15;144(2):263-272. PMID: 30368776.
239. Verjee LS, Verhoekx JS, Chan JK, Krausgruber T, Nicolaidou V, Izadi D, Davidson D, Feldmann M, Midwood KS, Nanchahal J. Unraveling the signaling pathways promoting fibrosis in Dupuytren's disease reveals TNF as a therapeutic target. Proc Natl Acad Sci U S A. 2013 Mar 5;110(10):E928-37. PMID: 23431165.
240. Virchow R. Die Cellularpathologie in lhrer Begründung auf Physiologische und Pathologische Gewebelehre. ed. Hirschwald, A. Berlin; 1858.
241. von der Heyde S, Sonntag J, Kaschek D, Bender C, Bues J, Wachter A, Timmer J, Korf U, Beißbarth T. RPPanalyzer toolbox: an improved R package for analysis of reverse phase protein array data. Biotechniques. 2014 Sep 1;57(3):125-35. PMID: 25209047.
242. Voutouri C, Mpekris F, Papageorgis P, Odysseos AD, Stylianopoulos T. Role of constitutive behavior and tumor-host mechanical interactions in the state of stress and growth of solid tumors. PLoS One. 2014 Aug 11;9(8):e104717. PMID: 25111061.
243. Wagner EF. Cancer: Fibroblasts for all seasons. Nature. 2016 Feb 4;530(7588):42-3. PMID: 26842052.
244. Wan L, Lin CW, Lin YJ, Sheu JJ, Chen BH, Liao CC, Tsai Y, Lin WY, Lai CH, Tsai FJ. Type I IFN induced IL1-Ra expression in hepatocytes is mediated by activating STAT6 through the formation of STAT2: STAT6 heterodimer. J Cell Mol Med. 2008 Jun;12(3):876-88. PMID: 18494930.
245. Wang Y, Gan G, Wang B, Wu J, Cao Y, Zhu D, Xu Y, Wang X, Han H, Li X, Ye M, Zhao J, Mi J. Cancer-associated Fibroblasts Promote Irradiated

Cancer Cell Recovery Through Autophagy. EBioMedicine. 2017 Mar;17:45-56. PMID: 28258923.

246. Watanabe K, Shiga K, Maeda A, Harata S, Yanagita T, Suzuki T, Ushigome H, Maeda Y, Hirokawa T, Ogawa R, Hara M, Takahashi H, Matsuo Y, Mitsui A, Kimura M, Takiguchi S. Chitinase 3-like 1 secreted from cancer-associated fibroblasts promotes tumor angiogenesis via interleukin-8 secretion in colorectal cancer. Int J Oncol. 2022 Jan;60(1):3. PMID: 34913066.
247. Weber CE, Kothari AN, Wai PY, Li NY, Driver J, Zapf MA, Franzen CA, Gupta GN, Osipo C, Zlobin A, Syn WK, Zhang J, Kuo PC, Mi Z. Osteopontin mediates an MZF1-TGF-β1-dependent transformation of mesenchymal stem cells into cancer-associated fibroblasts in breast cancer. Oncogene. 2015 Sep 10;34(37):4821-33. PMID: 25531323.
248. Wei SC, Fattet L, Tsai JH, Guo Y, Pai VH, Majeski HE, Chen AC, Sah RL, Taylor SS, Engler AJ, Yang J. Matrix stiffness drives epithelial-mesenchymal transition and tumour metastasis through a TWIST1-G3BP2 mechanotransduction pathway. Nat Cell Biol. 2015 May;17(5):678-88. PMID: 25893917.
249. Wessel D, Flügge UI. A method for the quantitative recovery of protein in dilute solution in the presence of detergents and lipids. Anal Biochem. 1984 Apr;138(1):141-3. PMID: 6731838.
250. Will R, Bauer K, Kudla M, Montero-Vergara J, Wiemann S, Jendrossek V, Peña-Llopis S, Vega-Rubín-de-Celis S. A Dual HiBiT-GFP-LC3 Lentiviral Reporter for Autophagy Flux Assessment. Methods Mol Biol. 2022;2445:75-98. PMID: 34972987.
251. Wolczyk D, Zaremba-Czogalla M, Hryniewicz-Jankowska A, Tabola R, Grabowski K, Sikorski AF, Augoff K. TNF-α promotes breast cancer cell migration and enhances the concentration of membrane-associated proteases in lipid rafts. Cell Oncol (Dordr). 2016 Aug;39(4):353-63. PMID: 27042827.
252. Wu F, Yang J, Liu J, Wang Y, Mu J, Zeng Q, Deng S, Zhou H. Signaling pathways in cancer-associated fibroblasts and targeted therapy for cancer. Signal Transduct Target Ther. 2021 Jun 10;6(1):218. PMID: 34108441.
253. Wu SZ, Roden DL, Wang C, Holliday H, Harvey K, Cazet AS, Murphy KJ, Pereira B, Al-Eryani G, Bartonicek N, Hou R, Torpy JR, Junankar S, Chan CL, Lam CE, Hui MN, Gluch L, Beith J, Parker A, Robbins E, Segara D, Mak C, Cooper C, Warrier S, Forrest A, Powell J, O'Toole S, Cox TR, Timpson P, Lim E, Liu XS, Swarbrick A. Stromal cell diversity associated with

immune evasion in human triple-negative breast cancer. EMBO J. 2020 Oct 1;39(19):e104063. PMID: 32790115.

254. Wu X, Chen X, Zhou Q, Li P, Yu B, Li J, Qu Y, Yan J, Yu Y, Yan M, Zhu Z, Liu B, Su L. Hepatocyte growth factor activates tumor stromal fibroblasts to promote tumorigenesis in gastric cancer. Cancer Lett. 2013 Jul 10;335(1):128-35. PMID: 23402812.
255. Wu X, Tao P, Zhou Q, Li J, Yu Z, Wang X, Li J, Li C, Yan M, Zhu Z, Liu B, Su L. IL-6 secreted by cancer-associated fibroblasts promotes epithelial-mesenchymal transition and metastasis of gastric cancer via JAK2/STAT3 signaling pathway. Oncotarget. 2017 Mar 28;8(13):20741-20750. PMID: 28186964.
256. Xie X, Lu J, Kulbokas EJ, Golub TR, Mootha V, Lindblad-Toh K, Lander ES, Kellis M. Systematic discovery of regulatory motifs in human promoters and 3' UTRs by comparison of several mammals. Nature. 2005 Mar 17;434(7031):338-45. PMID: 15735639.
257. Xu K, Tian X, Oh SY, Movassaghi M, Naber SP, Kuperwasser C, Buchsbaum RJ. The fibroblast Tiam1-osteopontin pathway modulates breast cancer invasion and metastasis. Breast Cancer Res. 2016 Jan 28;18(1):14. PMID: 26821678.
258. Yang X, Lin Y, Shi Y, Li B, Liu W, Yin W, Dang Y, Chu Y, Fan J, He R. FAP Promotes Immunosuppression by Cancer-Associated Fibroblasts in the Tumor Microenvironment via STAT3-CCL2 Signaling. Cancer Res. 2016 Jul 15;76(14):4124-35. PMID: 27216177.
259. Yarden Y, Pines G. The ERBB network: at last, cancer therapy meets systems biology. Nat Rev Cancer. 2012 Jul 12;12(8):553-63. PMID: 22785351.
260. Yarden Y, Sliwkowski MX. Untangling the ErbB signalling network. Nat Rev Mol Cell Biol. 2001 Feb;2(2):127-37. PMID: 11252954.
261. Yarilina A, Ivashkiv LB. Type I interferon: a new player in TNF signaling. Curr Dir Autoimmun. 2010;11:94-104. PMID: 20173389.
262. Yeon JH, Jeong HE, Seo H, Cho S, Kim K, Na D, Chung S, Park J, Choi N, Kang JY. Cancer-derived exosomes trigger endothelial to mesenchymal transition followed by the induction of cancer-associated fibroblasts. Acta Biomater. 2018 Aug;76:146-153. PMID: 30078422.
263. Yu Y, Xiao CH, Tan LD, Wang QS, Li XQ, Feng YM. Cancer-associated fibroblasts induce epithelial-mesenchymal transition of breast cancer cells through paracrine TGF-β signalling. Br J Cancer. 2014 Feb 4;110(3):724-32. PMID: 24335925.
264. Zeisberg EM, Potenta S, Xie L, Zeisberg M, Kalluri R. Discovery of endothelial to mesenchymal transition as a source for carcinoma-

associated fibroblasts. Cancer Res. 2007 Nov 1;67(21):10123-8. PMID: 17974953.

265. Zhang Q, Chai S, Wang W, Wan C, Zhang F, Li Y, Wang F. Macrophages activate mesenchymal stem cells to acquire cancer-associated fibroblast-like features resulting in gastric epithelial cell lesions and malignant transformation *in vitro*. Oncol Lett. 2019 Jan;17(1):747-756. PMID: 30655826.
266. Zhang Y, Weinberg RA. Epithelial-to-mesenchymal transition in cancer: complexity and opportunities. Front Med. 2018 Aug;12(4):361-373. PMID: 30043221.
267. Zhu A, Ibrahim JG, Love MI. Heavy-tailed prior distributions for sequence count data: removing the noise and preserving large differences. Bioinformatics. 2019 Jun 1;35(12):2084-2092. PMID: 30395178.

SUPPLEMENTS

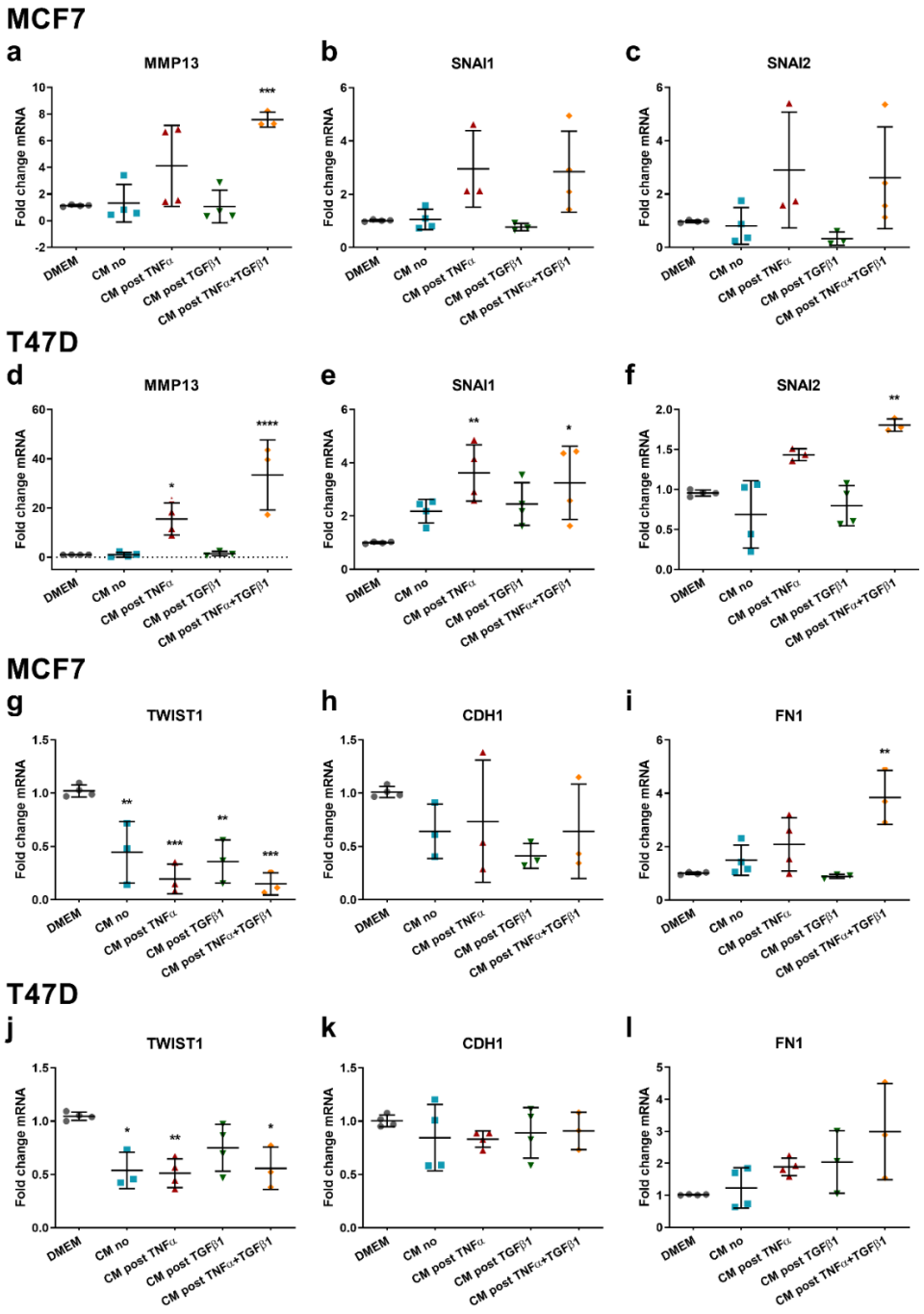

Figure S1. Expression of EMT markers by MCF7 and T47D cells after treatment with CAF-conditioned media. Immortalized CAF1 cells were stimulated with cytokines (10 ng/ml hrTNFα and/or 2 ng/mL hrTGFβ1) for 24h prior to collecting the CM. The breast cancer cells were treated with the CM for 24h and then lysed for RNA isolation. qPCR analysis was performed to evaluate the effect of the CM on the gene expression of selected EMT markers. Each dot is a biological replicate and the average of three technical replicates. The error bars are SEM. Statistical analysis was performed using a one-way-ANOVA test followed by Bonferroni correction, significance levels: * $p \leq 0.05$, ** $p \leq 0.01$, *** $p \leq 0.001$, **** $p \leq 0.0001$. Figure taken from: Christina Schniederjohann. Impact of cancer-associated fibroblast secreted SPARC on luminal A breast cancer cells. Bachelor thesis. 2019.

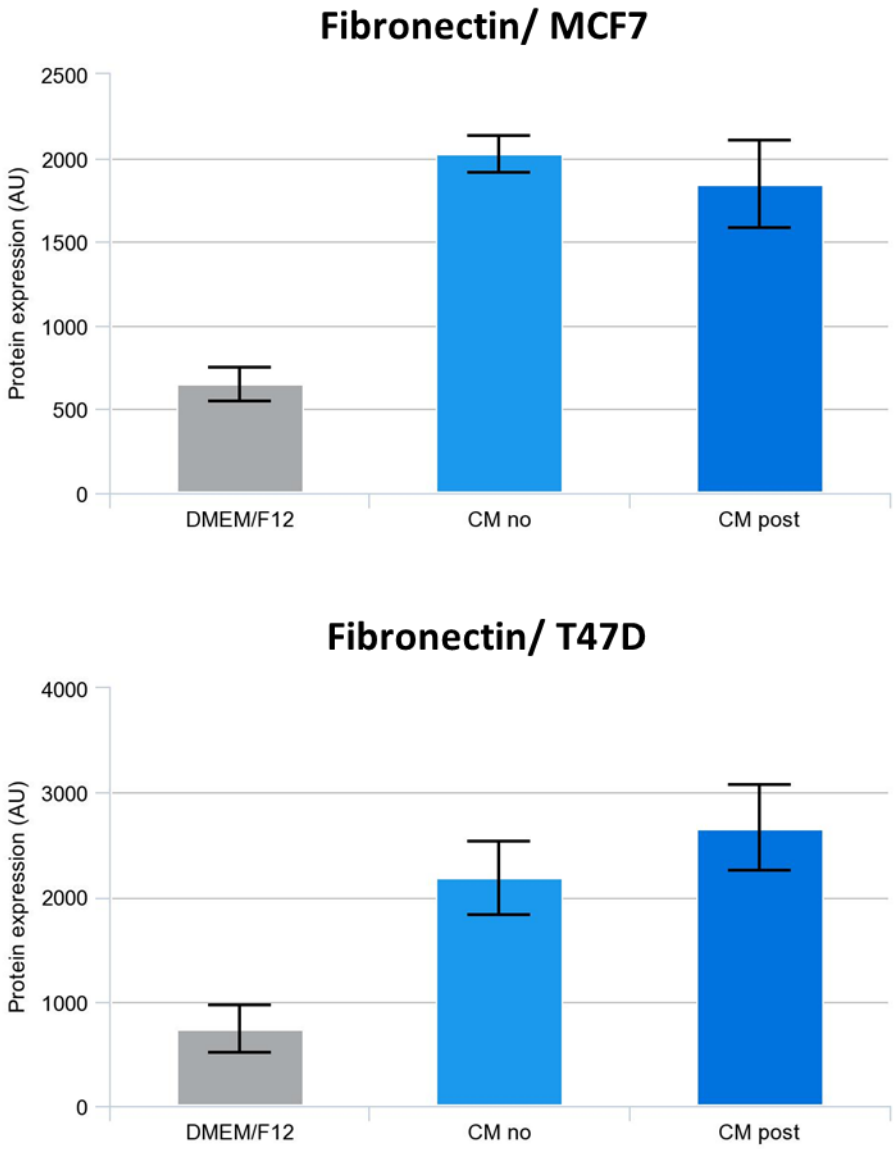

Figure S2. Fibronectin expression in Luminal A breast cancer cells after treatment with CAF1 CM as determined via RPPA. Breast cancer cells were treated for 24h with CM from immortalized CAF1 cells which were priorly stimulated for 24h with 10 ng/ml hrTNFα and 2 ng/ml hrTGFβ1 (CM post) or unstimulated (CM no). Treatment with DMEM/F12 was used as a control. Total protein lysates were isolated from the treated cell cultures and analyzed via RPPA for the protein expression of fibronectin. Each bar is the average of 3 biological replicates. The error bars are SD.

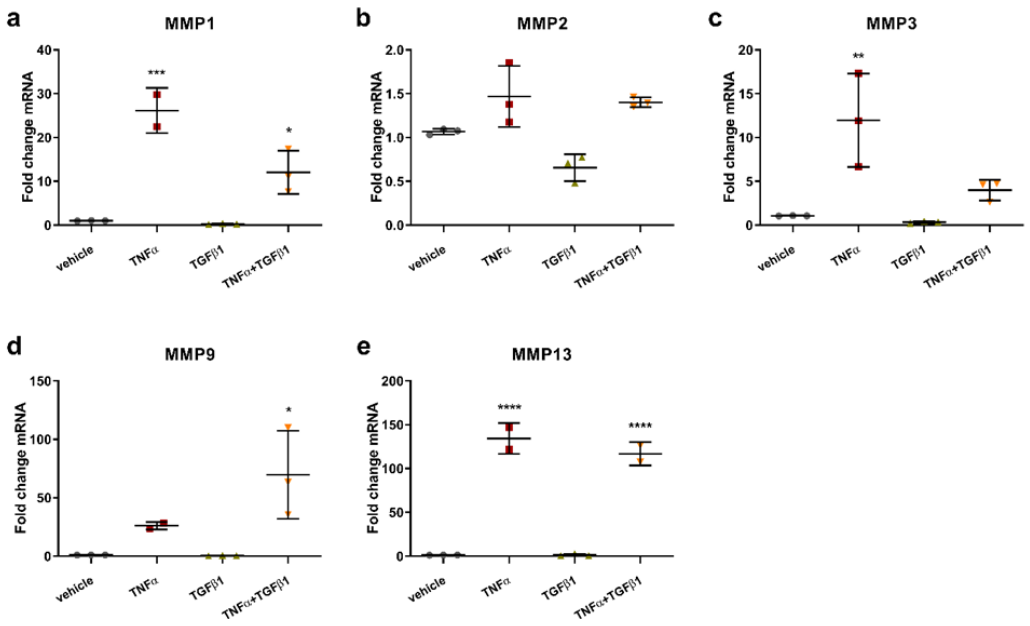

Figure S3. Expression of *MMP* genes in the CAF1 cells after treatment with TNFα and TGFβ1. Immortalized CAF1 cells were stimulated with 10 ng/ml hrTNFα and/or 2 ng/mL hrTGFβ1 for 24h prior to being lysed for RNA isolation. qPCR analysis revealed upregulation of *MMP* expression in response to the TNFα stimulation. Each dot is a biological replicate and the average of three technical replicates. The error bars are SEM. Statistical analysis was performed using a one-way-ANOVA test followed by Bonferroni correction, significance levels: * $p \leq 0.05$, ** $p \leq 0.01$, *** $p \leq 0.001$, **** $p \leq 0.0001$. Figure taken from: Christina Schniederjohann. Impact of cancer-associated fibroblast secreted SPARC on luminal A breast cancer cells. Bachelor thesis. 2019.

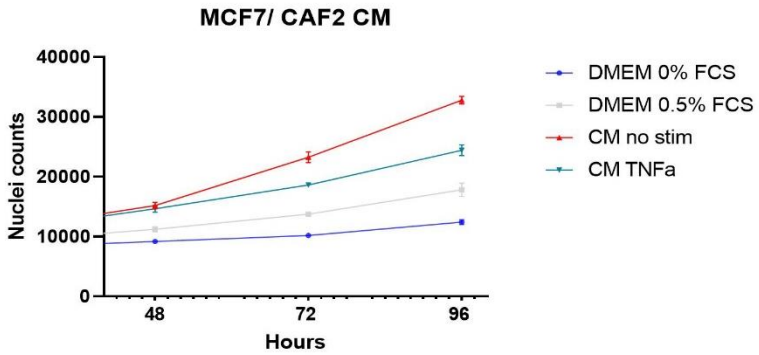

Figure S4. Nuclei counts of MCF7 cell after treatment with CM from TNFα-stimulate CAFs. Primary CAF2 cells were stimulated with 10ng/ml hrTNFα or solvent (H_20, no stim) for 24h prior to CM collection. MCF7 monocultures were treated with the CAF2 CM for 48h, 72h and 96h. At the respective time point the cells were stained with Hoechst 33342 and the nuclei were counted. The cells stopped proliferating upon treatment with CM from the TNFα-activated CAF2 cells most likely due to the toxic effects of TNFα. The error bars are SD.

Table S1. Expression levels of *FAP, C5AR2, ACTA2* & *FN1* as determined by RNA-Seq.
The numbers correspond to TPM (transcripts per million) values. The RNA-Seq data was generated by Dr. Mireia Berdiel-Acer, Dr Simone Borgoni and Dr. Emre Sofyali (with the help of the DKFZ Core Facility) and analyzed by Dr. Birgitta Michels. *C5AR2* codes for GPR77.

Gene	CAF1	CAF2	MCF7	T47D
FAP	298.776	284.462	0.007	0.000
C5AR2	0.012	0.012	39.136	43.462
ACTA2	447.096	235.341	3.072	70.172
FN1	3833.532	5256.774	2.284	20.827

Table S2. Expression levels of the *STAT* genes as determined by RNA-Seq.
The numbers correspond to TPM (transcripts per million) values. The RNA-Seq data was generated by Dr. Mireia Berdiel-Acer, Dr Simone Borgoni and Dr. Emre Sofyali (with the help of the DKFZ Core Facility) and analyzed by Dr. Birgitta Michels.

Gene	CAF1	CAF2	MCF7	T47D
STAT1	152.051	237.977	127.895	119.219
STAT2	207.387	206.427	49.589	57.034
STAT3	126.701	81.068	36.197	145.451
STAT4	5.101	5.035	1.598	0.068
STAT5A	14.244	7.005	1.615	6.312
STAT5B	34.198	42.047	38.098	55.699
STAT6	109.527	179.926	40.443	108.269

Abbreviations

αSMA	Alpha smooth muscle actin
ACTA	Actin alpha 2, Alpha Smooth muscle actin
ACTB	Actin beta
ADAM	A disintegrin and metalloproteinase domain containing protein
Akt	Protein kinase B
ANOVA	One-way analysis of variance
anti-CTLA-4	anti-Cytotoxic T-lymphocyte-associated protein 4
ATRA	All trans retinoic acid
BCA	Bicinchoninic acid assay
BL1	Basal-like 1
BL2	Basal-like 2
BMSC	Bone marrow derived stromal cell
BSA	Bovine serum albumin
BsAbs	Bispecific antibodies
C3	Complement C3
CAF	Cancer-associated fibroblast
CD10	Cluster of differentiation 10, neprilysin
CD29	Cluster of differentiation 29, integrin beta 1
CD44	Cluster of differentiation 44 antigen
CDH2	Cadherin 2, N-cadherin
CDK4/6	Cyclin-dependent kinase 4/6
cGAS	Cyclic GMP-AMP synthase
CCL2	Chemokine ligand 2
CM	Conditioned medium
CMFDA	5-Chlormethylfluorescein diacetate
COL1A1	Collagen type I alpha 1 chain
COL1A2	Collagen type I alpha 2 chain
CSC	Cancer stem cell
CT	Cycle threshold
CXCL1	C-X-C motif chemokine ligand 1
CXCL12	C-X-C motif chemokine ligand 12

DDA	Data-dependent acquisition
DDX58	DExD/H-Box Helicase 58
DCIS	Ductal carcinoma *in situ*
DCN	Decorin
DEG	Differentially expressed gene
DIA	Data-independent acquisition
DMEM	Dulbecco's modified Eagle's medium
DMSO	Dimethyl sulfoxide
DNA	Deoxyribonucleic acid
DoRothEA	Discriminant Regulon Expression Analysis
DPBS	Dulbecco's phosphate buffered saline
ECM	Extracellular matrix
EDTA	Ethylenediaminetetraacetic acid
EGFR	Epidermal growth factor receptor
ELISA	Enzyme-linked immunosorbent assay
EMT	Epithelial-to-mesenchymal transition
EndMT	Endothelial-to-mesenchymal-transition
ER	Estrogen receptor
ERBB2	Erb-B2 receptor tyrosine kinase 2
ERK	Extracellular signal-regulated kinase
FACS	Fluorescence-activated cell sorting
FAP	Fibroblast activation protein
FCS	Fetal calf serum
FDA	Food and Drug Administration
FDR	False discovery rate
FGF2	Fibroblast growth factor 2
FLISA	Fluorescence-linked immunosorbent assay
FN1	Fibronectin 1
FSP-1	Fibroblast-specific protein 1
GAPDH	Glyceraldehyde 3-phosphate dehydrogenase
GFP	Green fluorescent protein
GOBP	Gene Ontology Biological Process
GPR77	G-protein coupled receptor 77

GPR30	G-protein coupled estrogen receptor 30
GSEA	Gene set enrichment analysis
HA	Hyaluronic acid
HCC	Hepatocellular carcinoma
HeLa	Henrietta Lacks
HER	Human epidermal growth factor receptor
HGF	Hepatocyte growth factor
HMGB1	High mobility group box 1
HPLC-MS	High-performance liquid chromatography-Mass spectrometry
HSPD1	Heat Shock Protein Family D (Hsp60) Member 1
hr	human recombinant
HRP	Horseradish peroxidase
HSC	Hematopoietic stem cells
iCAF	Inflammatory cancer-associated fibroblast
IFIH1	Interferon induced with helicase C domain 1
IFIT	Interferon-induced protein with tetratricopeptide repeats
IFNAR1	Interferon-alpha/beta receptor alpha chain
IFNβ1	Interferon beta 1
IFNα	Interferon alpha
IFNγ	Interferon gamma
IGF	Insulin-like growth factor
IHC	Immunohistochemistry
IkB	Inhibitor of NF-κB
IKKβ	Inhibitor of nuclear factor kappa-B kinase subunit beta
IL-1R1	Interleukin-1 receptor 1
IL-1RAP	Interleukin-1 receptor accessory protein
IL-β1	Interleukin beta 1
IL6	Interleukin 6
IL10	Interleukin 10
IRF	interferon regulatory factor
ISG	Interferon-stimulated gene
ISGF3	Interferon-stimulated gene factor 3
ISRE	Interferon-sensitive response element

JAK	Janus kinase
LAMC2	Laminin subunit gamma 2
LAR	Luminal androgen receptor
LC3	light chain 3
LFQ	Label-free quantification
Lum	Luminal
Ly6C	Lymphocyte antigen 6 complex
mAb	monoclonal antibody
MAPK	Mitogen-activated protein kinase
MCF7	Michigan Cancer Foundation 7
MDR	Multidrug resistance
MHC	Major histocompatibility factor
miRNA	microRNA
MMP	Matrix metalloproteinase
MMTV-PyMT	Mouse mammary tumor virus-polyoma middle tumor-antigen
MSC	Mesenchymal stem cell
MSigDB	Molecular Signatures Database
MYLK	Myosin light chain kinase
myCAF	Myofibroblastic cancer-associated fibroblasts
NES	Normalized enrichment score
NF	Normal fibroblast
NAb	Neutralization Antibody
NF-κB	Nuclear factor kappa-light-chain-enhancer of activated B cells
NSCLC	Non-small cell lung cancer
OAS1	2'-5'-oligoadenylate synthetase 1
P/S	Penicillin/streptomycin
PD-1	Programmed cell death protein 1
PDGFR	Platelet-derived growth factor receptor
PD-L1	Programmed cell death ligand 1
PDPN	Podoplanin
PI3K	Phosphatidylinositol 3-kinase
PR	Progesterone receptor
PROGENy	Pathway RespOnsive GENes

PVDF	Polyvinylidene fluoride
qPCR	quantitative Polymerase Chain Reaction
RELA	V-Rel Avian Reticuloendotheliosis Viral Oncogene Homolog A
RIPA	Radio-Immunoprecipitation Assay
RNA	Ribonucleic acid
RNA-Seq	RNA sequencing
ROCK	Rho-associated coiled-coil containing protein kinase
ROS	Reactive oxygen species
ROX	Carboxyrhodamine
RPPA	Reverse phase protein array
RT	Room temperature
S100A4	S100 Calcium Binding Protein A4
SAA3	Serum amyloid A3
SCRG1	Stimulator of chondrogenesis 1
SDF1a	Stromal cell-derived factor 1a
SDS-PAGE	Sodium dodecyl sulfate polyacrylamide gel electrophoresis
SEM	Standard Error of the Mean
siRNA	short interfering RNA
SMAD	Homologue of SMA (small worm) and MAD (Mothers Against Decapentaplegic)
SMO	Smoothened
SOX9	SRY-Box Transcription Factor 9
SPP1	Secreted phosphoprotein 1
STAT	Signal transducer and activator of transcription
STING	Stimulator of interferon genes
TAM	Tumor-associated macrophage
TBS-T	Tris-buffered saline with Tween®20
TGFβ1	Transforming growth factor β1
TGFBR	Transforming growth factor β receptor
TIMP	Tissue inhibitor of metalloproteinases
TME	Tumor microenvironment
TNBC	Triple negative breast cancer
TNC	Tenascin C

TNFα	Tumor necrosis factor α
TNFR	Tumor necrosis factor receptor
TPM	Transcripts per million
TYK2	Tyrosine kinase 2
UPL	Universal probe library
VEGF	Vascular endothelial growth factor
VIM	Vimentin
WB	Western Blot
ZEB	Zinc Finger E-Box Binding Homeobox